Dynamic Stiffness and Damping Prediction on Rubber Material Parts, FEA and Experimental Correlation

Zorion Kareaga Laka

Lea Artibai Ikastetxea S. Coop.

and

London Metropolitan University

PhD - Doctor Europaeus

2016

Abstract

The final objective of the present work is the accurate prediction of the dynamic stiffness behaviour of complex rubber parts using finite element simulation tools. For this purpose, it becomes necessary to perform a complex rubber compound material characterisation and modelling work; this needs two important previous steps. These steps are detailed in the present document together with a theoretical review of viscoelastic visco-elasto-plastic models for elastomers.

Firstly, a new characterisation method is proposed to determine the degree of cure of rubber parts. It is known that the degree of cure of rubbers bears heavily on their mechanical properties. This method consists of the correlation of swelling results to rheometer data achieving a good agreement.

Secondly, the influence of the strain rate used in static characterisation tests is studied. In this step, a new characterisation method is proposed. The latter characterisation method will be used to fit extended hyperelastic models in Finite Element Analysis (FEA) software like ANSYS. The proposed method improves the correlation of experimental data to simulation results obtained by the use of standard methods.

Finally, the overlay method proposed by Austrell concerning frequency dependence of the dynamic modulus and loss angle that is known to increase more with frequency for small amplitudes than for large amplitudes is developed. The original version of the overlay method yields no difference in frequency dependence with respect to different load amplitudes. However, if the element in the viscoelastic layer of the finite element model are given different stiffness and loss properties depending on the loading amplitude level, frequency dependence is shown to be more accurate compared to experiments. The commercial finite element program Ansys is used to model an industrial metal rubber part using two layers of elements. One layer is a hyper viscoelastic layer and the other layer uses an elasto-plastic model with a multi-linear kinematic hardening rule. The model, being intended for stationary cyclic loading, shows good agreement with measurements on the harmonically loaded industrial rubber part.

Acknowledgements.

First of all, I would like to thank all the people at the Materials Department in Leartiker and Lea-Artibai Ikastetxea S. Coop. The completion of this thesis is not only an individual achievement but also a collective success. I am especially grateful to Jose Javier Egurrola for his support, friendship and continuous encouragement.

Many thanks to my different supervisors in Leartiker; especially to Aitor Arriaga during my thesis studies, Rikardo Pagaldai for his continuous advices, and Asier Retolaza my right hand man and how to forget my fellow sufferers Mikel Isasi, Jon Anakabe and Joana Kano in Leartiker. I would also like to express my sincere thanks to my different research group leaders; Jose Javier Egurrola, Amaia Egia, Ainara Basurko and Rafael Atxurra

I especially want to express my sincere gratitude to my supervisors Dr. Ane Miren Zaldua in Leartiker and Dr. Mathew Philip in London Metropolitan University for their helpful discussion, suggestions and corrections.

My best gratitude to Iñigo Aspiazu and Jon Plaza at Cikautxo Scoop. in Berriatua, for their kind collaboration at the experimental testing phase.

I would like to express my heartfelt thanks to my entire family and friends, for their support and motivation throughout the years.

Eskerrik asko bihotz bihotzez Ixaie, Manex, Libe, Aitxe, Ama eta Anaiei.

Eskerrik asko!

Zorion Kareaga Laka

Markina-Xemein, July 2016.

Contents

CHAPTER 1 LITERATURE REVIEW

Sarrera

Historikoki produktu berriak diseinatu behar direnean piezen prototikoak eraiki eta entseiatuz beren funtzioa beteko dutela bermatu izan ohi da, kontrako kasuan prototipoak berreraiki eta berriz balidazio prozesu guztia martxan jarriz. “Froga-akats” sistema hau oso garestia izanik ANSYS, ABAQUS, NASTRAN en gisako element finituen softwareak sortu ziren pieza fisikoak eraiki orduko nolakoa izango litzakeen beren portaera aurre ikusteko. Software hauek pieza birtuala modelizatu, materialeen propietateak asignatu eta karga konkretu batzuen aurrean piezaren portaera aurreikusteko gai dira.

Kautxuen munduan enpresa bakoitzak bere materialeen formulazio konkretuak erabili ohi ditu eta formula horiek “sekretuak” izan ohi dira. Guzti honek esan nahi duena zera da, milaka formulazio aurkitu ditzakegula aplikazio eta eraldatzaile bakoitzaren arabera eta material estandarizatu gutxi daudela merkatuan. Gainera, kautxuen propietate mekanikoak aldakorrak dira bulkanizazio gradu, tenperatura, entseiatzen erabilitako karga eta entseiu motaren garrantzi handia dutelarik. Guzti hau kontutan izanik, kautxuzko piezen propietate mekanikoak aurreikusi nahi baldin baditugu, kautxu hori nola karakterizatu behar den argi eduki behar da. Zer propietate simulatu nahi den argi dugunean, materialea horren arabera karakterizatu beharko da.

Esan bezala, kautxuaren bulkanizazio graduak eta bulkanizazio tenperaturak propietate mekanikoen gain zerikusi haundia dute. Hauetaz gain, kautxua ez lineala izanik, aztertzen gauden deformazio-maila ere kontutan hartu beharrekoa da. Ez linealtasun hori “karbono beltza” edo “negro de carbono” karga erreforzantea kautxuaren formulazioan gehitzean areagotu egiten da. Historikoki karga erreforzante hauek dituzten kautxuak materialeen modelu biskoelastikoekin modelizatu izan ohi dira baina arazoak egon dira karga erreforzante ugari duten kautxuen propietateak simulatu nahi izan direnean.

Tesi honen helburu nagusia aurretik aipaturiko arazoak sahiestea da:

(1) Lehen zatiak kautxu berdinarekin egindako pieza desberdinen bulkanizazioa neurtu edo alderatzeko metodo berri bat aurkezten du [1,2] (ikusi Annex I-A eta Annex I-B).

(2) Bigarren zatiak materialeen egokitzapenerako karakterizazio metodo berri bat aurkezten du, non metodo honek modelo matematiko estatikoak simulazio ez estatikoak egiten erabiltzea ahalbidetzen duen.

(3) Tesiaren azken zatiak kautxusko piezen zurruntasun dinamiko eta amortiguazio ahalmena simulatzeko metodo berri bat aurkezten du, non amplitude eta frekuentzi desberdinak aztertzen direlarik [3] (ikusi Annex III).

Introduction

The use of calculation codes, based on the finite element method in the design phase of new industrial products, has fundamental results when reducing the costs as opposed to manufacturing physical prototypes and utilising “trial and error” tests. The general use of software like NASTRAN, ABAQUS or ANSYS permits: the modelling of the part or the assembly under study, the input of the material mechanical properties; the solving of loading conditions and the visualisation and evaluation of the obtained results.

Due to the special mechanical properties of elastomers, there are several possibilities to perform different compounds to solve rubber parts requirements. Because of that wide range of possibilities, each rubber manufacturer uses their own rubber mixtures. Therefore, it is not very common to find standard rubber compounds. In addition, the mechanical properties of rubber compounds change with degree of cure, temperature, load conditions, testing type and so on. Hence, to characterise correctly the mechanical behaviour of the studied rubber compound, all these factors must be taken into account.

When using finite element software it is really important to feed the material properties correctly. The first step of any simulation is the mechanical characterisation of the material. The material type studied is rubber. This

characterisation must be in accordance with the simulation that will be performed. To achieve this objective, the degree of cure of the testing sample used to characterise the mechanical properties of the studied rubbers and the rubber part to be simulated must be as similar as possible. In addition, the strain ranges need to be in accordance with both characterisation and simulations.

The filler content has a noticeable influence in dynamic properties of elastomers. Dynamic stiffness and loss angle of elastomers increases with higher filler content. Fillers can also introduce a nonlinear dynamic behaviour shown as an amplitude dependence of the dynamic stiffness and loss angle. Although it is a bit inappropriate, the linear viscoelastic stiffness and loss measures are used also for the nonlinear dynamics of filled rubbers. In this thesis, storage *G'* and loss modulus *G"* are used to characterise the cyclic dynamic behaviour of a particular rubber used to validate the proposed modelling method. While unfilled rubber can be properly modelled by purely viscoelastic models, filled rubbers, show a pronounced amplitude dependence of the storage and a loss modulus for filled and highly filled natural rubber as it is explained in later sections. The frequency dependence shows a steeper slope for smaller amplitudes than for larger amplitudes in both storage and loss modulus. The original version of the overlay method proposed by Austrell cannot capture the mentioned slope variance that depends on amplitude. In a wide frequency range, as shown here, it is important to be able to model this behaviour. In this thesis it is shown how different dynamic stiffness and loss values in the elements of the viscoelastic mesh in the overlay can solve the problem.

To reach the objective of this thesis, the experimental work is divided in three chapters:

(1) The first relates the degree of cure of different rubber components by means of swelling [1,2] (see Annex I-A and Annex I-B). The correlated components should be manufactured by different methods. For that purpose it is proposed a material characterisation method.

(2) The second part proposes a novel conditioning method applicable in quasi-static characterisations when mechanical properties should be influenced by the strain rate.

(3) The last part of the thesis proposes a new procedure to predict the dynamic stiffness and damping on rubber material parts when an elastomer is tested in a defined frequency/amplitude ranges [3] (see Annex III).

The second and the third parts includes mechanical tests as a finite element analysis and experimental correlations.

Note that the materials used in both experimental works are different for the convenience. First, in CHAPTER 2, the proposed swelling method is validated for materials references CK-NR-1 and CK-EPDM-1. Second, in CHAPTER 3 the static characterisations and posterior fitting and simulations are performed with the material called CKR. Lastly, the dynamic properties of NR1, NR2 and CKR are characterised to be used in the research developed in CHAPTER 4. Eventually, five materials are used in total.

Aim of the thesis

The aim of the thesis is double:

1. First, to propose two new experimental procedures to get appropriate data for fitting hyperelastic and visco-elastoplastic models used to predict either quasi-static or dynamic stiffness or rubber-made units (a new methodology to determine the degree of cure and a new material conditioning approach):

- *Degree of cure:*

When the same rubber formulation is used to manufacture different geometries, it is really important to obtain the best possible degree of cure. To obtain the same degree of cure in different geometries where the thicknesses, the used moulds and the cure times are different for each type of rubber part, requires a rigorous control of various parameters. Consequently, as the specimens used in laboratory tests to characterise the mechanical properties of the material (rubber compound) and the rubber parts manufactured for industrial purposes are different geometries and are manufactured in different moulds, the first step consists in a several swelling tests to control degree of cure of each type of pieces.

The objective of the present step (CHAPTER 2) is to develop a very simple and effective method to evaluate/measure the degree of cure or the state of cure. The expression “state of cure of a vulcanizate” means the degree to which a property of the vulcanizate has approached the maximum attainable value as a result of change in time or temperature of cure. It is rather directly related to the degree of crosslinking, but this latter never reaches a maximum; it increases with time. To achieve this objective, a new method is developed. It consists of swelling measurements in solvents. ODR measurements and tensile tests are also done to correlate its results to the swelling values.

- *Material Conditioning method*

The objective is to improve the extended material conditioning methods applied in the static characterisation of rubbers when used in FEA software.

By the use of the presented conditioning method, the classic hyperelastic models can be used for non-static simulations.

In the materials fitting to these hyperelastic models, some experimental data are required. For this type of materials some parameters, such as the degree of cure or the testing method of the characterisation samples, have a noticeable influence. It is impossible to take all the variables into the hyperelastic material model. So, there are short cuts to solve their influence. One way to solve these factors is to have an influence on the material characterisation tests, testing them at determined strain-rates and cycling them before the recording of the valid data curve. The last factor is known as the Mullis effect, which consists of the relaxation of the elastic stiffness of the tested rubber part after each load cycle. In some tests the Mullins effect is not eliminated completely.

This CHAPTER 3 focuses on the experimental investigation, the curve fitting representation and the numerical simulation of filled elastomers in non-static tests. The aim of the CHAPTER 3 is to propose a new characterisation procedure to feed available hyperelastic material models in standard Finite Element software (FEA). Yeoh's 3rd order constitutive model is used to validate the proposed method in Ansys sofware.

2. Second, to propose a new methodology to take into account the observed frequency and strain dependency in filled rubbers when predicting the dynamic stiffness using finite element codes. In order to predict the dynamic properties of any industrial rubber part, a Multilinear with equivalent Viscoelastic approach model (MLVE model) is developed.

- *Dynamic stiffness*

This behaviour is not so studied as the quasi-static field. It is extensive used way to characterise this behaviour is the use of visco-elastic, visco-hyperelastic, visco-elastoplastic mathematical material models. These types of models are based on linear and nonlinear spring-dashpot systems built in parallel and series combinations.

The work performed in CHAPTER 4 addresses the methods to model dynamically loaded rubber components. Different systems use rubber isolators for dynamic vibroacoustical improvement; so there is a great need to understand their properties and properly predict the dynamic stiffness of this type of parts.

The aim of this step is, therefore, to develop rubbers dynamic properties prediction method on the modelling of rubber isolators in the 0-500Hz frequency range, taking into account both the frequency and the amplitude dependent properties of the material. It is the intention of such a study to propose a modelling procedure that could provide accurate prediction of dynamic stiffness of rubber parts and that could be implemented in commercial finite element method software.

In summary, this thesis develops a method to generate correct material input data in ANSYS to obtain a reasonable correlation level when simulating non-static and dynamic tests. For this purpose, the objective is to use the most practical material models, in order to establish a reliable simulation method in an industrial oriented environment.

The literature review remarks the main areas revised in the literature. For convenience, the literature review has been divided in four main parts: the first one recounts the basic concepts of elasticity and hyperelasticity. The aim of this first chapter is to clarify the basic concepts for better understanding of all chapters of the thesis. The second part deals with static modelling of elastomers; the third one refers to the dynamic behaviour of rubber compounds and the last part describes the dynamic modelling of elastomers.

1.1 Literature review. Part 1. From elasticity to hyperelasticity: Basic concepts

1.1.1 Rubber: Basics concepts

Although elastomers can be made of any of a wide variety of different organic substances, all of them are polymers consisting of very long molecular chains. Natural and synthetic rubbers known as elastomers are amorphous polymers to which several ingredients are added, creating a rubber compound. The important process of vulcanization (heating and chemical reaction) converts the plastic raw elastomeric material into a material of solid and elastic consistency where these materials become rubber.

Vulcanization is a chemical process by which the long molecular chains are linked together, forming a stable and more solid molecular structure. The cross-linking is obtained using activators, curing agents (sulphur or peroxides) and accelerators. The vulcanization process starts when the mixture is heated up to the cure activation temperature (120-200ºC) depending on the mentioned mixture formulation. Their viscoelastic nature gives them elasticity and also the ability to dissipate energy. Their strength is high, especially under conditions of shear and compression.

After being properly compounded and moulded into an engineered product, the material at some point will be subject to an external force. When a solid body is deformed, an internal reactive force called stress, acting across a unit area, tends to resist this deformation. Rubber is unique in being soft, highly extensible and highly elastic having an additional ability to dissipate energy [4].

The final properties of the vulcanized rubber depend mainly on the choice of the rubber, the mixture composition, the production process, and the product design. Depending on the type and amount of additives and the degree of vulcanization, rubber vulcanizates can provide different properties with respect to hardness, elasticity or tensile strength.

The mission of additives is to:

a) Change the characteristics of the vulcanized rubber (e.a. fillers to increase hardness).

b) Facilitate the product manufacturing (e.a. plasticizers)

c) Reduce the cost of the mixture (e.a. certain degrees of carbon black).

A standard formula should be something as shown in the following Table 1.1:

ADITIVE	**Phr**
Elastomer	100
Filler (s)	0 to 100
Plasticizer (s)	0 to 50
Sulfur	0 to 2.5
ZnO	5
Stearic acid	2
Accelerator (s)	1 to 10
Peroxide	6
Coagent	2
Anti O_2	2
Anti O_3	2
Wax	2
Others	2
Processing aids	2

Table 1.1: General formulation. The intention of this table is to show that rubber formulations are complex and can be composed by a lot of ingredients. Phr indicates parts per hundred of rubber.

Rubbers, in both dry and latex forms, are grouped and symbolized on the basis of the chemical composition of the polymer chain in the following manner [5]:

M Rubbers having a saturated carbon chain of thepolymethylene type rubbers have carbon and nitrogen in the polymer chain

N No rubber has so far been symbolized in the “N“ group.

O Rubbers having carbon and oxygen in the polymer chain

Q Rubbers having silicon and oxygen in the polymer chain

R Rubbers having an unsaturated carbon chain, e.g. natural rubber and synthetic rubbers derived at least partly from conjugated dienes

T Rubbers having carbon, oxygen and sulfur in the polymer chain

U Rubbers having carbon, oxygen and nitrogen in the polymer chain

Z Rubbers having phosphorus and nitrogen in the polymer chain

Table 1.2 shows mostly used rubbers and the classification in their corresponding group. Table 1.3 shows the summary of material properties of different rubbers and the behaviour of each rubber type.

To carry out this work two rubber types are selected. The first part of the experimental work which deals with the determination of the degree of cure of rubber compounds is performed with peroxide cured EPDM and a sulfur cured NR rubbers. In the second part which is about the dynamic properties of rubber it is considered that the most suitable rubber is NR, both because of its excellent elastic behaviour and its ability to dissipate energy.

R Group	
Rubber	**Symbol**
Acrylate-butadiene	ABR
Butadiene	BR
Chloroprene	CR
Epoxidized natural rubber	ENR
Hydrogenated NBR	HNBR
Isobutene-isoprene	IIR
Isoprene	IR
α-methylstyrene-butadiene	MSBR
Acrylonitrile-butadiene	NBR
Acrylonitrile-isoprene	NIR
Natural rubber	NR
Vinylpyridine-butadiene	PBR
Vinylpyridine-styrene-	PSBR
Styrene-butadiene	SBR
Styrene-isoprene-butadiene	SIBR

O Group	
Rubber	**Symbol**
Polychloromethyloxirane	CO
Epichlorohydrin copolymer	ECO
Polypropilene oxide	GPO

U Group	
Rubber	**Symbol**
Polyester urethane	AU
Polyether urethane	EU

M Group	
Rubber	**Symbol**
Copolymer of ethyl acrylate	ACM
Copolymer of ethyl acrylate and ethylene	AEM
Copolymer of ethyl acrylate and acrylonitrile	ANM
Chloropolyethylene	CM
Chlorosulfonylpolyethylene	CSM
Terpolymer of ethylene, propylene and diene	EPDM
Ethylene-propylene copolymer	EPM
Ethylene-vinyl acetate copolymer	EVM
Copolymer of tetrafluoroethylene and propylene	FEPM
Perfluoro rubber	FFKM
Fluoro rubber	FKM
Polyisobutene	IM
Fully hydrogenated acrylonitrile-butadiene copolymer	NBM

Q Group	
Rubber	**Symbol**
Silicone rubber having methyl and fluorine substituent	FMQ
Silicone rubber having methyl, vinyl and fluorine	FVMQ
Silicone rubber having only methyl substituent groups	MQ
Silicone rubber having methyl and phenyl substituent	PMQ
Silicone rubber having methyl, vinyl and phenyl	PVMQ
Silicone rubber having methyl and vinyl substituent	VMQ

Table 1.2: Mostly used rubbers and their classification in groups [5]

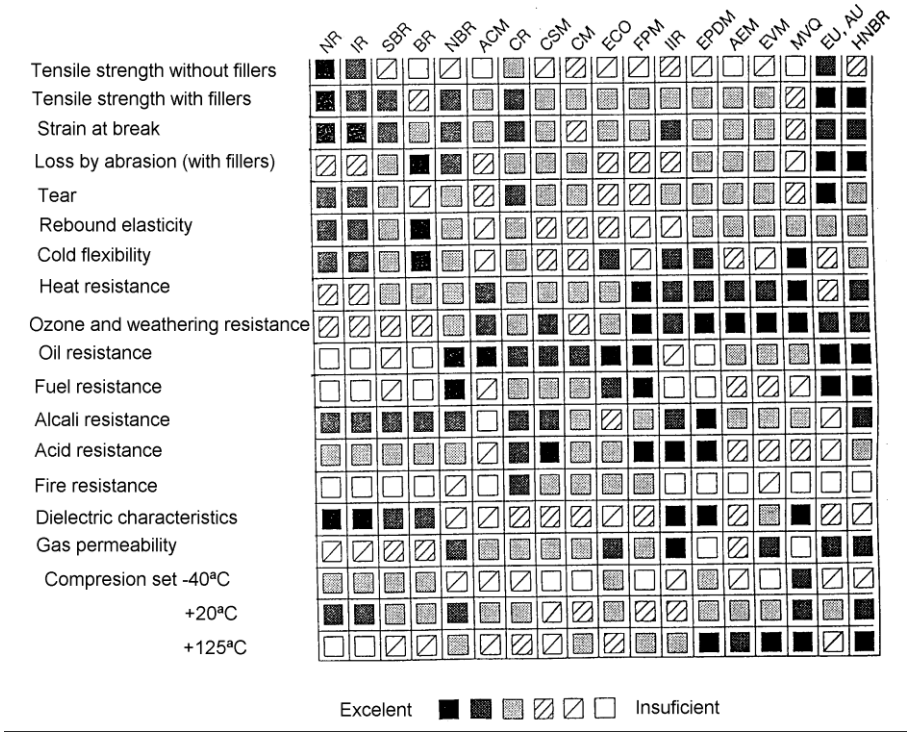

Table 1.3: Types of rubber and their properties [6]

1.1.2 Hyperelasticity of Rubber

One of the most notable properties of hyperelastic materials is their capability to be extended or elongated hundreds per cent of their initial length without plastic deformations. Then, it implies that these materials are able to recover their initial configuration when the sample is unloaded. Another elastomers property is their low elastic modulus *E* (≈0.5-10 MPa).

Under small deformations elastomers are linearly elastic solids. Thus this type of materials fulfils Hooke's law. Hooke's law of elasticity is an approximation where the extension of a spring is in direct proportion with the load added to it as long as this load does not exceed the elastic limit. Materials for which Hooke's law is a useful approximation are known as linear-elastic or "Hookean" materials (Eq. 1.1 and Eq. 1.2). It can be modelled as a spring (Figure 1.1). The elastic spring can be expressed as,

$$F = K.\delta \qquad \textit{Eq. 1.1}$$

$$\sigma = E.\varepsilon \rightarrow E = \sigma / \varepsilon \qquad \textit{Eq. 1.2}$$

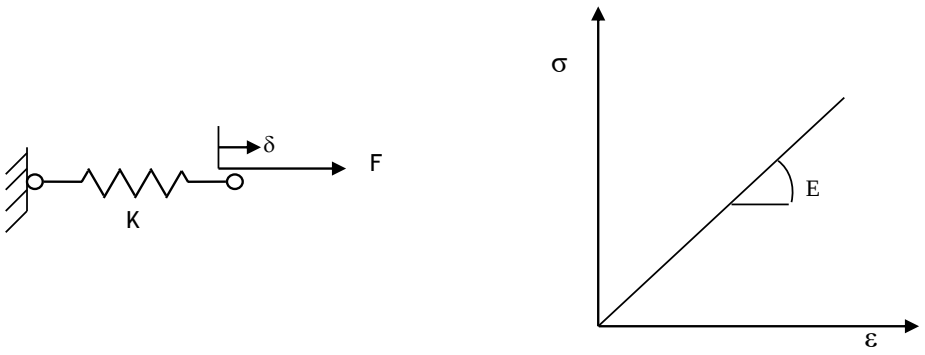

Figure 1.1: Linear elastic spring.

where σ and ε represents the tensile stress and strain respectively. Young's modulus *E* is a fundamental measure of the *K* material stiffness. The higher its value is, the more resistant the material has to be stretched. The tensile stress σ is defined in terms of force per unit area.

For the three dimensional cases, Hooke's law must be generalised [7]. In this type of cases, any point of a loaded body could be modelled as a cube (Figure 1.2), which is deformed in three principal directions. This cube is in a load balance; so in the opposite face to the applied load, there is a reaction.

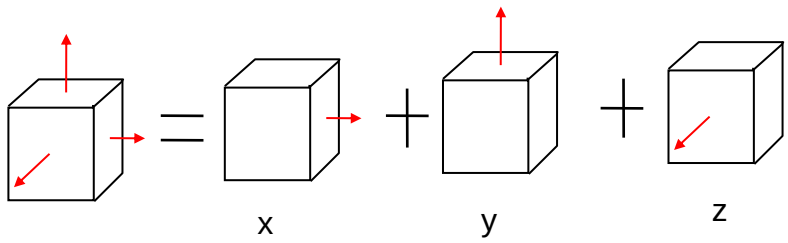

Figure 1.2: Superposition method representation

$$\sigma_{x,y,z} = \frac{F_{x,y,z}}{A_{x,y,z}} \qquad \textit{Eq. 1.3}$$

The Generalised Hooke's law is applicable only for isotropic materials; the strain for each direction is calculated as follows:

$$\varepsilon_x = \frac{1}{E}\left[\sigma_x - \nu\left(\sigma_y + \sigma_z\right)\right] \qquad \textit{Eq. 1.4}$$

$$\varepsilon_y = \frac{1}{E}\left[\sigma_y - \nu\left(\sigma_z + \sigma_x\right)\right] \qquad \textit{Eq. 1.5}$$

$$\varepsilon_z = \frac{1}{E}\left[\sigma_z - \nu\left(\sigma_x + \sigma_y\right)\right] \qquad \textit{Eq. 1.6}$$

Instead of elongating or compressing a sample, it may be subject to various shearing or twisting motions. The ratio of the shear stress τ to the shear strain γ defines the shear modulus *G* which is extended to define elastomers hyperelasticity constitutive models (ESED functions) discussed later instead of the young modulus *E*. The relation between both strain states –uniaxial and shear- shown in Eq. 1.8 is developed in Annex II-A.

$$G = \frac{\tau}{\gamma} \qquad \textit{Eq. 1.7}$$

$$G = \frac{E}{2(1+\nu)} \qquad \textit{Eq. 1.8}$$

When the material is considered incompressible the Poisson's ratio υ [7] is close to 0.5; so from the previous Eq. 1.8, it is assumed that the young modulus is three times the shear modulus. Most materials have Poisson's ratio values greater than 0 and smaller than 0.5. Referring to the elastomer materials, this ratio is close to 0.5 because of its incompressibility (Eq. 1.13). Then,

$$E = 3G \qquad \textit{Eq. 1.9}$$

In addition, the Bulk compression modulus *k*, about 2000MPa, is very high and the low shear modulus *G*, about 0.2-5 MPa, gives its low compressibility property.

The Bulk modulus *k* is a material constant which defines the material resistance to volume change when subject to compression loading. The demonstration of where is the bulk modulus is in Annex II-B.

$$k = \frac{E}{3(1-2\nu)} \qquad \textit{Eq. 1.10}$$

For convenience, the positive volumetric strain is defined as a decrease in volume.

From Eq. 1.8 and Eq. 1.10, the other material constants, such as Young modulus *E*, shear modulus *G* and Poisson's ratio ν can be obtained as follows:

$$E = 3k(1-2\nu) \qquad \textit{Eq. 1.11}$$

$$E = 2G(1+\nu) \qquad \textit{Eq. 1.12}$$

$$\nu = (3k - 2G)/(6k + 2G) \qquad \textit{Eq. 1.13}$$

Each material property can be determined from the above equations as long as two of them are known. The Poisson's ratio ν is difficult to measure, hence it is better to characterise the other two parameters (*E* and *G*). *Peng et al* [8] showed a method to determine the bulk modulus.

The Young modulus *E* is always positive therefore $1-2\nu > 0$ must be positive, consequently $\nu < 0.5$. In addition, the Poisson's ratio range goes from $0 \le \nu \le 0.5$. When this ratio takes the extreme value of $\nu = 0{,}5$ then $k = \infty$ which implies that $\varepsilon_v = 0$, so the volume doesn't change. This is one of the classical assumptions in the hyperelastic calculations.

Usually the ESED function studied in later sections uses a material compressibility constant *d*. This is found from the initial slope (*k*, small strain bulk modulus) of collected pressure vs. volume data as explained for example by *Charlton and Yang* [9]:

$$d = 2/k \qquad \textit{Eq. 1.14}$$

Gent [10]: This linear behaviour can be assumed in some rubber calculations because in many cases, they are low loaded. However, the Hooke's law proportionality does not hold for all elastic bodies; there are materials and bodies whose behaviour is elastic although this elasticity is nonlinear (Figure 1.3:).

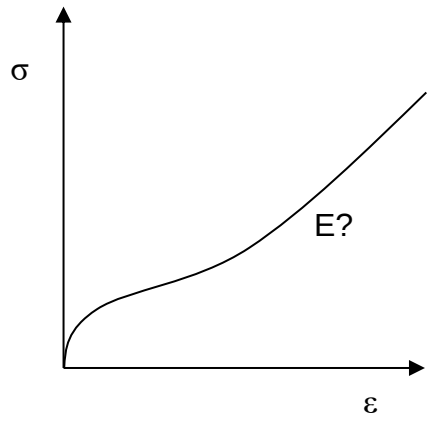

Figure 1.3: Rubber compounds nonlinear elasticity

To improve the Hooke's law, another definition arises that considers the reversibility of nonlinear elastic deformations. As the body deforms, it stores internal energy due to the strain or deformation: it is called the strain energy *W*. The reversibility of elastic deformations and the independence of the path (previous deformation histories) of elastic bodies lead us to assume the existence of a strain energy potential for the elastic body, from which the stresses can be derived. In case of elastomeric materials, the stress tensor is derived from strain energy density functions (ESED) based on thermodynamic laws *Oden* [11].

The materials that fulfil Eq. 1.15 named Green elastic constitutive law are known as hyperelastic materials. Therefore, a hyperelastic material is one whose strain energy at any time is given by a function of the Cauchy-Green deformation tensor.

$$\sigma_{ij} = \frac{\partial W}{\partial \varepsilon_{ij}} \qquad \textit{Eq. 1.15}$$

So, the stress tensor may be obtained by derivation of the next equation,

$$W(\varepsilon_{ij}) = \int_0^{\varepsilon_{ij}} \sigma_{ij} d\varepsilon_{ij} \qquad \textit{Eq. 1.16}$$

The strain energy per unit volume in the reference configuration *W* and its dependence on the strain measure are the subject of this section. A general assumption is that *W* depends on all the components of the strain measure, giving

$$W = W(B) \qquad \textit{Eq. 1.17}$$

The mathematical ESED Models used to characterise the quasi-static behaviour of hyperelastic materials are defined by stretches λ instead of uniaxial strains $\boldsymbol{\varepsilon}$.

When a complex three dimensional part is tested, the strain state of the deformed geometry is composed by a combination of principal and shear strains. Hence, the following definitions are focused to solve these three dimensional complexities using for it the principal elongations λ_1, λ_2, λ_3 by the large elastic deformations.

In order to determine the straining of the body and consequently the $[B]$ matrix (the left Cauchy Green tensor), we need to know how the distance between neighbouring particles in the reference configuration is affected by the deformation. This can be achieved by considering the length changes of an infinitesimal material line element. This line element is obtained by the following differential

$$dx_i = \frac{\partial x_i}{\partial X_j} dX_j \qquad \textit{Eq. 1.18}$$

where *X* referees to the particle reference configuration or position and *x* is the current location.

The explicit matrix expression of the above equation is:

$$\begin{Bmatrix} dx_1 \\ dx_2 \\ dx_3 \end{Bmatrix} = \begin{bmatrix} \frac{\partial x_1}{\partial X_1} & \frac{\partial x_1}{\partial X_2} & \frac{\partial x_1}{\partial X_3} \\ \frac{\partial x_2}{\partial X_1} & \frac{\partial x_2}{\partial X_2} & \frac{\partial x_2}{\partial X_3} \\ \frac{\partial x_3}{\partial X_1} & \frac{\partial x_3}{\partial X_2} & \frac{\partial x_3}{\partial X_3} \end{bmatrix} \begin{Bmatrix} dX_1 \\ dX_2 \\ dX_3 \end{Bmatrix} \qquad \textit{Eq. 1.19}$$

which can be expressed in compact matrix notation as

$$dx = FdX \qquad \textit{Eq. 1.20}$$

The matrix $[F]$ is:

$$F_{ij} = \frac{\partial x_i}{\partial X_j} \qquad \textit{Eq. 1.21}$$

The ESED function is a function of the left Cauchy-Green deformation tensor,

$$[B] = [F][F]^T \qquad \textit{Eq. 1.22}$$

Being $[F]$ the deformation tensor that relates the undeformed and deformed configurations; so $W = W(\varepsilon_1, \varepsilon_2, \varepsilon_3)$, $W = W(\lambda_1, \lambda_2, \lambda_3)$ and $W = W([B])$.

This ESED function can be expressed as $W = W(\lambda_1, \lambda_2, \lambda_3, n_1, n_2, n_3)$ by the principal stretches and the principal directions. This expression can be simplified in $W = W(\lambda_1, \lambda_2, \lambda_3)$ for isotropic materials. Finding the roots of the characteristic polynomial of $[B]$, we obtain the principal stretches. However, in the same way, it is easier to find the roots using the strain invariants instead of using the principal stretches:

$$W = W(I_1, I_2, I_3) \qquad \textit{Eq. 1.23}$$

$$I_1 = tr([B]) = \lambda_1^2 + \lambda_2^2 + \lambda_3^2 \qquad \textit{Eq. 1.24}$$

$$I_2 = \frac{1}{2}[tr^2([B]) - tr([B]^2)] = \lambda_1^2\lambda_2^2 + \lambda_1^2\lambda_3^2 + \lambda_2^2\lambda_3^2 \qquad \textit{Eq. 1.25}$$

$$I_3 = \det([B]) = \lambda_1^2\lambda_2^2\lambda_3^2 \qquad \textit{Eq. 1.26}$$

If the material is considered to be incompressible at this time, the samples initial volume and the final volume must be equal (see Figure 1.4); therefore the third invariant can be simplified as follows:

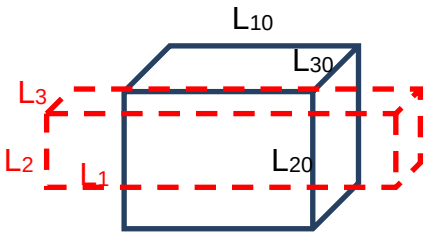

Figure 1.4: Representation of the undeformed (in blue) and deformed (in red) shapes of a testing bar.

$$V_f = V_0 \Rightarrow L_1L_2L_3 = L_{10}L_{20}L_{30} \Rightarrow \frac{L_1}{L_{10}}\frac{L_2}{L_{20}}\frac{L_3}{L_{30}} = 1 \Rightarrow \lambda_1\lambda_2\lambda_3 = 1 \qquad \textit{Eq. 1.27}$$

$$I_3 = \det([B]) = \lambda_1^2\lambda_2^2\lambda_3^2 = (\lambda_1\lambda_2\lambda_3)^2 = 1^2 = 1, \text{ so } I_3 = 1 \qquad \textit{Eq. 1.28}$$

Then, the previous Eq. 1.23 can be simplified in the next expression,

$$W = W(I_1, I_2) \qquad \textit{Eq. 1.29}$$

As the third principal stretch can be expressed as,

$$\lambda_3 = \frac{1}{\lambda_1 \lambda_2} \qquad \textit{Eq. 1.30}$$

the invariants I_1 and I_2 yield in,

$$I_1 = \lambda_1^{\,2} + \lambda_2^{\,2} + \frac{1}{\lambda_1^{\,2}\lambda_2^{\,2}} \qquad \textit{Eq. 1.31}$$

$$I_2 = \lambda_1^{\,2}\lambda_2^{\,2} + \frac{1}{\lambda_2^{\,2}} + \frac{1}{\lambda_1^{\,2}} \qquad \textit{Eq. 1.32}$$

The constitutive law for a hyperelastic, isotropic and incompressible material is derived by the use of an energy principle *Malvern* [12], *Beatty* [13]. The constitutive law is given by:

$$[t] = 2\left[\left(\frac{\partial W}{\partial I_1} + I_1 \frac{\partial W}{\partial I_2}\right)[B] - \frac{\partial W}{\partial I_2}[B]^2\right] + p[\varphi] \qquad \textit{Eq. 1.33}$$

where $[\varphi]$ is the 3X3 unitary matrix.

Where [*t*] is the Cauchy stress tensor(true stress or force per deformed area) and *p* is the pressure defined as

$$p = \frac{1}{3}(t_{11} + t_{22} + t_{33}) \qquad \textit{Eq. 1.34}$$

So the deviator stress could be written as,

$$[s] = [t] - p[\varphi] \qquad \textit{Eq. 1.35}$$

The general constitutive laws are derived from the above equation by eliminating the pressure stress.

The only part of the stress that causes strain in an incompressible body is the deviatory part because the volume does not change.

In the case of the deformation without shear, the left Cauchy-Green deformation tensor can be expressed as:

$$[B]=[F][F]^T=\begin{bmatrix}\lambda_1^2 & 0 & 0\\ 0 & \lambda_2^2 & 0\\ 0 & 0 & \lambda_3^2\end{bmatrix} \qquad \textit{Eq. 1.36}$$

$$[B]^2=\begin{bmatrix}\lambda_1^4 & 0 & 0\\ 0 & \lambda_2^4 & 0\\ 0 & 0 & \lambda_3^4\end{bmatrix} \qquad \textit{Eq. 1.37}$$

$$t_1=2\frac{\partial W}{\partial I_1}\lambda_1^2+2\frac{\partial W}{\partial I_2}\left(\left(\lambda_1^2+\lambda_2^2+\lambda_3^2\right)\lambda_1^2-\lambda_1^4\right)+p \qquad \textit{Eq. 1.38}$$

$$t_2=2\frac{\partial W}{\partial I_1}\lambda_2^2+2\frac{\partial W}{\partial I_2}\left(\left(\lambda_1^2+\lambda_2^2+\lambda_3^2\right)\lambda_2^2-\lambda_2^4\right)+p \qquad \textit{Eq. 1.39}$$

$$t_3=2\frac{\partial W}{\partial I_1}\lambda_3^2+2\frac{\partial W}{\partial I_2}\left(\left(\lambda_1^2+\lambda_2^2+\lambda_3^2\right)\lambda_3^2-\lambda_3^4\right)+p \qquad \textit{Eq. 1.40}$$

t_i = Principal Cauchy Stress in i direction

λ_i = Principal stretch in i direction

1.1.3 Finite element analysis (FEA) or Finite element method (FEM)

1.1.3.1 Introduction

The Finite Element Analysis (FEA) is a computer simulation technique used in engineering analysis. It consists in a numerical method for solving problems of engineering and mathematical physics. The FEA method is useful for problems with complicated geometries, loadings, and material properties where analytical solutions cannot be obtained. It was first developed in 1943 by Richard Courant, who utilized the Ritz method of numerical analysis and minimization of variational calculus to obtain approximate solutions to vibration systems. Later, *Turner et al* [14] established a broader definition of numerical analysis. The paper centres on the "stiffness and deflection of complex structures".

FEA is used for the determination of stresses and displacements in mechanical objects and systems. However, it is also routinely used in the analysis of many other types of problems, including those in heat transfer, fluid dynamics and electromagnetism. FEA is able to handle complex systems that defy closed-form analytical solutions. The object or system being investigated is represented by a geometrically similar model consisting of multiple, linked, simplified representations of discrete regions. Equations of equilibrium, in conjunction with applicable physical considerations such as compatibility and constitutive relations, are applied to each element, and a system of simultaneous equations is constructed. The system of equations is solved for unknown values using the techniques of linear algebra or nonlinear numerical schemes, as appropriate. While being an approximate method, the accuracy of the FEA method can be improved by refining the mesh in the model using more elements and nodes.

In this section, a general description of the basic theory behind finite element analysis will be followed by a discussion on element types commonly available for application. The generic procedure for applying finite elements will also be summarised in terms of geometry definition and mesh creation, material properties, boundary and loads conditions, and interpretation of results.

1.1.3.2 Structural Finite Element Analysis. Theoretical Basis.

Geometry can be idealised as being composed of many small, discrete pieces called finite elements. The problem can now be characterised by large numbers of simultaneous equations.

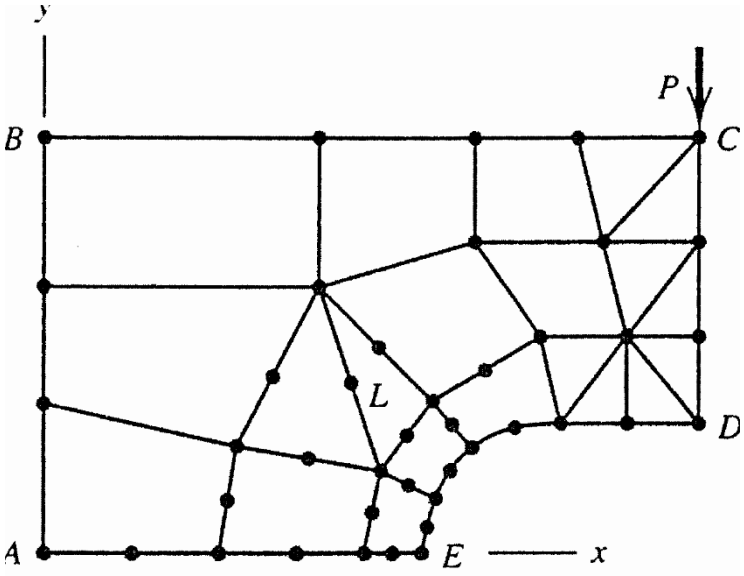

Figure 1.5: Example of a finite element model in 2D [15].

When a load is applied to the structure, all of the elements must deform in a fashion that guarantees equilibrium of forces between the elements. In addition, the deformation of the modelled structure must remain compatible.

Displacement function.—

Characterises the displacements within an element as a function of space. The choice of displacement function affects the accuracy of the element in approximating actual displacements, strain, and stress behaviour over the volume of the element. Since strains are first derivatives of displacements, a linear displacement function leads to the approximation of constant strains and stresses within the element. Similarly, a quadratic displacement function simulates linear stress and strain fields within an element. For the three-node triangular elements shown in Figure 1.5, with the x axis lying along one edge of the triangle, and with displacements (U_i, V_i) in two coordinate directions (x,y) at each node (i), a total of six nodal displacements (degrees of freedom) can

be defined in terms of the deformation field for the element. This requires functions with a total of six coefficients:

$$u = a + bx + cy \qquad \textit{Eq. 1.41}$$

$$v = d + ex + fy \qquad \textit{Eq. 1.42}$$

where *a*, *b*, *c*, *d*, *e*, and *f* are unknown constants.

Element displacements in terms of nodal displacements.

Using the previous Eq. 1.41 and Eq. 1.42 to evaluate the displacement at each node (i),

$$U_i = a \qquad \textit{Eq. 1.43}$$

$$U_i = a + bX_j \qquad \textit{Eq. 1.44}$$

$$U_i = a + bX_k + cY_k \qquad \textit{Eq. 1.45}$$

where X_j, X_k and Y_k define known coordinate locations. A similar set of equations can be written to define the coefficients *d, e*, and *f* in terms of the nodal y displacements. Using matrix manipulation it is possible to represent the *u* and *v* displacements within an element in terms of nodal displacements as

$$\begin{Bmatrix} u(x,y) \\ v(x,y) \end{Bmatrix} = [N] \begin{Bmatrix} Ui \\ Vij \\ Vj \\ Uk \\ Vk \end{Bmatrix} = [N]\{\delta\} \qquad \textit{Eq. 1.46}$$

where [*N*] is the shape function matrix and $\{\delta\}$ is the vector of nodal displacements.

Strains as a function of nodal displacements.—

The two dimensional definitions of strain in terms of displacement are:

$$\varepsilon_x = \frac{\partial u}{\partial x} \qquad \textit{Eq. 1.47}$$

$$\varepsilon_y = \frac{\partial u}{\partial y} \qquad \textit{Eq. 1.48}$$

$$\gamma_{xy} = \frac{\partial u}{\partial y} + \frac{\partial v}{\partial x} \qquad \textit{Eq. 1.49}$$

Eq. 1.47 and Eq. 1.49 are used to calculate the strains within the element in terms of its nodal displacements. Using matrix notation again, the above relationships can be expressed as

$$\{\varepsilon\} = \begin{Bmatrix} \varepsilon_x \\ \varepsilon_y \\ \gamma_{xy} \end{Bmatrix} = [B]\{\delta\} \qquad \textit{Eq. 1.50}$$

where [B] is a matrix that can be defined in terms of derivatives of the shape function elements.

Stresses in terms of strains.—

In order to relate stresses to strains, a material constitutive model is necessary. For simple linear elasticity, the plane stress constitutive relations are

$$\sigma_x = \frac{E}{1-\nu^2}\left(\varepsilon_x + \nu\varepsilon_y\right) \qquad \textit{Eq. 1.51}$$

$$\sigma_y = \frac{E}{1-\nu^2}\left(\varepsilon_y + \nu\varepsilon_x\right) \qquad \textit{Eq. 1.52}$$

$$\tau_{xy} = \frac{E}{2(1+\nu)}\gamma_{xy} \qquad \textit{Eq. 1.53}$$

where *E* is the elastic modulus and ν is the Poisson's ratio. Using matrix notation,

$$\begin{Bmatrix}\sigma_x\\ \sigma_y\\ \tau_{xy}\end{Bmatrix} = [D]\begin{Bmatrix}\varepsilon_x\\ \varepsilon_y\\ \gamma_{xy}\end{Bmatrix} = [D][B]\{\delta\} \qquad \textit{Eq. 1.54}$$

where [D] is the material matrix formed using Eq. 1.52 and Eq. 1.53.

Nodal forces in terms of displacements.—

A load is transmitted from one finite element to another through forces at the node points of the elements, which can be represented as $\{F\}$. These nodal forces in the two coordinate directions are related to the nodal displacements through a set of element equilibrium equations. These equilibrium equations can be defined by equating the external work accomplished by the nodal forces when subjected to an arbitrary set of virtual nodal displacements, $d\{\delta\}$, to that of the internal energy stored in the element's volume as its stress is subjected to the virtual strain field, resulting from the same nodal displacements.

This relationship can be expressed as:

$$\left(d\{\delta\}\right)^T\{F\} = \int_{Vol} d\{\varepsilon\}^T\{\sigma\}dVol \qquad \textit{Eq. 1.55}$$

Since the virtual strains can be related to the virtual nodal displacements as

$$d\{\varepsilon\} = [B]d\{\delta\} \qquad \textit{Eq. 1.56}$$

the element equilibrium takes the form of

$$(d\{\delta\})^T\{F\} = d\{\delta\}^T \int_{Vol} [B]^T [D][B]\{\delta\} dVol \qquad \textit{Eq. 1.57}$$

The relationship between the nodal forces $\{F\}$ and the nodal displacements $\{\delta\}$ can be written as,

$$\{F\} = [K]_e\{\delta\} \qquad \textit{Eq. 1.58}$$

where $[K]_e$ is the element stiffness matrix defined as

$$[K]_e = \int_{Vol} [B]^T [D][B] dVol \qquad \textit{Eq. 1.59}$$

1.1.3.3 Types of Finite Elements

Elements can be categorised as one, two and three-dimensional solid elements and beam, plate and shell elements.

The complexity of the analysis, the amount of engineering and computer time increase significantly when moving from 1-D to 2-D and 3-D analysis. Many real part geometries and loadings are certainly 3-D in nature. When 2-D and 1-D elements are used, assumptions must be made relative to the distribution of stress and strain in the other directions.

One-dimensional elements.—

Bar or truss elements are simple, one-dimensional elements. Their length is calculated from the nodal positions defining the bar ends. The cross-sectional

area is defined by the modeller. These elements are simple spring elements and have very limited use in plastic part modelling.

Two-dimensional elements.—

Include plane stress, plane strain and axisymmetric elements. The plane stress assumption (that stress in the thickness direction is zero) is used when the component's deformation is independent of the dimension perpendicular to the plane of description and its thickness in that direction is small (thin snap fits). The plane strain assumption (that strain in the thickness direction is zero) is used when the component is thick relative to the planar dimensions.

In the axisymmetric elements, the stresses, strains, and loads do not vary in the circumferential direction. These elements are often quite useful because they account for fully 3-D behaviour.

Three-dimensional elements.—

3-D elements are typically either tetrahedrons or hexahedrons. One of the most common is the rectangular hexahedron with eight nodes, one at each corner. Such elements will be used when precise studies of local stress distributions around geometric details like notches are needed.

In this thesis, 2-D and 3-D elements will be evaluated for simple and complex geometries.

Shell elements.—

All the nodes describing the geometry of these elements are at the midsurface of the component. The thickness of the element is usually specified as either a nodal or an element parameter.

The degrees of freedom associated with the nodes of these elements now include rotations as well as translations.

In this thesis, shell elements will not be evaluated.

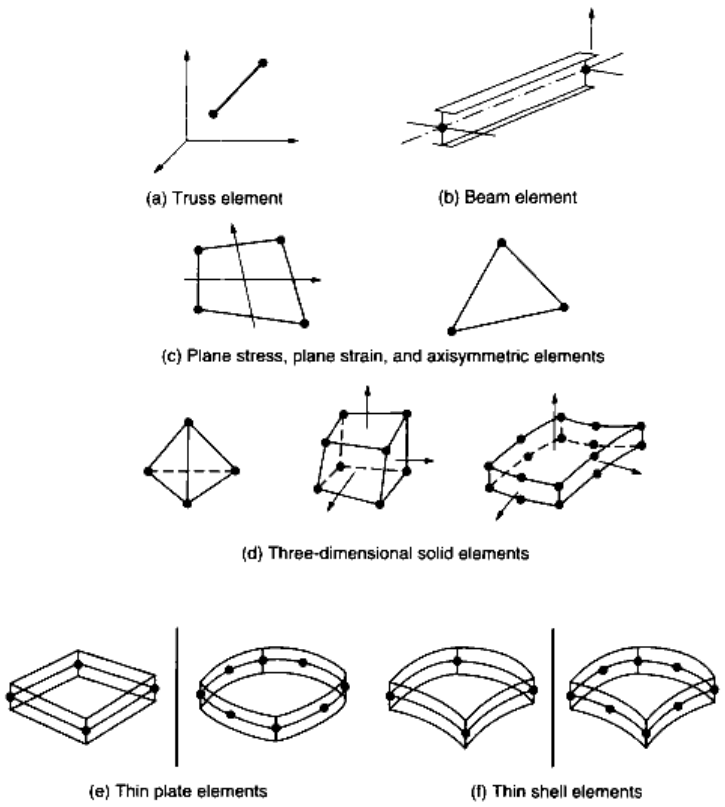

Figure 1.6: Basic element types found in FEA software.

1.1.3.4 Finite Element Analysis Procedure.

The study of a component or a system of different parts (an assembly) requires in any finite element based software three main steps which consist of pre-processing, solving and post-processing.

Pre-processing.—

The pre-processing step is related to the preparation of the geometry and mesh. In some cases no geometry is available since the mesh is directly imported from another FEA code. When the geometry is modelled, it can be imported from CAD software or can be directly created in the finite element programme. In both cases, the general aim of the geometrical modelling is to obtain the simplest representation of the part (eliminating small details that will not affect the overall response) in order to make the meshing process easier.

Meshing consists of dividing the geometry into elements that are connected to one another at the nodal points. The meshing of the part is automatic in most of the codes and the user has to specify the element type and the mesh size

to be used. Selecting coarser meshes results in a faster solution time but limits the accuracy of the analysis.

This step also comprises the specification of material properties, which can be complicated depending on the materials to be studied and the complexity of the analysis.

Solution.—

The solution phase is related to the specification of the boundary conditions and loads that are imposed to the component or system of components and the solving of the problem.

The boundary conditions can be in the form of restrictions of degrees of freedom (DOF) in the X, Y, Z directions, or in the form of contact regions in between different areas of the same part or between different parts.

The load type varies with the analysis type but in general structural problems, forces, displacements, pressures, temperatures, velocities or accelerations are applied.

Post-processing.—

The post-processing phase is related to the visualization of the results in a graphical form. Deformed shapes, stresses, strains, reaction results and graphs can be plotted between other quantities and the output should be compared with admissible parameters in our design. An adequate post-process should evaluate critically the validity of the obtained results, for example, in a static analysis the applied forces and the obtained reaction results.

Evaluating the obtained results, design modification or optimization works can be carried out.

1.1.3.5 Ansys Parametric Design Language (APDL)

Commercial finite element method software as Ansys or Abaqus have implemented algorithms to perform finite element analysis (FEA). This type of

software displays a friendly environment for users. In addition, this type of software gives the choice to include several options as calculations, material models, macros, and so on by parametric programming languages or subroutines.

APDL stands for ANSYS Parametric Design Language [16], a scripting language that can be used to automate common tasks or even build a model in terms of parameters (variables). APDL also encompasses a wide range of other features such as repeating a command, macros, if-then-else branching, do-loops, scalar, vector and matrix operations.

1.2 Literature review. Part 2. Static modelling of elastomers

The static tests performed to measure the mechanical properties of materials are executed at very low speeds (see section 3.1.4-A). Hence, as a minimum speed is required to do the static tests, also they are known as quasi-static tests.

This part of the literature review is divided in two sections: the first one relates to the quasi-static material constitutive description and the second section describes the ordinary quasi-static characterisation methods for performing simulations in finite element analysis (FEA).

1.2.1 Hyperelastic material models: Static modelling of elastomers by elastic strain energy density functions (ESED Functions)

There are two rather different approaches to study the rubber elasticity. On the one hand, the statistical or kinetic theory attempts to derive elastic properties from some idealized model of the structure of vulcanized rubber. On the other hand, the phenomenological theory treats the problem from the viewpoint of continuum mechanics. This approach constructs a mathematical framework to characterise hyperelastic behaviour so that stress analysis and strain analysis problems may be solved without reference to microscopic structure or molecular concepts.

The statistical-thermodynamic theory of a molecular .— This theory was originally developed by *Kuhn and Grün* [17]; additional contributions were made by *James and Guth* [18] and also *Flory and Rehner* [19]. *Treloar* [20] comprehensively reviewed the molecular theory of rubber-like elasticity, the base of which is on the fundamental statistical property of the elastomer molecules and the network entropy of deformation.

The work of deformation per unit volume is:

$$W = \frac{1}{2} NkT(\lambda_1^2 + \lambda_2^2 + \lambda_3^2 - 3) \qquad \textit{Eq. 1.60}$$

where *N* is the number of network chains in a unit volume, *k* is the Boltzmann's constant, λ_i are the principal extension ratios and *T* is the temperature in Kelvin. Additionally, developing this theory summarized in e.a. [21], the next relation can be imposed:

$$G = NRT \qquad \textit{Eq. 1.61}$$

Hence,

$$W = \frac{1}{2} G\left(\lambda_1^2 + \lambda_2^2 + \lambda_3^2 - 3\right) \qquad \textit{Eq. 1.62}$$

Thus, the strain energy function represented by Eq. 1.62 involves only one physical constant *G*, the shear modulus, which may be determined from the degree of crosslinking in the rubber.

Substituting Eq. 1.30 in Eq. 1.62,

$$W = \frac{1}{2} G\left(\lambda_1^2 + \lambda_2^2 + \left[\lambda_1 \lambda_2\right]^{-2} - 3\right) \qquad \textit{Eq. 1.63}$$

Thus, for an incompressible material, *W* is a function of two independent variables; in this case, they are chosen to be λ_1, λ_2.

This theory predicts a simple relationship between the stress and the strain. In simple shear, the shear stress is linearly related to the shear strain by the shear modulus *G*. The form of the relationships is similar to all elastomers that are only scaled by the magnitude of the distance between cross-links. It predicts well the initial elastic modulus at small strains. But it breaks down as the chain extension approaches strains of 50% for an unfilled elastomer. The high strain behaviour caused by the effects of a finite extensibility is of course neither predicted nor the marked nonlinearity is at moderate strains. The phenomenological theories, to be discussed next, are not restricted by any particular physical interpretation. They largely concentrate on trying to

represent the high strain behaviour of unfilled elastomers with attempts to extend these ideas to represent the behaviour of filled elastomers.

Rivlin [22] has shown that the statistical theory is the natural extension of Hooke's law of large deformations, hence the material that obeys it is called Neo-Hookean.

Replacing Eq. 1.24 by Eq. 1.62,

$$W = \frac{1}{2} G\left(I_1 - 3\right) \qquad \textit{Eq. 1.64}$$

Deviations from the theory are apparent, especially in uniaxial extension, where, at low strains (below about 50%), the measured modulus is too high in relation to its value at moderate strains (up to 400%). At even higher strains, a rapidly rising modulus is seen, which is also not predicted by the theory presumably due to the finite extensibility of the chains.

Phenomenological theory of rubber-like elasticity.— Before the deviations of the statistical theory, a general treatment of the stress-strain relation of rubberlike solids, that began with *Mooney* [23] and was further developed by *Rivlin* [24], shown from the concept of an ideal elastic solid, assuming that the material is only isotropic in elastic behaviour in the un-strain state; no volume change occurs on deformation (the energy cannot be dissipated). Its mechanical behaviour may be described by means of an ESED function or Helmoltz free energy of deformation per unit volume of material referred to the undeformed state, which is a single-valued function of the state of deformation. Based on the symmetry considerations, appropriate measures of strain - regardless the choice of axes - are given by three strain invariants I_1, I_2, and I_3, $W = W(I_1, I_2, I_3)$.

When the material is unstrained, I_1, I_2 and I_3 take the values 3, 3 and 1 respectively. It can be shown that if the linear stress-strain relations of classical elasticity are to be applied for a sufficiently small deformation of the material,

W can be approximated with any desired degree of accuracy by a power series in $I_1 - 3$, $I_2 - 3$ and $I_3 - 1$. Thus, we may write:

$$W = \sum_{i+j+k=1}^{\infty} C_{ijk} (I_1 - 3)^i (I_2 - 3)^j (I_3 - 1)^k \qquad \textit{Eq. 1.65}$$

For an incompressible material where $I_3=1$, the coefficient $C_{00}=0$ since the undeformed state is considered to be that in which the strain energy is zero. So the function is simplified; consequently:

$$W = \sum_{i+j=1}^{\infty} C_{ij} (I_1 - 3)^i (I_2 - 3)^j \qquad \textit{Eq. 1.66}$$

Mooney [23] developed the first phenomenological theory in 1940 prior to the development of the statistical theory:

$$W = C_{10}(I_1 - 3) + C_{01}(I_2 - 3) \qquad \textit{Eq. 1.67}$$

Typically this expression and other similar stored energy functions were written in terms of the three strain invariants. The initial value of the Young modulus and the shear modulus can be calculated:

$$E_0 = 6\left(C_{10} + C_{01}\right) \qquad \textit{Eq. 1.68}$$

$$G_0 = \frac{E_0}{3} \qquad \textit{Eq. 1.69}$$

The Mooney ESED contained two elastic constants C_{10} and C_{01} Eq. 1.67 and was simplified by the Neo-Hookean, as given in Eq. 1.70, when $C_{10}=G/2$ and $C_{01}=0$ or in terms of the strain invariants as

$$W = C_{10}\left(I_1 - 3\right) \qquad \textit{Eq. 1.70}$$

This model lies in the fact that the statistical theory of rubber elasticity arrives at the same strain energy function Eq. 1.64. (*Treloar* [20]) and *Yeoh* [25] showed that only a small strain range could be fitted to a carbon black filled elastomer. The Mooney expression appears to be unsuitable for modelling the behaviour of filled elastomers. It has also been pointed by *Charlton and Yang* [9] that the Mooney constants determined from tensile data are inadequate to predict the behaviour in other modes of deformation.

Tschoegl [26] suggested that the failure of the Mooney-Rivlin equations arises from not taking enough terms of the Rivlin series Eq. 1.66. *James and Green* [27] fitted test data to highly carbon black filled elastomers with various high order expansions of the Rivlin series. They reported that a third order deformation expansion with 5 terms, Eq. 1.71, gave better predictions beyond the range of the input data than the expansion of a higher order or of a higher number of terms:

$$\begin{aligned} W &= C_{10}(I_1 - 3) + C_{01}(I_1 - 3) + C_{20}(I_1 - 3)^2 \\ &+ C_{11}(I_1 - 3)(I_2 - 3) + C_{30}(I_1 - 3)^3 \end{aligned} \qquad \textit{Eq. 1.71}$$

Gregory [28] noted that a simple relationship existed between stress/strain data obtained in uniaxial tension, uniaxial compression and simple shear. Other empirical relationships for *W* have been developed by *Varga, Ogden, Valanis-Landel* [29–31]. These diverge from the Rivlin type of relationship in that some discard the principle that the strain invariants I_1 and I_2 are even-powered functions of the extension ratios and some are written in terms of strains or extension ratios rather than in terms of strain invariants. Based on extension ratios, *Ogden* [30] proposed the next relation for incompressible elastomers,

$$W = \sum_{n=1}^{N} \frac{\mu_n}{\alpha_n} \left(\lambda_1^{\alpha_n} + \lambda_2^{\alpha_n} + \lambda_3^{\alpha_n} - 3 \right) \qquad \textit{Eq. 1.72}$$

where μ_n are constants and the α_n are not necessarily integers, and may be either positive or negative. This representation includes the statistical theory $(\alpha_1 = 2)$ and the Mooney equation $(\alpha_1 = 2, \alpha_2 = -2)$ as special cases. *Ogden* [30] showed that a three-term expression is required to represent tension, pure shear and equi-biaxial extension for an unfilled elastomer, containing six adjustable parameters. The degree of agreement with the experiment is quite satisfactory for unfilled elastomers. Ogden's formulation has the merit to be mathematically simple, although the magnitudes of a large number of independent constants have to be determined- since all the terms in the equation have an identical form. According to *Sawyers and Rivlin* [32] the Ogden model is a special case of the Rivlin ESED and *Treloar* [20] affirmed that the two formulations are equivalent. In the same way, *Valanis-Landel* [31] proposed the next relation based in extension ratios,

$$W = 2G_0 \sum_{i=1,3} \left(\lambda_i \left(\ln \lambda_i - 1 \right) \right) \qquad \textit{Eq. 1.73}$$

Gent [33] developed a function that describes reasonably the whole range of strains especially the large strain behaviour with the upturn in the stress-strain behaviour that is due to the finite extensibility of the chains. It would give some confidence in the use of a model if the parameters had some molecular/physical significance. In this respect, the function may be written as:

$$W = -C_{10} (I_m - 3) \ln \left[1 - \frac{(I_1 - 3)}{(I_m - 3)} \right] \qquad \textit{Eq. 1.74}$$

where I_m is the limiting value of I_1 corresponding to the deformation when the network is fully stretched.

The previous relation could be written as:

$$W = -\frac{E}{6} J_m Ln\left[1 - \frac{(I_1 - 3)}{J_m}\right] \qquad \textit{Eq. 1.75}$$

E and J_m are physical constants: E is the small strain tensile or Young modulus and J_m denotes a maximum value for $(I_1 - 3)$. At small strains, this equation reduces to Eq. 1.60 from the statistical theory where C_{10} is equal to the shear modulus G or NkT. This ESED function is claimed to have the advantage that it reduces the description of the stress-strain behaviour of an elastomer to two parameters having a clear physical meaning.

The general observation that can be made for unfilled materials is that $\partial W/\partial I_1 >> \partial W/\partial I_2$ and the examination of data published by *Fukahori and Seki* [34] also supports the contention that for filled elastomers $\partial W/\partial I_2$ by comparison with $\partial W/\partial I_1$ was numerically close to zero. If it could be assumed that $\partial W/\partial I_2$ was equal to zero, then the difficulties of measuring the relationships for I_2 could be ignored, and filled elastomer characterisation would be significantly simplified. This approach was originally suggested by *Gregory* [28] who observed, on the basis of measurements of the stress-strain behaviour of carbon filled natural-rubber elastomers, that a simple relationship existed between shear, tension and compression data for a number of different compounds. *Davies et al* [35] confirmed this observation with carbon black filled materials. The observation on filled materials showed that the mechanical behaviour, that could be described using the first strain invariant, could only be true if $\partial W/\partial I_1$ was independent of I_2 and if the magnitude of $\partial W/\partial I_1$ was significantly greater than $\partial W/\partial I_2$. From this consideration, the review shows that there is no unique solution. The choice of a function will depend on the particular situation. The first one will generally need to be accurate at small and moderate strains (<100%) unlike the second one which would be required to predict moderate and large strains accurately.

Yeoh [25], using the work of *Gregory* [28], proposed to take only the first three terms of the Rivlin series to obtain the following cubic function for filled elastomers:

$$W = C_{10}(I_1 - 3) + C_{20}(I_1 - 3)^2 + C_{30}(I_1 - 3)^3 \qquad \textit{Eq. 1.76}$$

This approach predicted the stress strain behaviour of filled elastomers well at large strain. The use of this function has been shown to permit the prediction of stress/strain behaviour in different deformation modes from data obtained in one simple deformation mode. But this leads to unstable functions predicting physically unrealistic behaviour under conditions outside the range of the experimental data. The initial value of the Young modulus and the shear modulus can be calculated as follows:

$$E_0 = 6C_{10} \qquad \textit{Eq. 1.77}$$

$$G_0 = 2C_{10} \qquad \textit{Eq. 1.78}$$

Yeoh's model [25] reported good ability to predict multi-axial data, including comparison with the published biaxial data of *James and Green* [27] for filled elastomers. Conceptually, this proposed function is a model with a shear modulus varying as a second-degree polynomial in $I_1 - 3$. The variation of the shear modulus in the case of carbon black elastomers is a fall of the modulus with increasing strain and arise at large deformations due to finite extensibility. This characteristic behaviour can be modelled if C_{20} is negative while C_{10} and C_{30} are positive.

Additional experimental evidence and those recent works by *Othman and Gregory* [36], *Davies et al* [35], *Gregory et al* [37], *Yeoh and Fleming* [38] have also suggested that it is appropriate and more reliable to make the ESED a function of I_1 for filled materials. Any inaccuracy resulting from making these

simplifying assumptions may not be too severe a limitation, as elastomers are only imperfectly elastic.

In the same way, another ESED function based on the previous consideration was developed by *Arruda-Boyce* [39]:

$$W = G_0 \sum_{i=1}^{5} \frac{C_i}{\lambda_m^{2i-2}} \left(I_1^i - 3^i \right) \qquad \textit{Eq. 1.79}$$

G_0 and λ_m are material parameters which represent the initial shear modulus and the locking stretch at which the strain/stress curve of the model stiffens significantly respectively. This function is also called the eight-chain model because it was developed based on a representative brick element where eight chains emanate from the centre of the cube to each corner. The values of C_i arise from statistical treatment of non-Gaussian Chains:

$$C_1 = \frac{1}{2} \ , \ C_2 = \frac{1}{20} , C_3 = \frac{11}{1050} , C_4 = \frac{19}{7000} , C_5 = \frac{519}{673750} \qquad \textit{Eq. 1.80}$$

Mullins effect and Phenomenological hyperelasticity.—

The ESED functions consider the energy cannot be dissipated (section 1.2.2). Two of the earlier constitutive models that account for softening have been developed by *Simo* [40] and *Godvinjee and Simo* [41] although these models are not generally available in finite element codes.

The problem described above is compounded as the hysteresis loop changes systematically on each cycle due to stress softening. *Hawkes et al* [42] have attempted to solve this problem by mathematically representing the stress-softening phenomenon with a strain energy function of the following form:

$$W_n = f(n) \ \ W_1 \qquad \textit{Eq. 1.81}$$

where W_1 and W_n are the ESED functions on the first and n^{th} number of cycles, and $f(n)$ is a decreasing function of n. This model developed for a constant maximum cyclic strain condition is obviously limited to this particular test condition and cannot be applied as a general case. In a general situation, the strain energy function depends not only on the previous number of cycles that the specimen has endured but also on the whole strain amplitude history.

Ogden and Roxburgh [43] proposed a pseudo elastic mathematical approximation which allows the prediction of the decrease in material stiffness modifying the initial value given by hyperelastic ESED material models. The model is a maximum load modification to the nearly and fully-incompressible hyperelastic constitutive models already available. In this model, the virgin material is modelled using one of the available hyperelastic potentials, and the Mullins effect modifications to the constitutive response are proportional to the maximum load in the material history. The Ogden-Roxburgh's model results in a scaled stress given by

$$S_{ij} = \eta S_{ij}^{0} \qquad \textit{Eq. 1.82}$$

where η is a damage variable which is defined as follows:

$$\eta = 1 - \frac{1}{r} erf\left[\frac{1}{m} W_m - W_0\right] \qquad \textit{Eq. 1.83}$$

where W_m is the maximum previous strain energy and W_0 is the strain energy for the hyperelastic material.

Some earlier models were proposed e.g. *Miehe* [44] and *Miehe and Keck* [45]. Newer proposal is implemented in *ANSYS software* [15]: The modified Ogden-Roxburgh pseudo-elastic model results in a scaled stress given by

$$\eta = 1 - \frac{1}{r} erf\left[\frac{W_m - W_0}{m + \beta W_m}\right] \qquad \textit{Eq. 1.84}$$

The modified Ogden-Roxburgh damage function requires and enforces the three damage material constants *r, m*, and β.

The material constants are selected to ensure $\eta\epsilon(0,1]$ over the range of application. This condition is guaranteed for $r > 0$, m > 0, and $\beta \geq 0$; however, it is also guaranteed by the less stringent bounds $r > 0$, $m > 0$, and $(m + \beta W_m) > 0$. The latter bounds are solution-dependent, so you must ensure that the limits for η are not violated if $\beta < 0$.

1.2.2 Hysteresis. Energy dissipation of strained/cycled elastomers: Mullins, Payne and crystallization effects

When an elastomer is tested, some energy is dissipated as heat. Such energy dissipation occurs due to various causes explained below:

Carbon black.— Carbon black fillers are added to rubber to increase stiffness, abrasion resistance, tear strength, and fatigue life. The mentioned fillers used in most rubber compounds have a noticeable influence in their mechanical properties as energy dissipation. The types of filler-rubber interactions are both physical and chemical, ranging from weak Van Der Waal forces to strong covalent linkages. *Hamed and Hatfield* [46] mentioned the number of each kind of the latter mentioned interactions is unknown.

Medalia et al [47–49] explained that carbon black consists of aggregates which are formed by fusion of particles in the flame. The aggregate is composed by spheroidal particles and these particles do not have an independent existence in carbon black. The aggregate is the smallest dispersible entity. The aggregates are associated into agglomerates held together by Van Der Waals bonds and a network, which can be completely separated into the constituent aggregates by a deformation of the rubber compound. In rubber, the void spaces within the aggregates are filled with rubber. This occluded rubber is partly shielded from deformation and thus acts as part of the filler rather than as part of the matrix. Rubber molecules interact with carbon black by physical absorption and by chemisorptions on active sites.

When an elastomeric material is strained, part of the applied energy is dissipated in overcoming viscous resistance to motion of the molecular chains

(viscoelastic behaviour) and in breaking or modifying the structure associated with the molecular or filler network. In unfilled vulcanized elastomers, the dissipation mechanisms associated with the molecular structure, mainly viscoelastic losses are not generally significant in terms of the deviation from elastic behaviour. In the case of filled elastomers, these dissipations are much more pronounced because the carbon black causes a large increase in the viscosity due to hydrodynamic effects (displacement of large particles through the elastomer matrix). The breakdown and the reformation of carbon particle aggregates are also believed to be one of the causes of the increased energy dissipation.

Mullins Effect or irreversible stress-softening.— When an elastomer is cyclically deformed, the stress-softening produced is known as the “Mullins Effect”. It was apparently first studied in detail by *Holt* [50] and later by *Mullins* [51], *Bueche* [52], *Hardwood et al* [53], *Hardwood and Payne* [54] (Figure 1.7). This stress-softening is irreversible at room temperature and occurs in filled and unfilled rubber-like materials and it is produced by the breaking of cross-links within the rubber network. The greatest softening occurs during the first cycle, but the effect continues at a decreasing rate in subsequent cycles. The softening due to the Mullins effect increases progressively with the increasing deformation and the number of loading and unloading cycles, which are the main causes of the filler-filler and rubber-filler de-adhesion.

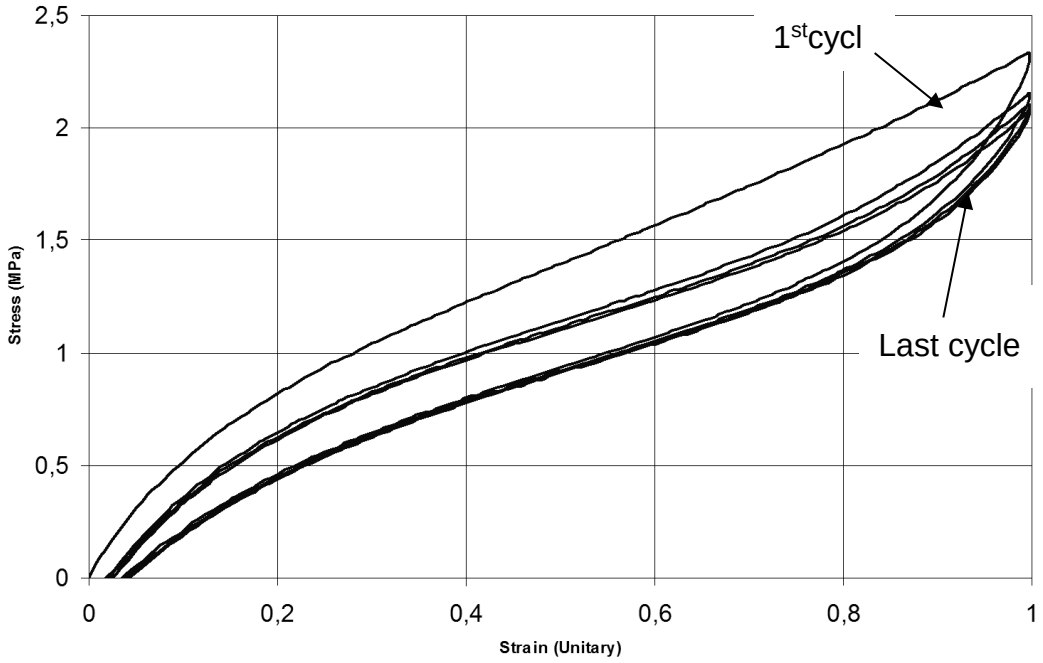

Figure 1.7: Mullins effect: The greatest softening occurs during the first cycle

The Mullins effect is a phenomenon typically observed in compliant filled polymers. It is characterised by a decrease in material stiffness during loading and it is readily observed during cyclic loading as the material response along the unloading path differs noticeably from the response that is along the loading path (Figure 1.7).

The various explanations suggested for the Mullins effect show that there is still no general agreement on the origin of this effect at the microscopic or mesoscopic scales. This behaviour was attributed to the de-bonding of the polymer from the filler particles, the molecular slippage, destruction-reformation of a filler network, and disentanglement of the rubber chains. Some theories of the possible physical explanation of the Mullins effect are reviewed in the next lines:

a) Rubber-filler interface bond rupture:

Bueche [52]: When a rubber part is stretched in horizontal direction, the filler particles must separate. With a very low stretch, the union between filler particles and rubber-chain C might rupture. Hence, if the rubber is allowed to retract to its initial value and is re-stretched, it will be softer, since the chains

which broke are no longer a resisting deformation. After breaking, a chain makes no further contribution to the stiffness and the softening effect results from this chain breakdown (Figure 1.8).

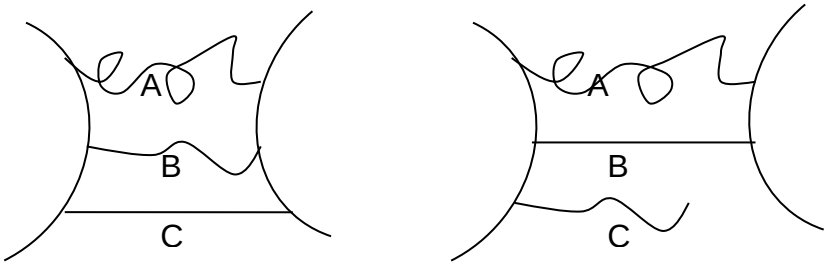

a) b)

Figure 1.8: Three molecular rubber-chains attached to two filler particles are represented. a) Un-stretched state: The adhesion between Chain C and the aggregates might break with a very low stretching cycle. The needed stretch to break the adhesions between filler particles and the rubber chains B and C will be greater respectively. b) Stretched state: the adhesion between Chain C and one of the carbon black particles is broken, and Chain A & B are stretched.

b) Molecules slipping: adsorption-desorption of polymeric chains at the filler interface

Howkink [55] proposed that molecules slip over the surface of the fillers and new bonds are instantaneously created along the chains. The new bonds would be of the same physical nature as the original ones, but would appear at different places along the rubber molecules (Figure 1.9).

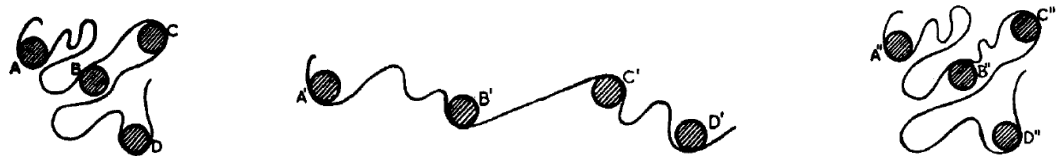

A)Original state B)Stretched C)After release of the stress

Figure 1.9: A molecular rubber-chain attached to some filler particles is represented. A) Un-stretched state. B) Stretched state: Molecules slip over the surface of the fillers. C) After release of the stress: carbon black particles as a rubber molecule, try to return to their initial possition.

c) The destruction-reformation of a filler network:

Kraus et al [56] proposed to attribute the main source of the stress-softening to the rupture of carbon-black structure or agglomerate, especially for highly reinforced materials (Figure 1.10)

A) B)

Figure 1.10: A carbon-black chain or agglomerate is represented. A) Un-stretched state B) Stretched state: The carbon-black agglomerate composed by several spherical aggregates, is broken down into two smaller agglomerates.

d) Disentanglement of the rubber chains

Hammed and Hatfield [46] proposed the other consideration. The removal of chain entanglements between particles associated with the strain axis may cause the stress-softening. The number of active chains is assumed to remain constant; only the entanglement density changes with respect to the extension.

A) B)

Figure 1.11: A) Un-stretched state B) Stretched state: a chain entanglement is removed

Mullins [51] explained that in filled rubber compounds, pronounced softening occurs due to a breakdown of aggregates of filler particles. This breakdown is essentially complete at very small deformations (strains up to about 0.1%)) and at larger deformations, softening due to this cause is relatively small. At intermediate and larger deformations, in both, unfilled and filled vulcanizates, most of the softening appears to be due to configurational changes of the rubber-molecular network due to non-affine, displacement of network junctions and entanglements during deformation and incomplete subsequent recovery to their original positions.

Reversibility of deformed rubber.—

Complete recovery in rubber vulcanizates reflects that no structural breakdown has occurred during deformation and thus, in these cases, the softening is due solely to a change in the configuration of the molecular network; this involves a rearrangement or displacement of the network junctions.

In some materials, appreciable residual deformation or set may be present after removal of the stress. This incomplete recovery associated with set reflects not only a breakdown of network junctions but also some reformation in the deformed state. Rupture of network chains connecting filler particles is an irreversible effect and would be expected to depend on the temperature and rate of pre-stressing. Any linkages broken and reformed while the rubber is deformed also contribute to softening and incomplete recovery after deformation. Recovery is normally much slower and less complete due to filler agglomerates and to filler aggregates attached to rubber-molecular network and displaced during deformation, hindering and limiting return to original equilibrium positions *Harwood and Payne* [54]. Hence, this incomplete recovery may derive from viscous flow in a network that is not crosslinked or from the rearrangement of a network formed by weak crosslinks or molecular entanglements. The softening recovers slowly on standing, but may be accelerated and made more complete by an increase in temperature.

Payne effect.—

The Payne effect appears when rubber parts are loaded cyclically at different load amplitudes where the magnitude of the dynamic stiffness of a rubber unit decreases as the excitation amplitude increases. In addition, the loss modulus plotted over amplitude shows a maximum where the storage modulus drops more rapidly. Several researchers review extensively the dynamic properties and the amplitude dependence of carbon black filled rubbers better explained in section 1.3.3, e.g., *Medalia* [47,49], *Harris and Stevenson* [57] and *Rendek and Lion* [58].

Strain-softening of the glassy polymer shell surrounding the particles surfaces

Another molecular mechanism responsible for the non-elastic behaviour, in the form of an increased high strain hysteresis, is strain-induced crystallisation which occurs particularly in natural rubber. At large extensions, the elastomer chains orientate and align resulting in the formation of crystallites. This crystallisation is an additional energy dissipation process which is observed as a more pronounced upturn in the stress-strain curve at large strains when compared with that of a non-strain crystallising elastomer.

1.2.3 Static mechanical properties characterisation: Uniaxial and shear strain states

When the mechanical properties of an elastomer compound have to be characterised, some experimental tests are required. This section presents the standard specimens used in the mechanical properties characterisation. The materials are characterised in simple strain states by standard specimens designed for this purpose.

Once the material behaviour is characterised experimentally in simple strain states, later on, the prediction of deformed geometries with complex strain states can be performed by the use of Commercial finite element method software such as Ansys or Abaqus. These types of software have implemented algorithms to fit the experimental curves of simple strain states to standard ESED functions reviewed in section 1.2.1.

The usually characterised strain states are the uniaxial tension or equibiaxial compression, the uniaxial compression or equibiaxial tension, the planar tension (pure shear) or planar compression and simple shear. With the addition of the hydrostatic stress, some of the previously mentioned strain states can be related to each other as it is shown in Figure 1.12

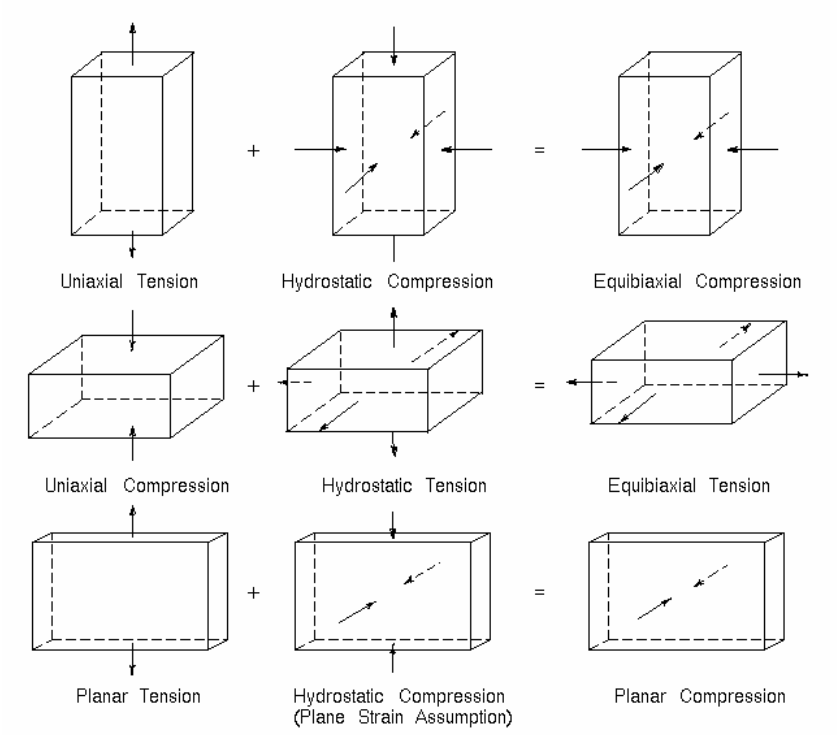

Figure 1.12: Uniaxial, equibiaxial and planar tension equivalences.

The most popular tests, because of their testing simplicity, are the tensile [59–61] (Figure 1.13-A) and compression [62–64] (Figure 1.13-B) tests which describe the uniaxial state and the shear planar test for the shear strain state (Figure 1.13-C). There are some drawbacks that make other tests difficult to perform: firstly, the equibiaxial testing device fabrication and maintenance (Figure 1.13-D); secondly, the bonding needed between the testing plates and the rubber in simple shear [65,66] (Figure 1.14); and lastly, because of the bulging (edge effects) of the rubber disc that indicates a non-uniform strain state (the surfaces of the rubber part in contact with the plates have to be correctly lubricated and the selection of the lubricant has to be carefully made). This latter effect is explained in section 3.1.2.1.

What is explained above does not imply that the rejection of one or two of the previously mentioned tests is unfeasible. In some cases, for some

mathematical models, it is possible to carry out the characterisation only with one type of the test samples [25].

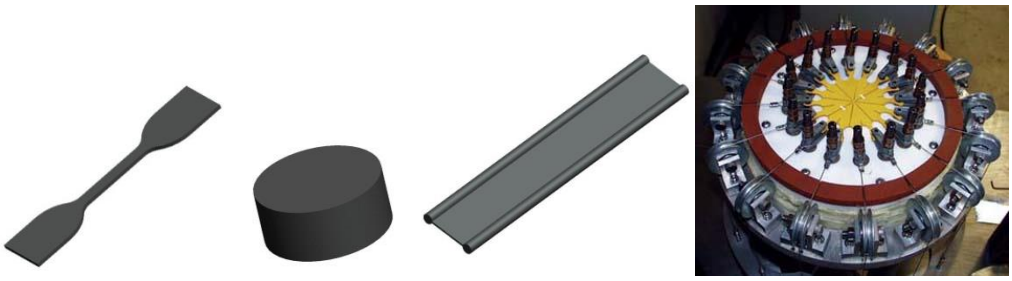

A) B) C) D)

Figure 1.13: A) *Tensile, B) compression, C) pure shear and D) equi-biaxial characterisation samples*

Figure 1.14: Simple shear characterisation sample

1.3 Literature review. Part 3. Dynamic behaviour of elastomers

1.3.1 Contribution of time in the stiffness relaxation of elastomers under constant load.

In this section the stress relaxation is studied. The stress relaxation is the variation of the stress with time, in response to an applied constant deformation ε_0, all at a constant temperature. The load acting on the body is decreasing gradually since the stress decays exponentially with a characteristic time constant. Once the material is relaxed, the stress is not zero and the long term modulus is E_∞ (Figure 1.15).

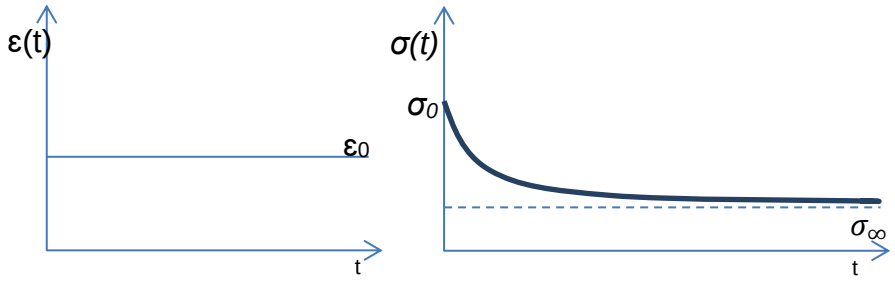

Figure 1.15: Stress relaxation curves. The testing sample is deformed and this deformation is maintained constant during the test. The maximum stress value is reached at time t_0 and it decreases gradually.

Unfilled elastomers.— The mechanical behaviour of this type of rubbers can be assumed as viscoelastic behaviour, and then, their behaviour can be reproduced by linear viscoelastic constitutive models. The mentioned models assume that the relaxation rate is proportional to the instantaneous stress σ_0 and that all the curves, for different values of applied strain (and instantaneous stress), are proportional (Figure 1.16).

When an unfilled rubber is cycled, such viscoelastic models consider that the hysteresis loop during cyclic deformation remains elliptic. They do not take into account the dependence of the material on the strain amplitude that is imposed. Hence, the viscoelastic models fit well the mechanical properties of unfilled rubbers but do not characterise correctly the filled rubbers properties.

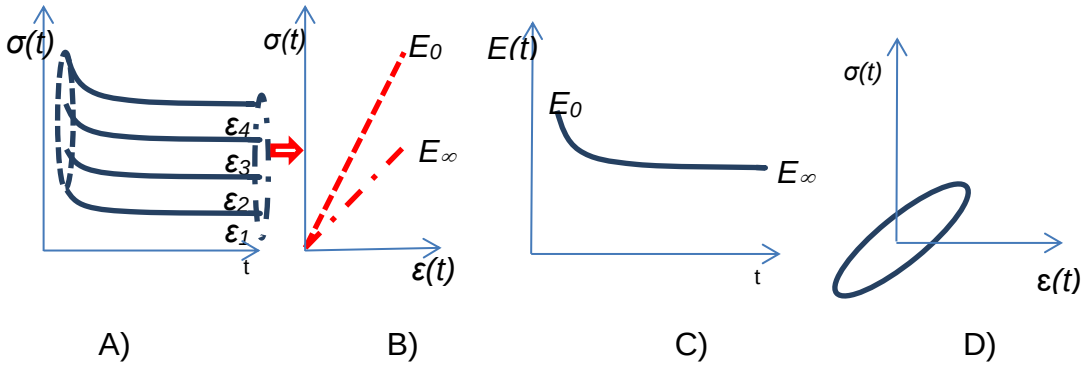

Figure 1.16: Stress relaxation: Linear viscoelasticity. A) Four stress relaxation tests done with four preloads are represented from ε_1 to ε_4. B) The modulus E depends only on the testing time (t). C) The modulus E does not depend on the preload and it is the same for all preloaded tests. Hence, the initial stress σ_0 and every $\sigma(t)$ are proportional to the applied deformation load ε_i. C) In a load cycle, the hysteresis loop is elliptical.

Filled elastomers.— In case of filled rubbers, the relaxation rate is not proportional to the stress and the different curves are not proportional to each other. Hence, the dynamic behaviour of filled elastomers cannot be characterised by classical viscoelasticity. In addition, when highly filled elastomers are cycled at large amplitudes and low frequencies, the hysteretic response diverges considerably from the elliptic shape shown in viscoelastic or unfilled materials. Stress in the filler phase and in the rubber-filler interfaces is responsible for the rate-independent contribution as observed in Figure 1.17.

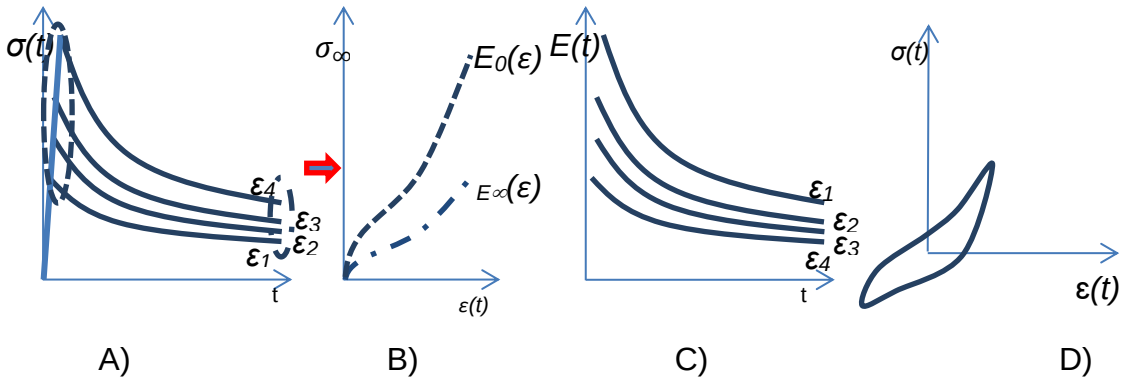

Figure 1.17: Nonlinear viscoelasticity. A) Four stress relaxation tests done with four preloads are represented from ε_1 to ε_4. B) The modulus E depends on the testing time (t) and on the load strain (ε_i). C) The modulus E depends on the strain load (ε_i). Hence, the initial stress σ_0 and every $\sigma(t)$ are not proportional and depend on the applied deformation load ε_i. C) The hysteresis loop is nonlinear.

1.3.2 Dynamic properties of unfilled elastomers: linear viscoelastic materials in cycled loads.

Dynamic mechanical properties refer generally to responses periodically varying strain or stresses. They are usually simply defined as a small sinusoidally varying strain or stress, for which the response is a small sinusoidally varying stress or strain, respectively, with the same frequency but generally out of phase. Then, the strain always lags slightly behind the stress (Figure 1.18). This phase shift between stress and strain exists because that part of the energy input is not recovered at the end of the cycle. Some of the energy input is stored and recovered in each cycle and some is dissipated as heat. Materials whose behaviour exhibits such characteristics are called viscoelastic. The phase angle is a measure of the damping, and thus, also a measure of hysteresis.

The mathematical approximations studied in this section are based on the linear viscoelastic theory.

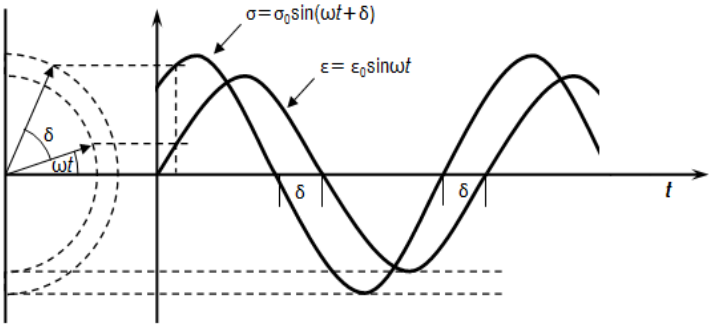

Figure 1.18: Phase shift between stress and strain.

If no damping is present in the system, the modulus is real but it becomes complex when damping exists as in the case of elastomers.

When a sample is subjected to oscillatory deformations, the strain varies sinusoidally with time as:

$$\varepsilon = \varepsilon_0 sin\omega t \qquad \textit{Eq. 1.85}$$

where ε_0 is the strain amplitude, ω the angular frequency (2π times the frequency in Hertz), and t the time. The stress σ will also oscillate sinusoidally with the angular frequency ω as illustrated in Figure 1.18

$$\sigma = \sigma_0 \sin(\omega t + \delta) \qquad \textit{Eq. 1.86}$$

where δ is the phase lag.

If Eq. 1.86 is expanded, it can be rewritten as:

$$\sigma = \sigma_0 \sin \omega t cos\delta + \sigma_0 \cos \omega t sin\delta \qquad \textit{Eq. 1.87}$$

From the last expression Eq. 1.87, the stress can be considered consisting of two components (Figure 1.19):

a) $\sigma_0 cos\delta$: in phase with the strain, proportional to $sin\omega t$

b) $\sigma_0 sin\delta$: 90º out of phase with the strain, proportional to $cos\omega t$

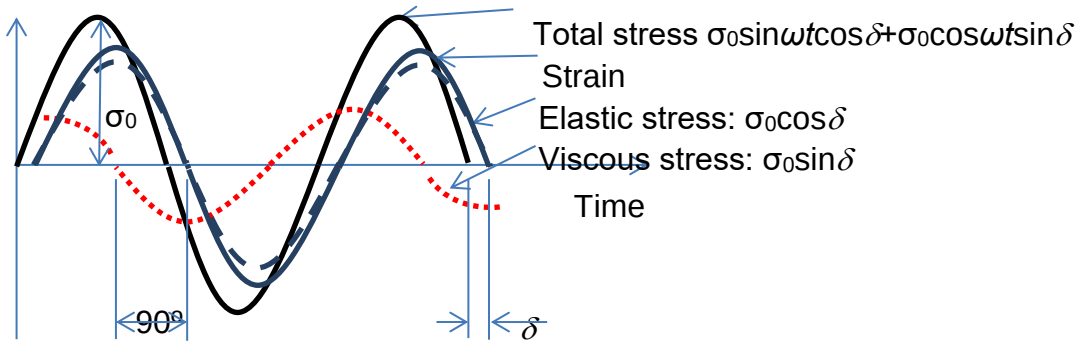

Figure 1.19: Stress components representation

Rewriting Eq. 1.87,

$$\sigma = \varepsilon_0 \, \mathrm{E}' \sin \omega t + \varepsilon_0 \, \mathrm{E}'' \cos \omega t \qquad \textit{Eq. 1.88}$$

The dynamic properties can be decomposed in storage modulus *E'* and loss modulus *E"* or equivalently, as complex modulus E* and phase angle δ (see Figure 1.20).

$$E' = \frac{\sigma_0}{\varepsilon_0} cos\delta \qquad \textit{Eq. 1.89}$$

$$E'' = \frac{\sigma_0}{\varepsilon_0} sin\delta \qquad \textit{Eq. 1.90}$$

$$E^* = \sqrt{E'^2 + E''^2} = \frac{\sigma_0}{\varepsilon_0} \qquad \textit{Eq. 1.91}$$

And the phase lag,

$$tan\delta = E''/E' \qquad \textit{Eq. 1.92}$$

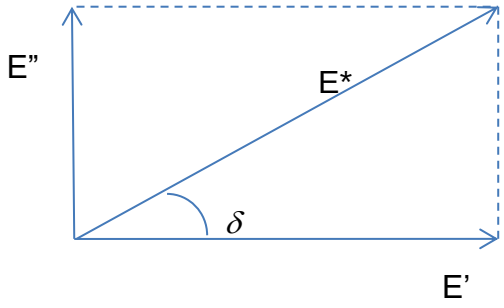

Figure 1.20: Phasor diagram

According to Eq. 1.91, the dynamic modulus is the ratio of the peak values of stress σ_0 and strain ε_0 even though these values are taken at different times. In fact, if strain and stress cycles are sinusoidal, the slope of the long axis is defined as the complex modulus E^* (Figure 1.21) and the hysteresis area takes the form of an elliptical loop. The elliptic hysteresis loop is associated with the dissipated energy.

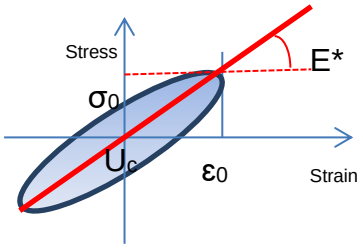

Figure 1.21: Linear viscoelastic hysteresis loop for harmonic excitation. Linear behaviour

The E' is the real part of the complex modulus (Figure 1.20). It is known as storage modulus because it defines the energy stored in the sample produced by the load strain. Likewise, E'' is the imaginary part of the complex modulus E^*. It is called loss modulus since it describes the dissipation of energy, which is evident when calculating the energy dissipated per cycle U_c (Annex II-C);

$$U_c = \frac{\varpi \varepsilon_0^{\,2}}{2} E'' \frac{2\pi}{\omega} \qquad \textit{Eq. 1.93}$$

$$U_c = \pi E'' \varepsilon_0^{\,2} \qquad \textit{Eq. 1.94}$$

This energy is represented by the area of elliptic hysteresis loop (Figure 1.21).

If the integral of U_c is evaluated for a quarter of a cycle, instead of the entire cycle, the first term gives the maximum stored elastic energy (W_c).

$$W_c = \frac{1}{2} E' \varepsilon_0^{\,2} \qquad \textit{Eq. 1.95}$$

If Eq. 1.89 is replaced in Eq. 1.95,

$$W_c = \frac{1}{2} \sigma_0 \varepsilon_0 \cos\delta \qquad \textit{Eq. 1.96}$$

where W_c is the maximum stored elastic energy, which is independent from the frequency.

From these energy expressions, we can deduce that:

$$E' = \frac{2W_c}{\varepsilon_0^{\,2}} \qquad \textit{Eq. 1.97}$$

$$E'' = \frac{U_c}{\pi \varepsilon_0^{\,2}} \qquad \textit{Eq. 1.98}$$

As it is explained above, the damping is the energy loss per cycle and it is compared to some values of potential energy stored in the component during the same cycle. However, there are numerous definitions of this energy based on the assumption of linear behaviour of rubber material.

Nashif et al [67] describes the loss factor as follows:

$$\eta = \frac{E''}{E'} = tg\delta = \frac{U_c}{2\pi W_c} \qquad \textit{Eq. 1.99}$$

Olsson and Austrell [68] or *Sjöberg and Kari* [69] applied another definition of damping which is obtained as the quotient between the energy lost per cycle U_c and a simplified potential energy multiplied by π:

$$D = \frac{U_c}{\pi \sigma_0 \varepsilon_0} \qquad \textit{Eq. 1.100}$$

Furthermore, this energy loss can be defined as [70]:

$$C = E^* \sin\delta / \omega \qquad \textit{Eq. 1.101}$$

$$C = \frac{\sigma_0}{\omega \varepsilon_0} \sin\delta \qquad \textit{Eq. 1.102}$$

Finally, the next ratio is called specific loss:

$$\frac{U_c}{W_c} = 2\pi tg\delta \qquad \textit{Eq. 1.103}$$

1.3.3 Dynamic properties of filled elastomers: non-linear viscoelastic materials in cycled loads.

Dynamic properties of filled/nonlinear elastomers in cyclic loading.- When the system is nonlinear, the hysteresis loop mentioned in the previous section 1.3.2, distorts and becomes parallel shaped (Figure 1.22). The dynamic behaviour of filled elastomers is not linear and this effect is observed in the hysteresis loop. These nonlinearities are produced because of the nonlinear elasticity of rubber and the filler structure breakdown and reforming. This filler structure modification produces a decrease of the dynamic modulus induced by the amplitude increasing.

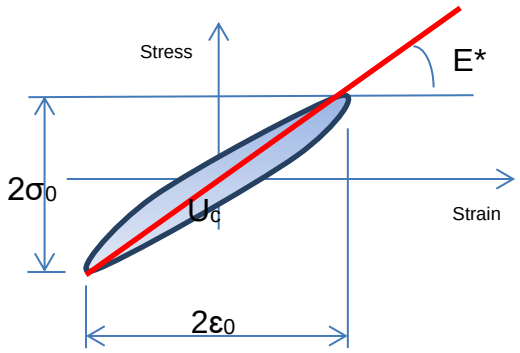

Figure 1.22: General hysteresis loop for harmonic excitation. Nonlinear behaviour

Strain amplitude dependence on the dynamic modulus: Payne effect.—

Strain amplitude dependence on the dynamic modulus has been thoroughly studied in the last years. Two phenomena are responsible for the stiffness dependence on the amplitude: on the one hand the well-known Mullins effect [50–53,55,56] which is related to the stress-softening produced when an elastomer is cyclically deformed as shown in Figure 1.7. On the other hand, the Payne effect. The term “Mullins softening” is sometimes used interchangeably with the Payne effect, but the former is a different phenomenon that occurs at larger strains. To investigate the Payne effect without the influence of the Mullins effect, all specimens are preconditioned with sufficient large strain amplitude so that the Mullins-effect is eliminated.

One of the earliest studies of this phenomenon was made by *Fletcher and Gent* [71] (afterwards called Payne effect [72–77]) who extended the studies of the mentioned effect. When a constant strain load at constant frequency is applied cyclically, the modulus decreases with increasing strain amplitude for a wide range of filler types and concentrations.

The investigations made by *Payne* [73] concluded that the elastomer modulus declines, increasing strain amplitude as a result of the breaking of the filler structure. As the molecular structure is composed of aggregates held together by Van Der Waals bonds, the modulus is almost recoverable due to the permanent breaking and recombination of the mentioned weak bonds in the filler network. *Huber et al* [78] described that the rate of these breaking and recombination processes generally differs but, under stationary conditions, they are equal and depend on the dynamic deformation amplitude. In Figure 1.23-A and Figure 1.23-B, where the dynamic mechanical properties are plotted as the storage *E'* and loss modulus *E"* respectively, it is observed that *E"* takes a maximum value in the strain range corresponding to the maximum rate of change of the storage modulus with amplitude.

At small amplitudes of oscillation, a small structure is broken down; the storage modulus *E',* which is large due to the filler structure, is not modified. Hence, *E"* is small even though the reformation of the structure is probably easier at these small separations of the black particles. At large amplitudes, the structure is so extensively broken down that the reformation of the structure is very much slower than the cycle time and *E"* is again low. A maximum in *E"* and phase angle are expected somewhere in the middle strain region where considerable structure breakdown occurs, but where reformation is also easier and faster. Consequently, the decrease in dynamic modulus *E** and increase in loss factor $tan\delta$ are not maintained in all range of amplitudes. At large amplitudes, the change in dynamic modulus *E** is softer than in intermediate ones as shown in Figure 1.23-C. The loss factor (Figure 1.23-D) shows a peak in the region where *E** decreases more markedly as shown for example by *Lindley* [79], *Payne and Whittaker* [76] and *Rendek and Lion* [58]. Theoretically, there is a critical amplitude where, bellow it, the storage *E'* and loss modulus *E"* do not change due to the amplitude variation.

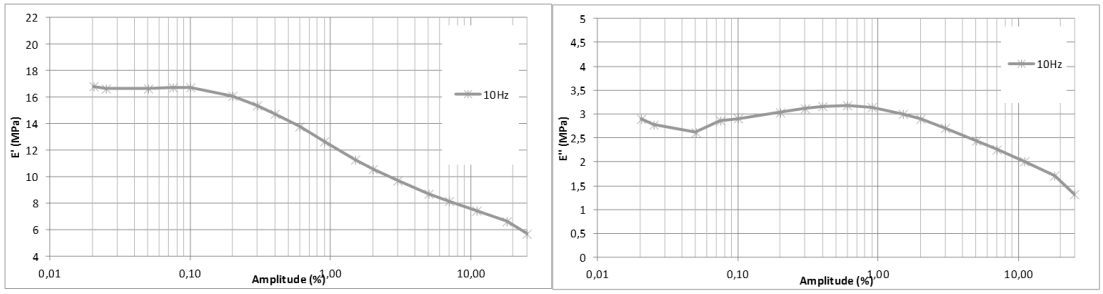

A) B)

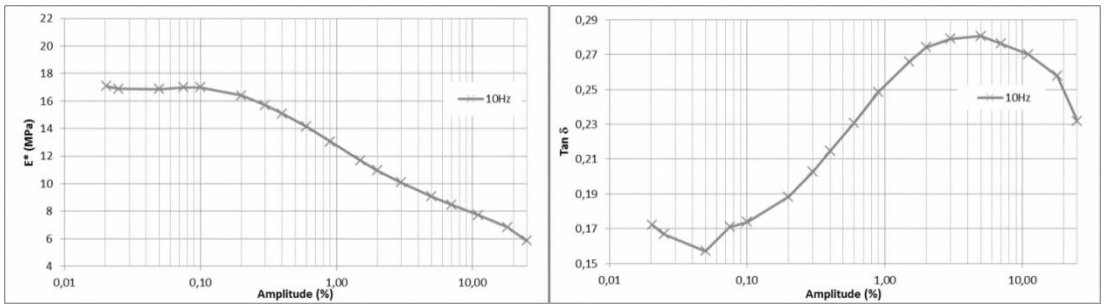

C) D)

Figure 1.23: Amplitude sweep test. Testing frequency: 10 Hz. Figures A, B, C and D are the storage E', loss E" and complex E modulus respectively and D is the tan δ (Figure reproduced from Rendek and Lion [58])*

Effect of fillers.— Carbon black fillers are added to rubber in order to increase both the dynamic modulus *E** and the phase angle δ (and hence the damping) of rubber. Consequently, these dynamic properties become amplitude-dependent. The magnitude of the mentioned dynamic properties depends on the type and the amount of filler.

In Figure 1.24, the variation of the dynamic properties of vulcanizates A to E over the normal operating range of shear strain is shown. The rubbers are all of approximately the same hardness (about 55 IRHD). This was accomplished using three different types of carbon-black, balancing the reinforcing effect and adding high-viscosity aromatic oil. *Harris and Stevenson* [57] who made experimental investigations of several nonlinear aspects of the dynamic behaviour of, especially, filled rubbers, which shows that the modulus increases, was greater at small amplitudes, particularly for vulcanizates with high proportions of filler.

Medalia's [47,49] work shows that the dynamic properties represent the viscoelastic properties of vulcanizates at deformations below about 25%, after reaching a pseudo-equilibrium state. The level and the variation of the damping through the strain range increased with enhancing the filler content. The filler agglomerate, which is broken down on cycling above a certain strain range, may reform, leading to a reduction in modulus and to a peak in damping. This material behaviour, even in shear, is clearly nonlinear [57]. *Fletcher and Gent* [71], *Lindley* [79] and more recently *Rendek and Lion* [58] carried out some experimental tests to study the amount of filler influence on the mentioned dynamic properties, which show again a stronger dependence on filled elastomers than on unfilled ones as it is observed in Figure 1.24.

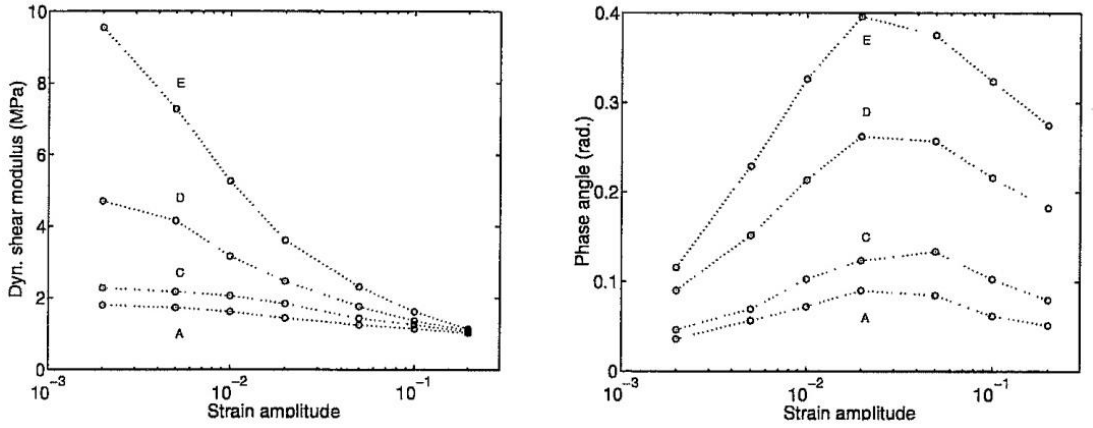

Figure 1.24: Amplitude dependence of dynamic shear modulus and phase angle for some filled natural rubbers of various filler contents (Reproduced from Harris and Stevenson [57]). From A to E, different compounds are represented, the amount of carbon-black being higher in E than in A). From C to E, they have the same type of filler.

Wang [80,81] carried out experimental investigations to show the impact of the filler network, both its strength and architecture on the dynamic modulus and its hysteresis during the dynamic straining. It was found that the filler network can substantially increase the effective volume of the filler due to the rubber trapped in the agglomerates, leading to high elastic modulus (Figure 1.25-B). During the cyclic straining, while the stable filler network can reduce the hysteresis of the filled rubber, the breakdown and reformation of the filler network would cause an additional energy dissipation resulting in the higher

hysteresis. The experiments were done at double strain amplitudes ranging from 0.2% to 120% with a constant frequency of 10Hz under constant temperatures of 0 and 70ºC and filler phr of 0 and 70.

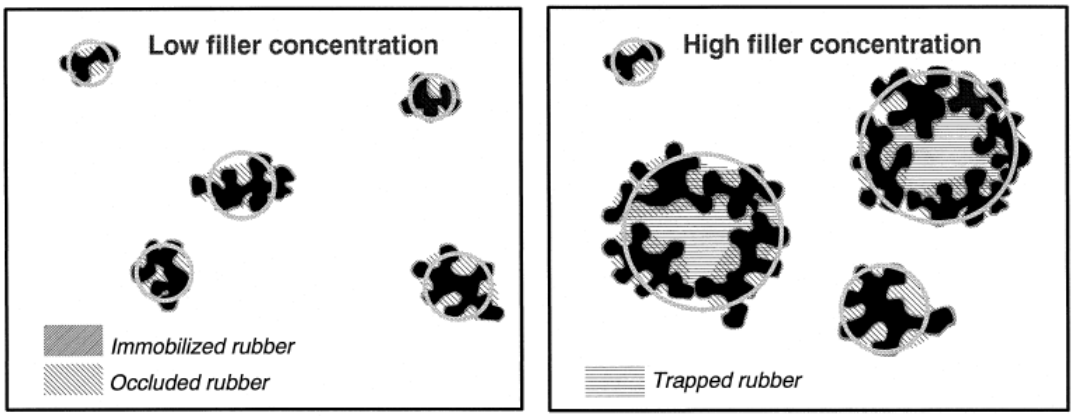

A) B)

Figure 1.25: A) Low filler concentration: Immobilized and occluded rubber representation around filler agglomerates. B) High filler concentration: Trapped rubber representation into filler agglomerates (Figure taken from Wang [81]).

Payne effect and the augmentation of the elastic modulus.— The augmentation of the elastic modulus at low amplitudes has been explained by *Payne* [73,76] or *Mullins and Tobin* [82] as being due to a network structure modification of carbon black particles (known as aggregates in *Medalia's* [47] studies). From Payne's viewpoint, the particles or aggregates are associated in agglomerate groups which, when deformed, are broken into smaller agglomerates of different dimensions. The particles or aggregates are fused carbon entities and are associated by the Van Der Waals or other secondary attractive forces into agglomerates (known as well as aggregates network).

At small deformations, the elastic modulus is higher because the carbon-black agglomerates, which are the "hardest" regions, are not broken. These agglomerates or "hard regions" must immobilize some rubber in addition to the occluded one within the aggregates (see Figure 1.25-A); thus, they cause an augmentation of the effective volume fraction beyond that limit, which is due to the aggregates themselves. In addition, as the effective volume fraction of the filler increases, the agglomerates ability to move into the matrix is diminished;

hence, elastic modulus increases. Both effects become more important as the amplitude is diminished or as the frequency is increased.

As the deformation is increased, the agglomerates are broken into smaller agglomerates. Therefore, the elastic modulus decreases because there are more mobile units or “soft” regions into the rubber matrix. At high deformations, the carbon-black agglomerates break down until the aggregates themselves are mobile units. The augmentation effect is of minor practical importance in well-dispersed formulation batches.

The agglomerates present at intermediate amplitudes may be identified with the “hard” regions. The breaking of the structure is often described as a frictional behaviour, which is an energy dissipation mechanism. Hence, the loss factor of the elastomer increases, as *Medalia* show in [49].

Reversibility.— In recent literature [83], it has been shown that the dynamic moduli of rubber are not only a function of the current deformation amplitude: they also depend on the history of deformation. Based on comprehensive experiments with sinusoidal excitations with changing amplitudes, *Wang et al* [84] demonstrated that the dynamic moduli of filled rubber exhibit a pronounced recovery behaviour, which can be interpreted as a thixotropic effect.

If firstly small dynamic strain amplitude is applied, followed by a larger one and finally the small amplitude again, different numerical values of dynamic moduli belonging to the same strain amplitude are observed. The small amplitude storage and loss modulus observed directly after switching from the large to the small amplitude is smaller than their values prior to the large amplitude cycles. But they show pronounced recovery behaviour and reach their original values after several minutes or a few hours. Experiments of this type can be found, for instance in [85].

The stress response attributed to the Mullins effect shows a similar behaviour but the recovery times are longer [83]. When an elastomer is tested with increasing and decreasing amplitude sweeps driven in series in the first decreasing amplitude sweep, a softening is observed. This softening is related

to the Mullis effect and it is irreversible. In the followings up and down amplitude sweeps, the material is pre-conditioned; so the Mullins effect is eliminated. Hence, the next up and down sweeps demonstrates the reversibility of the rubber compound, where the stiffness does not change (Figure 1.26).

From Figure 1.26, another conclusion can be deduced: The Payne's effect is reversible because the second and subsequent amplitude sweeps give the same result.

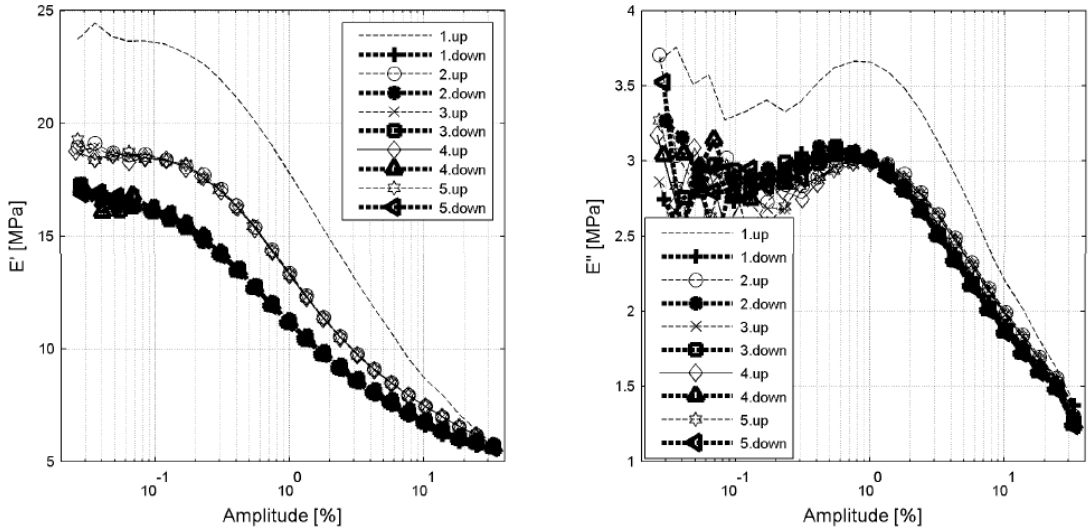

Figure 1.26: Reversibility of the Payne effect. Thin lines belong to increasing or up-amplitude sweeps (dynamic amplitude increases) and fat lines to decreasing or down-amplitude sweeps (dynamic amplitude decreases). (Figure taken from Rendek and Lion [58])

<u>Pre-load in harmonic tests</u>.—

To study the dynamic behaviour of a rubber part, sinusoidally varying strain or stress harmonic tests are commonly used. The rate of the dynamic load can be defined as both unique frequency as frequency range. Generally, this type of tests consists of an initial static pre-stress of the testing specimen continuing with a dynamically applied sinusoidally varying strain or stress. In addition, it is common to perform amplitude/frequency sweeps, increasing them in linear steps where the other parameter (frequency/amplitude) is maintained constant.

When an elastomer part is tested in dynamic sinusoidal experiments, the dynamic modulus is larger than the static modulus of the preload (Figure 1.27).

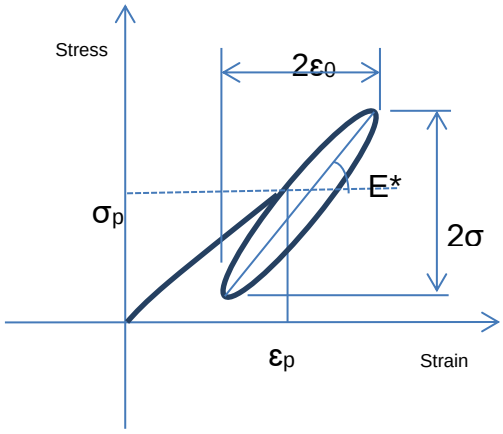

Figure 1.27: Static pre-load and dynamically applied load

$$E^* = \frac{\sigma_0}{\varepsilon_0} \qquad \textit{Eq. 1.104}$$

$$E = \frac{\sigma_p}{\varepsilon_p} \qquad \textit{Eq. 1.105}$$

where σ_p and ε_p are the stress and strain captured in the pre-load static test and σ_0 and ε_0 are the stress and strain captured in the harmonic test.

The dynamic properties of rubber change with the influence of pre-strain, amplitude, frequency and temperature. The temperature increasing has a stress softening effect and the increasing of frequency has a stress stiffening effect.

The dynamic modulus *E** increases and the phase angle or loss factor decreases as preload is increased, as shown in works of *Nashif et al* [67], *Rendek and Lion* [58] and [86] (Figure 1.28). *Rendek and Lion* [58] carried out different static pre-strain to continue with the same amplitude-sweep tests. They observed that the pre-strain does not have any influence in the material stiffening in the full strain range of amplitudes when this pre-strain is smaller than 60%.

For preloads higher than the latter percentage, the influence in the material stiffening is considerable, which increments the storage *E'* and loss *E"* modulus. The loss modulus is less sensitive to changes in the preload which is responsible for the loss factor decreases. The observed dependence on the pre-strain can be explained by the progressive hyperelastic behaviour of elastomers (Figure 1.29).

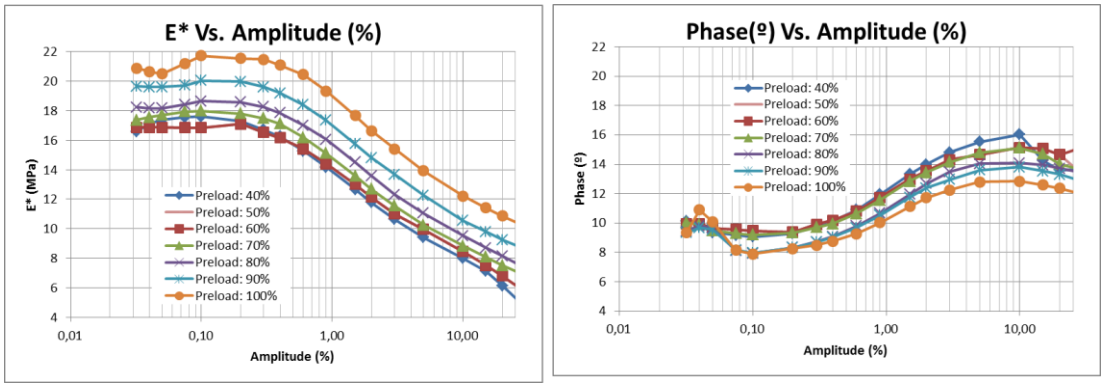

Figure 1.28: Influence of the preload and later cyclic amplitude in elastomers dynamic properties. Left graph: Complex or dynamic modulus E. Right graph: phase angle δ (Figure reproduced from [58]).*

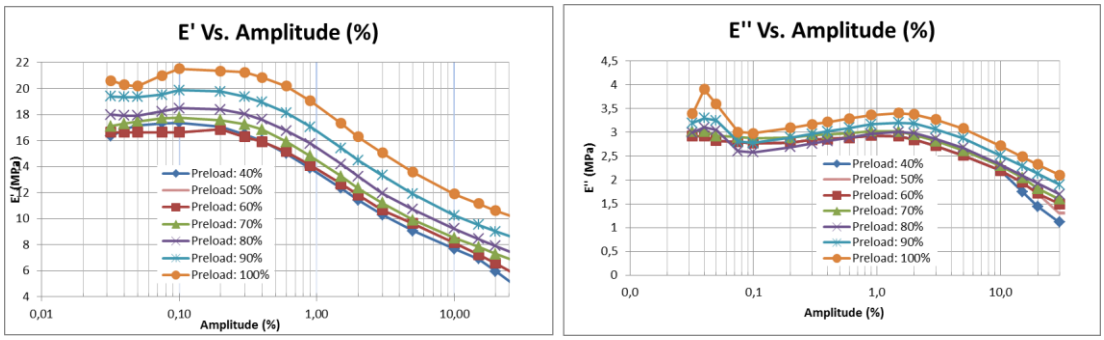

Figure 1.29: Influence of the preload and later cyclic amplitude in elastomers dynamic properties. Left graph: Storage modulus E'. Right graph: Loss modulus E" . (Figure reproduced from [58]).

Frequency or strain rate dependence in harmonic tests.—

The dynamic stiffness *E** of elastomeric materials increases as frequency is increased. This stiffening effect is due to the possible configurational changes of the polymer molecules within the rubber compound matrix are reduced when

the frequency is increased. Hence the expected storage modulus is greater if the frequency is increased [76,77,87].

The storage *E'* and loss modulus *E"* exhibit pronounced frequency dependences (Figure 1.30-A and B). The unfilled elastomer shows much weaker frequency dependence than filled elastomers. As filler content increases, the stiffening of the storage modulus *E'* and loss modulus *E"* are greater as frequency increases. The effect of the filler amount in both moduli in a frequency range is more detailed in the experimental work in section 4.2

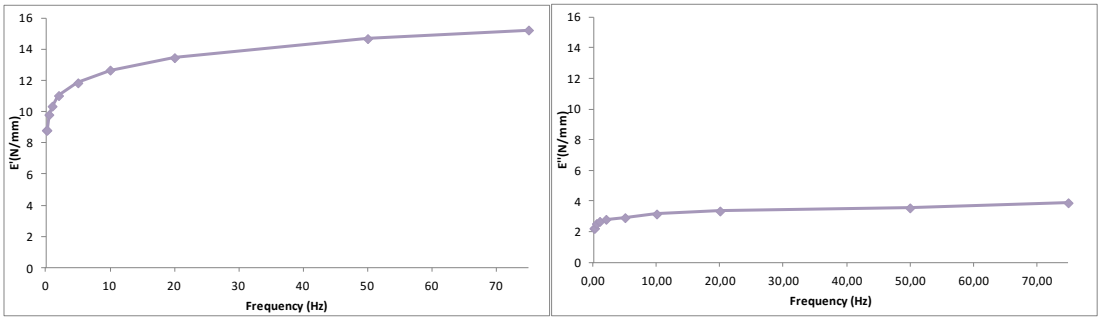

A B

Figure 1.30: Influence of the frequency in the material stiffening. A) Storage modulus E' vs. frequency. B) Loss modulus E'' vs. frequency.

In dynamic characterisations, when the specimen is tested in harmonic frequency sweeps, the material needs a certain time to achieve a stationary or constant value of its dynamic modulus when the frequency/strain-amplitude has changed. It is called micro-structural relaxation time or cyclic relaxation time (CSR) [88].

Stress stiffening due to frequency at small amplitudes.—

The Payne effect explained before describes why the dynamic stiffness of elastomers is higher when the amplitude is smaller. In addition, filled elastomers stiffen more markedly when frequency is increased. The slope of the frequency sweep is more pronounced when the strain amplitude is smaller (see Figure 1.31-A,C and Figure 1.32). This effect can be produced because the elastomer behaviour is more a composite behaviour at small amplitudes than at higher amplitudes; as the bonds between aggregates and the elastomer matrix are broken, its behaviour is more similar to an unfilled

elastomer. As the molecular structure is composed of aggregates held together by Van Der Waals bonds, the modulus is almost recoverable upon return to small amplitudes. It implies that the filler structure largely reforms for an amplitude cycle. For small amplitudes, the dynamic modulus, which is large due to the filler structure, is not modified. This effect is studied more thoroughly in the experimental work in section 4.2.

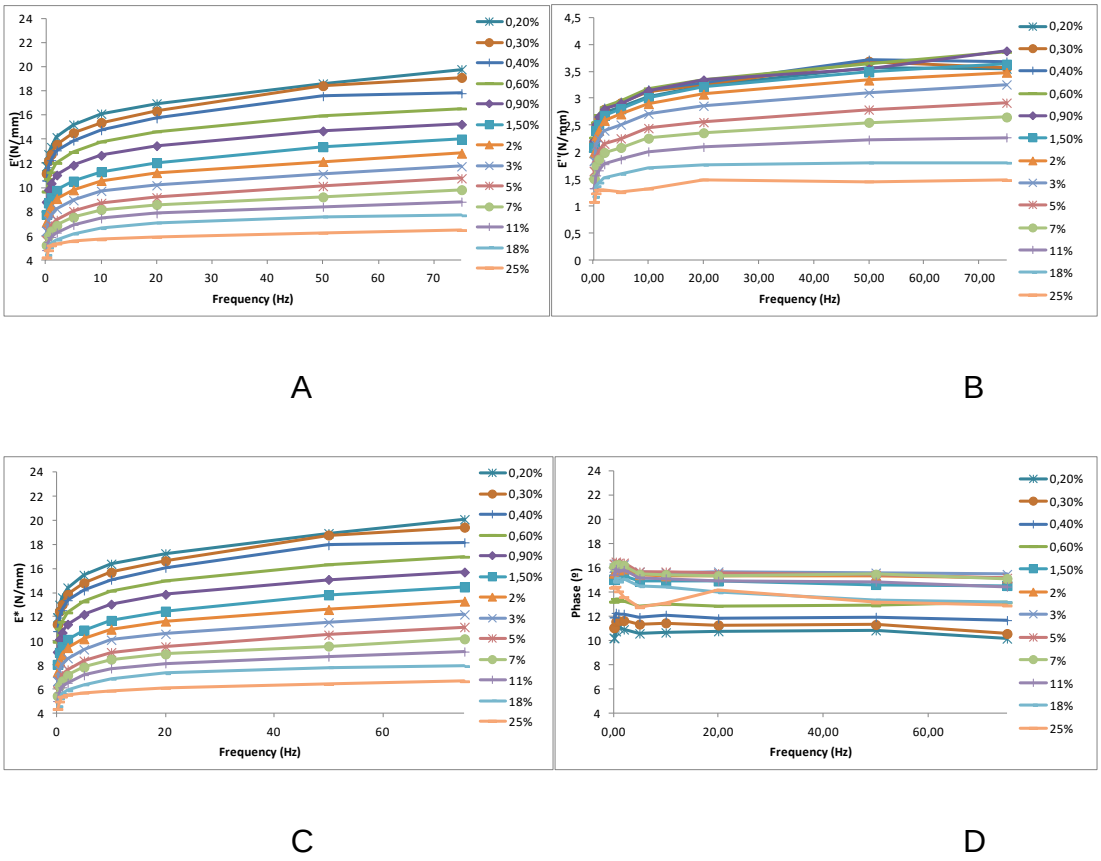

Figure 1.31: Frequency sweeps with different double strain amplitudes. Figures A, B, C and D are the storage, loss and complex modulus respectively and D is the phase angle (Figures calculated from Rendek and Lion [58])

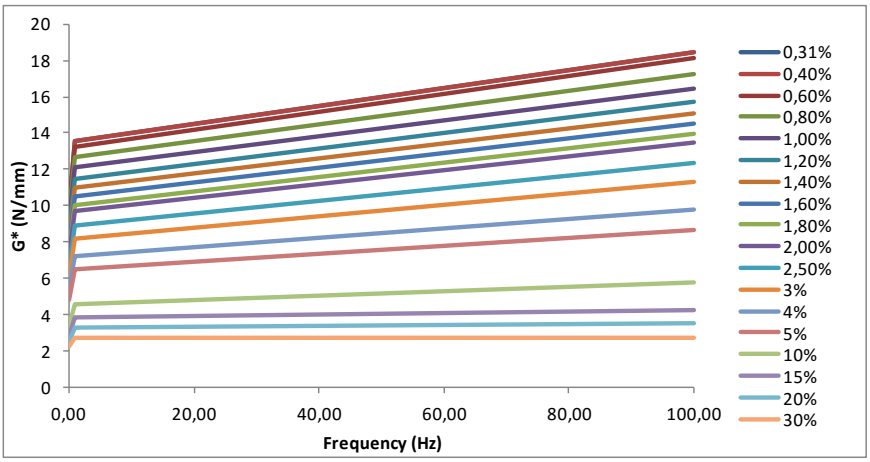

Figure 1.32: Influence of the frequency in the material stiffening. 18 frequency sweeps are presented. Each frequency sweep between 0.01-100 Hz is done at changing the peak to peak amplitude (Figure calculated from results taken from [89])

1.3.4 Frequency-temperature correspondence

Dynamic properties of rubber are dependent on frequency, amplitude and temperature, which can be observed in the dynamic modulus and damping results. This dependency exists due to the reorganization of the rubber network during the dynamic test.

Ward [7]: There is a certain relationship between frequency and temperature in dynamic viscoelastic measurements. This relationship is based on a Boltzmann Superposition Principle or “time-temperature superposition”. Hence, it is possible to convert temperature changes into frequency changes to study the frequency dependency of viscoelastic properties at a given temperature. Consequently, it is possible to predict viscoelastic properties over a wide frequency range at an arbitrary temperature.

Ferry [90] (WLF) carried out several studies based on the principle of “time-temperature superposition” related to the amount of horizontal shift and temperature. They found an empirical equation associated to the latter principle. The equation can be used to fit (regress) discrete values of the shift factor a_T vs. temperature T. When this *WLF* Eq. 1.106 is defined, it is used to estimate the temperature shift factor for temperatures not tested. Hence, the master curve can be applied to other temperatures. For a given reference temperature T_r, this equation determines the amount of horizontal shift a_T, for data measured at T_r, and T. This horizontal shift quantity is called the “shift factor”,

$$log(a_T) = \frac{-C_1(T - T_r)}{[C_2 + (T - T_r)]} \qquad Eq.\ 1.106$$

where T_r is the reference temperature chosen to construct the master curve and C_1, C_2 are empirical constants adjusted to fit the values of shift factor a_T.

For the construction of the master curve, it is necessary to make several dynamic tests. These tests consist of multiple frequency sweeps at different temperatures (i.e. Figure 1.33).

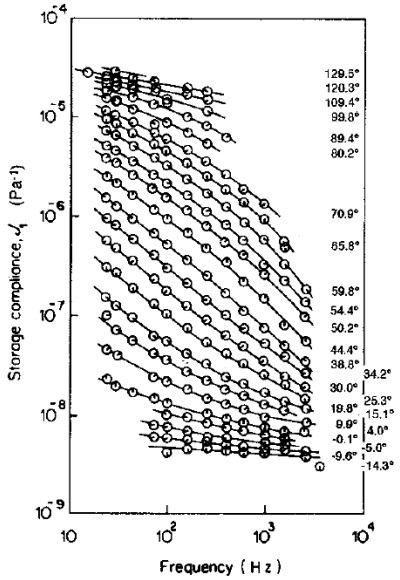

Figure 1.33: Master curve of a polymer in the glass transition region plotted against frequency at 24 temperatures. (Figure taken from Ferry [90])

Having data above T_g, it is possible to predict the behaviour (compliance, storage modulus, etc.) of viscoelastic materials for temperatures $T>T_g$, and/or for times/frequencies longer/slower than the time available for experimentation. With the master curve and associated *WLF* equation, it is possible to predict the mechanical properties of the polymer out of time scale of the machine, thus extrapolating the results of multi-frequency analysis to a broader range, out of measurement range (Figure 1.34).

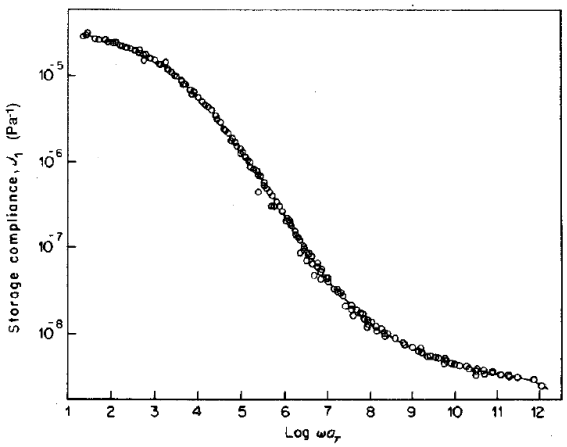

Figure 1.34: Application of suitable shift factors to the data of Figure 1.33. The storage compliance is predicted over a wide frequency range at an arbitrary temperature. (Figure taken from Ferry [90]).

The horizontal shift on a logarithmic time-scale is shown in Figure 1.34. *WLF* [91] found an approximately identical shift factor-temperature relation for all amorphous polymers. For most elastomers, C_1 and C_2 assume the following values: C_1=8.86 and C_2=101.6 [49,92].

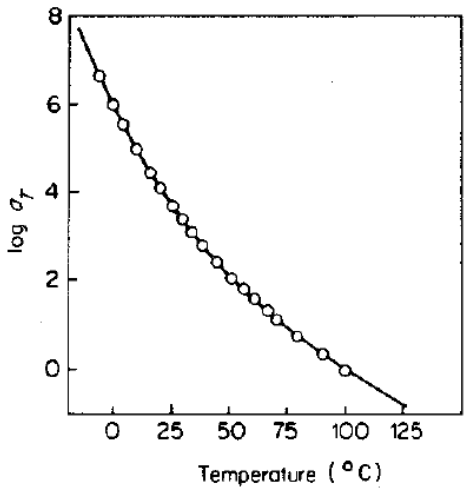

Figure 1.35: Representation of the WLF equation. Temperature dependence of the shift factor at used in plotting Figure 1.34. (Figure taken from Ferry [90] Ch.11)

When the selected T_r is the glass transition T_g, this *WLF* equation holds only in the temperature range between the glass transition T_g and a temperature 100ºC higher than that temperature. Moreover, if T_r is in the range of temperature of transition or rubbery region (Figure 1.35), this equation applies over a temperature range T_r±50ºC.

When the rubber part is working above the glassy region or glass transition temperature (T_g), the constants are positive. However, when the constants are obtained with data at temperatures below T_g, negative values of C_1, C_2 are obtained.

1.3.5 Amplitude-temperature correspondence

Rendek and Lion [58]: As it is shown in Figure 1.36, the Payne-effect depends strongly on the temperature. The amplitude dependence is more pronounced at lower temperatures than at higher ones.

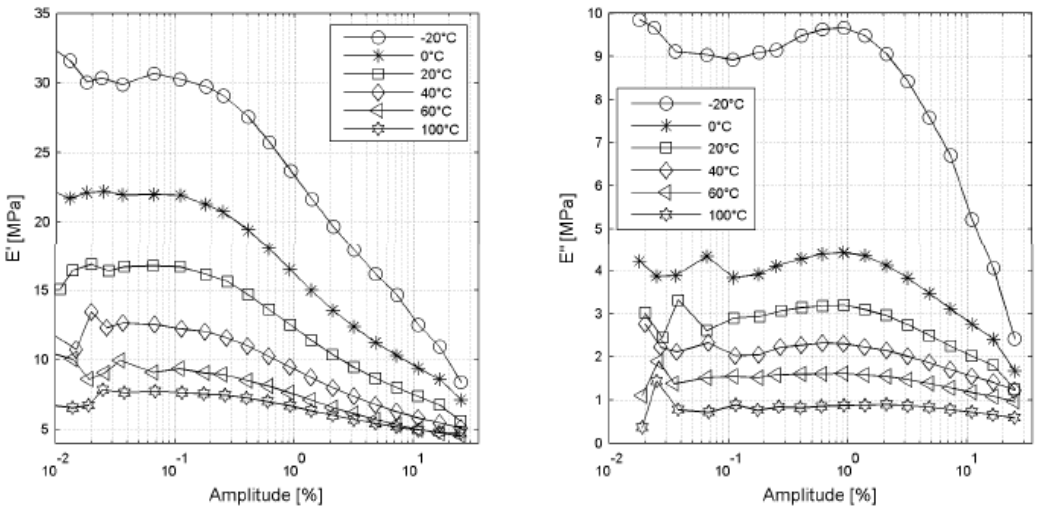

Figure 1.36: Amplitude-temperature correspondence at 10Hz (Figure taken from [58])

Miller and Warnaka [93] demonstrated the applicability of shifting techniques to the strain-frequency and strain-temperature relationships which have shown good correlation with the experiments.

1.4 Literature review. Part 4. Dynamic modelling of elastomers

As seen in section 1.3.2, when a rubber part is subjected to a sinusoidal deformation, the resulting stress does not have to be in phase with the said load deformation (as it would be for perfect elastic solids). However, this response is not 90 degrees out of phase (as in the case of perfectly viscous liquid). This delay in the response is somewhere in between. As mentioned in that section, it is considered that the dynamic behaviour of rubber is viscoelastic. On the contrary to what happens in linear elastic materials, viscoelastic material depends on the complete history of deformation. Several approaches to the analytical modelling of the rheological behaviour of a linear viscoelastic system are available in the literature. A classical approach uses a mechanical model comprising a combination of linear springs and dashpots. Viscoelastic models consider that the hysteresis loop during a cyclic deformation remains elliptic. These models do not take into account the dependence of the material on the strain amplitude imposed. These considerations are correct in the case of unfilled rubbers (proportionality in the relaxation rate and between different pre-strained curves Figure 1.16), but it is not correct for filled rubbers (where both proportionalities do not happen in such types of elastomers Figure 1.17).

In order to develop a model with a reasonable behaviour for a wide range of frequencies, there are two different ways to go. On the one hand the use of the hereditary or convolution integrals (section 1.4.1.1). This method consists of a series of Maxwell elements in parallel, resulting in Prony series. The wider frequency range supposes the need to use more Maxwell elements with a consequent increase in material constants. This thesis is focused on this method. On the other hand the use of Fractional derivatives (section 1.4.1.2). The last method is more recent than the first one, its main advantage being the reduction in a number of material constants.

Several approaches have been presented in the literature. The first approaches, which the authors call's triboelastic models, omit the frequency-dependence on mechanical properties in the theory of rate-independent plasticity *Coveney and Johnson* [94,95]. These triboelastic models were

modified to take into account the rate-dependency of elastomers *Coveney and Johnson* [96]. Other models are based on the phenomenological theory of viscoelasticity, e.g. [97–99].

The first model giving a qualitative and quantitative interpretation of the Payne effect (reviewed in section 1.3.3) on a physical level is the so-called Kraus model. In brief, it characterises the amplitude dependence of the dynamic moduli under periodic loads. It has been discussed in detail, e.g. in *Ulmer* [100]**.** He assumed that physical Van der Waals contacts between neighbouring aggregates are continuously broken and restored under periodic loads. Under the assumption of a constant strain amplitude $\Delta\varepsilon$, frequency and temperature, the microstructure of the material tends to a stationary state which is characterised by a constant number of aggregate constants. To represent the amplitude dependence of the dynamic moduli, the stationary number of constants is nonlinear function of $\Delta\varepsilon$. The so-called Kraus model is specified by Eq. 1.107 and Eq. 1.108 and describes the experimentally observed dependence of the storage modulus G' and the dissipation or loss modulus G'' on $\Delta\varepsilon$, i.e. the monotonic decrease of G' and sigmoidal behaviour of G'' [72].

$$G' = G'_\infty + \frac{G'_0 - G'_\infty}{1 + (\frac{\Delta\varepsilon}{\Delta\varepsilon_c})^{2m}} \qquad \textit{Eq. 1.107}$$

$$G'' = G''_\infty + \frac{2(G''_m - G''_\infty)(\frac{\Delta\varepsilon}{\Delta\varepsilon_c})^{m}}{1 + (\frac{\Delta\varepsilon}{\Delta\varepsilon_c})^{2m}} \qquad \textit{Eq. 1.108}$$

The material constant $\Delta\varepsilon_c$ is the strain amplitude belonging to the maximum G_m'' of the loss modulus; G_∞' and G_∞'' are the asymptotic values of G' and G'' for large $\Delta\varepsilon$; G_0' is the value of storage modulus for small amplitudes, and m is a phenomenological exponent.

Kraus [101] model specified by Eq. 1.107 and Eq. 1.108 is a very successful method of representing the behaviour of the dynamic moduli perceived during

experiments at a constant frequency. Nevertheless, some more or less small modifications are necessary and have been proposed by *Ulmer* [100]. Although the model is appropriate to represent the material amplitude dependence, the whole set of material parameters has to be determined again if the frequency changes. In addition, this model cannot be used for calculations in the time domain under arbitrary loading histories. For this purpose, *Lion* [102] developed a new model based on the previously mentioned models. *Lion* [102] assumes that the amplitude dependent parts of storage and dissipation modulus are not independent of each other, as frequently assumed. This model [102] is able to represent the frequency dependence of the material parameters of $G'(\Delta\varepsilon)$ and $G''(\Delta\varepsilon)$ models developed by *Kraus* [101] and improved by *Ulmer* [100]. However, the identification of the parameters is complicated. *Lion et al* [72] developed a 6 parameters model based on the theory of linear viscoelasticity. Since the linear viscoelasticity is unable to describe any kind of amplitude dependence, they introduce a non-linearity into the model. For this purpose, he uses fractional derivatives. This model is formulated in the time domain. It can relate the stress to any strain history (arbitrary function of time) and it is not restricted to the steady-state response to a deformation that varies sinusoidally with time (frequency domain theory). The frequency is between 10 and 60 Hz and the strain amplitude between 0.1 and 5%. Although the model describes the general trend of amplitude and frequency dependence, the loss modulus is weakly underestimated. New models are proposed, e.g. *Lion* [83], *Höfer* [89]. *Rendek and Lion* proposed three more models which take into account the initial static pre-deformation [58,103,104]. The last mentioned researchers implemented successfully a subroutine in a finite elements software ANSYS, which could simulate the mechanical properties of three dimensional industrial parts under dynamic loadings.

In the other way, the dynamic properties of elastomers are often characterised by mathematical schematization, which allows the physical behaviour of the material to be analytically simulated. This is achieved by defining models, also known as rheological models, which can be structured in such a way that they reproduce the response of the material to any kind of excitation. In particular, by means of different ways of assembling spring, viscous damping and

Coulomb friction sliding elements connected in series or in parallel. Several researchers use three types of the mentioned elements to represent the dynamic behaviour of elastomers. The first type of element contemplates the completely relaxed stiffness of the elastomer (generally modelled by a linear or nonlinear spring); the second type characterises the amplitude dependence of the elastomer (normally modelled by elastoplastic elements) and lastly, the third type of element which characterises the rate or frequency dependent behaviour of elastomers (viscoelastic models).

Berg [98,105] proposed a one-dimensional model with a relationship between force and motion based on a superposition of elastic, friction and viscous forces. The proposed model has five parameters. The viscous model with only one set of spring and damper in series is a conservative model since it underestimates the hysteresis. It does not take into account the dependence on the preload and temperature. *Sjöberg and Kari* [69] improve Mats Bergs model, extending the viscous part of the model. The frequency dependence is modelled by a fractional calculus element, which permits the correct characterisation of the frequency dependence underestimated in Bergs model. The use of fractional derivatives has the potential to give appropriate frequency dependence with very few (spectral) terms; essentially a model consisting of a very large number of Maxwell elements is replaced by a single fractional derivative Maxwell element. Although they provide a compact way of presenting a wide spectrum, fractional time derivatives cannot alone model nonlinear behaviour. The model proposed by *Sjöberg and Kari* [69] was applied by *Garcia et al* [106,107].

Austrell [99] presented FEM based method which avoids the subroutine implementation. His work was directed to develop a simple method which allowed the simulation of dynamic properties with the combination of general constitutive models implemented in commercial finite element methods. Austrell's model consists of 5 constants simple model composed by a linear spring, an elastoplastic and a viscoelastic elements. The mentioned model was improved to fit better the dynamic behaviour of elastomers with a consideration of various elastoplastic and viscoelastic elements in the model by *Olsson and Austrell* [68] with the subsequent increment in material

constants. After, the model was improved by an introduction of a hyperelastic spring instead of elastic spring by *Olsson and Austrell* [108–110] using the same overlay method. The overlay method is used to combine various constitutive models programmed in commercial finite element software. As shown in Figure 1.37, this method consists of the mesh superposition where the object to simulate is meshed and the mesh is copied at the same location. Next, the nodes are merged obtaining a final model composed of a number of superposed meshes with common nodes. As said before, the use of the overlay or mesh superposition technique avoids the implementation of new complex constitutive models. *Austrell* [108] research shows how this overlay method can be used. For this purpose, *Austrell* [108] used three superposed meshes, where one mesh was characterised by an elastic or hyperelastic properties of rubber, the second mesh which characterised the Payne effect and the third mesh related with the rate-dependent properties of rubber. One mesh or elements layer for each elastoplastic or viscoelastic element is needed. As filler content increases, the nonlinearity of the rubber dynamic behaviour is increased, which requires the use of more VE or/and EP elements to obtain more accurate fitting of the material model to the experimental results. As the number of the elastoplastic constitutive elements increases, the number of needed meshes also increases; this enlarges the calculation time.

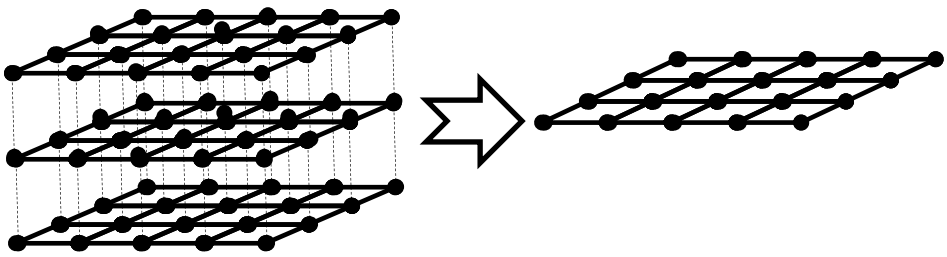

Figure 1.37: Overlay model. The object to simulate is meshed and the mesh is copied as many times as required at the same location. Each mesh is characterised by the required material model. This example is the simplest overlay model presented by Austrell [99]

On the research of the hysteresis loop at a constant frequency, *Ahmadi* [111] evaluated the Multi-linear Kinematic Hardening Plasticity (ML) rule implemented for example in the ANSYS and Abaqus FE codes that could

provide the appropriate stress-strain hysteresis loops for filled rubber. The model was shown to give similar results as that achieved by the overlay of several FE meshes of elastic-perfectly-plastic (EP) material studied in Austrell and Olsson's work, resulting in substantial reduction in computation time compared with the "overlay" approach. On the other hand, in the research of the rate-dependence, *Gil-Negrete et al* [112] and *Gil-Negrete* [113] reduced the number of material constants of the model proposed by *Olsson and Austrell* [108–110] using fractional derivatives and simplifying all viscoelastic elements in a unique element.

One of the most recent models was proposed by *Ahmadi and Muhr* [114] which consist of a simple time-domain model. This model requires a few numbers of material constants and is in accordance with the *Kraus* [101] and *Davies et al* [35] models.

1.4.1 Strain rate characterisation by means of viscoelasticity

1.4.1.1 The hereditary theory for viscoelasticity: Stress relaxation for unfilled rubbers: Constant strain (ε_0)

Viscoelasticity will be described by other means: the hereditary or convolution integrals. These integral, are used because the stress is not only a function of the actual strain, but also of the previous strain history, which is what hereditary integrals take into account. These integrals can express all facts contained in the constitutive equations of the models presented previously. Hence, it can describe the behaviour of the viscoelastic materials.

Linear viscoelastic material can be represented by the following Boltzmann superposition integral. According to this expression, the current stress is determined by the superposition of stress responses to the complete spectrum of increments of strains

$$\sigma(t) = \int_0^t E(t-\tau)\frac{d_\varepsilon(\tau)}{d_\tau}d_\tau \qquad \textit{Eq. 1.109}$$

Where *E(t)* is the relaxation modulus, and $E(t) = \varepsilon(t) = 0\ for -\infty < t < 0$

Eq. 1.109 is founded on general principles; hence, it is valid for any linear viscoelastic material irrespective of the model used to express the material function, *E(t)*. Different phenomenological models of the behaviour of linear viscoelastic materials are available in the literature.

1.4.1.2 Fractional derivative viscoelasticity

To obtain accurate predictions, the generalised Maxwell model solved with hereditary integrals needs to increase the number of parameters associated to the model and may make it difficult to fit. This increment in the number of parameters is due to the expansion of the Prony series (Eq. 4.43, Eq. 4.44).

A general form of the stress-strain equation in differential operators is given by *Fung* [115],

$$\sum_{i=0}^{N} a_i \frac{d^{pi}\sigma}{d_{t^{pi}}} = \sum_{j=0}^{M} b_j \frac{d^{qj}\varepsilon}{d_{t^{qj}}} \qquad \textit{Eq. 1.110}$$

Where p_i and q_j are real constants with $0 \leq p_i, q_j \leq 1$. The ordinary time derivatives acting on the time-dependent stress and strain fields in Eq. 1.110 are replaced with corresponding fractional-order time derivatives. A fractional time-derivative of order α is defined, in an integral form, as *Bagley and Torvik* [116].

And now, the generalised Maxwell model can be written as follows *Nashif* [67]:

$$\sigma + \sum_{i=0}^{N} a_i \frac{d^{pi}\sigma}{d_{t^{pi}}} = E_\infty \varepsilon \sum_{j=0}^{M} b_j \frac{d^{qj}\varepsilon}{d_{t^{qj}}} \qquad \textit{Eq. 1.111}$$

Fractional derivatives can be defined through the Riemann-Liouville convolution integral *Oldham* [117],

$$D_t^{\alpha} f(t) = \frac{d^N}{dt^N}\left[\frac{1}{\Gamma(N-\alpha)}\int_0^t \frac{f(\tau)}{(t-\tau)^{\alpha-N+1}}d\tau\right] \quad \alpha+1 \geq N > \alpha \geq 0 \qquad \textit{Eq. 1.112}$$

Where α is the arbitrary order of derivative; *N*, the smallest integer, larger than the order of the fractional differentiation α, and Γ denotes the gamma function defined as:

$$\Gamma(n) = \int_0^{\infty} t^{n-1}e^{-t}dt \ (n > 0) \qquad \textit{Eq. 1.113}$$

Several researchers [69,112,118–121] have used this method to define the behaviour of various types of materials where elastomers are included in time domain or frequency domain.

Enelund [118] developed a fractional derivative model of linear viscoelasticity based on the decomposition of the displacement field into an anelastic part and elastic part.

The fractional derivatives are not applied in this work.

CHAPTER 2 DETERMINING THE STATE OF CURE OF RUBBER BY MEANS OF SWELLING.

2.1 Theoretical background

In the present chapter, we want to develop a very simple and quick method to evaluate (measure) the degree of cure achieved by the material. The term “state of vulcanizate” means the degree to which some property of the vulcanizate has approached to maximum attainable value as a result of change in time or temperature of cure. It is rather directly related to the degree of crosslinking.

Rubber parts are manufactured using processes such as compression moulding, injection moulding, extrusions, calendaring and so on. In all cases, first the rubber takes the shape of the part to be manufactured, and, later on, it vulcanizes to achieve the final properties. Vulcanization is known as the process during which a number of bonds (so called crosslinks) between the rubber molecules are formed, so that a viscous and tacky material is converted into an elastic material. As a consequence, a polymer network is created, resulting in a three-dimensional structure (Figure 2.1). Three requirements have to be fulfilled for a material to show rubber-like properties:

(1) the presence of long chain-like molecules with freely rotating links;

(2) weak secondary forces between the molecules;

(3) an interlocking of the molecules at a few places along their length to form a three-dimensional network.

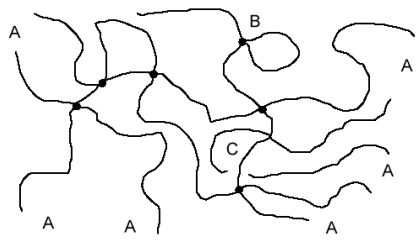

Figure 2.1: Model of a rubber network: A: loose chain ends, B: elastically inactive loop, C: chain entanglement, chemical crosslink [122].

Due to the introduction of crosslinks, the chains are prevented from sliding from each other and the rubber becomes elastic. Besides chemical crosslinks, chain entanglements contribute to the elasticity of the polymer network. They can be either of permanent or temporary nature. The concept of entanglements has been discussed, and even questioned during many decades. Today, however, it is more or less accepted that entanglements contribute to the elastic forces in rubber materials. When filler is incorporated, polymer-filler interactions appear and will also contribute to the three-dimensional network. Opposing these three mechanisms of networking are loose chain ends and elastically ineffective loops. The former increases the free volume of the material by their non-restricted mobility (no crosslinks that tighten the chain end). Chain loops may be formed during vulcanization and will lower the number of elastically effective chains in the material.

The term “crosslink density” deserves a more elaborate explanation. It can be expressed as the number of crosslink points or number of elastically effective chains per unit volume. These two quantities are proportional to each other, and their exact relationship depends on the functionality of the crosslink points, i.e. the number of chains that start from the crosslink. Henceforth crosslink density will be defined as the number of crosslink points per unit volume. Furthermore, crosslink density is inversely related to the average molecular weight of the chains between the crosslinks, which is also a way to express the network properties. The value of crosslink density may be in the order of 10^{-3} to 10^{-5} mol/cm3 for a typical rubber material, corresponding to 15 to 1500 monomer units between the crosslinks. Crosslink density is fundamental for polymeric networks as it determines many physical properties of the resulting material. Figure 2.2 shows how some properties of a rubber material generally depend on the crosslink density [1,2].

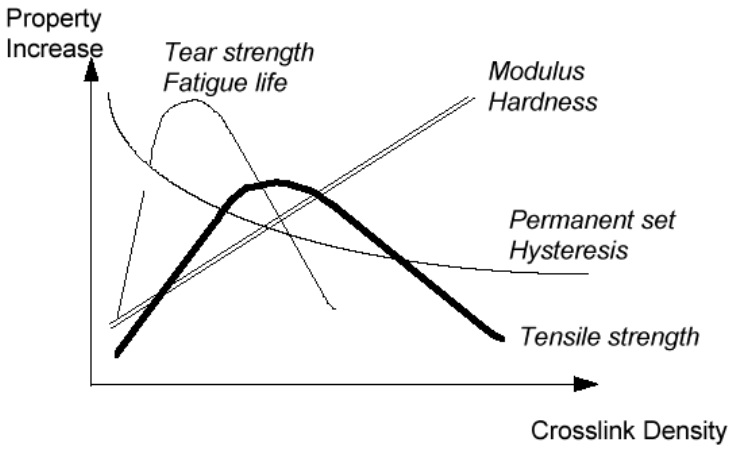

Figure 2.2 Dependence of some properties of a rubber material on crosslink density [122]

This vulcanization process requires a time, which basically depends on the formulation recipe and the cure temperature, and in some cases pressure. For instance, when using a compression or injection moulding process, the heated mould transfers heat to the material; its temperature increases, and cure reactions start. Depending on the cure time, a certain crosslink density will be achieved, and as detailed in Figure 2.2, this leads to specific values of the physical properties.

Several techniques are available to study the kinetics of curing or vulcanization. *Arrillaga et al* [123] discusses their application and usefulness, with the aim of defining the kinetics by empirical/phenomenological approaches, to realise curing simulations. This includes techniques such as ODR, MDR and DSC. Nevertheless, the aim of the present work was not to have a procedure to obtain the complete cure curve, but to have a procedure to determine the degree of cure achieved in partially cured samples.

According to literature, crosslink density can be measured in different ways:

- Stress-strain measurements using the Mooney-Rivling equation [2,23]
- Determination of the elastic modulus at a certain temperature in the rubbery plateau range [124]
- By determination of the residual exothermicity [125]
- By swelling measurements using the *Flory-Rehner* equation [126]

The current work is concerned with the use of swelling measurements to evaluate the degree of cure achieved in several parts. ODR measurements and tensile tests are also done to correlate the results obtained to the swelling value. Although the use of residual exothermicity measured by DSC was considered as a useful procedure to evaluate the degree of cure, this procedure was not utilized for the present study because of its poor resolution, related to the low exothermal peak of rubber formulations and the very small samples that need to be used. The degree of cure is determined as a ratio between the residual heat given by a partially cured sample and the heat given by a non-cured sample [127].

The swelling based procedure was finally used to evaluate differences in curing degree values across the thickness, for a real industrial part manufactured with the rubber formulations studied in the present work.

The determination of equilibrium swelling volumes is one of the best methods for characterising crosslinked structures. The rate of swell as well as the equilibrium swell of a vulcanizate in a solvent has been shown to be a function of the state of cure. Either the molecular weight between crosslinks or its reciprocal, the number of effective network chains per unit volume of rubber may be used as an indication of the cure state. Curing degrees are usually determined by applying the *Flory-Rehner* formula [128], which is:

$$\overline{M_c} = \frac{\rho V_0 \left(V_r^{1/3} - V_r/2\right)}{-Ln\left(1-V_r\right) - V_r - \mu V_r^2} \qquad \textit{Eq. 2.1}$$

where ρ is the density of the material (rubber formulation), V_0 is the molar volume of solvent, μ is the value of the rubber-solvent interaction parameter and V_r is the polymer volume fraction in the swollen vulcanizate, which is a function of the swollen rubber mass, dried rubber mass, density of the formulation, and density of the solvent used for swelling.

Warley and Del Vecchio [127] proposed a similar expression to calculate the crosslink density in (mol/cm3):

$$-\nu = \frac{Ln(1-V_r)+V_r+\mu.V_r^2}{V_0.(V_r^{1/3}-V_r/2)} \qquad \textit{Eq. 2.2}$$

Where ν is the crosslink density, in mol/cm3, which can be rewritten as:

$$-\nu = \frac{\rho}{M_c} \qquad \textit{Eq. 2.3}$$

This is true for non-filled formulations. The calculation becomes much more complex when testing carbon-black loaded formulations [128],[129,130]. The polymer-Solvent interaction parameter must be also determined, using the two solvent procedure described by *Hayes* [131].

In this work, two types of geometries are used. The first one is used to characterise the static and dynamic properties of elastomers (characterisation specimen) and the second one is the industrial geometry, which is used to do the mechanical properties predictions and after correlating the mentioned predictions with the experimental tests. To avoid external parameters iterations, the degree of cure of both (characterisation specimen and industrial part) must be as similar as possible. To compare their degree of cure, an internal procedure was developed and published, based on swelling measurements *Arrillaga, Kareaga, Retolaza and Zaldua* [1,2] (Annex I-A and B).

2.2 Swelling measurements

Due to the complexity of the swelling procedures presented in section 2.1, the option of using just the value of the swelling degree was chosen. The swelling degree is defined as:

$$\%\, swelling = \left[\frac{m_1 - m_0}{m_0}\right] 100 \qquad Eq.\ 2.4$$

where m_0 is the samples weight before swelling, and m_1 is the samples weight after swelling.

To apply this technique, it is necessary to use appropriate solvents (ciclohexane for apolar and acetone for polar elastomers could be a good choice). It should give a sufficient swelling rate in the range of 90-100% and a low evaporation rate. From the solvents tested, ciclohexane was the only one fulfilling these requirements. Samples cured at different times were available from the ODR tests and tensile tests specimens. Samples (0.4 to 0.5 g) were immersed into a bottle containing 6 ml of solvent and maintained into the solvent 24 h. Before measuring m_1 the sample was dried briefly with tissue. It is necessary to recall that the swelling degree measured in this way is an average value because in reality, there is a distribution of the curing degree across the thickness of the sample.

2.3 Materials. Rubber compounds

The present study was based on the use of two rubber formulations, one based on a NR cured with sulfur and the other on an EPDM cured by peroxides. They are proprietary developments and were manufactured at Cikautxo S.Coop. Company.

Table 2.1: summarizes the complete recipe for both formulations, which were prepared in a 150 l internal mixer.

CK-NR 1	*phr*
BR	30
NR	70
Inhibitor	1
Stearic acid	1.5
ZnO	4
Antiozone wax	4
PAN	1
TMQ	0.5
N539	91
Aromatic oil	12
CZ	1.5
Sulfur 80%	1.8
4,4' dithiomorfoline	1.1
PVI	0.2

CK-EPDM 1	*phr*
EPDM, 50% propylene, 5% diene	70
EPDM, 70% propylene, 5% diene	30
MgO	6
TMQ	1
Polyethylen glycol	2
Stearic acid	1
N-539	58.3
Paraffinic oil	29
Slipping wax	4
Perkadox 14/40	5.5
Vulcanization Co-agent	3.5

Table 2.1: Compound recipes. CK-NR 1 and CK-EPDM 1 are natural rubber based and EPDM based formulations respectively. Both elastomers are provided by the company Cikautxo Scoop.

2.4 Rheological tests

All tests were conducted according to the ASTM D2084 standard. The sample was put into a temperature controlled die cavity fitted with a bi-conical disk (rotor) oscillating in a sinusoidal way, at a frequency of 1.57 Hz and an amplitude of +/-3º (see Figure 2.3). The torque counteracting the disk oscillation is monitored over the test time. ODR not only measures the scorch or induction period, but also the cure rate and the state of cure. Thus, the complete cure curve can be recorded and the torque level is correlating to the degree of crosslinking. Three different cure characteristics occur and are illustrated in Figure 2.4.

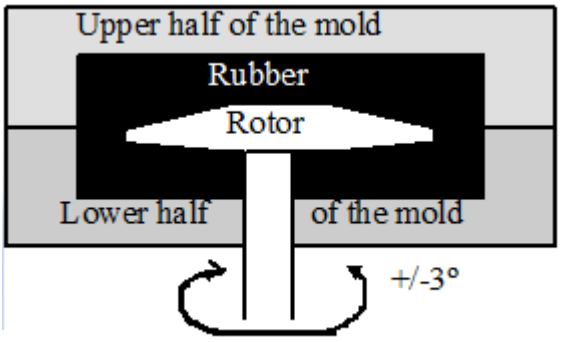

Figure 2.3: ODR testing system. The elastomer covers completely the acting rotor and it is vulcanized in the heated mold.

Test operation mode was as follows: First, the dies and the rotor are heated to the test temperature. A sample taken from an environment held at room temperature is introduced in the preheated chamber and the dies are closed. Immediately, at the closing of the dies, the system automatically adjusts the time to zero. As the sample is at room temperature when introduced into the dies, a decrease of temperature is observed in the chamber. A short time elapses before the test temperature is restored. Tests were made at 165º and 150º for CK-NR 1 and 180ºC and 160º for CK-EPDM 1.

Tests were done with at least 5 samples for each case, and an average was set for later evaluation. Figure 2.4: If the minimum torque (*point a*) is set to "degree of cure α"=0 and the maximum torque (*point b*) to "degree of cure α"=1, then the cure curve α vs. t (t=time) can be calculated for each temperature according to the following equation:

$$\alpha_{(t)} = \frac{Torque_{(t)} - Torque_{(\min)}}{Torque_{(\max)} - Torque_{(\min)}} \qquad \textit{Eq. 2.5}$$

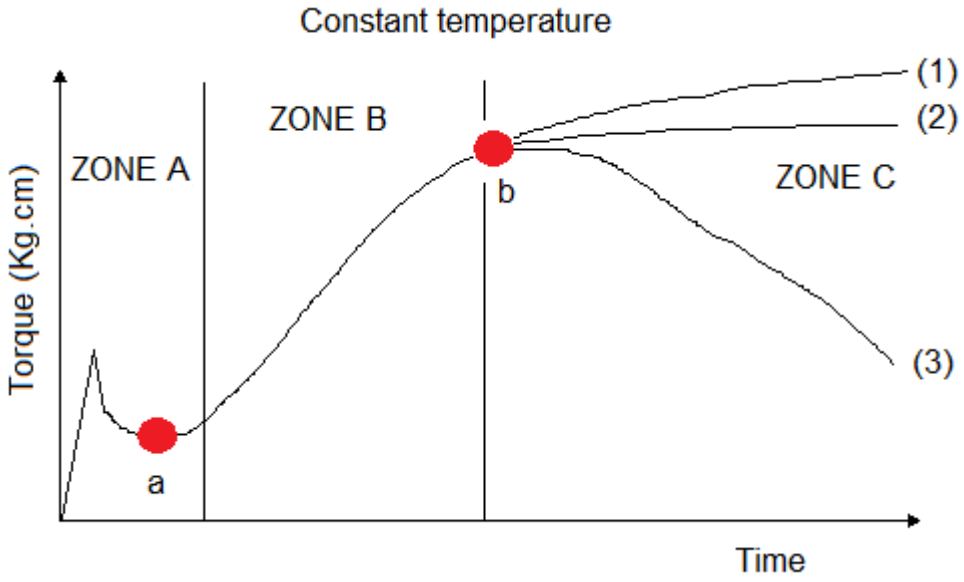

Figure 2.4: ODR test result showing the points of minimum 'a' and the"ideal vulcanization" torque 'b'. Vulcanization curves showing (1)-marching behaviour, (2) – plateau level, and (3) - reversion.

The ODR results are divided in three main zones:

- ZONE A: Induction period or scorch time (*ti*): The time from the start of the measurement to the onset of the crosslinking process (i.e. when the curve begins to slope upwards) is called scorch time, also defined as induction period. It represents time interval at the curing temperature during which no crosslinking can be defined.

- ZONE B: Curing or crosslinking stage: Following the induction period, crosslinking occurs at a rate which is dependent on temperature and the nature of the composition.

- Zone C: Reversion or overcure stage: When the crosslinking has proceeded to a full cure, subsequent heating produces an overcure which may be evidenced by continued stiffening or by reversion. The upper curve (1) shows a marching behaviour that can be observed for chloroprene rubber, EPDM and SBR-based compounds. (2) Plateau level: It is the ideal behaviour where the cure level reaches a plateau (equilibrium), typically for NBR. (3) shows a reversion, a phenomenon that appears for example, when NR is vulcanized with a conventional sulfur system, as described by *Crowther et al* [132].

2.5 Geometries and testing conditions

2.5.1 ODR samples

The CK-NR 1 formulation was tested at two temperatures, 165ºC and 150ºC. CK-EPDM 1 was tested also at two temperatures, 180 and 160ºC. Sufficiently long cure times were set to see the complete curve. Once the complete cure curves were obtained, further measurements were made at the same temperatures, but using intermediate test times, as described below:

- CK-NR 1, tested at 165ºC: 100, 120, 150, 180, 220, 300, 600 and 1000 s.
- CK-NR 1, tested at 150ºC: 260, 290, 320, 350, 390, 430, 470 and 720 s.
- CK-EPDM 1 , tested at 180ºC: 60, 90, 110, 140, 200, 300 and 500 s.
- CK-EPDM 1 , tested at 160ºC: 100, 210, 320, 440, 550, 660 and 900 s.

These times are intermediate values within the cure range and the reversion/plateau range. After reaching the test time, the samples were removed as quickly as possible from the ODR and were immersed into iced water to stop curing.

2.5.2 Tensile tests

The tensile test specimens were pressed on a REP V37 injection machine. CK-NR 1 was injected at a 165ºC mould temperature with curing times of 60, 90, 120 160, 200, 260, 290, 320, 350, 390, 430, 470 and 720 s. CK-EPDM 1 was injected at 180ºC mould temperature with curing times of 30, 60, 80, 100, 210, 320, 440, 550, 660 and 900 s.

After moulding, samples were removed as quickly as possible from the mould and immersed into iced water to stop further curing. Five samples were manufactured at each cure time and then, tensile tests were done according to the ASTM D412-97 to get the information on modulus at 100 and 200 % elongation.

2.5.3 Industrial part

To evaluate the test method with regard to its applicability, the degree of cure variation across the thickness of an industrial part (Reference: Volkswagen 7H0-253-144) was checked. Parts were manufactured with both formulations (Table 2.1). Figure 2.5 displays the part studied; it's a rubber-metal part, where rubber has a maximum thickness of about 15 mm. Two types of samples were analysed. Sample 1 was cut from the external layer of the rubber part (that one in contact with the mould) and sample 2 was taken from the centre of the rubber part. Test conditions complied to section 2.2 with a solvent-rubber ratio of 15:1.

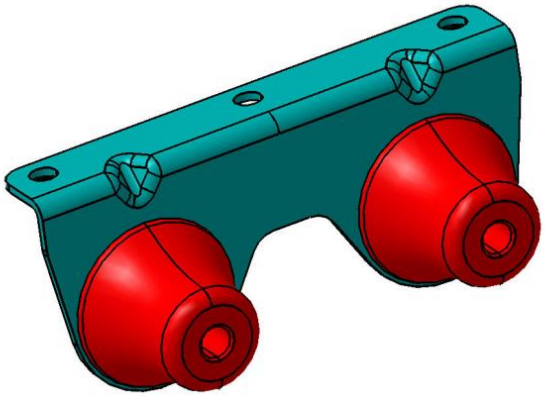

Figure 2.5: Industrial part studied in the present work. Volkswagen Reference 7H0-253-144

2.6 Results and discussion

2.6.1 Rheometer traces

Figure 2.6 and Figure 2.7 show the ODR tests results obtained for both rubber formulations. CK-NR 1 exhibits a clear reversion phenomenon (being typical for sulfur cured formulations), both when testing at 150 and 165ºC. This is represented as a torque decrease after achieving the maximum value. CK-EPDM 1 is an EPDM crosslinked with peroxide. When testing at low temperature, 160ºC, the decompositions rate of the peroxide is low. This slow down the cure kinetics and it seems that the trace arrives at the plateau after 900 s. Nevertheless, the maximum torque achieved at 180ºC was slightly higher. This means that at 160ºC, the maximum degree of cure was not attained.

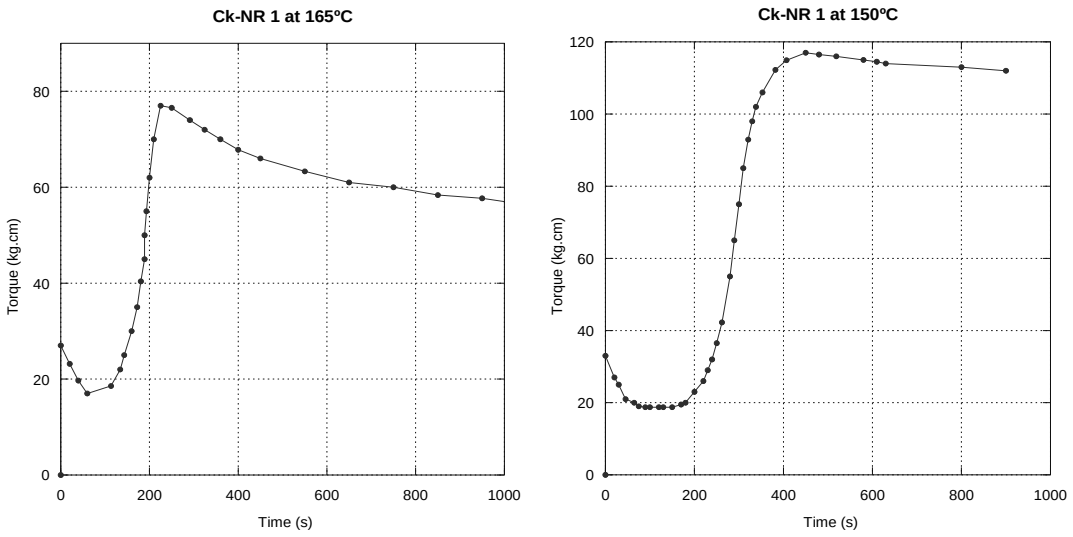

a) b)

Figure 2.6: Vulcanization curves by ODR for CK-NR 1; a) tests done at 165ºC; b) test done at 150ºC.

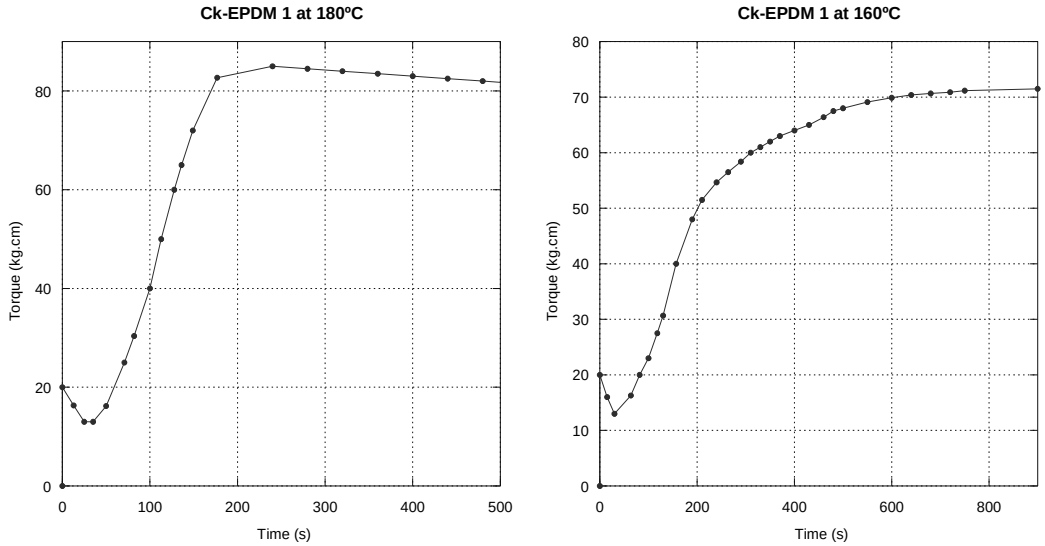

a) b)

Figure 2.7: Vulcanization curves by ODR for CK-EPDM 1; a) tests done at 180ºC; b) test done at 160ºC.

Using the information of the aforementioned curves and Eq. 2.5, the curing degree curves detailed in Figure 2.8 and Figure 2.9 can be calculated from torque values. The degree of cure was set at zero up to the point where the torque starts to increase after achieving the minimum value. This period is defined as the induction or scorch time.

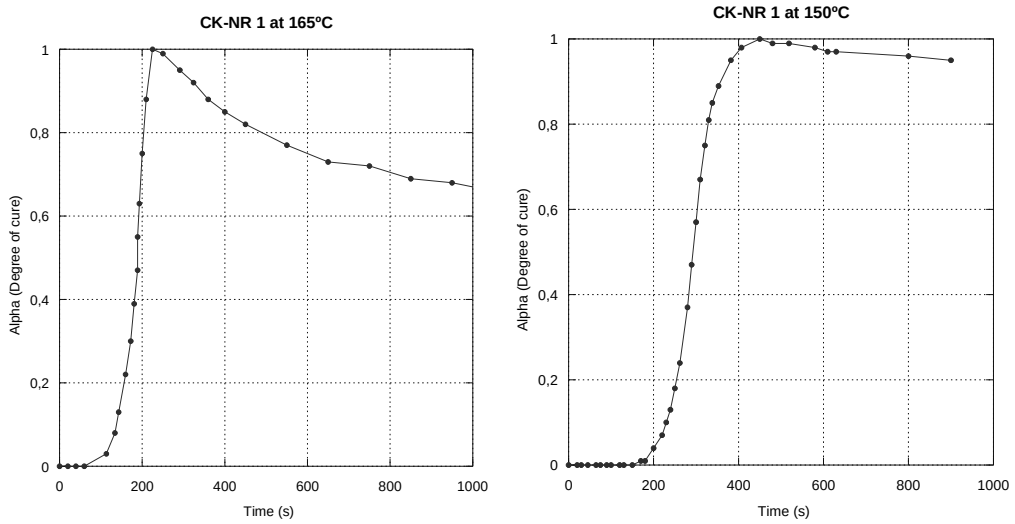

a) b)

Figure 2.8: Cure curves defined as degree of cure (α) versus time data, obtained from ODR torque values, for CK-NR 1; data at 165ºC; b) data at 150ºC

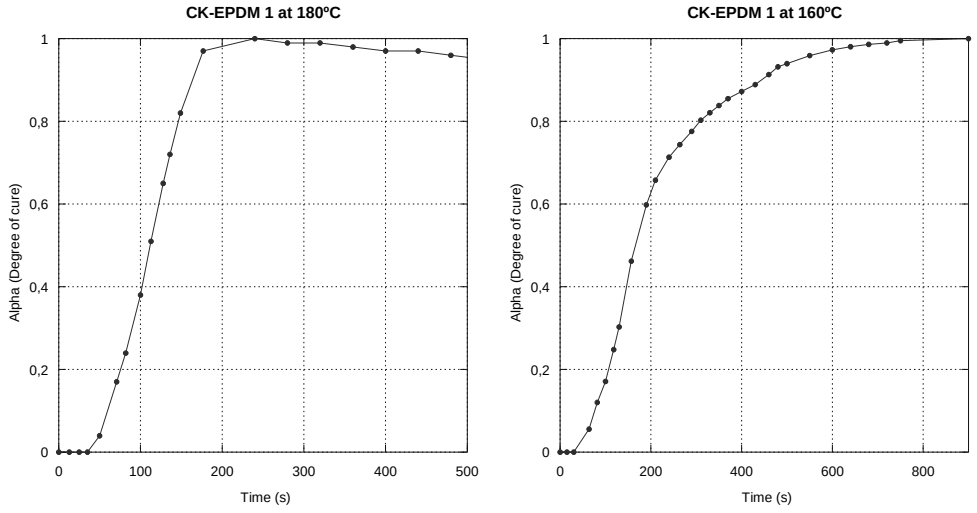

a) b)

Figure 2.9: Cure curves defined as degree of cure (α) versus time data, obtained from ODR torque values, for CK-EPDM 1; data at 180ºC; b) data at 160ºC

2.6.2 Swelling of ODR samples

As already discussed in section 2.5.1, additional tests were performed with keeping the compound in the ODR chamber for the specified times and the resulting samples being checked for swelling. Figure 2.10 and Figure 2.11 represent the swelling values obtained vs. curing time:

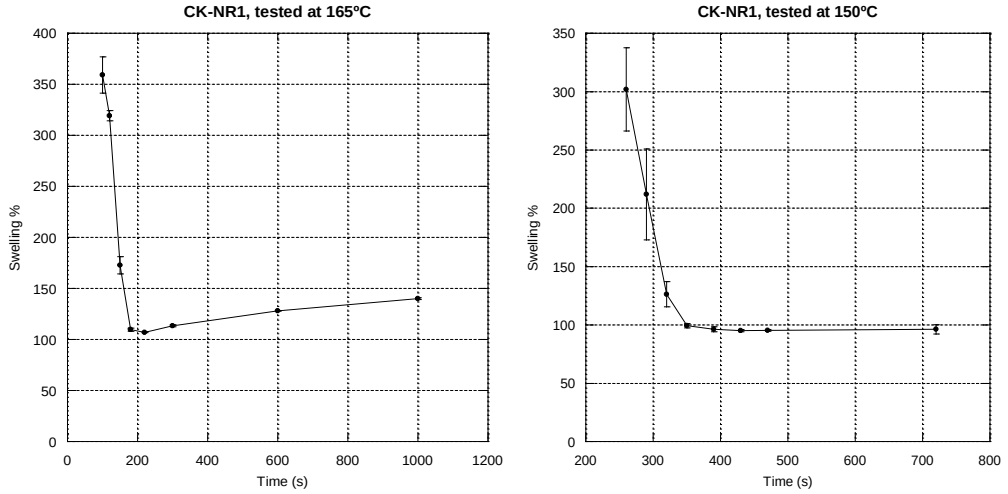

a) b)

Figure 2.10: Swelling degree value as a function of cure time set for the ODR samples, for CK-NR 1 formulation; data at 165ºC; b) data at 150ºC

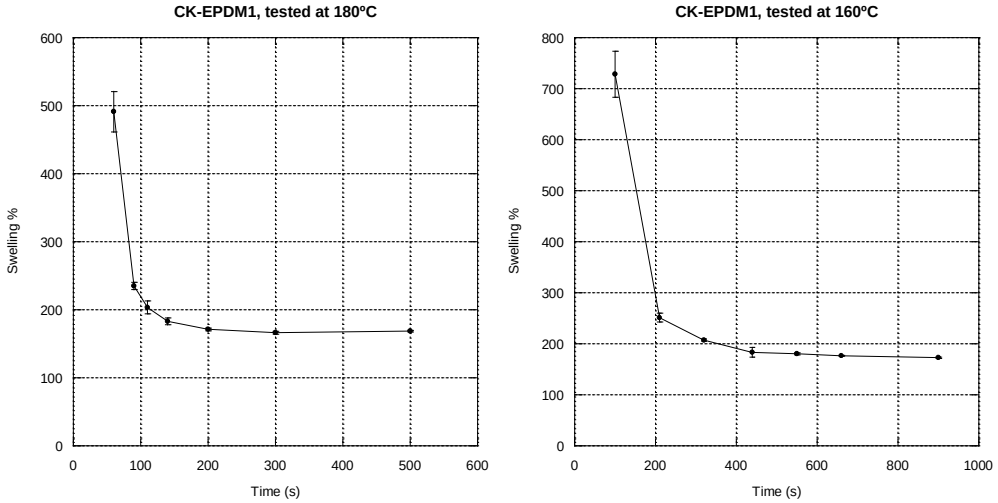

a) b)

Figure 2.11: Swelling degree value as a function of cure time set for the ODR samples, for CK-EPDM-1 formulation; data at 180ºC; b) data at 160ºC

The NR formulation gives a higher torque at the maximum cure point when test is done at lower temperature (see Figure 2.6). The number of crosslinks per unit volume becomes higher. This behaviour is verified by the swelling results (see Figure 2.10) where the minimum value of swelling (that is related to the maximum crosslink density) is at 107% for the material having been cured at 165ºC and goes down to 95% at curing temperature of 150ºC. A higher torque value means a lower swelling ratio. Once the optimum cure point is achieved (that is the minimum swelling point), the NR exhibits its reversion character, which results in an increase of the swelling ratio as detailed in Figure 2.10.

The EPDM formulation was cured with peroxides. In this case, as illustrated in Figure 2.7, the material gives a higher maximum torque when the test is done at higher temperature (180ºC instead of 160ºC). When a temperature of 160ºC is applied, the peroxide does not decompose completely so that the curing remains incomplete. When the information of the swelling tests is evaluated (see Figure 2.11), a minimum swelling ratio of about 166% is achieved at a temperature of 180ºC whereas the minimum value at 160ºC is 172%. This means that the cure reaction is not completed at 160ºC. Again, a higher torque values correlate to a lower swelling ratio. A small torque decay, as time goes on, is exhibited at 180ºC, which is also represented as an increase of swelling ratio.

For both NR and EPDM, there is a match in time for the time values at which the material reaches the maximum torque value in ODR tests and the time value for which the minimum value of swelling ratio is achieved; which means that there is an equivalence of maximum torque and minimum swelling ratio.

According to these results, when vulcanizing a rubber formulation, it is necessary to take the cure temperature into account because it affects the decomposition of the curing agents, and also the cure time. In addition to that, it could lead to reversion phenomena depending on the composition of the formulation.

A match can be found between the torque values measured in the ODR test (and each torque value can be associated to a specific degree of cure) and the swelling ratios. In this way, once this relationship has been defined for the

rubber formulation to be studied, it is possible to determine the curing degree of a rubber part using the swelling method discussed above. So, it is not necessary to apply the methods described in the literature (being much more complex) and that are based on the *Flory-Rehner* relationship [128].

2.6.3 Tensile testing and swelling of tensile test samples

Tensile test specimens were manufactured in accordance with section 2.5.2, three samples each for tensile testing and swelling. The results are collected in Figure 2.12 and Figure 2.13 (tensile tests) and in Figure 2.14 and Figure 2.15 (swelling tests).

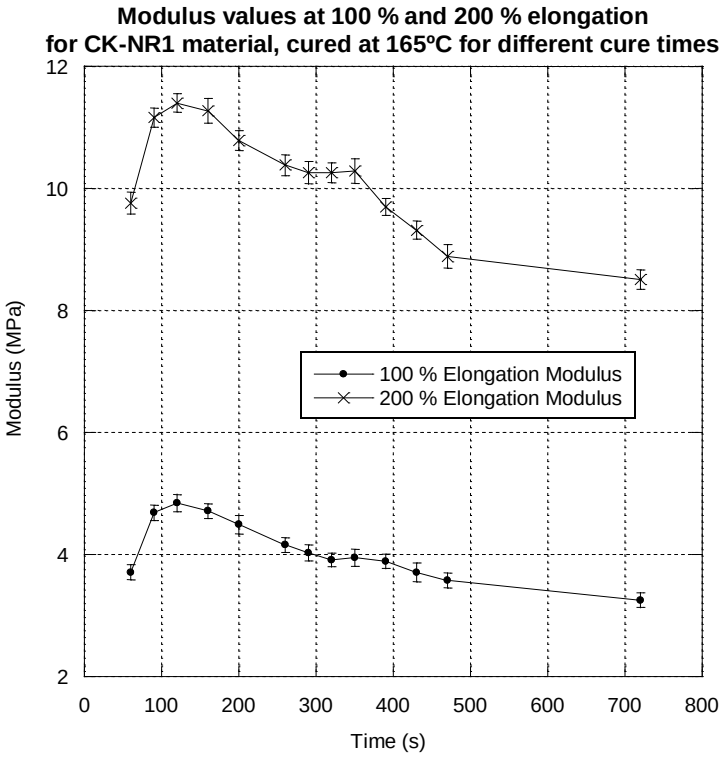

Figure 2.12: Variation of the modulus value at 100 and 200 % of deformation for CK-NR 1 samples cured at 165ºC for different cure times.

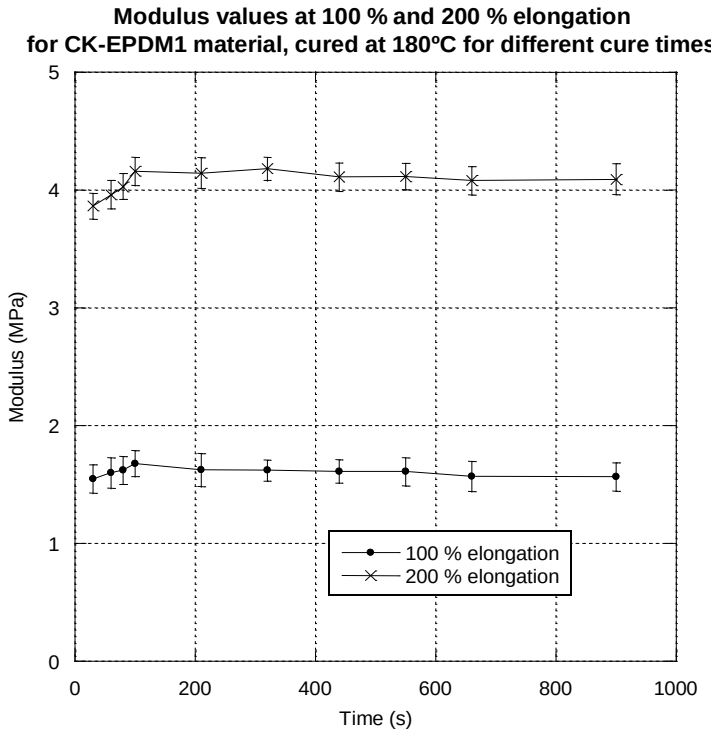

Figure 2.13: Variation of the Modulus value at 100 and 200 % of deformation for CK-EPDM 1 samples cured at 180ºC for different cure times.

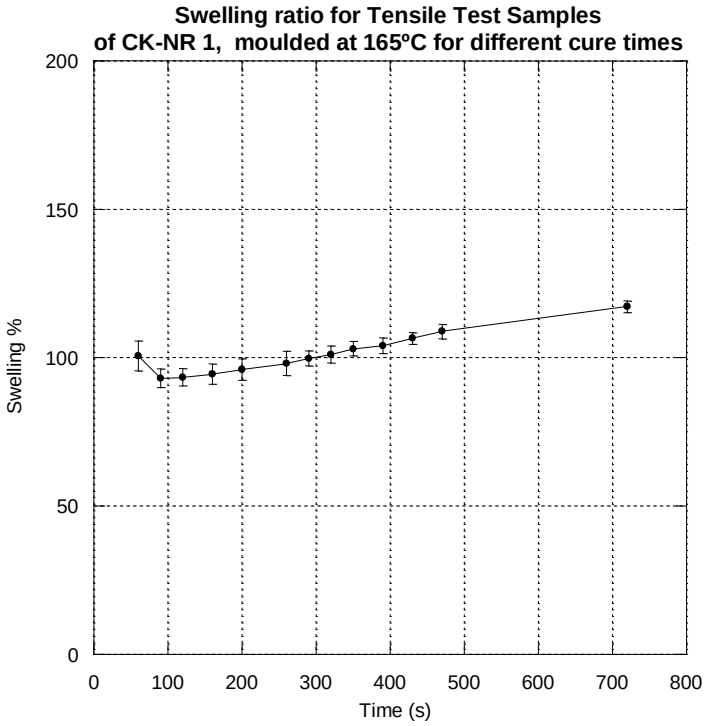

Figure 2.14: Variation of swelling ratio for the samples of CK-NR 1 cured at 165ºC for the different cure times.

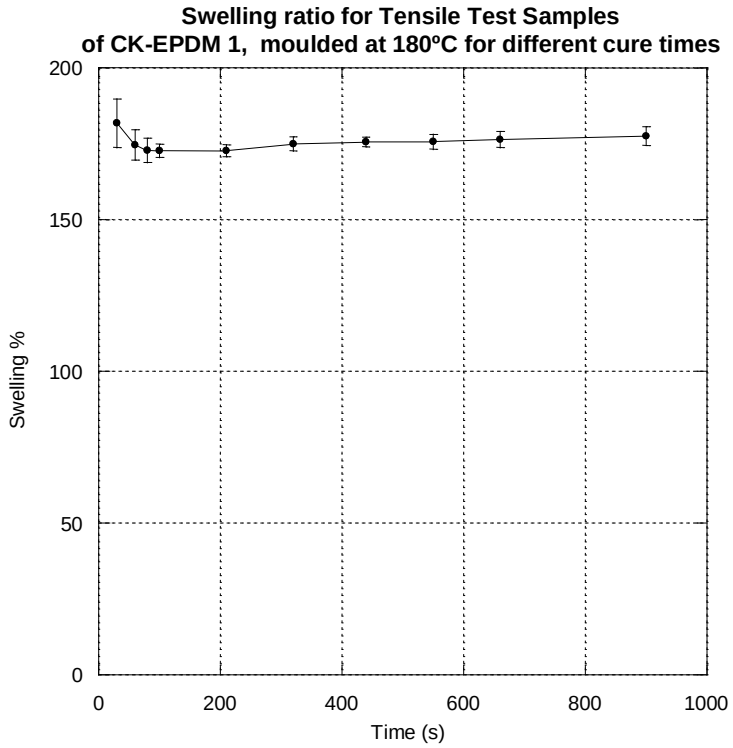

Figure 2.15: Variation of Swelling ratio for the samples of CK-EPDM 1 cured at 180ºC for different cure times.

Regarding CK-NR 1, there occurs an initial increase of moduli up to a maximum followed by an on-going decrease. That decrease is associated with the reversion character exhibited by the formulation. CK-EPDM 1 shows a similar increase at the beginning, but almost no reversion behaviour. The maximum value is maintained.

Figure 2.14 and Figure 2.15 display a minimum swelling ratio point. Values of about 93 and 172% are attained for NR (165ºC) and EPDM (180ºC) samples respectively. The values are close to the minimum swelling values seen for ODR samples tested at 150ºC (NR) and 160ªC (EPDM), i.e. tested at lower temperatures than the mould temperature for manufacturing the tensile samples. This means a direct relationship of swelling values from ODR and tensile test samples cannot be deduced, because the manufacturing process and, as a consequence, the thermal history of those samples are completely different. Concerning the curing degrees measured by swelling, both methods (ODR and tensile) do not lead to equivalent results. Analogous to the ODR samples, however, the tensile specimens have a match in time for the point of

minimum swelling ratio and the point of maximum modulus value (both at 100 and 200% elongation).

2.6.4 Swelling of industrial parts

Preparation and testing of the samples followed the section 2.5.3. The results are presented in Table 2.2. Both materials show that the external layer leads to lower swelling ratio values than the core material, which is related to differences in the degree of cure. According to results presented in Figure 2.10 and Figure 2.11, where samples from the ODR tests were swollen under similar conditions, the NR formulation arrives to a minimum level of about 95% of swelling ratio for a completely cured sample. This value matches the value measured for the external layer of the industrial part. So, it can be concluded that the external layer of the NR part is completely cured. The internal layer reaches about 102%, which corresponds to an incomplete cure. Considering the swelling values obtained for the ODR samples, it can be deduced that the swelling behaviour gives a good indication of the degree of cure. Referring to the EPDM formulation, ODR test samples attain a minimum swelling ratio of about 170% for a complete curing stage. Results from the industrial part show that the external layer achieves these values, whereas the internal layer gives higher swelling ratios, which corresponds to an incomplete cure again.

Material	Sample nº1	Sample nº2	Sample nº3	Average
CK-NR 1 – External layer	96.56	95.06	96.76	96.13
CK-NR 1 – Internal layer	101.99	101.27	102.24	101.84
CK-EPDM 1-External layer	169.04	169.14	170.57	169.59
CK-EPDM 1-Internal layer	175.56	175.95	176.56	176.02

Table 2.2: Swelling ratios measured in industrial part ref. 7h0-253-144.

CHAPTER 3 STATIC CHARACTERISATION METHODS. STRAIN-RATE DEPENDENT MECHANICAL CHARACTERISATION AND CORRELATION WITH A HYPERELASTIC STRAIN ENERGY FUNCTION IN ANSYS

3.1 Theoretical background

As mentioned in previous sections, there are very few standard rubber components. In addition, the static/dynamic mechanical properties of the standard rubber components are not characterised as in metals or thermoplastic materials.

To make predictions of stiffness of complex parts, the first step is to characterise the mechanical properties of simple states of deformation of the material of the said parts. Subsequently, these simple behaviours are used to fit the parameters of the hyperelastic models. Finally, using finite element programs can predict the behaviour that will have the aforementioned complex parts. This means that, on the one hand, it must be used one or several parts to characterise simple deformation states. On the other hand, we will have another complex part with a state of complex deformation.

Because of the complexity of the rubber mechanical behaviour, mathematical models based on Elastic Strain Energy Density have been developed by several researchers as it is shown in section 1.2.1, from the beginning of the 20th century until now. These models have been implemented in FEA software as Ansys, Abaqus or Marc to make complex calculus simpler. But these models do not have the capability to intrinsically take into account the rate dependency of the material. So, the simplest way to solve this problem is to influence the material characterisation step. Another way to characterise the rate-dependency could be using viscoelastic models, which are not covered in this present work.

Although some tests are considered static, they must be performed with a minimum testing rate (near zero testing rates supposes time consuming which increases the cost of the test). Hence, we can find ‘static’ tests performed by testing rates of 100%/min, 20 mm/min, 100 mm/min or 500 mm/min. It is

known, when a complex rubber part is tested with a constant testing rate, the deformation strain tensor of the finite element mesh is composed by principal and shear strain components. The gradient of the strain range of the tensor should be wide. Therefore, the strain rate of the elements should be different.

As seen before, some experimental data are required to calibrate the ESED functions (hyperelastic models). This work is directed to characterise the stiffness of rubber depending on three parameters – strain level, number of conditioning cycles and strain-rate in each strain level-. After, this input will be the input to calibrate any ESED function.

The aim of this chapter is to provide a new material conditioning method improving the existing mechanical conditioning methods. The new conditioning method allows to build a single curve where each strain level characterised by the strain rate is due. Hence, the classic hyperelastic models developed to simulate static mechanical properties can be used for 'non-static' simulations.

Before making a prediction of a static test of a complex part (eg an industrial part) one should know the process to be followed in experimental trials to perform an adequate characterisation of the material.

3.1.1 Degree of cure

The mechanical properties of rubber compounds are greatly influenced by the degree of cure (Figure 2.2). Therefore, both the testing specimens used to (section 3.1.2) characterise mechanical properties of rubbers as the part to be predicted and its mechanical behaviour by means of FEA must have the same degree of cure. For this purpose, the method presented in CHAPTER 2 is applied in order to achieve the same vulcanization degree between both testing sample used in the characterisation step as in the industrial part.

3.1.2 Simple strain states

For engineering purposes, the behaviour of materials is characterised in the simplest strain states. The next subsections review the uniaxial and shear planar states of strain which will be applied in future characterisation of materials.

3.1.2.1 Uniaxial strain state

For uniaxial tension test (Figure 3.1), λ is positive and negative for compression. In the other two directions, they are equal in case of incompressible materials:

$$\lambda_1 = \lambda$$
$$\lambda_2 = \lambda_3 = 1/\sqrt{\lambda} \qquad \textit{Eq. 3.1}$$

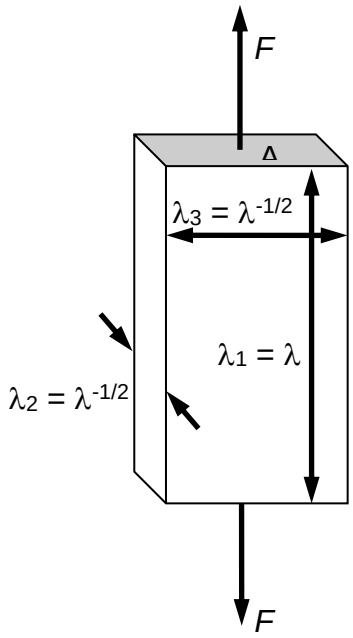

Figure 3.1: Uniaxial strain state

In this case of deformation state, there is only one nonzero principal stress component; then the Cauchy stress tensor is written as:

$$t = \begin{bmatrix} t & 0 & 0 \\ 0 & 0 & 0 \\ 0 & 0 & 0 \end{bmatrix} \qquad \textit{Eq. 3.2}$$

where

$$t = F/a \qquad \textit{Eq. 3.3}$$

and *F* is the force applied in the principal direction and *a* is the deformed cross section area perpendicular to the loaded direction. The relation between deformed and undeformed areas is defined as follows:

$$a = \frac{1}{\lambda} A \qquad \textit{Eq. 3.4}$$

So, the Cauchy or the real stress can be expressed by the force and undeformed or initial cross section area as:

$$t = F\lambda / A \qquad \textit{Eq. 3.5}$$

For uniaxial deformations described in terms of the stretch ratio λ, the deformation tensor that relates the undeformed and deformed configurations is

$$[F] = \begin{bmatrix} \lambda & 0 & 0 \\ 0 & \frac{1}{\sqrt{\lambda}} & 0 \\ 0 & 0 & \frac{1}{\sqrt{\lambda}} \end{bmatrix} \qquad \textit{Eq. 3.6}$$

The Cauchy Green tensor and its inverse matrix are defined as follows:

$$[B] = \begin{bmatrix} \lambda^2 & 0 & 0 \\ 0 & \frac{1}{\lambda} & 0 \\ 0 & 0 & \frac{1}{\lambda} \end{bmatrix} \qquad \textit{Eq. 3.7}$$

$$[B^{-1}] = \begin{bmatrix} \frac{1}{\lambda^2} & 0 & 0 \\ 0 & \lambda & 0 \\ 0 & 0 & \lambda \end{bmatrix} \qquad \textit{Eq. 3.8}$$

and its invariants of deformation are:

$$I_1 = tr(B) = \lambda^2 + \frac{2}{\lambda} \qquad \textit{Eq. 3.9}$$

$$I_2 = tr(B^{-1}) = 2\lambda + \frac{1}{\lambda^2} \qquad \textit{Eq. 3.10}$$

$$I_3 = \det(B) = 1 \qquad \textit{Eq. 3.11}$$

The true stress versus stretch response in uniaxial deformations can then be determined, *Rivlin* [22]:

$$t = 2\left(\lambda^2 - \frac{1}{\lambda}\right)\left[\frac{\partial W}{\partial I_1} - \lambda\frac{\partial W}{\partial I_2}\right] \qquad \textit{Eq. 3.12}$$

and the nominal or engineering stress (load per unit initial area) versus stretch is:

$$\sigma = 2\left(\lambda - \frac{1}{\lambda^2}\right)\left[\frac{\partial W}{\partial I_1} + \frac{1}{\lambda}\frac{\partial W}{\partial I_2}\right] \qquad \textit{Eq. 3.13}$$

Then,

$$F = 2A\left(\lambda - \frac{1}{\lambda^2}\right)\left[\frac{\partial W}{\partial I_1} + \frac{1}{\lambda}\frac{\partial W}{\partial I_2}\right] \qquad \textit{Eq. 3.14}$$

where *F* is the tensile force and *A* is the initial cross sectional area.

The only stresses σ and deformations ε appear in principal directions without any shear appearance. In the case of the hyperelastic materials, the young modulus is different for each strain. However, the initial Young modulus E_0 can be calculated considering the unit stretch as:

$$E_0 = \lim_{\lambda \to 0} \frac{\partial \sigma}{\partial \lambda} = 6\left[\frac{\partial W}{\partial I_1} + \frac{\partial W}{\partial I_2}\right]_{I_1 = I_2 = 3} \qquad \textit{Eq. 3.15}$$

For a complete uniaxial strain state characterisation, the component is compressed and tensioned in the required range of deformations. To characterise this strain state in a wide range of deformations, the normal way is to characterise the uniaxial compression (Figure 1.13-B and Figure 3.2) and uniaxial tension (Figure 1.13-A and Figure 3.5) separately.

The compression specimen presented in The International Standards [62–64], for example, defines the geometry and the methods to use to characterise the mechanical properties of rubber compounds in uniaxial compression.

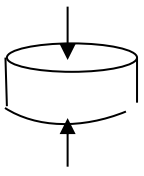

Figure 3.2: Compression characterisation sample

The standard compression test specimens should be 29mm in diameter and 12.5mm in thickness (Figure 3.2). The cylinder is compressed between two parallel plates. To avoid friction in the rubber-plate interface that produces the appearance of shear deformations, the plates and the cylinder faces are lubricated. The used oil must be incompatible with the rubber compound to avoid the absorption by the latter. Anyway, in deformations greater than 30-50 % depending on the tested compound, the lateral side straight verticality becomes a round shape (Figure 3.3). This is the so called bulging effect and it means that shear deformation appears and the test is not completely uniaxial in advance. So the test may be stopped (e.g. in Figure 3.4, from experience, this effect starts at around 32% of deformation).

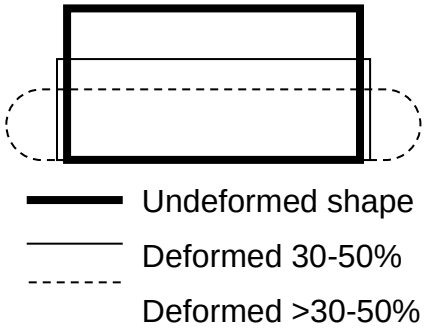

Figure 3.3: Representation of the bulging effect

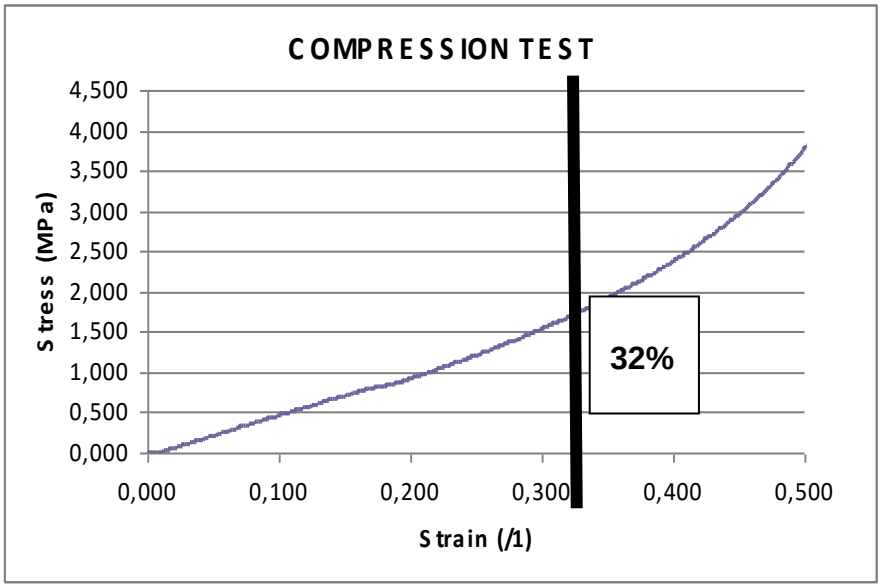

Figure 3.4: Change from pure uniaxial to complex deformation state at the strain of 32%.

On the other hand, for example, the International Standard [59–61] defines the geometry and the testing methods to characterise uniaxial tensile properties. The double-dumbbell sample used in tensile tests is shown in Figure 1.13 and Figure 3.5 and the tensile typical curve in Figure 3.6.

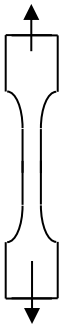

Figure 3.5: Tensile characterisation sample

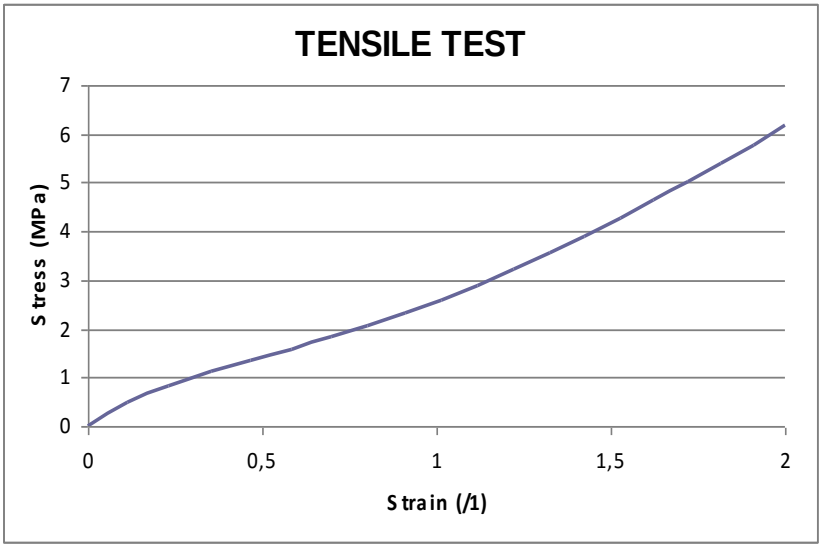

Figure 3.6: Typical tensile curve

In Figure 3.6 it is shown the strain/stress nonlinear behaviour. The initial decrease in modulus up to around 40% (in this example) may be due to the changes in the filler-filler and rubber-filler interactions. The subsequent increase in modulus at large deformations is probably due to finite extensibility of the rubber network [51].

Finally, both compression and tension uniaxial tests are joined to get a complete uniaxial response. The final graph looks like Figure 3.7.

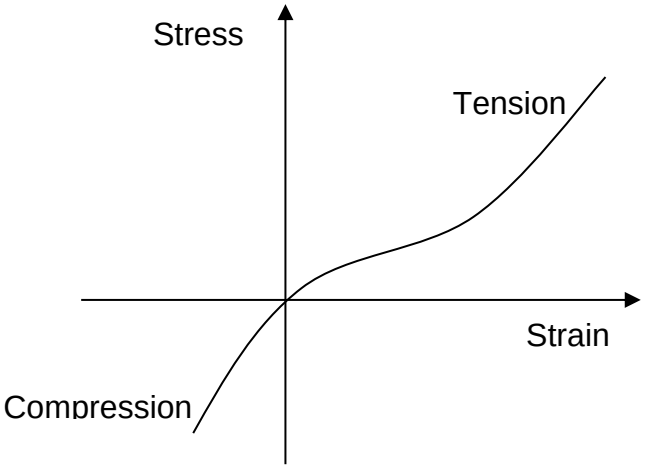

Figure 3.7: Complete uniaxial response. Compression-tension uniaxial curve

3.1.2.2 Shear planar or pure shear strain state

The pure shear or shear planar specimen is not defined in any International Standard (ISO) (Figure 3.8). Not much information is available in bibliography concerning the shear planar specimen. The length of the sample must be more or less 10 times its height and a lot wider (more than a hundred times). The dimensions of the specimen in this work are: length=300mm, height=35mm, thickness=2mm.

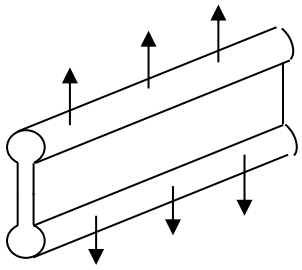

Figure 3.8: Pure shear or shear planar characterisation specimen

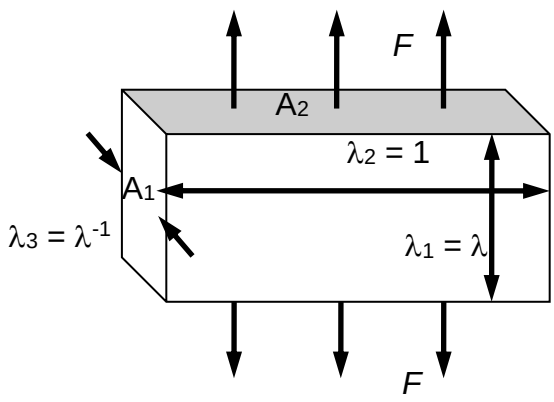

Figure 3.9: Pure shear or shear planar strain state

The principal elongations in shear planar are related as follows (Figure 3.9):

$$\lambda_1 = \lambda \qquad \lambda_2 = 1 \qquad \lambda_3 = 1/\lambda \qquad \textit{Eq. 3.16}$$

$$[F] = \begin{bmatrix} \lambda & 0 & 0 \\ 0 & 1 & 0 \\ 0 & 0 & 1/\lambda \end{bmatrix} \qquad \textit{Eq. 3.17}$$

$$[B] = FF^t = \begin{bmatrix} \lambda^2 & 0 & 0 \\ 0 & 1 & 0 \\ 0 & 0 & \dfrac{1}{\lambda^2} \end{bmatrix} \qquad \textit{Eq. 3.18}$$

$$[B^{-1}] = \begin{bmatrix} \dfrac{1}{\lambda^2} & 0 & 0 \\ 0 & 1 & 0 \\ 0 & 0 & \lambda^2 \end{bmatrix} \qquad \textit{Eq. 3.19}$$

In this case, the strain invariants are equal and they could be defined as:

$$I_1 = tr(B) = I_2 = tr(B^{-1}) = 1 + \lambda^2 + \frac{1}{\lambda^2} \qquad \textit{Eq. 3.20}$$

There are two non-zero principal stress components, thus the Cauchy stress tensor is:

$$[t] = \begin{bmatrix} t_1 & 0 & 0 \\ 0 & t_2 & 0 \\ 0 & 0 & 0 \end{bmatrix} \qquad \textit{Eq. 3.21}$$

The relation between the initial and deformed areas is:

$$a_1 = \frac{1}{\lambda} A_1 \qquad \textit{Eq. 3.22}$$

$$a_2 = A_2 \qquad \textit{Eq. 3.23}$$

where A_1 and A_2 are the undeformed and a_1 and a_2 are the deformed cross section areas.

Therefore,

$$t_1 = \frac{F_1 \lambda}{A_1} \qquad \textit{Eq. 3.24}$$

$$t_2 = \frac{F_2}{A_2} \qquad \textit{Eq. 3.25}$$

where F_1 and F_2 are the forces that develop in direction 1 and 2.

It is possible to predict the pure shear with the Rivlin's relations as follows:

$$\sigma_1 = F_1 / A_1 = 2\left(\frac{\partial W}{\partial I_1} + \frac{\partial W}{\partial I_2}\right)\left(\lambda - \frac{1}{\lambda^3}\right) \qquad \textit{Eq. 3.26}$$

$$\sigma_2 = F_2 / A_2 = 2\left(\frac{\partial W}{\partial I_1} + \frac{1}{\lambda^2}\frac{\partial W}{\partial I_2}\right)\left(1 - \frac{1}{\lambda^2}\right) \qquad \textit{Eq. 3.27}$$

In practice $\lambda>1$, therefore only the first relation is used for the evaluation of laboratory tests.

3.1.3 Strain rate dependence on the dynamic stiffness of rubber compounds

In the case of rubber compounds, the strain rate used in characterisation tests has a considerable influence on their mechanical properties. The hyperelastic ESED models seen in section 1.2.1 do not take into account the influence of the deformation rate used in the experimental test or the stress relaxation that occurs in a rubber part during the test or once it has been deformed (see Figure 3.10-A and D respectively). Some examples of strain-rate influence are represented in Figure 3.10-B.

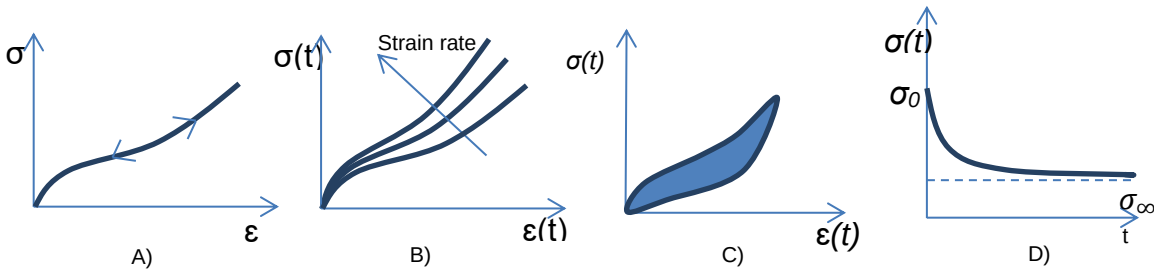

Figure 3.10: A) Hyperelastic models curve representation (Static test). B) Stiffness increases with strain rate C) In an experimental load cycle, the material is relaxed and the energy represented by the hysteresis area is lost as heat. D) When a rubber part is deformed and this deformation is maintained in time, the initial stress σ_0 is relaxed σ_∞.

Figure 3.11 and Figure 3.12 show the testing rate influence in static tests. In these figures, the strain rate dependence on rubbers stiffness is checked performing tension tests with different testing rates. As it is shown in Figure 3.11, the stiffness of the studied rubber is increased at higher testing rates.

These tests are carried out with shear planar characterisation specimens shown in Figure 3.8 and manufactured with the natural rubber based compound called CKR (
Table *3.1*).

In Figure 3.12, it is plotted the stresses at each strain rate when the testing specimen is deformed 30%. The obtained results suppose the normalized error of 7.73% (Eq. 3.29) between the higher and lower testing rates

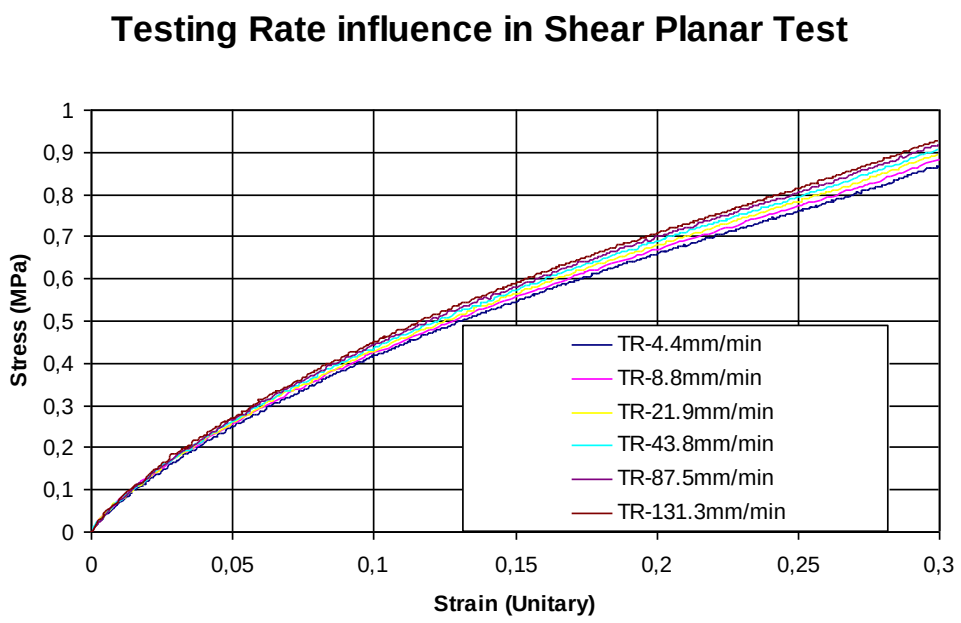

Figure 3.11: Evolution of the stress-strain behaviour (stiffness) depending on the used testing speed.(Material: CKR)

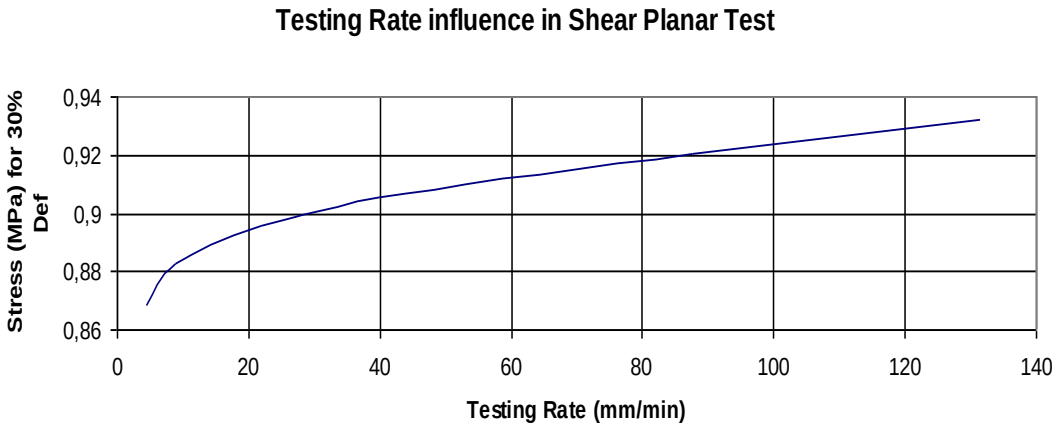

Figure 3.12: Strength of the Rubber compound (CKR) at 30% of deformation tested at different testing rates in mm/min.

3.1.4 Standard mechanical conditioning methods

Due to the presence of the Mullins effect (section 1.2.2) in elastomeric parts, all parts involved both in material characterisation and simulated parts must be cycled the same number of times. The Mullis Effect consists of the relaxation of the elastic stiffness of the tested rubber part after each load cycle. This effect is more pronounced during the first cycle, but it is still detectable after several cycles (see Figure 1.7).

To simplify finite element simulations, the strain energy function can be derived after softening the elastomer for a given number of cycles in an attempt to stabilise its stress-strain behaviour. In order to avoid the use of Mullins damage functions, elastomers may be conditioned. These latter methods are usually called conditioning.

There are different procedures to characterise elastomeric materials which have been extensively studied by *Charlton et al* [9], *Austrell* [99], *James and Green* [27], *Chow and Cundiff* [133] and *Yeoh* [25]. In short, these techniques are explained bellow:

A) Unconditioned test:

The part is tested at a very low strain-rate until the required strain. On the first cycle loading, the viscous behaviour affects both the loading and the unloading curves. The strain energy functions referred to earlier are usually derived by fitting the first loading curve. Certainly, this method almost overestimates the elastic strain energy in a specimen. A number of attempts have been made to obtain an approximate solution to the problem. *Kawabata et al* [134] used an average of loading and unloading curves. *Gent and Kim* [135] suggested that the area under the unloading curve should be used to calculate the elastic strain energy. Furthermore, they calculated that an overestimation, ranging from 35-130%, depending on the imposed strain of the elastic strain energy occurred in carbon black filled NR and SBR elastomers if the loading curve was used. It is hence currently better to use a particular well-defined solution for a particular problem. On the one hand, *Yeoh* [25] uses a testing speed of 50%/min after the correlation with 10%/min, because of the similarity of the

results and the time efficiency of the first one. On the other hand, *Austrell* [99] recommends 3%/min if the characterisation sample will not be cycled. Furthermore, *Yang et al* [136] and *Przybylo and Arruda* [137] use a strain rate of 1.10-2/s. *Moreau et al* [138] arrived at the same conclusion, i.e. that results obtained at 2mm/min, 20mm/min and 100mm/min are approximately equivalent; hence the test rate of 20mm/min is being selected for the measurements.

B) One-level conditioning

In order to take into account the *Mullins* [51] effect in the characterisation phase, the samples are tested up to the selected strain for a number of cycles. The preconditioning cycles are not registered and the last curves are selected. *Austrell* [99] recommends 5 preconditioning cycles and 3 more to take a representative stress/strain curve. An example of such a method was proposed by *Yeoh* [25] to cycle the test piece from zero strain to a selected strain for five cycles and takes the average of the sixth to the eighth cycle as the representative stress-strain behaviour (Figure 3.13):

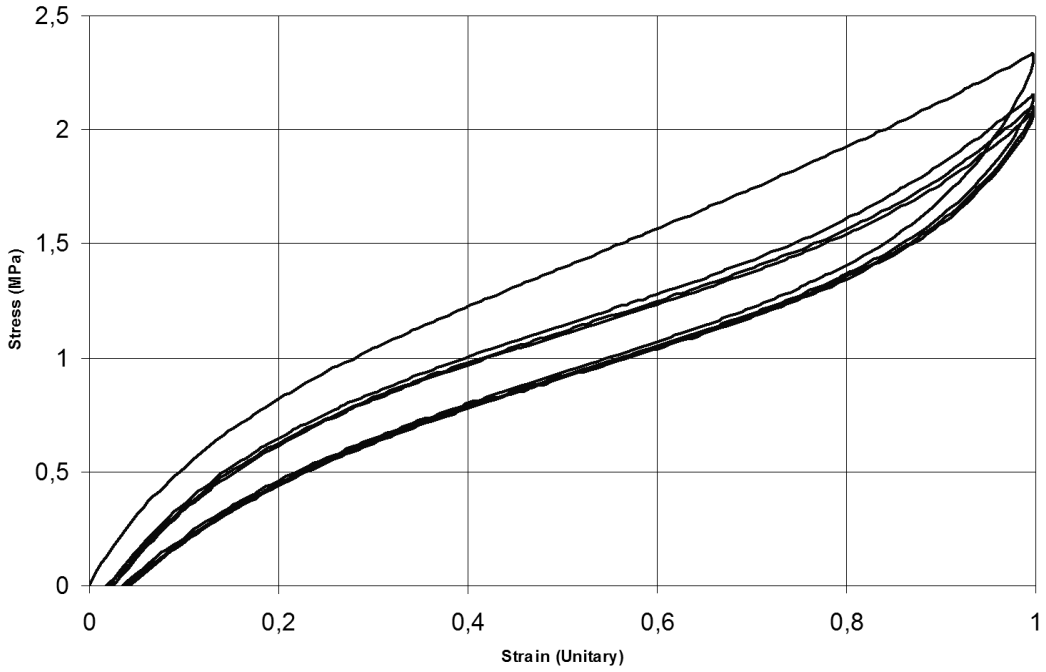

Figure 3.13: One-level conditioning method.

C) Progressive conditioning

The objective of using this method is to obtain a representative curve of the material preconditioning a number of times (five, for example) up to predefined strains that go from small to large deformations (Figure 3.14). After that, three more cycles are performed and the representative curve is taken. The selected levels could be 2, 5, 10, 20, 50 and 100%; obviously, the curve should be of better quality as long as more levels are defined.

Chow and Cundiff [133] proposes to repeat from zero strain at this deformation level during eight cycles and the average of the stress strain maxima in the sixth to the eighth loading cycle was taken. This average stress gives a single point on the stress-strain curve. Collectively, the recorded averages of stress strain maxima at each deformation level defined a quasi-equilibrium stress versus strain curve for the material.

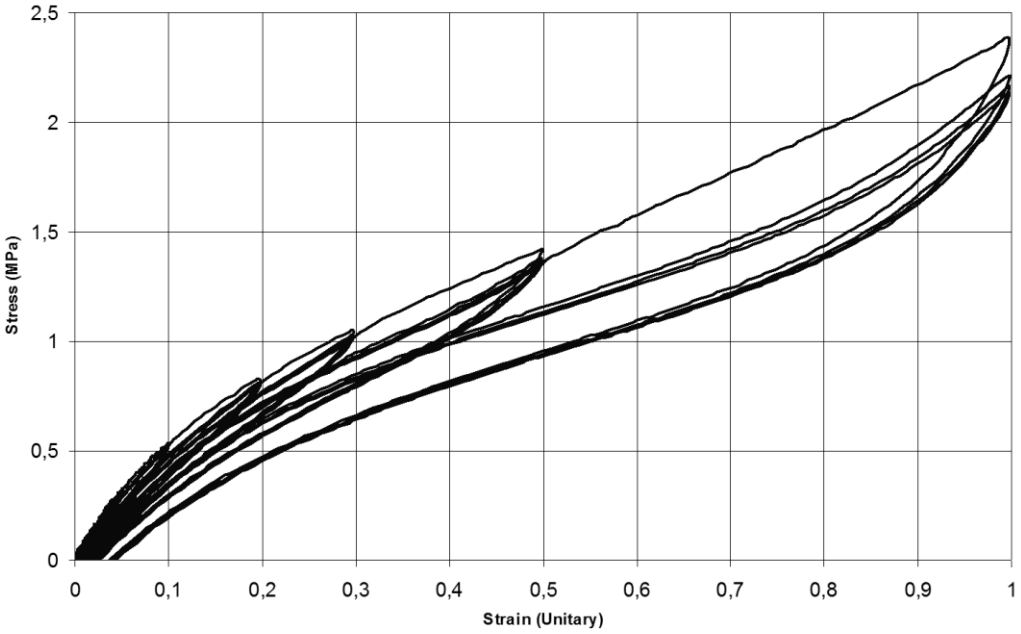

Figure 3.14: The progressive conditioning method.

D) Intermittent conditioning

This method consists of a static strain up to the selected strain and a subsequent stress relaxation. Afterwards, the sample is strained up to the next

selected static strain continuing with the stress relaxation. This sequence is repeated up to the largest stretch selected (Figure 3.15).

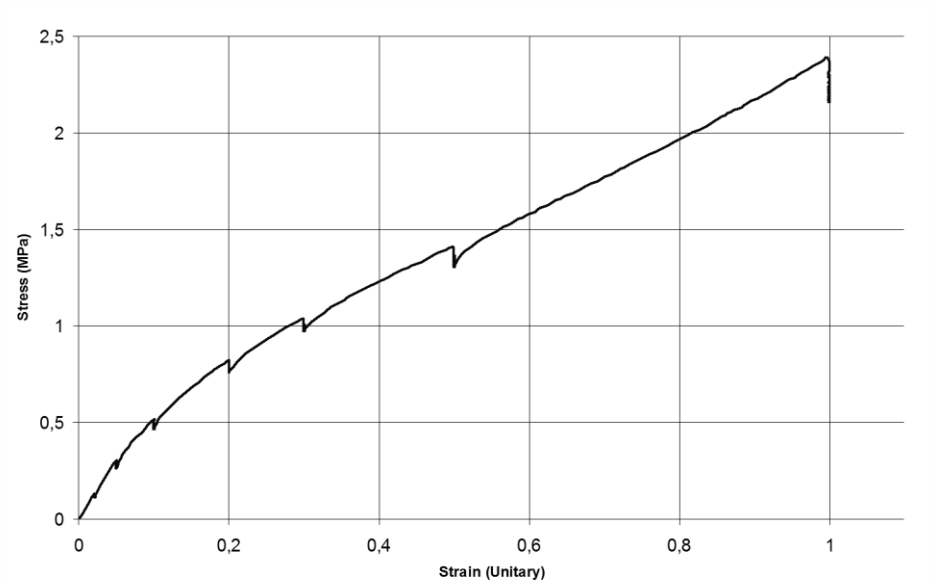

Figure 3.15: The intermittent conditioning method

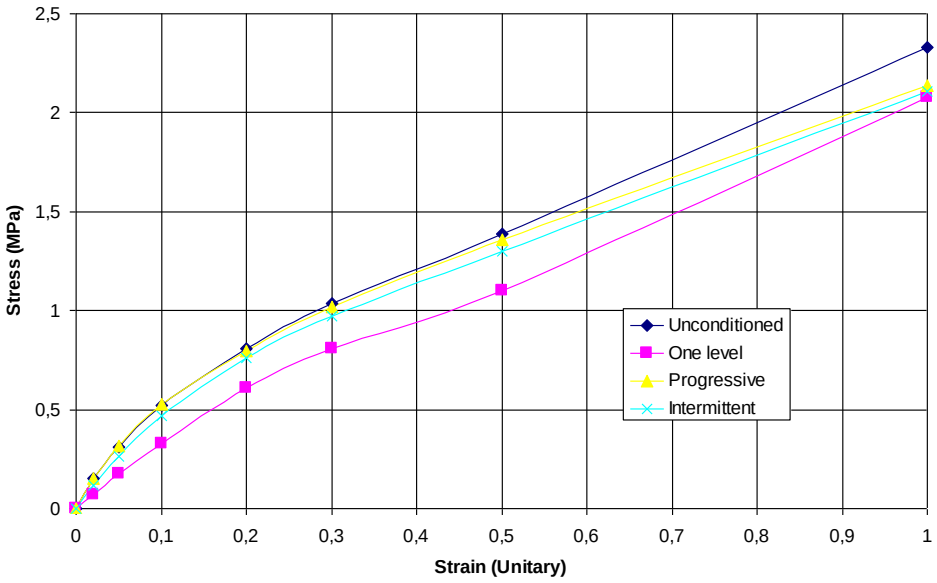

Figure 3.16: Comparison of different rubber conditioning methods. The unconditioned sample and the one level conditioning method give the highest and the lowest stiffness's respectively. The rubber compound used to correlate the conditioning methods is the NR based CKR rubber compound (
Table 3.1).

Such procedures will clearly work quite well for a component for which the approach represents approximately its only loading cycles. However, it clearly cannot have a general applicability for components loaded in a more complex manner.

3.1.5 ESED Function to perform the simulations by means of FEA.

The present work is carried out using the finite element code Ansys v11, where the experimental data of the characterisation samples are fitted to *Yeoh's* [25] model defined as,

$$W = C_{10}(I_1 - 3) + C_{20}(I_1 - 3)^2 + C_{30}(I_1 - 3)^3. \qquad \textit{Eq. 3.28}$$

This approach predict the stress strain behaviour of filled elastomers well at large strain. Moreover, this function permit the prediction of stress/strain behaviour in different deformation modes from data obtained in one simple deformation mode (see section 1.2.1).

In order to numerically check the error between the experimental data and the simulation, the normalized least-square method is used. This least-square method gives equal weight to all data points. The calculated residual is the output that helps evaluating how precisely the fit was performed. The equation for the normalized error calculation is the following one:

$$E_{normalized} = \sqrt{\sum_{i=1}^{N} \frac{\left(\sigma_i^{trial} - \sigma_i^{experiment}\right)^2}{\left(\sigma_i^{experiment}\right)^2}} \qquad \textit{Eq. 3.29}$$

where $\sigma^{experiment}$ are the stresses used to calibrate the *Yeoh's* model and σ^{trial} are the calculated stresses using this model. Finally, '*i*' denotes each strain point.

3.2 Experimental work

3.2.1 Geometry definition

The characterisation and simulation procedure will be presented with an industrial example. The studied geometry is an exhaust hanger shown in Figure 3.17:

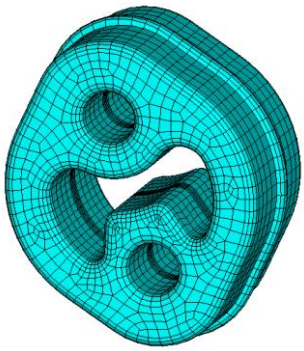

Figure 3.17: Industrial case: Exhaust hanger industrial case. Meshed geometry.

3.2.2 Material definition

The selected rubber to perform this work and its composition are detailed in Table 3.1.

CKR	*phr*
BR	30
NR	70
ZnO	4
Stearic acid	1
Peptizing agent	1
Antiozonant Microwax	3.5
Aminic antioxidant	1.5
Aminic antiozonant	3
Aromatic oil	5
N539	50
Sulfur	1.4
CZ	1

Table 3.1: The selected rubber compound is CKR and its composition in parts per hundred of rubber.

This material was manufactured by Cikautxo Scoop.

3.2.3 Functional requirements

The experimental testing conditions of the exhaust hanger are defined as follows:

- 3 pre-conditioning cycles will be performed before the last load cycle which will be the accepted curve.
- The load consists of a positive tension load of 8mm.
- The testing rate or the speed given to perform the tension is 100 mm/min (or 1.66mm/sec).

That means that the testing time t_t is 4.8 seconds.

3.2.4 Initial FEM simulation

In order to determine the strain range to characterise, an initial simulation is performed. Hence, as required in the functional requirements, the finite element model is loaded 8mm to obtain the mentioned deformation range. In this step, we randomly use selected material properties (E=1 MPa and Poisson's ratio= 0.499) and the results are plotted in the following Figure 3.18:

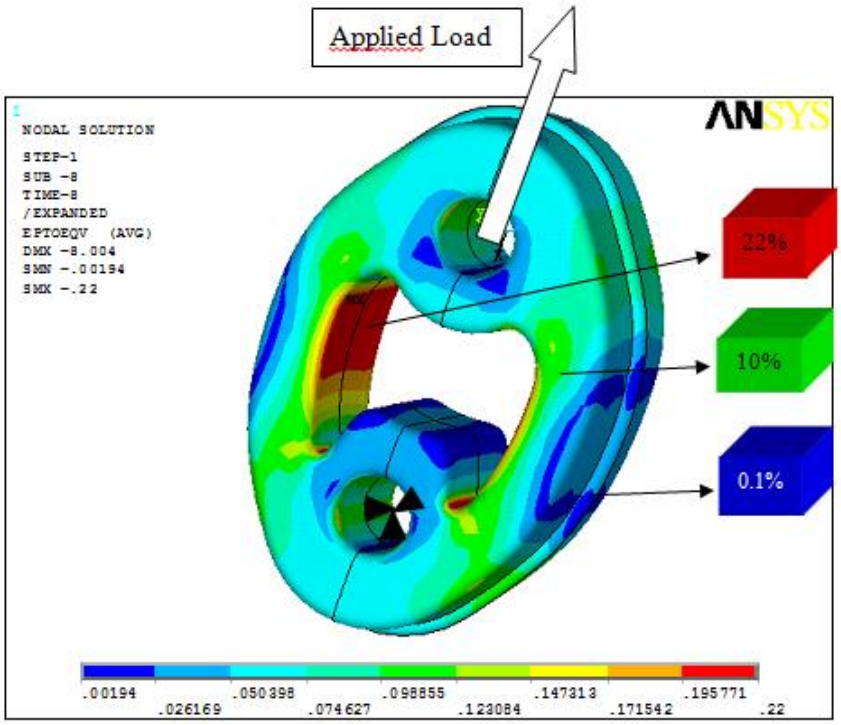

Figure 3.18: Initial FEM simulation

The material is characterised in a range between zero and the maximum strain that has been calculated in the former simulation (22%). To assure an adequate characterisation, this range is augmented to 30%.

3.2.5 Material testing: Mechanical Properties Characterisation

This section is directed to create experimental data curves to be used as input data. Later, the mainly generalised conditioning methods are presented in subsection 3.2.5.1 and an additional conditioning method is proposed in subsection 3.2.5.2 is correlated.

In order to build the characterisation curves, the material needs to be tested at some increasing strain levels. First, the maximum strain of *22%* of the deformed mesh is calculated in the initial FEM simulation (section 3.2.4). After, the characterisation strain range is defined between 0 and 30% to assure the adequate characterisation of the mechanical properties of the exhaust hanger. Finally, the conditioning strain levels for the last two progressive conditioning methods are defined as 1, 2, 5, 10, 20 and 30%. In addition, the material properties are tested with the same number of cycles as in the industrial part; the material is cycled four times at each strain level. The last curve of each level is the selected one to build the definitive material curve. In addition, each strain level is tested as the same strain rate given in the elements with the same deformation of the industrial part. Then, the strain rate for each strain level given in the industrial case is calculated as follows:

First, the test duration in the exhaust hanger's example can be calculated as follows:

$$t_t = \frac{Load}{Speed} \qquad Eq.\ 3.30$$

where t_t is the test duration, *Load* is the applied displacement and *Speed* is the testing rate.

Second, the strain rate for each strain level is calculated,

$$StrainRate = \frac{\varepsilon}{t_t} \qquad Eq.\ 3.31$$

where ε is the strain level.

Finally, the testing speed for each strain set can be calculated and tested for every characterisation test sample as follows:

$$Speed = \frac{\varepsilon}{100} D / t_t \qquad Eq.\ 3.32$$

where D is the original length between clamps.

Finally, from Eq. 3.31 and Eq. 3.32 the testing speed for each strain set can be calculated as follows:

$$Speed = \frac{D.StrainRate}{100} \qquad Eq.\ 3.33$$

3.2.5.1 Standard conditioning procedures

1.- <u>Unconditioned test</u>: The first type consists of a unique tension test at a very slow strain rate. The strain rate is defined as 5%/min of the initial length of the sample.

The first two, both compression and pure shear characterisations, are performed controlling the displacement and the speed of the testing machine actuator. **Due to the complexity of the strain rate controlling method, the third, the uniaxial tension test is an exception. This specimen is characterised with the aid of a non-contact video extensometer (see Figure 3.19). Hence, the strain and strain rates of each level are controlled in strain (%/min) and not in speed (mm/min) as they are done in the compression and pure shear tests. The testing conditions for each specimen are detailed in Table 3.2

Specimen type	***Strain Level Nº***	*Strain (%)*	*Strain Rate (%/min)*	*Displacement (mm)*	*Testing speed (mm/min)*
Compression	1	30	5	4.05	0.7
Shear planar	1	30	5	10.5	1.8
Tensile	1	30	5	**	**

Table 3.2: Testing conditions of each specimen type.

Figure 3.19: Non-contact video extensometer

2.- *Progressive conditioning method*: The characterisation sample is tested as many times as the industrial part (3+1 in this case) at a very slow strain rate. The selected rate of 15%/min is an intermediate value between the ones proposed by *Austrell* [99] and *Yeoh* [25], 3%/min and 50%/min respectively. The testing conditions for shear planar, compression and tensile essays are detailed in Table 3.3, Table 3.4 and Table 3.5 respectively:

Strain Level Nº	*Strain (%)*	*Strain Rate (%/min)*	*Displacement (mm)*	*Testing speed (mm/min)*
1	1	15	0.35	5.3
2	2	15	0.7	5.3
3	5	15	1.75	5.3
4	10	15	3.5	5.3
5	20	15	7	5.3
6	30	15	10.5	5.3

Table 3.3: Rate used in each set of 3+1 cycled stretch for the Shear Planar Samples on their respective tests

Strain Level Nº	*Strain (%)*	*Strain Rate (%/min)*	*Displacement (mm)*	*Testing speed (mm/min)*
1	1	15	0.135	2
2	2	15	0.27	2
3	5	15	0.675	2
4	10	15	1.35	2
5	20	15	2.7	2
6	30	15	4.05	2

Table 3.4: Rate used in each set of 3+1 cycled stretch for the Compression Samples on their respective tests

Strain Level Nº	*Strain (%)*	*Strain Rate (%/min)*
1	1	15
2	2	15
3	5	15
4	10	15
5	20	15
6	30	15

Table 3.5: Rate used in each set of 3+1 cycled stretch for the Dumb-bell Samples on their respective tests

3.2.5.2 Proposed material conditioning procedure; Progressive conditioning with equivalent strain-rates

The presented conditioning method consists of a number of loading cycles performed at several strain levels that go from small to large deformations. Therefore, this method is similar to the progressive conditioning method reviewed in section 3.1.4 changing the strain rate from the previous strain level to the next as seen in Figure 3.20.

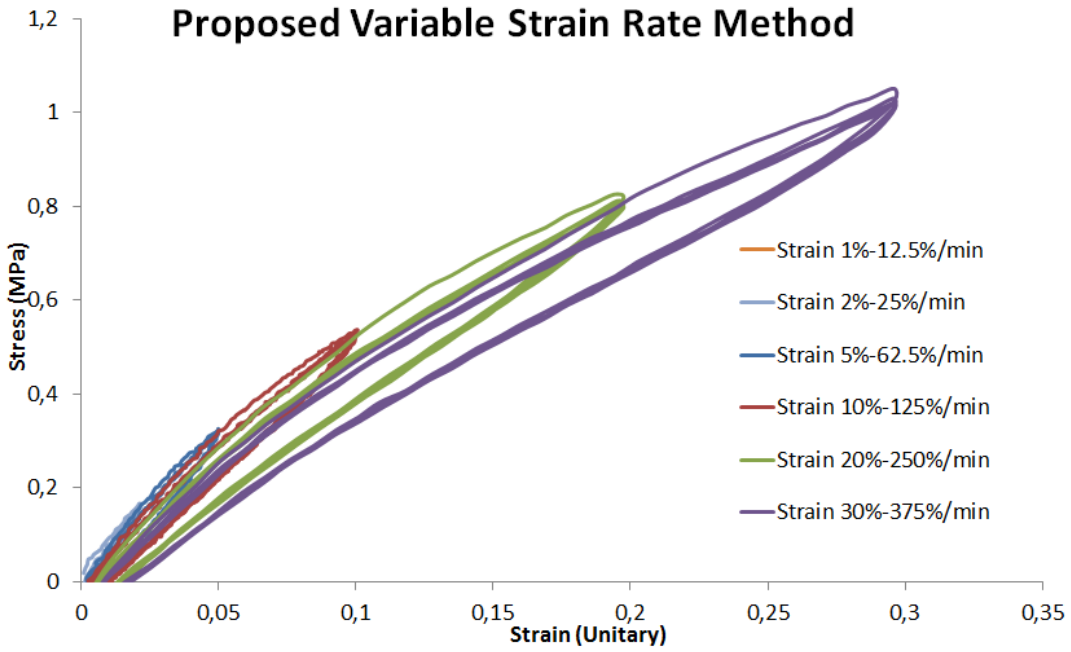

Figure 3.20: Shear planar mechanical conditioning test (3+1 cycles). In the progressive conditioning the sample is stretched in six strain levels.

Shear planar, compression and tensile specimens testing conditions are detailed in the following data tables (Table 3.6, Table 3.7 and Table 3.8):

Strain Level Nº	*Strain (%)*	*Strain Rate (%/min)*	*Displacement (mm)*	*Testing speed (mm/min)*
1	1	12.5	0.35	4.4
2	2	25	0.7	8.8
3	5	62.5	1.75	21.9
4	10	125	3.5	43.8
5	20	250	7	87.5
6	30	375	10.5	131.3

Table 3.6: Proposed characterisation method: Rates used in each set of 3+1 cycled stretch for the Shear Planar Samples on their respective tests

Strain Level Nº	*Strain (%)*	*Strain Rate (%/min)*	*Displacement (mm)*	*Testing speed (mm/min)*
1	1	12.5	0.135	1.7
2	2	25	0.27	3.4
3	5	62.5	0.675	8.4
4	10	125	1.35	16.9
5	20	250	2.7	33.8
6	30	375	4.05	50.6

Table 3.7: Proposed characterisation method: Rates used in each set of 3+1 cycled stretch for the Compression Samples on their respective tests

Strain Level Nº	*Strain (%)*	*Strain Rate (%/min)*
1	1	12.5
2	2	25
3	5	62.5
4	10	125
5	20	250
6	30	375

Table 3.8: Proposed characterisation method: Rates used in each set of 3+1 cycled stretch for the Dumb-bell Samples on their respective tests

3.3 Results and discussion

3.3.1 Conditioning methods correlation in pure shear

In the later simulations performed by means of FEA, the selected ESED function is the Yeoh's model. In order to simplify the procedure, the *Yeoh's* model parameters can be fitted to shear planar experimental data [25].

In Figure 3.21, the conditioning methods presented in section 3.2.5.1 and 3.2.5.2 are correlated in shear planar. The unconditioned and progressive conditioning method seems to be very similar where the deviation is 1% between each other. The conditioning method, which gives the highest stiffness, is given by the progressive conditioning with equivalent strain rates. The later conditioning method has 1% and 5% of deviation at the unitary strain of 0.1 and 0.3 (/1) respectively.

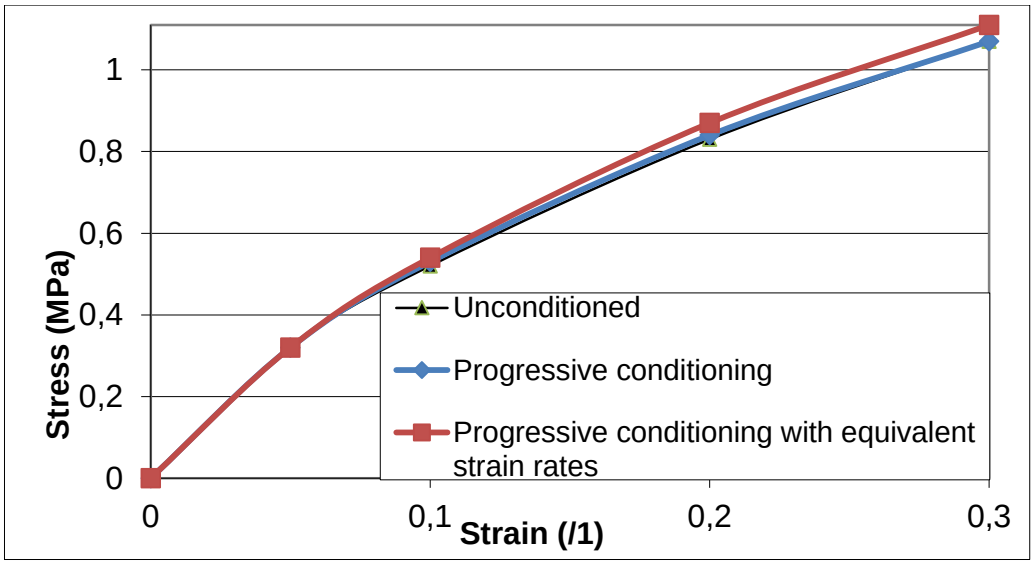

Figure 3.21: Comparison of different rubber conditioning methods.

3.3.2 Yeoh's models fitting to shear planar experimental data and its validation in tension and compression.

In order to verify that the use of shear planar experimental test is sufficient to calibrate *Yeoh's* model, the next verifications are carried out. The material fitting is performed by the use of ANSYS software and this material is called MAT1. Later, on the one hand, the pure shear specimen used to calibrate the *Yeoh's* model and, on the other hand, the tests of the other two experimentally tested tension and compression geometries are simulated by virtual meshes by means of FEA. Finally, the previous simulations are compared with their experimental data (see Figure 3.22).

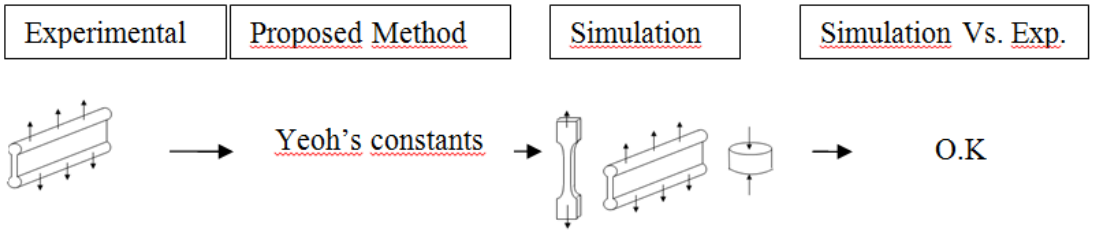

Figure 3.22: First, Yeoh's ESED function is fitted to shear planar experimental data. Second, the MAT1 characterisation is validated by means of reverse engineering.

The shear planar experimental data presented in this validation process is the experimental performed with the progressive conditioning with equivalent

strain rates (Figure 3.21). The Yeoh's parameters C_{10}, C_{20} and C_{30} calculated in the fitting process are 0.85407,-0.82742, 1.1348 MPa respectively.

The next Figure 3.23-A,B and C shows the experimental and simulation correlation in tensile, pure shear and compression specimens respectively. The mean and maximum normalized error (Eq. 3.29) gives values below 5 and 14.8 % respectively.

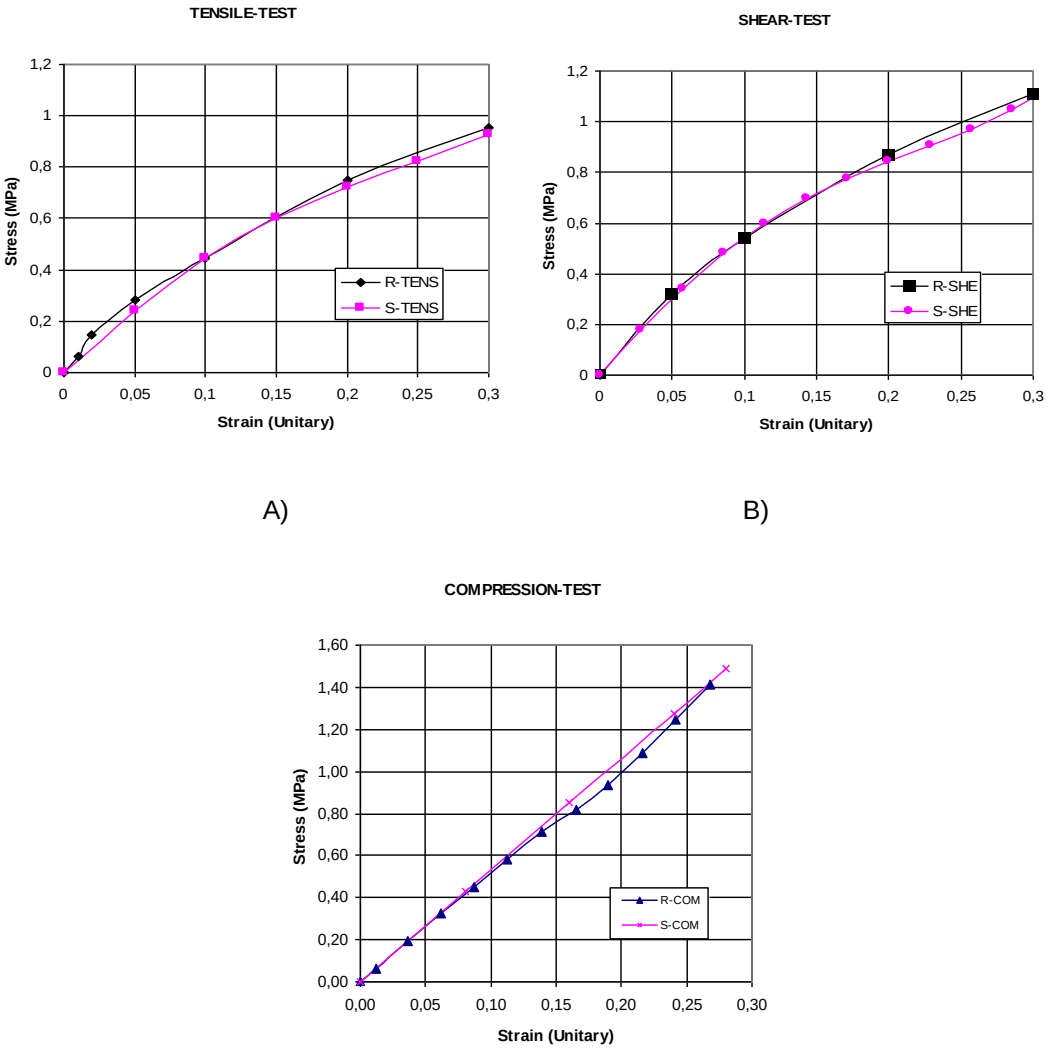

Figure 3.23: Simulation and correlation with the experiments of: A) Dumb-bell (tensile test), B) Shear planar test and C) Compression test. R- and S- means experimental and simulation result.

The agreement in the experimental and simulations correlation is acceptable.

3.3.3 Exhaust hanger: Simulations correlation to experimental data

The next table presents the *Yeoh's* parameters obtained by fitting the model to the studied three conditioning methods. These parameters will be used to do the stiffness predictions of the industrial case by means of FEA.

Method	C_{10}	C_{20}	C_{30}
Unconditioned	0.84622	-0.99511	1.4672
Progressive conditioning	0.85218	-0.95689	1.3503
Strain rate variable conditioning	0.85407	-0.82742	1.1348

Table 3.9: Yeoh's parameters (MPa) obtained in the fitting of the model to the shear planar experimental tests. Yeoh's parameters obtained from the different conditioning methods.

The comparison of the simulations of the industrial part (exhaust hanger) and the experimental tests using the previously mentioned three characterisation methods (section 3.2.5) is shown in Figure 3.24 and the normalized errors are presented in Table 3.10.

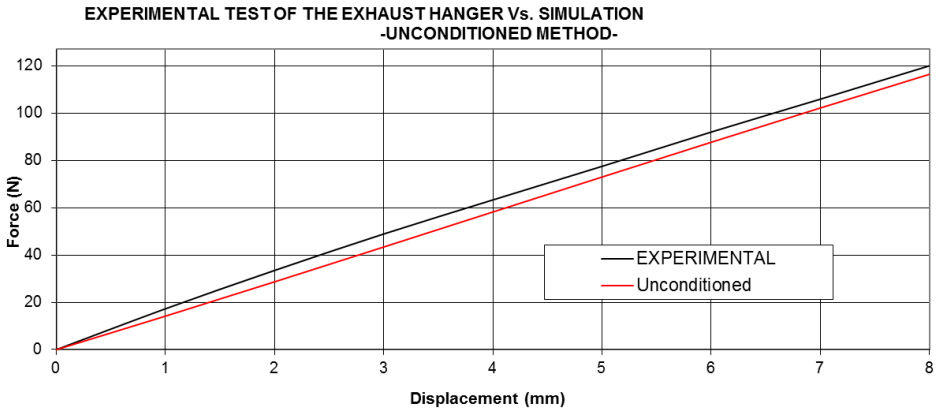

A)

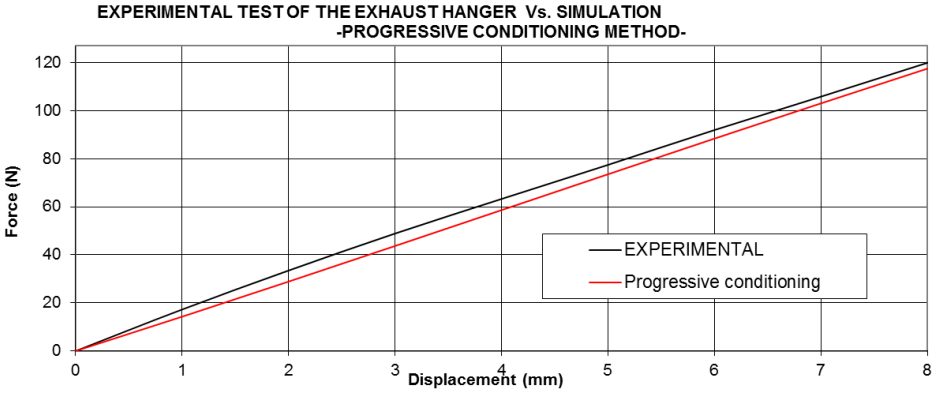

B)

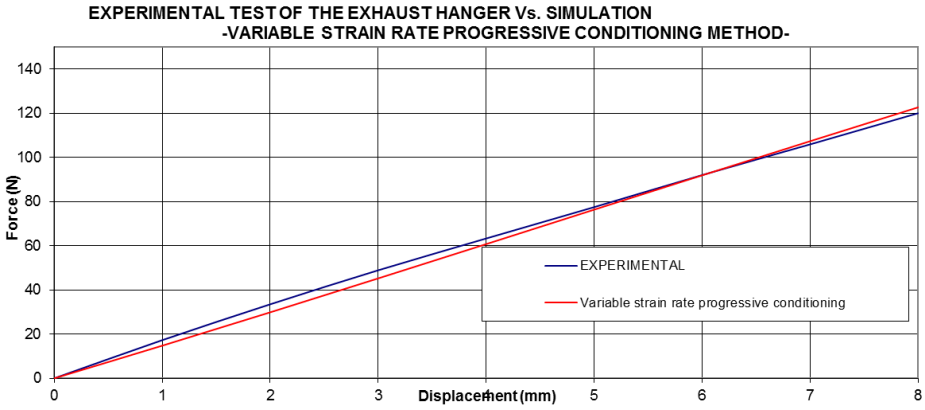

C)

Figure 3.24: Comparison of the industrial part experimental test and their simulations. The simulations are performed with Yeoh's parameters presented in Table 3.9. The simulations are performed with the fitting carried out with A) Unconditioned, B) Progressive conditioning and C) Variable strain rate in progressive conditioning methods.

Method	*Desviation %*	*Max desviation %*
Unconditioned	8.57	18
Progressive conditioning	7.81	17
Variable strain rate in progressive conditioning	5.25	15

Table 3.10: The simulations error respect to the Exhaust Hanger Experimental data. The maximum deviation is given when the tension load is 1 mm

The unconditioned method, which consists of a unique tension test using a quasi-static speed of 5%/min, does not take into account the Mullins effect. In order to evaluate this effect in both -the characterisation samples as in the industrial part- the best procedure is the application of the same number of conditioning cycles in both tests. However, this method does not contemplate the strain-rate dependence, which is one of the main factors to define the stiffness of the rubber. Hence, the global error is the highest.

The progressive conditioning method, which consists in the application of the same number of conditioning cycles in both tests using a very low testing speed of 15%/min, is very similar to the first method. This time, the influence of the Mullins Effect is evaluated as in the industrial part. Nevertheless, the global error remains high.

The proposed method (progressive conditioning with equivalent strain rates) gives the best results compared to the other two methods. In addition, correlating established first and second characterisation methods and the proposed method, the normalized errors are 2.97%, and 2.22% for the first and the second methods respectively.

In synthesis, the proposed characterisation method permits to describe all the main variables in the characterisation phase according to the definition of the loads and deformations applied to the industrial part. Then, the most proper method to predict the industrial part behaviour is the one proposed in this research.

CHAPTER 4 MODELLING THE DYNAMIC PROPERTIES OF RUBBER. AMPLITUDE AND FREQUENCY DEPENDENCY OF RUBBERS

This section is directed to review the behaviour of unfilled, filled and highly filled rubber compounds under cyclic dynamic loads. For this purpose, three rubber compounds are characterised dynamically with different frequency and amplitude conditions [139].

4.1 Theoretical background

4.1.1 Simple shear strain state

The simple shear is the more popular specimen type to characterise the dynamic properties of elastomers. This section reviews the simple shear state of strain which will be applied in this CHAPTER 4 to carry out the characterisation of the dynamic properties of elastomers.

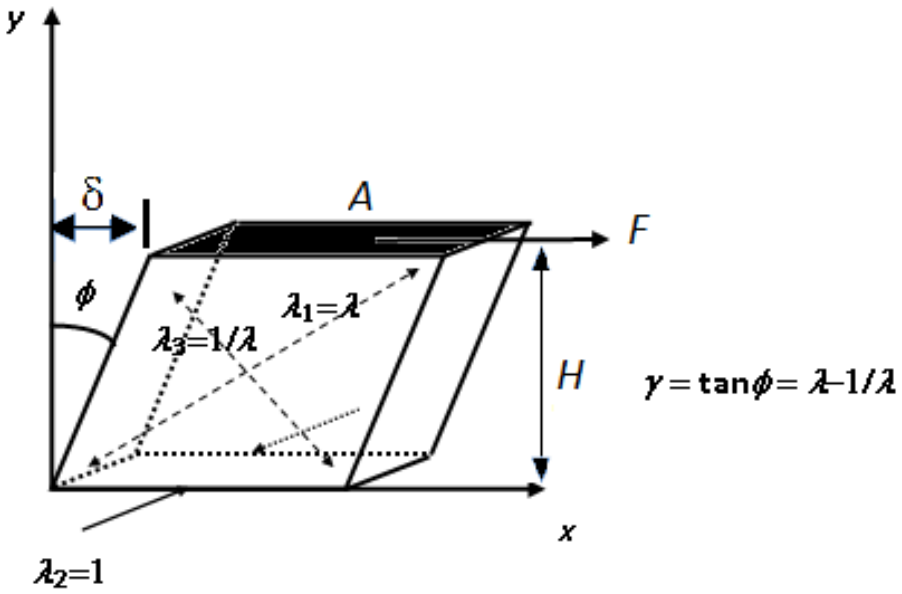

Figure 4.1: Simple shear: deformed shape

X_i *and* x_i are the coordinates in the original and deformed configuration respectively (Figure 4.1) and, in the simple shear case, the deformation is determined by:

$$x_1 = X_1 + \tan\phi X_3$$
$$x_2 = X_2 \qquad \textit{Eq. 4.1}$$
$$x_3 = X_3$$

where,

$$\tan\phi = \delta/H \qquad \textit{Eq. 4.2}$$

and where ϕ, δ, F and H are defined as the shear angle (direct shear strain), shear displacement , force and thickness respectively (Figure 4.1). There is only a displacement in the first direction, being proportional to X_3.

For simple shear deformations described in terms of the stretch ratio λ, the deformation gradient is:

$$[F] = \begin{bmatrix} 1 & 0 & \tan\phi \\ 0 & 1 & 0 \\ 0 & 0 & 1 \end{bmatrix} \qquad \textit{Eq. 4.3}$$

The Cauchy Green tensor and its inverse are:

$$[B] = FF^t = \begin{bmatrix} 1+\tan^2\phi & 0 & \tan\phi \\ 0 & 1 & 0 \\ 0 & 0 & 1 \end{bmatrix} \qquad \textit{Eq. 4.4}$$

$$[B^{-1}] = \begin{bmatrix} 1 & 0 & -\tan\phi \\ 0 & 1 & 0 \\ -\tan\phi & 0 & 1+\tan^2\phi \end{bmatrix} \qquad \textit{Eq. 4.5}$$

so the strain invariants in this strain state are equal

$$I_1 = tr(B) = I_2 = tr(B^{-1}) = 3 + \tan^2 \phi \qquad \textit{Eq. 4.6}$$

and the shear stress according to Rivlin's was found to be

$$\tau = 2\left[\frac{\partial W}{\partial I_1} + \frac{\partial W}{\partial I_2}\right]\tan \phi \qquad \textit{Eq. 4.7}$$

where τ is the shear stress and ϕ the rotation angle (Figure 4.1).

In this strain state, the area is not affected by the deformation and force *F* is applied on area *A* in parallel direction:

$$\tau = F/A \qquad \textit{Eq. 4.8}$$

Inserting Eq. 4.2 and Eq. 4.8 into Eq. 4.7, we arrive at the relation between shear forces and shear displacement in simple shear test:

$$F/A = 2\left[\frac{\partial W}{\partial I_1} + \frac{\partial W}{\partial I_2}\right]\delta/H \qquad \textit{Eq. 4.9}$$

For small strains used in linear theory of elasticity where the shear angle approach zero:

$$\tan \phi = \delta/H \approx \gamma \qquad \textit{Eq. 4.10}$$

As,

$$G_0 = \tau / \gamma \qquad \textit{Eq. 4.11}$$

The initial shear modulus can be obtained from Eq. 4.7 in the following way:

$$G_0 = \lim_{\tan\theta \to 0} \frac{\partial \tau}{\partial \gamma} = 2\left[\frac{\partial W}{\partial I_1} + \frac{\partial W}{\partial I_2}\right]_{I_1=I_2=3} \qquad \textit{Eq. 4.12}$$

Hence, comparing Eq. 4.12 and Eq. 3.15 for incompressible linear materials, the relation between the elastic and the shear modulus is $E_0=3G_0$. This equation reinforces the relation of the shear modulus and Young modulus concluded in section 1.1.2 (Eq. 1.9); it is valid for small displacements in elastomers.

In order to characterise the simple shear mechanical behaviour of rubber compounds, there are at least two types of generalised shear specimens that are explained in the next lines:

1.- Quadruple simple-shear testing specimen (Figure 4.2): This simple shear characterisation sample is defined in the *International ISO Standard* 1827:1991 [66] and in the Spanish *Spanish UNE Standard* 53630:2010 [65]:

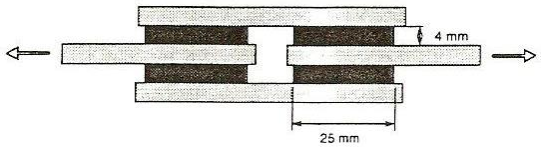

Figure 4.2: Quadruple simple shear characterisation sample

2.- Dual simple-shear testing specimens: This characterisation sample is defined in *ASTM D 945-92* [140].

The deformation achieved via these tests only approximates simple shear. In large deformations, the analysis neglects non-uniform deformation, loss of

plane strain conditions, and normal deformation to the shear plane, *Przybylo and Arruda* [137]. To solve this problem, there are two proposals:

- *Option A.-* The same authors *Przybylo and Arruda* [137] proposal is a single cubic specimen where the normal deformation to the shear plane was restricted by a special shear test fixture designed to fix the shear platen separation (Figure 4.3).

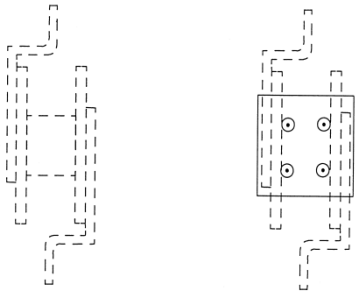

Figure 4.3: Dual simple shear characterisation sample: option A

- *Option B.-* Two rubber cylinders are connected to metal cylinders. The lateral ones are fixed and the central one is moved in the vertical direction. The recorded force is twice the shear force on each cylinder, and the loading head displacement is the deformation of each cylinder (Figure 4.4). However, finite element calculations of the test specimen show that a shear modulus obtained from this test has to be increased by 6 percent to yield the same values as the ideal simple shear test, indicating that a perfect simple shear load case is not obtained [141].

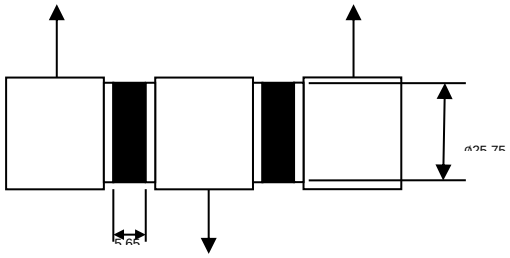

Figure 4.4: Dual simple shear characterisation sample: option B

Pure shear studied in subsection 3.1.2.2 and simple shear are related as explained in Annex II-D and E.

4.1.2 EPVE Model: Elastoplastic-Viscoelastic material model

In the experimental work (section 4.2) the behaviour of rubber under several amplitude and frequency conditions is studied. Section 4.3 is directed to develop a new FEM model which has the ability to fit the mentioned rubber behaviour. The model proposed in the section 4.3 is based on Austrell and Olsson's work. Hence, this section 4.1.2 is directed to review the model of the latter authors called EPVE (elastoplastic-viscoelastic) model in this report.

The present thesis develops the work started by *Austrell* [99] and continued by *Olsson and Austrell* [68,108] using an overlay method. The proposed model is presented in *Kareaga et al* [3] attached as Annex III The overlay method is used to combine various constitutive models programmed in commercial finite element software. As shown in Figure 4.28 or Figure 4.21, this method consists of the mesh superposition where the object to simulate is meshed and the mesh is copied at the same location. Then, the nodes are merged obtaining a final model composed of a number of superposed meshes with common nodes. The use of the overlay or mesh superposition technique explained in section 4.1.3.3 avoids the implementation of new complex constitutive models.

Both EPVE and the proposed MLVE with equivalent viscoelastic approach models are composed by several rheological elements. Consequently, a brief summary of mathematical approaches is reviewed.

In this work, the elastoplastic, multilinear and viscoelastic parts are called EP, ML and VE respectively.

4.1.2.1 Amplitude-dependence characterisation by means of elastoplasticity. Generalised frictional solid model.

This section develops the EP or generalised friction model. This model will be used to characterise the ML part of the proposed MLVE model with equivalent viscoelastic approach. The review is basically extracted from the work of *Austrell* [99,141] and *Olsson* [68,109].

Coulomb friction element.—

Figure 4.5: A) Coulomb friction element. B) Representation of possible stress situations

This element consists of two blocks which can slide against each other (Figure 4.5-A). This element cannot be applied by itself because it provides an infinite horizontal slope when it acts. Hence, this element cannot characterise the nonlinear cycle (Figure 4.5-B).

No sliding occurs while a stress equal to σ_{ff} is not developed in the element. Therefore, bellow the latter friction stress, the element blocks are fixed to each other; so, no strain is produced in these conditions.

In brief, the next situations can be produced:

$\sigma_f = 0$ when $\sigma \langle \sigma_{ff}$

$\sigma_f = \sigma_{ff}$ when $\sigma \rangle \sigma_{ff}$

$\sigma_f = \sigma_{ff}$ when $\varepsilon \rangle 0$

$\sigma_f = -\sigma_{ff}$ when $\varepsilon \langle 0$

Where σ, σ_f and σ_{ff} are the acting stress, stress in the frictional element and the yield stresses respectively.

Elastoplastic element.—

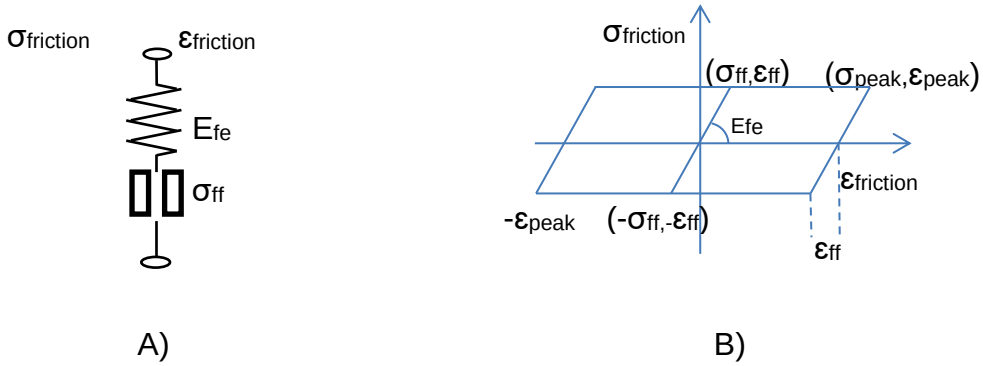

Figure 4.6: A) an elastoplastic element. B) Hysteresis loop for harmonic excitation of amplitude $\varepsilon_{0=}\varepsilon_{peak}$.

This model consists of a spring and friction elements in series (Figure 4.6-A). It is similar to the Maxwell model but, in this instance, the dashpot is substituted by the Coulomb friction element.

As in the previous element, while the stress in the chain is less than σ_{ff}, the two blocks in the Coulomb element are fixed together and a linear response is given by the spring. Once the maximum stress level σ_{ff} is reached, sliding in the Coulomb element occurs.

In brief, the next situations can be produced:

- $\sigma_{friction} = E_{fe}\varepsilon_{friction}$ while $\varepsilon_{friction} < \varepsilon_{ff}$
- $\sigma_{friction} = \sigma_{ff}$ while $\varepsilon_{friction} \geq \varepsilon_{ff}$

where $\varepsilon_{ff} = \sigma_{ff}/E_{fe}$ denotes the strain level at which sliding is produced.

When a cyclic load is applied, the hysteresis loop adopted by this model is represented in Figure 4.6-B, which is the same for any frequency.

According to section 1.3.2, the stiffness can be calculated as follows:

When $\varepsilon_{friction}>\varepsilon_{ff}$ then,

$$|E^*| = \sigma_{peak}/\varepsilon_{peak} \qquad Eq.\ 4.13$$

The area U_c which represents the dissipated energy for strain cycle, is:

$$U_c = 4\sigma_{ff}\left(\varepsilon_{peak} - \varepsilon_{ff}\right) = 4\sigma_{ff}\left(\varepsilon_{peak} - \sigma_{ff}/E_{fe}\right) \qquad Eq.\ 4.14$$

While $\varepsilon_{peak} < \varepsilon_{ff}$, no sliding is produced and this model behaves as a linear spring. Consequently, the modulus will be E_{fe} and no damping is present.

The hysteresis loop can be evaluated using the next algorithm presented in [99]. As shown previously, the strain is the summation of elastic and frictional strain $\varepsilon_{friction} = \varepsilon_{fe} + \varepsilon_{ff}$. Hence, the incremental relation used to obtain the algorithm is:

$$\Delta\varepsilon_{friction} = \Delta\varepsilon_{fe} + \Delta\varepsilon_{ff} \qquad Eq.\ 4.15$$

The stress-strain relationship must be evaluated for the increments of strain and stress. The objective is to obtain the stress increment $\Delta\sigma_{friction}$ which can be derived from the elastic part because the stress is the same in both elastic and friction elements given by:

$$\sigma_{friction} = E_{fe}\varepsilon_{fe} \qquad Eq.\ 4.16$$

In that way, the stress increment can be expressed as,

$$\Delta\sigma_{friction} = E_{fe}\Delta\varepsilon_{fe} \qquad Eq.\ 4.17$$

The required final stress is evaluated from the known current stress. To evaluate the latter value, a trial stress is determined from the assumption that the strain increment is purely elastic:

$$\sigma_{trial} = \sigma_{friction} + E_{fe}\Delta\varepsilon_{friction} \qquad Eq.\ 4.18$$

where $\sigma_{friction}$ is the current stress.

The maximum stress is limited to $-\sigma_{ff}<\sigma_{friction}<\sigma_{ff,}$ then,

- If $\sigma_{friction} > \sigma_{ff}$, at least one part of the strain increment is plastic. If this increment is considered as purely plastic, then, $\Delta\varepsilon_{fe} = 0$; hence:
- If $|\sigma_{trial}| > \sigma_{ff}$, then $\sigma_{friction} = \pm\sigma_{ff}$

When the previous condition is fulfilled, the stress has to be scaled back. This factor is defined as $\alpha = \sigma_{friction}/\sigma_{trial}$, then the stress $\sigma_{friction} = \alpha\sigma_{trial}$.

- If $|\sigma_{trial}| \leq \sigma_{ff}$, then $\sigma_{friction} = \sigma_{trial}$ and the strain increment is purely elastic.

Finally, the algorithm used to evaluate the stress is defined as [99]:

$i = 1,2,3$ ...

$\Delta\varepsilon_{friction} = \varepsilon_{friction}^{i+1} - \varepsilon_{friction}^{i}$

$\sigma_{trial} = \sigma_{friction}^{i} + E_{fe}\Delta\varepsilon_{friction}$

$\alpha = \sigma_{friction}/\sigma_{trial}$

If $\alpha > 1\ then\ \alpha = 1$

$\sigma_{friction}^{i+1} = \alpha\sigma_{trial}$

A simple frictional solid model.—

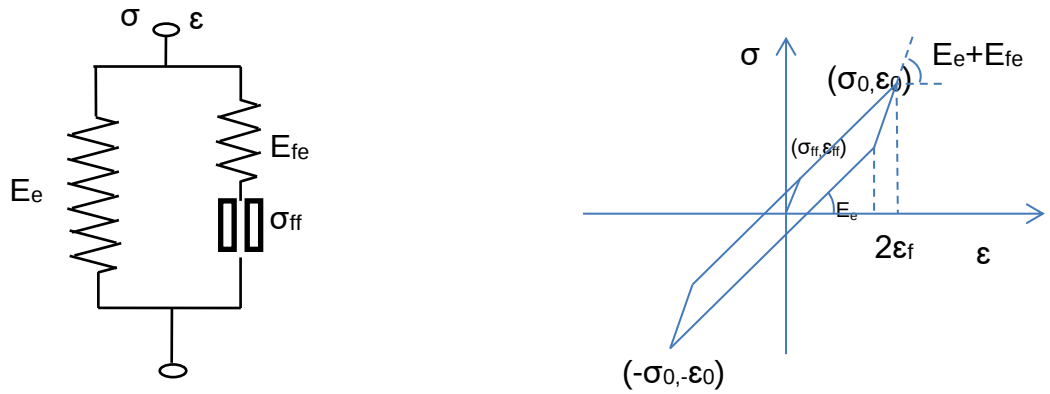

A) B)

Figure 4.7: A) A simple frictional solid model B) Hysteresis loop for harmonic excitation of amplitude ε_0.

This model describes better the dynamic modulus and damping than the simple elastoplastic element. When the stress in the elastoplastic element is less than σ_{ff}, the two blocks in the Coulomb element are fixed together and a linear response is given by the spring. Hence, the response of the whole model is linear, given by the addition of two linear springs. However, when the maximum stress level σ_{ff} is reached, sliding in the coulomb element occurs and the model behaves nonlinearly (Figure 4.7-A-B).

$$\sigma = \sigma_e + \sigma_{friction} \qquad \textit{Eq. 4.19}$$

In this model two situations may appear:

1.- $\varepsilon < \varepsilon_{ff} = \frac{\sigma}{E_{fe}+E_e} = \frac{\sigma_{friction}}{E_{fe}} = \sigma_e/E_e$: no sliding is produced in the Coulomb element and the elasoplastic chain behaves as a linear spring. Hence, there will be no hysteresis and damping will be zero. Then, the modulus E given by the whole model will be the summation of both springs E_e+E_{fe}; therefore the stress of the whole model is defined as

$$\sigma = E_e\varepsilon + E_{fe}\varepsilon \qquad \textit{Eq. 4.20}$$

2.- $\varepsilon \geq \varepsilon_{ff} = \sigma_{ff}/E_{fe}$: sliding occurs in the Coulomb element then

$$\sigma = E_e\varepsilon + \sigma_{ff} \qquad \textit{Eq. 4.21}$$

$$|E^*| = \frac{\sigma_{peak}}{\varepsilon_{peak}} = \frac{\sigma_0}{\varepsilon_0} = \frac{\sigma_{ff} + E_e\varepsilon_0}{\varepsilon_0} = E_e + \frac{\sigma_{ff}}{\varepsilon_0} \qquad \textit{Eq. 4.22}$$

The difference with the elastoplastic element is due to the peak stress value, which is higher than the friction Zener model because of the elastic spring contribution in parallel. However, the hysteresis area is the same as in the elastoplastic element (Eq. 4.14).

In addition to what is explained in section 1.3.1, this model can be used to simulate sinusoidal dynamic tests. If the mentioned test is simulated with the latter model, in contrast to what happens in the viscoelastic Zener model, the dynamic modulus changes with the load strain amplitude (Figure 4.8): $E^*_1 > E^*_2$.

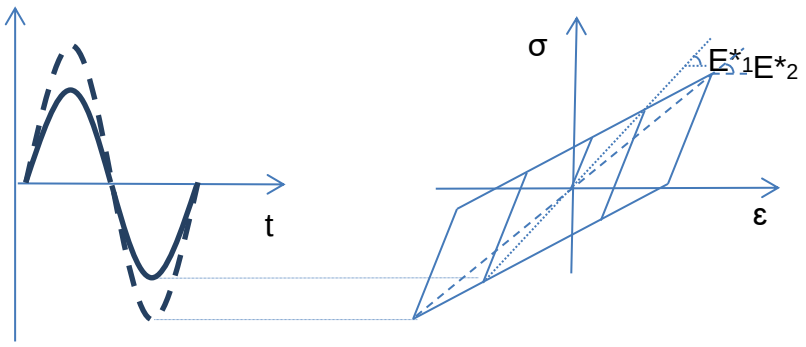

A) B)

Figure 4.8: Sinusoidal Dynamic test: A simple frictional solid model. Nonlinear plasticity. The dynamic modulus changes with the load strain amplitude. A) Two sinusoidal loads with different strain amplitude are presented. B) The dynamic modulus changes with the load strain amplitude: $E^*_1 > E^*_2$.

Generalisation of the simple frictional solid Model.—

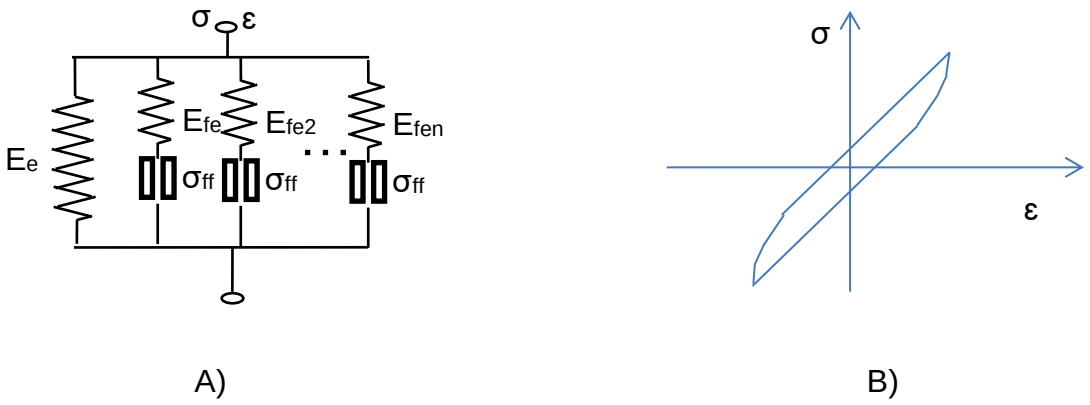

Figure 4.9: A) Generalised frictional solid model B) Hysteresis loop for harmonic excitation of amplitude ε_0.

The Zener model is a good approximation to rubber material behaviour but it could be optimized including *N* elastoplastic chains in parallel. In this way, the hysteresis loop gets a smoother shape and fits better to experimental results (Figure 4.9 & Figure 4.10).

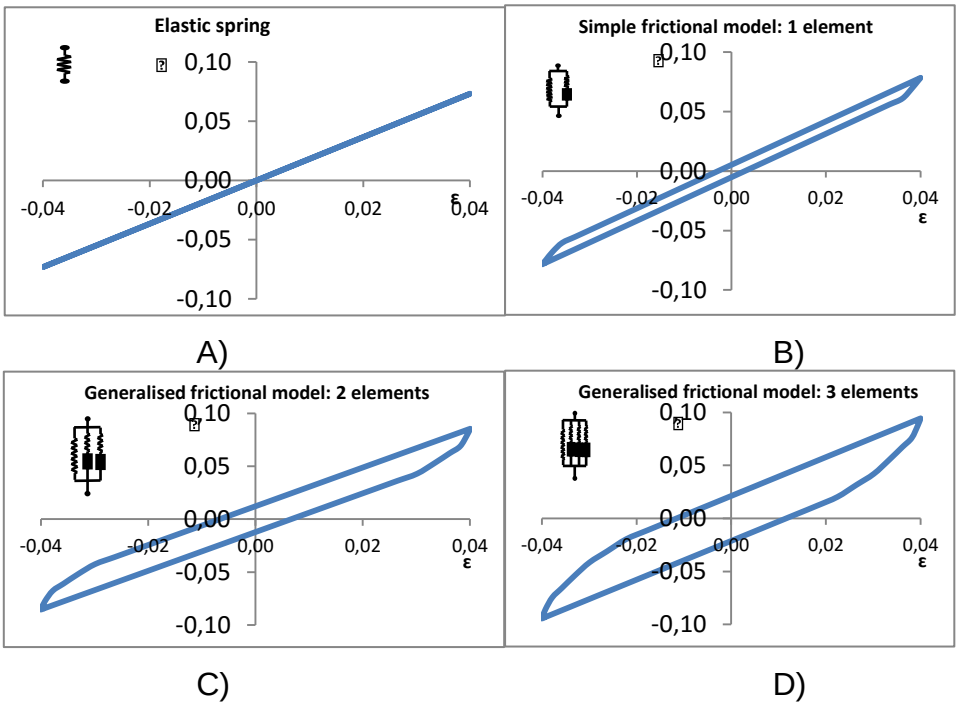

Figure 4.10: Static characterisation: A) Elastic spring. B) Simple frictional model. C) Generalised two frictional elements model. D) Generalised three frictional elements model.

Total stress is calculated by adding the stress of each element:

$$\sigma = \sigma_e + \sum_{i=1}^{N} \sigma_{friction}^{i} \qquad \textit{Eq. 4.23}$$

In this model, two situations may appear again:

1.- $\varepsilon < \varepsilon_{ffi} = \sigma_{friction,i}/E_{fe,i}$: no sliding occurs in the Coulomb element and the friction Maxwell chain behaves as a linear spring. Hence, there will be no hysteresis and damping will be zero and

$$\sigma_{friction}^{i} = E_{fei}\varepsilon \qquad \textit{Eq. 4.24}$$

2.- $\varepsilon \geq \varepsilon_{ffi} = \sigma_{ffi}/E_{fe,i}$: sliding occurs in the Coulomb element then

$$\sigma_{friction}^{i} = \sigma_{ffi} \qquad \textit{Eq. 4.25}$$

The fitting procedure of the mentioned model can be performed as proposed by *Austrell* [99] or by *Ahmadi et al* [111].

a) <u>Parameters evaluation method Nº1</u>: <u>Initial loading curve fitting</u>:

This method was proposed by *Austrell* [99] and a similar method was also used by *Ahmadi et al* [111].

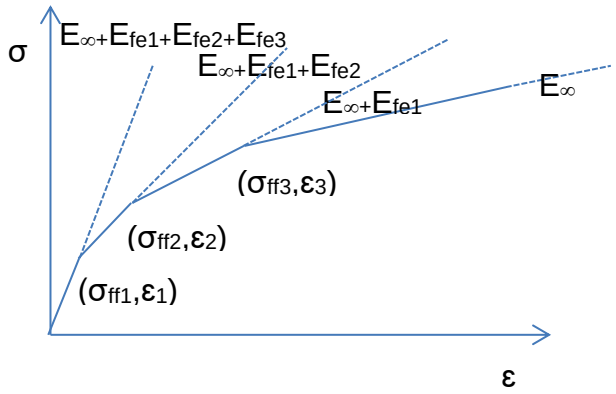

Figure 4.11: Initial loading curve of the generalised frictional solid model

The model parameters can be obtained from the initial loading curve (Figure 4.11). Each friction Maxwell chain yield in the order 1,2,3,…. The parameters of each element are determined directly as follows:

$$E_{fei} = \frac{\sigma_{ffi} - \sigma_{ffi-1}}{\varepsilon_i - \varepsilon_{i-1}} - \frac{\sigma_{ffi+1} - \sigma_{ffi}}{\varepsilon_{i+1} - \varepsilon_i} \qquad \textit{Eq. 4.26}$$

And the yield stress of each element is defined as

$$\sigma_{ffi} = E_{fei}\varepsilon_i \qquad \textit{Eq. 4.27}$$

These equations can be rewritten in function of the strain and stress to obtain the breakpoints directly:

$$\sigma_i = \sum_{j=1}^{i-1} E_{fej}\varepsilon_j + \left(E_\infty + \sum_{j=i}^{n} E_{fej} \right) \varepsilon_i \qquad \textit{Eq. 4.28}$$

$$\varepsilon_i = \sigma_{ffi} / E_{fei} \qquad \textit{Eq. 4.29}$$

In the case of the first point where *i=1*, the first term of Eq. 4.28 disappears.

b) <u>Parameters evaluation method Nº2: Load cycle fitting presented in this thesis</u>:

This characterisation method is developed in section 4.3.1.1.

The hyperelastic spring.—

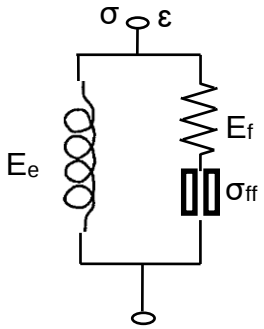

Figure 4.12: Nonlinear frictional solid model

The generalised frictional solid model should be improved using a nonlinear spring instead of linear one, as *Austrell et al* [108] proposed, where the nonlinear spring is modelled by a hyperelastic model (see section 1.2.1). To simplify the fitting of the model, initially the nonlinear spring may be considered as a linear spring to calculate the approximated initial shear modulus *G*. The previously calculated initial shear modulus can be used to fit the nonlinear model using the equivalences of the mentioned modulus with C_{ij} constant of the hyperelastic models. For example, according to *Yeoh* [25],

$$W = C_{10}(I_1 - 3) + C_{20}(I_1 - 3)^2 + C_{30}(I_1 - 3)^3. \qquad \textit{Eq. 4.30}$$

For simple shear, the shear stress of the Yeoh's model is given as a function of the shear strain γ as follows, *Olsson and Austrell* [110],

$$\tau = 2C_{10}\gamma + 4C_{20}\gamma^3 + 6C_{30}\gamma^5 \qquad \textit{Eq. 4.31}$$

On the one hand, parameter C_{10} governs the initial shear modulus G_0

$$C_{10}=G_0/2 \qquad \textit{Eq. 4.32}$$

and C_{20} as C_{30} the nonlinear elastic response. Its equivalence with shear modulus *G* (from [108]) can be written as follows:

$$W = \frac{G_0}{2}(I_1 - 3) - 0.1\frac{G_0}{2}(I_1 - 3)^2 + 0.06\frac{G_0}{2}(I_1 - 3)^3 \qquad \textit{Eq. 4.33}$$

Another hyperelastic models and its equivalences with *G* modulus are detailed in section 1.2.1.

4.1.2.2 Rate-dependence characterisation by means of Prony series. Linear viscoelasticity of rubber

For a pure viscous material, all internal stresses are a function of the instantaneous strain rate. This material may not recover its original shape, even when the applied stress is removed. The mechanical energy supplied to the system is dissipated as heat. Reciprocally, pure elastic material efforts are based only on the instantaneous deformation. This material recovers its original shape upon removal of the applied stress.

A classical approach to the description of the response of materials which exhibit viscoelastic properties is based on the analogy with the response of mechanical elements. This involves the construction of viscoelastic models by combination of mechanical elements that simulate pure viscous and elastic properties, and therefore represent linear viscoelastic behaviour. Some of the most studied combinations of spring and dashpots are the Kelvin-Voigt model, Maxwell model or the Zener model. Discussions on these models may be found in *Austrell* [99] and *Gil-Negrete* [113]. Some other authors as *Park* [142] have done a good review of the work done in the field of classical viscoelasticity using generalised standard mechanical models for the characterisation of viscoelastic dampers.

Since the actual materials show nonlinear behaviour under large deformations, these models are only suitable for small displacement amplitudes, and are not suitable for predicting a continuous deformation or flow behaviour of the real materials.

For a viscoelastic material, internal stresses are a function not only of the instantaneous deformation (deformation, strain rate, etc.), but also the

deformation history. In real materials, the most recent history is more important than the most distant, so they may be defined as materials with weak memory.

In the case where both stress and deformation are of infinitesimal magnitude, their relationships over time can be described by means of linear differential equations with constant coefficients. It will define a linear viscoelastic behaviour, which means that the relationship between stress and deformation is only a function of time and does not depend on the magnitude of the load. More specifically, it only defines the proportionality of the relaxation rate to the instantaneous stress σ_0 and all the tests done with different initial strains are proportional.

These models are purely phenomenological. They do not enlighten the molecular and physical processes that take place, but they are particularly useful for predicting the response of a material under conditions of creep and relaxation and even under complex loading conditions. In addition, they can give a clearer picture of the general nature of the viscoelastic response.

These time domain viscoelastic models can provide an accurate description of the frequency dependent behaviour of rubber materials.

A classical approach to the modelling of linear viscoelastic behaviour employs a mechanical model composed of linear springs and dashpots, and the stress-strain equation for such a model involves standard differential operators. A general form of the stress-strain equation in differential operators is given by *Fung* [115] in Eq. 1.110.

In Annex II-F, one-dimensional simple material models have been described in terms of their constitutive differential equations.

Generalisation of the Maxwell model.—

This model is based on the Zener model. One or more Maxwell chains are added to that model to improve the fitting of experimental data (Figure 4.13).

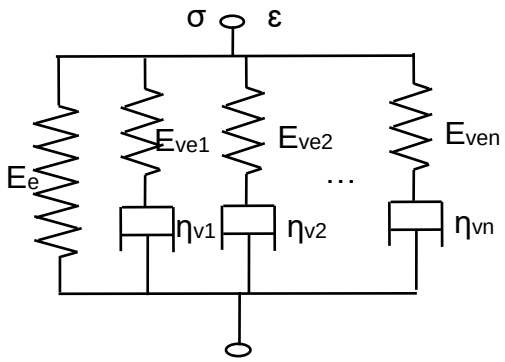

Figure 4.13: Generalisation of the Maxwell model.

Considering a relaxation test, the total stress in this model will be obtained with the addition of the elastic stress to the solitary spring of stiffness E_e which is known as E_∞, plus the summation of stresses in each Maxwell element.

These viscoelastic models can be written so that they can characterise the mechanical behaviour as a function of both time and frequency. When these models are written according to time, they can be used for characterising the creep and stress relaxation tests. This thesis will examine the last mentioned tests because these latter are the most related to the objectives of this thesis.

The generalised Maxwell model (Figure 4.13), widely used to characterise the modulus functions of linear viscoelastic media, consists of a spring and *N* Maxwell units connected in parallel *Tschoegl* [143].

$$\sigma_0 = \sigma_\infty + \sum_{i=1}^{N} \sigma_{ve,i} \qquad \textit{Eq. 4.34}$$

$$\sigma = \varepsilon_0 \left(E_\infty + \sum_{i=1}^{N} E_{ve,i} e^{\frac{-t}{\tau_i}} \right) \qquad \textit{Eq. 4.35}$$

$$E_{ve}(t) = E_\infty + \sum_{i=1}^{N} E_{ve,i} e^{-\frac{t}{\tau_i}} \qquad \textit{Eq. 4.36}$$

where τ_i is the relaxation time for each Prony component E_{vei}.

In this model, when the time is zero (*t=0),* the instantaneous modulus E_o is

$$E_0 = E_\infty + \sum_{i=1}^{N} E_{vei} \qquad Eq.\ 4.37$$

where E_∞ is the long term or the relaxed modulus at ($t=\infty$) , and E_{vei} and τ are the relaxation modulus and relaxation time respectively; the relaxation time of the i^{th} Maxwell element defined by $\tau_i = \eta_i / E_{vei}$ where η_i is the viscosity of the dashpot unit. The typical term under the summation symbol in the previous equation represents the relaxation modulus of the i^{th} Maxwell unit. The series expression in the equation is often referred to as a Prony series.

Findley et al [144] studied some common models including the generalised Voigt model and generalised Maxwell model.

Prony series in time domain.—

This section is developed in detail in Annex II-G.

The Prony series can be used to characterise the variation of relaxation modulus of elastomers subjected to a constant deformation Eq. 4.36,

If we call *E(t)* the relaxation modulus of tensile stresses. The limits take the following values:

$$E_\infty = \lim_{t \to \infty} E(t)$$

$$E_0 = E(0)$$

A dimensionless relaxation modulus is defined as follows:

$$\alpha_i = \frac{E_{ve,i}}{E_0} \qquad Eq.\ 4.38$$

The summation of α_i should be less than or equal to 1. If the summation of α_i is equal to 1, that means that *E* (t=∞)=0.

Hence, Prony series can be rewritten as follows,

$$E(t) = E_0\left[\alpha_\infty + \sum_{i=1}^{N} \alpha_i e^{-\frac{t}{\tau_i}}\right] \qquad Eq.\ 4.39$$

If two extremes of time are studied, one extreme is the instantaneous shear moduli at time *t* equal to 0 which gives the full stiffness. Hence,

$$E(0) = E_0\left[\alpha_\infty + \sum_{i=1}^{N} \alpha_i\right] \qquad Eq.\ 4.40$$

This implies that the summation of the input relative moduli α_i must be less than or equal to 1.

On the other extreme, where time is infinite, the relative modulus α_∞ represents the percentage of remaining stiffness, which is given by:

$$E(\infty) = E_0[\alpha_\infty] \qquad Eq.\ 4.41$$

In brief, T_i is the relaxation time for each Prony component $E_{ve,i}$. E_o is the instantaneous modulus (t=0) whereas E_∞ is the long-term modulus ($t=\infty$).

Prony series in frequency domain.—

In addition to the explained in section 1.3.1, this model can be used to simulate sinusoidal dynamic tests.

Prony series generally defined in time domain can be converted to frequency domain with the application of the Fourier transformation. This section is developed in detail in Annex II-H. The final equations obtained in Annex II-H are the same as those given by *Bergström* [145]:

$$E^*(\omega) = E_\infty + \sum_{j=1}^{n} E_{vej} \frac{i\omega\tau_j}{1 + i\omega\tau_j} \qquad \textit{Eq. 4.42}$$

$$E'(\omega) = E_0 - \sum_{i=1}^{N} E_{ve,i} + \sum_{i=1}^{N} \frac{E_{ve,i}\tau_i^2\omega^2}{1 + \tau_i^2\omega^2} \qquad \textit{Eq. 4.43}$$

$$E''(\omega) = \sum_{i=1}^{N} \frac{E_{ve,i}\tau_i\omega}{1 + \tau_i^2\omega^2} \qquad \textit{Eq. 4.44}$$

Note that this model do not depend on the imposed amplitude.

4.1.2.3 Complete response modelling. Combination of rate and amplitude dependence: Elastoplastic-viscoelastic model (EPVE model)

This section explores how the models explained in sections 4.1.2.1 and 4.1.2.2 could be used to characterise the dynamic properties of filled rubbers in various frequency and amplitude conditions.

The nonlinearization of the pure viscoelastic Maxwell model can be performed with the addition of frictional elements. The studied friction models are rate-independent, which means that no viscous effects are modelled.

The simplest model of the generalised Maxwell model is obtained connecting the Zener model and the corresponding frictional model in parallel (Figure 4.14). The total response of the model is the sum of the mentioned frictional and Zener models $\sigma = \sigma_{elastic} + \sigma_{viscous} + \sigma_{friction}$. It takes into account the elastomers elasticity, its strain rate-independent hysteresis (which is used to characterise the amplitude dependence) and the strain rate-dependence all together.

This simplest model was studied by *Austrell* [99] which consist of a simple five-parameter model (Figure 4.14).

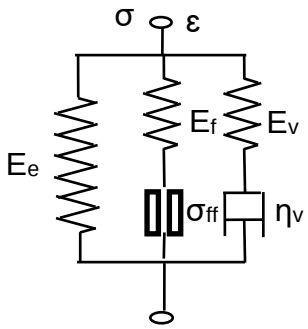

Figure 4.14: Nonlinear viscoelasticity. Five-parameter model.

This five-parameter model can be expanded by the addition of more viscous and frictional elements in parallel (Figure 4.15) obtaining better fittings to experimental data.

$$\sigma = \sigma_{elastic} + \sum_{i=1}^{N} \sigma_{friction}^{n} + \sum_{j=1}^{M} \sigma_{viscous}^{m} \qquad \textit{Eq. 4.45}$$

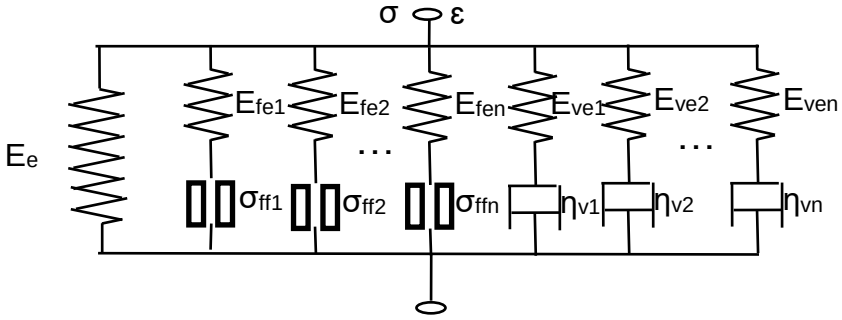

Figure 4.15: EPVE Model: Generalised Maxwell model.

Olsson [146] concluded that this model has limitations. On the one hand, the model assumes the independence between frequency and amplitude which was demonstrated that it is not completely correct in some materials. The use of Prony series to characterise the rate-dependency implies that the model does not take into account the amplitude. Hence, the frequency dependence will be the same for all amplitudes and the frequency sweeps done with different amplitudes will be perfectly parallel. Then, the EPVE model does not take into account the change of the stiffening slope as frequency increases at different amplitudes. The latter stiffening effect is reviewed in section 1.3.3 and verified with our materials in the experimental section 4.2.

On the other hand, the mentioned generalised Maxwell model does not include any damage effects. *Olsson* [146] concludes that the model was valid for correctly conditioned materials without damage effects. He studied the possibility to introduce the Mullins effect using Miehe's model [44].

4.1.3 Finite element method theory and application with ANSYS

4.1.3.1 Preliminary considerations

As mentioned before, the elastoplastic-viscoelastic model (EPVE model) is composed by three types of different simple material models. It is needed to take into account how these models are programmed in the FE-Code that it will be used to feed the models parameters correctly. This time, the FE-Code that is used is ANSYS 14.0

On the one hand, this section is focused on defining the material models used in ANSYS to build the generalised Maxwell model and, on the other hand, it focuses on the explanation of the way to transform the parameters obtained in the characterisation step in parameters used by ANSYS.

The characterisation sample is the simple shear specimen. Then, the obtained parameters are shear modulus G_0 for elastic springs, shear yield τ_{ff} stress for Coulomb friction elements and relaxation G_{ve} modulus and relaxation time τ_t for Maxwell elements.

The material models used in ANSYS to characterise the EPVE model are:

1.- The elastic behaviour can be modelled as (linear) elastic spring where Young modulus E_0 is required, or as hyperelastic (nonlinear) spring where the initial shear modulus G_0 is required for Neo-Hookean constitutive model.

2.- Elastoplastic model: Bilinear kinematic (BKIN) where initial Young modulus E_0 and the tensile yield stress σ_{ff} are required.

3.- Viscoelastic or Prony series: where dimensionless relaxation modulus and relaxation times are required. The relation between relaxation modulus and dimensionless relaxation modulus is described in section 4.1.2.2.

Elastomers are considered isotropic and completely incompressible so that the relation *E=3*G* (Eq. 1.9) is applied.

The shear modulus *G* is normally obtained by pure shear specimen test. This time, the used specimen is the simple shear specimen. In Annex II-D and E, the equivalence between both pure and simple shear specimens for small strains is demonstrated.

To convert shear yield stress τ_{ff} in tensile yield stress σ_{ff} as required in ANSYS the relation (see Annex II-I),

$$\sigma_{ff} = \sqrt{3}.\tau_{ff} \qquad Eq.\ 4.46$$

4.1.3.1.1 Elasto Plastic Constitutive Models in Finite Element Analysis. ANSYS Software.

In this section, different elasto-plastic models will be described in order to clarify the possibilities that these constitutive models offer in codes such as ANSYS.

The FEA code ANSYS offers a huge variety of material models. Inside the structural analysis group (thermal, fluid, electromagnetic, acoustic, piezoelectric, piezoresistive and thermoelectric materials could also be defined), mainly linear or nonlinear materials can be defined.

For linear materials, elastic properties are defined which can be further classified as isotropic, orthotropic or anisotropic. The simplest option is to consider the material isotropic since only two constants are needed to define the material card. These two constants are the elastic modulus (*E* in ANSYS) and the Poisson's ratio (*PRXY* in ANSYS). In the case of the orthotropic behaviour, 9 constants are needed to be defined. And in the case of the anisotropic behaviour, up to 21 constants could be specified.

For an elastic isotropic consideration, the elastic modulus and Poisson's ratio can be calculated from a standardised tensile test.

Concerning the present thesis, the interest has not only been centred on the definition of the elastic properties but also on the generation of material data cards above the yield point. Due to this, nonlinearity and plasticity have to be also considered in the material specification. This can be carried out by the use of nonlinear material models in ANSYS. Inside the nonlinear material models, elastic and inelastic classifications can be found. Elastic nonlinear material models cover mainly hyperelastic material equations for elastomeric material behaviour. They also cover multilinear elastic behaviour, but none of them are useful for hysteretic studies.

Inelastic nonlinear material models are the so-called elasto-plastic material constitutive equations. These material models were originally created to characterise metallic materials behaviour. These constitutive models can also be classified into different groups in ANSYS: rate independent (studied in this thesis work), rate dependent, non-metal plasticity, cast-iron and shape memory alloy.

The rate independent consideration does not take into account testing rate effects in the stress-strain properties of the material. This approach can be used for cycled elastomeric materials when the component to be studied is required to support quasi-static loading conditions with no change of time (no transient effects).

The hardening rule describes the changing of the yield surface with progressive yielding, so that the conditions (i.e. stress states) for subsequent yielding can be established.

4.1.3.1.2 Yielding.

The yield criterion is used to relate multiaxial stress state with the uniaxial case. Tensile testing on specimens provides uniaxial data, which can easily be plotted on one-dimensional stress-strain curves.

The actual structure usually exhibits a multiaxial stress state. The yield criterion provides a scalar invariant measure of the stress state of the material which can be compared with the uniaxial case.

A common yield criterion is the Von Mises equation (also known as the octahedral shear stress or distortion energy criterion). In ANSYS notation, the Von Mises equivalent stress for a 3D space with normal (σ) and shear (τ) stresses is defined as:

$$\sigma_0 = \sqrt{\frac{1}{2}\left[\left(\sigma_x - \sigma_y\right)^2 + \left(\sigma_y - \sigma_z\right)^2 + \left(\sigma_z - \sigma_x\right)^2 + 6\left(\tau^2{}_{xy} + \tau^2{}_{yz} + \tau^2{}_{xz}\right)\right]} \qquad \textit{Eq. 4.47}$$

In tensor form, Eq. 4.47 can be expressed as:

$$\sigma_0 = \sqrt{\frac{3}{2} s : s} \qquad \textit{Eq. 4.48}$$

where s is the deviatoric stress, defined as the summation of the stress tensor and the hydrostatic stress:

$$\begin{aligned} s &= \sigma + pI \\ p &= -\frac{1}{3}\left(\sigma_x + \sigma_y + \sigma_z\right)\big) \end{aligned} \qquad \textit{Eq. 4.49}$$

The stress state can be separated into hydrostatic (dilatational) and deviatoric (distortional) components. The hydrostatic stress p is associated with the energy of volume change whereas the deviatoric stress s is associated with the change in shape.

$$\sigma = s - pI \qquad \textit{Eq. 4.50}$$

The Von Mises yield criterion states that only the deviatoric component causes yielding. If plotted in 3D principal stress space, the Von Mises yield surface is a cylinder. The cylinder is aligned with the axis $\sigma_1=\sigma_2=\sigma_3$. Note that if the stress state is inside the cylinder, no yielding occurs. This means that if the material is under hydrostatic pressure ($\sigma_1=\sigma_2=\sigma_3$), no amount of hydrostatic pressure will cause yielding.

Another way to view this is that stresses which deviate from the axis ($\sigma_1=\sigma_2=\sigma_3$) contribute to the Von Mises stress calculation *s*.

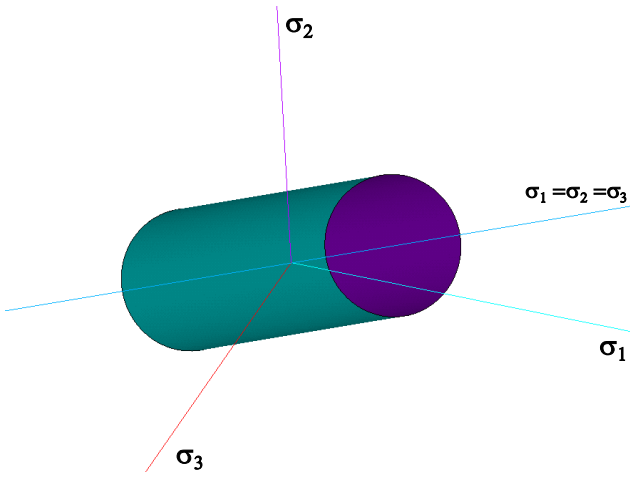

Figure 4.16: Von Mises yield surface in 3D space.

If viewed normal to the axis $\sigma_1=\sigma_2=\sigma_3$, the Von Mises yield criterion will look as shown below:

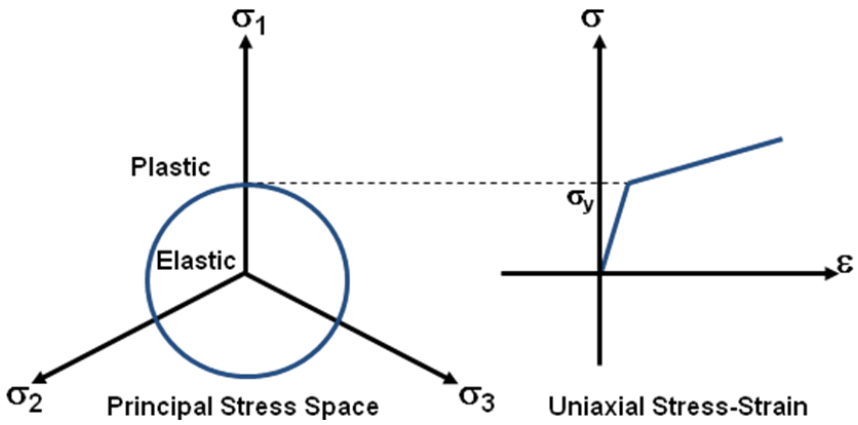

Figure 4.17: Von Mises yield surface in $\sigma_1=\sigma_2=\sigma_3$ axis.

Inside the yield surface, as mentioned earlier, behaviour is elastic. Note that the multiaxial stress state can exist anywhere inside the cylinder. At the edge of the cylinder (circle), yielding will occur. No stress state can exist outside the cylinder. Instead, hardening rules will describe how the cylinder changes with respect to yielding.

4.1.3.1.3 Hardening Rules.

The hardening rule determines how the yield surface changes (size, centre, shape) with plastic deformation. The hardening rule determines when the material will yield again if the loading is continued or reversed. This is in contrast to elastic-perfectly-plastic materials which exhibit no hardening – i.e., the yield surface remains fixed.

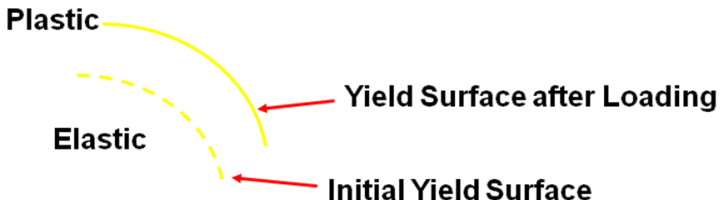

Figure 4.18: Evolution of yield surface as plastic deformation is being produced.

Two hardening rules are available: work or isotropic hardening and kinematic hardening. In work hardening, the yield surface remains centred about its initial centreline and expand in size as the plastic strains develop.

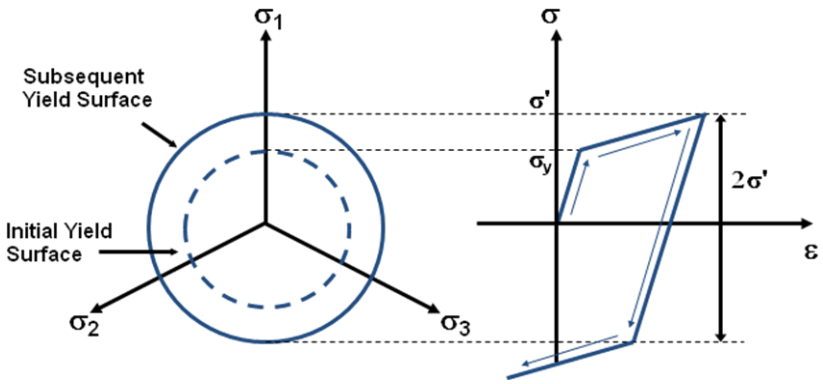

Figure 4.19: Isotropic hardening, evolution of yield surface.

Kinematic hardening assumes that the yield surface remains constant in size and the surface translates in stress space with progressive yielding.

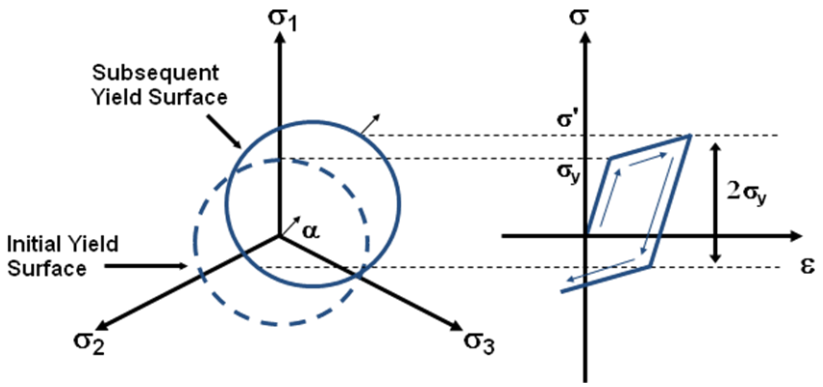

Figure 4.20: Kinematic hardening, evolution of yield surface.

This is in contrast to elastic-perfectly-plastic materials which exhibit no hardening – i.e., the yield surface remains fixed.

Different hardening behaviours can be specified inside the rate independent formulation in ANSYS:

- Isotropic Hardening Plasticity.
- Kinematic Hardening Plasticity.
- Combined Kinematic and Isotropic Hardening Plasticity.

Isotropic Hardening is appropriate for large strains with proportional loading. It is not suitable for cyclic loading applications.

Kinematic Hardening can be used for cyclic loading since it includes the Bauschinger effect (the greater the tensile cold working, the lower the compressive yield strength). However, kinematic hardening is recommended for situations where the strain levels are relatively small (less than 5-10 % true strain).

Combined isotropic and kinematic hardening is an advanced plasticity option which uses the Chaboche Hardening model. This results in the translation and expansion of the yield surface. The combined hardening can be used for large strain and cyclic loading applications.

When elastomeric components are subjected to small straining under cyclic loads, as it will be the case of the studies performed in this thesis work, the kinematic hardening option seems to be the adequate choice.

In all the hardening models, two different yielding criteria can be used in ANSYS: the Von Mises yield criterion and the anisotropic Hill's yield criterion. Hill's criterion can be thought of as an extension of the Von Mises yield criterion to cover anisotropic yielding but will not be studied in this thesis. In this latter, elastomers are considered as isotropic; hence, the Von Mises yield criterion will be used.

ANSYS offers different approximations to input the experimental uniaxial tensile tests. The input true stress-true strain curve can be modelled as a bilinear trace, as a multilinear curve or as a nonlinear curve. With the bilinear trace, the material behaviour is described by a bilinear stress-strain curve starting at the origin with positive stress and strain values. The initial slope of the curve is taken as the elastic modulus of the material. At the specified yield stress, the curve continues along the second slope defined by the tangent modulus (having the same units as the elastic modulus). The tangent modulus cannot be less than zero nor greater than the elastic modulus. In this thesis project, when BKIN model is used, the modulus of the second slope is zero, which means that the material has a perfectly plastic behaviour when it is deformed over the yield strain.

In the multilinear option, a multilinear curve is used instead of a bilinear curve. The uniaxial behaviour is described by a piece-wise linear total stress-total strain curve, starting at the origin, with positive stress and strain values. The curve is continuous from the origin through 100 (maximum) stress-strain points. The slope of the first segment of the curve must correspond to the elastic modulus of the material and no segment slope should be larger. No segment can have a slope less than zero. The slope of the stress-strain curve is assumed to be zero beyond the last user-defined stress-strain data point. Up to 20 temperature-dependent stress-strain curves can be included. This option seems to be the best choice to input the elastomers cyclic quasi-static behaviour.

The nonlinear option uses an equation to fit the input stress-strain curve. This equation can be of the form of the Voce or power law hardening and it is specially indicated to metallic materials where there is a smooth pass from the elastic to the plastic zone.

4.1.3.2 Viscoelastic constitutive model: Prony series. ANSYS Software.

Viscoelasticity describes material response which contains an elastic and viscous part. The elastic response is instantaneous and recoverable and the viscous response occurs over time (anelastic) is non-recoverable. The rate effect is such that there is a limiting behaviour for fast and slow loading. As strain rate decreases, the bulk/shear modulus also decreases. For high strain rates, the elastic response is the limiting behaviour. For low strain rates, the 'viscous' response is the limiting behaviour.

In mechanical solutions from ANSYS [15], viscoelasticity is implemented through the use of Prony series. The shear and volumetric responses are separated and the well-known relationships between shear modulus *G* and bulk modulus *k* are described by Eq. 1.10.

Instead of having constant values for *G* and *K* (and by extension, elastic modulus *E* and Poisson's ratio ν), these are represented by Prony series in viscoelasticity.

For shear strain state, equations Eq. 4.36 and Eq. 4.38 can be rewritten as:

$$G(t) = G_\infty + \sum_{i=1}^{N} G_i e^{-\frac{t}{T_i^G}} \qquad \textit{Eq. 4.51}$$

$$\alpha_i^G = \frac{G_i}{G_o} \qquad \textit{Eq. 4.52}$$

As with other material behaviour, deviatoric and volumetric terms are separated. Hence, from previous equations, the next relations can be written:

$$G(t) = G_0 \left[\alpha_\infty^G + \sum_{i=1}^{N} \alpha_i^G e^{-\frac{t}{T_i^G}} \right] \qquad \textit{Eq. 4.53}$$

$$K(t) = K_0 \left[\alpha_\infty^K + \sum_{i=1}^{M} \alpha_i^K e^{-\frac{t}{T_i^K}} \right] \qquad \textit{Eq. 4.54}$$

These equations imply that the shear and bulk moduli are represented by a decaying function of time *t*. Simply stated, the user provides pairs of relative moduli $\alpha_{G,i}$ and relaxation time $T_{G,i}$, which represent the amount of stiffness lost at a given rate. Similar behaviour can be defined for bulk modulus with a separate set of *M* values of relative moduli $\alpha_{k,i}$ and relaxation times $T_{k,i}$

4.1.3.3 The overlay technique in finite element method software.

The present thesis develops the work started by *Austrell* [99] and continued by *Olsson and Austrell* [68,108] using an overlay method. The overlay method is used to combine various constitutive models programmed in commercial finite element software. Such an approach allows the use of material models implemented in classical FE-codes avoiding programming a new complex material models subroutine.

As shown in Figure 4.21, this method consists of the mesh superposition where the object to simulate is meshed and the mesh is copied at the same location. Then, the nodes are merged obtaining a final model composed of a number of superposed meshes with common nodes. *Austrell* [108] research shows how this method can be used.

For this purpose, the latter researcher used three superposed meshes: one mesh was characterised by an elastic or hyperelastic properties of rubber, the second mesh characterised the Payne effect and the third mesh was related with the rate-dependent properties of rubber. One mesh or the elements layer is needed for the viscoelastic model and one for each elastoplastic element. As the filler content increases, the nonlinearity of the rubber dynamic behaviour is increased, which requires the use of more VE or/and EP elements to obtain more accurate fitting of the material model to the experimental results. As the number of the constitutive elements increases, the number of needed meshes also increases, which enlarges the calculation time.

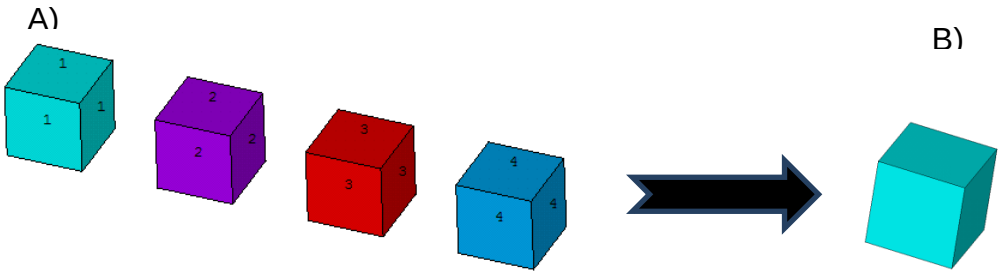

Figure 4.21: A) Example of four brick elements: The first element is characterised by the viscohyperelastic material. The elements number 2, 3 and 4 are characterised by the plasticity (BKIN) model that obey Von Mises yield criteria. B) The elements 2, 3 and 4 are displaced and superposed with the element number 1 and the nodes are merged.

As it is commented in previous sections, the total stress is obtained by the addition of several mechanical elastic, viscoelastic and plastic elements. A direct generalisation for three dimensional stress states would be to add the elastic or hyperelastic, elastoplastic and viscoelastic stress tensors. Hence, the total stress tensor $[\sigma]=[\sigma_e]+[\sigma_{ve}]+[\sigma_{ep}]=[\sigma_{eve}]+[\sigma_{ep}]$

In ANSYS, when Prony series are defined, the spring of the EPVE model is introduced as a long term relaxation modulus. Hence, two stress tensors are required: on the one hand, the elasto-viscoelastic or hyper-viscoelastic, and, on the other hand, the elastoplastic (Von Mises Bilinear Kinematic) material models.

The elastoplastic part of the stress tensor is given by a summation,

$$\sigma^{ep} = \sum_{i=1}^{N} \sigma_i^{ep} \qquad \textit{Eq. 4.55}$$

The elasto-viscoelastic or hyper-viscoelastic stress contribution is given by the following summation:

$$\sigma^{eve} = \sigma^{e} + \sum_{i=1}^{N} \sigma_i^{ve} \qquad \textit{Eq. 4.56}$$

The EPVE model used in the experimental chapter employs three terms of the mentioned elastoplastic and elasto-viscoelastic summations.

4.2 Experimental research: Rubber dynamic properties and its characterisation in simple shear

4.2.1 Geometry and testing conditions

The simple shear specimen, which consists of a 25mm diameter and 6 mm thick rubber cylinder, is used to characterise the dynamic properties as shown in Figure 4.22. This type of geometry avoids the introduction of some factors that could have an influence on the experimental results such as contact frictions, and it permits a rigid fixture between the testing tools and the tested part.

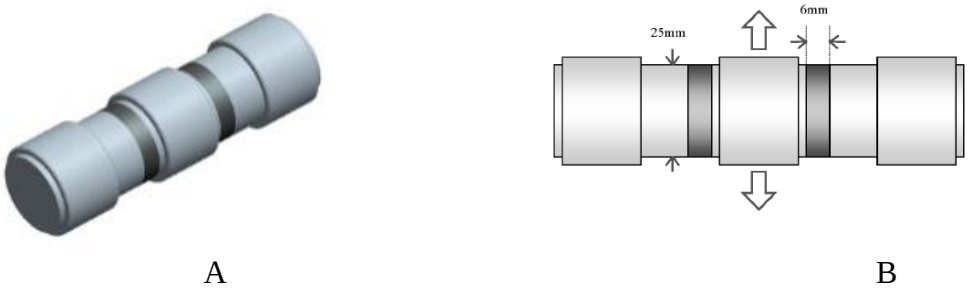

A B

Figure 4.22: Simple Shear specimen: A) Cylindrical double shear test piece. In black, two rubber cylinders of 25mm diameter and 6 mm thickness sandwiched between three metal end pieces. B) The two metal end pieces are fixed and the central piece is moved along the direction shown by the arrows (Figure taken from [147]).

To assure the repeatability of the dynamic characterisation tests, some considerations are taken into account:

(1) The laboratory atmosphere is adjusted to 23ºC and 50% of relative humidity.

(2) 5 simple shear specimens are tested per condition and the mean curve of these curves is presented.

(3) One frequency sweep per amplitude, where the starting frequency is 0.05Hz with 5Hz linear step increments up to 500.05Hz.

Each specimen is preconditioned at each of the eight different amplitudes, cycling 10 times, and then the frequency sweep starts. Each specimen is

tested in the defined frequency sweep at the mentioned eight shear strains, from the lower to the higher. At the end of the characterisation procedure, eight frequency sweeps are captured, one frequency sweep per amplitude. Once the eight frequency sweeps are finished, the tests are repeated again to assure that no relaxation factor has any influence on the initial results.

The tests in elastomer NR1, NR2 and CKR are presented also in the work of *Kareaga* [139] (Annex IV); they consist of eight different amplitude frequency sweeps: from 0.05Hz to 500.05 Hz. The input peak amplitudes to characterise the mentioned elastomers dynamic properties are 0.1, 0.2, 0.31, 0.41, 0.82, 1.23, 2.05 and 4.1 %.

In this thesis, all the characterisation process with each specimen is made with the same clamping device and testing machine where the specimen is mounted only once.

4.2.2 Material definition: Rubber compounds used in the experimental work

For this work, three materials or rubber compounds are used. Two of them are natural rubber based rubber compounds NR1 and NR2; and the third one is a randomly selected elastomer provided by the company Cikautxo Scoop. The formulation of the first two natural rubber based elastomers is very similar, where the unique difference between both is the carbon black quantity. One of them is low filled formulae and the second one is highly filled formulae (Table 4.1).

NR1	*phr*
SMR CV 60	100
ZnO	5
SFR N-774	80
TMQ	1
IPPD	1.5
Zinc Stearate	3
MBS	1.5
TBTD	0.9
Sulfur	0.8

NR2	*phr*
SMR CV 60	100
ZnO	5
SFR N-774	30
TMQ	1
IPPD	1.5
Zinc Stearate	3
MBS	1.5
TBTD	0.9
Sulfur	0.8

CKR(MCN6887)	*phr*
BR	30
NR	70
ZnO	4
Stearic acid	1
Peptizing agent	1
Antiozonant Microwax	3.5
Aminic antioxidant	1.5
Aminic antiozonant	3
Aromatic oil	5
N539	50
Sulfur	1.4
CZ	1

Table 4.1: Formulation recipes. NR1 and NR2 are natural rubber based formulations. Their unique difference consists of the carbon black quantity. The third formula CKR is randomly selected industrial elastomer provided by the company Cikautxo Scoop.

4.2.3 Material test system

Dynamic tests have been carried out in Cikautxo S.Coop. The MTS servohydraulic test systems are precisely configured to characterise dynamic properties of several materials and components. Specifically, the MTS Model 831.50 (10 kN, Elastomer Testing System with FlexTest 60 Control System) 1000 Hz is shown in Figure 4.23. The MTS Model 831.50 is a high frequency elastomer test system incorporating all the necessary elements to provide static and dynamic characterisation data for elastomeric components and materials. The standard configuration features a frequency range of 0.01 to 1000 Hz with ±50N to ±10 kN force range and ±0.005 to ±20 mm dynamic displacement range.

Acceleration compensation is built into the force measurement system and is used on both the strain gauge load cell and the piezoelectric load washer. Accuracy at high frequency is ensured by utilizing acceleration based displacement measurement with the accelerometer located at the specimen interface of the piston rod.

Figure 4.23: MTS Model 831.50 (10 kN) 1000 Hz. Elastomer Testing System

The results given by the characterisation device have the structure of the following figure:

Dynamic Characterization 73,02881 Sec
Analysis Method: Sine Regression
Time Data File:

Specified Frequency	Specified Mean Level	Specified Dynamic Amplitude (p-p)	Frequency	Load Mean Level	Load Dynamic Amplitude (p-p)	Load Vector	Displacement Mean Level	Displacement Dynamic Amplitude (p-p)	Phase	K*	K'	K"	Tan Delta	Energy
Hz	N	mm	Hz	N	N	deg	mm	mm	deg	N/mm	N/mm	N/mm	unitless	N-mm
0,05	0	0,5	0,05	-1,29844	188,8753	10,39336	-1,06572	0,500428	10,39336	377,4272	371,2345	68,08982	0,183415	13,39387
5,05	0	0,5	5,052632	0,101987	213,7403	10,88911	-1,0574	0,500427	10,88911	427,1157	419,4253	80,68588	0,192372	15,87633
10,05	0	0,5	10,05016	-3,58639	217,5122	11,01295	-1,06752	0,500548	11,01295	434,5485	426,5458	83,01214	0,194615	16,35045
15,05	0	0,5	15,05882	-0,10714	219,7473	11,18353	-1,05731	0,500022	11,18353	439,4751	431,1299	85,23723	0,197707	16,74489
20,05	0	0,5	20,05658	-2,28159	221,712	11,35298	-1,0612	0,501002	11,35298	442,537	433,8779	87,11468	0,200782	17,17346

Figure 4.24: An example of a frequency sweep where the amplitude remains constant. The starting frequency is 0.05Hz with 5Hz linear step increments up to 20.05Hz

The simple shear specimens were tested in order to characterise the rate-dependent or frequency dependent properties of elastomers.

K' and *K"* (MPa) dynamic storage and loss stiffness respectively - data were reported by the software of the testing machine. The shear storage and loss modulus can be obtained as follows:

$$G' = K' \frac{thk}{A} \qquad Eq.\ 4.57$$

Where *K'* is the dynamic storage stiffness given by the division between the load given by the load cell (N) and the displacement given by the LVDT or axial accelerometer of the material test system (MTS); *thk* is the thickness of the simple shear specimen (mm) and *A* is the cross sectional area (mm^2). It must be taken into account that, if the used testing specimen type is dual simple-shear, this area *A* has to be multiplied by two. Then,

$$G' = K' \frac{thk}{2A} \qquad Eq.\ 4.58$$

and,

$$G'' = K'' \frac{thk}{2A} \qquad Eq.\ 4.59$$

4.2.4 Results and discussion

As mentioned before, formulation recipes of three elastomers are presented in Table 4.1. These elastomers are highly filled, filled and unfilled, NR1, CKR and NR2 respectively. The characterisation results of each elastomer are divided into two groups. On the one hand, four graphs will be presented defining the dynamic properties versus frequency (Hz); these properties are simple shear storage *G'*, loss *G"*, dynamic *G** modulus and phase angle δ (Figure 4.25-Figure 4.27 from A to D). On the other hand, the same dynamic properties versus shear strain amplitude γ_0 are presented (Figure 4.25-Figure 4.27 from E to H).

The most widely studied parameters in literature are the storage *G'* and loss *G"* modulus: they are the dynamic properties which give the most valuable information. The dynamic stiffness *G** and phase angle δ can be derived from them. Hence, the conclusions will be focused mostly on these two modulus *G'*

and *G"* and the other two dynamic properties *G** and phase angle δ will be presented as additional information. Moreover, the dynamic stiffness *G** has the same tendencies as the storage modulus *G'.*

Frequency versus dynamic properties.—

As it can be seen from Figure 4.25 to Figure 4.27 in A and C graphs, if frequency is increased, storage *G'* and dynamic modulus *G** increase too. This stiffening effect due to the frequency increasing is more pronounced as the amplitude tends to zero. However, in frequency sweeps performed at higher amplitudes, the change in frequency does not almost affect the magnitude of *G'* and *G**.

Loss modulus *G"* and phase angle δ, as shown in Figure 4.25 to Figure 4.27 in B and D graphs, an increase as frequency is increased. When studying the highest amplitudes, the increase of the loss modulus *G",* due to the frequency increase, becomes less significant.

Amplitude versus dynamic properties.—

The magnitudes of storage *G'* and dynamic *G** modulus shown from Figure 4.25 to Figure 4.27 in E and G graphs decrease as the amplitude is increased. As it is shown in the mentioned graphs, this reduction in the stiffness is more pronounced as the testing frequency is higher.

The maximum of the loss modulus *G"* shown from Figure 4.25 to Figure 4.27 in graph F is given at an amplitude where the storage modulus *G'* shown in the same figures in graphs E drops more rapidly. The phase angle δ (graph H) increases as the frequency is increased. The magnitude of loss modulus *G"* arises as frequency is increased, but this effect becomes less significant as the amplitude increases.

The effect of the amount of filler on dynamic properties.—

In general, the dynamic stiffness of all testing conditions is greater in elastomers with a higher content of filler. On the one hand, the storage modulus *G'* and the dynamic stiffness *G** arise as much as the amount of filler

is increased; this is due to its reinforcing effect. The stiffening of the storage *G'* and dynamic modulus *G** that plotted over frequency, the slope at low amplitudes have more noticeable influence as a filler content of the elastomer increases. On the other hand, the offset between *G'* and *G** versus the frequency curves at the tested amplitudes is more noticeable in elastomers with a greater amount of filler. Finally, as the filler content tends to zero, the amplitude and frequency dependence tend to be negligible whereas the material behaviour tends to be linear.

If we compare the B graphs of each elastomer from Figure 4.25 to Figure 4.27, the loss modulus magnitude increases with increasing the filler content. The slope of *G"* versus frequency decreases as the amplitude increases in highly filled and filled rubbers, as it is shown in Figure 4.25 to Figure 4.26 in graph B.

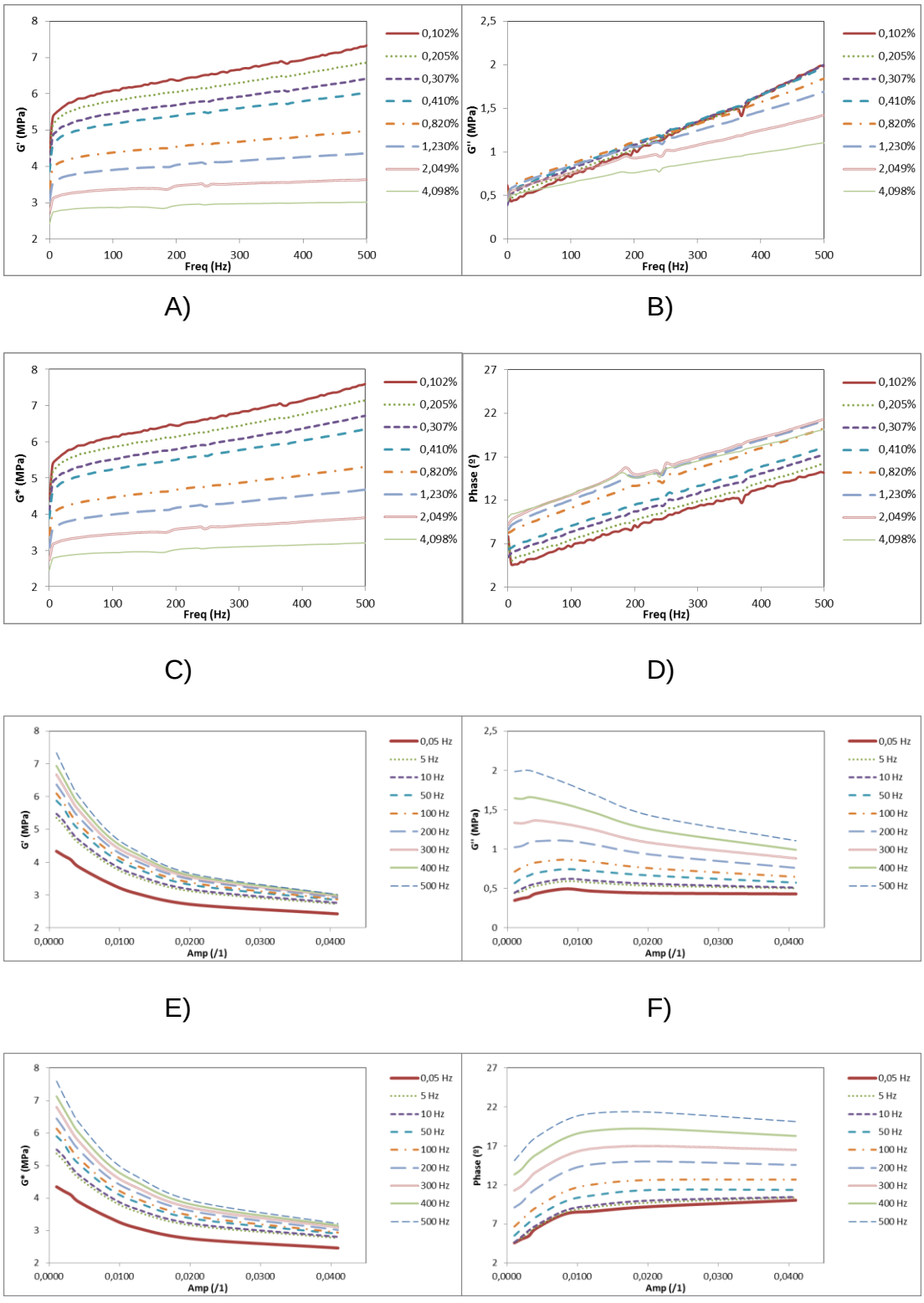

Figure 4.25: Dynamic results of NR1: First, the dynamic properties G', G'', G and δ versus frequency (Hz) are represented, A), B) ,C) and D) respectively. Next, the dynamic properties G', G'', G* and δ versus shear strain (/1) are represented, E), F), G) and H) respectively.*

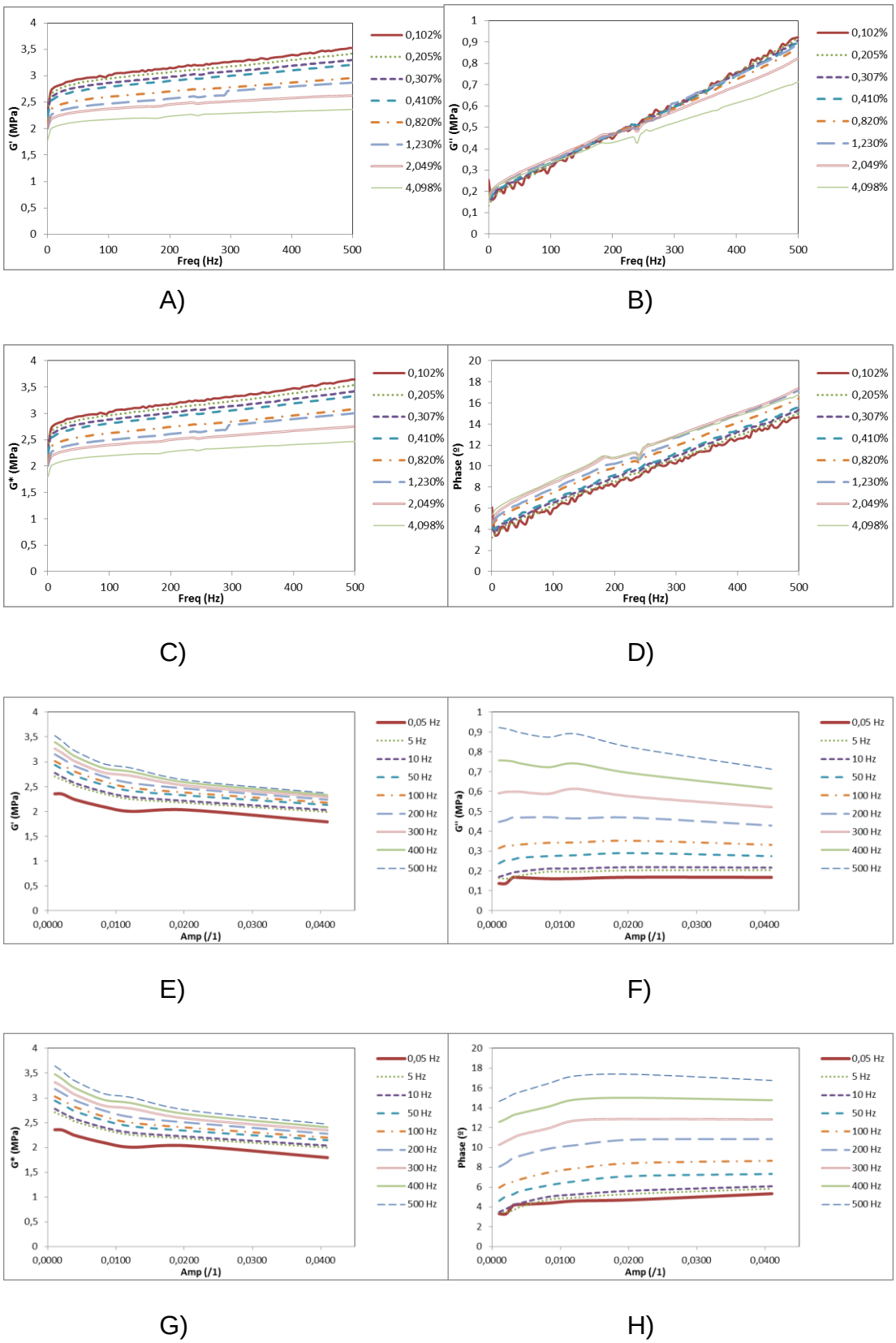

Figure 4.26: Dynamic results of CKR: First, the dynamic properties G', G'', G and δ versus frequency (Hz) are represented, A), B) ,C) and D) respectively. Next, the dynamic properties G', G'', G* and δ versus shear strain (/1) are represented, E), F), G) and H) respectively.*

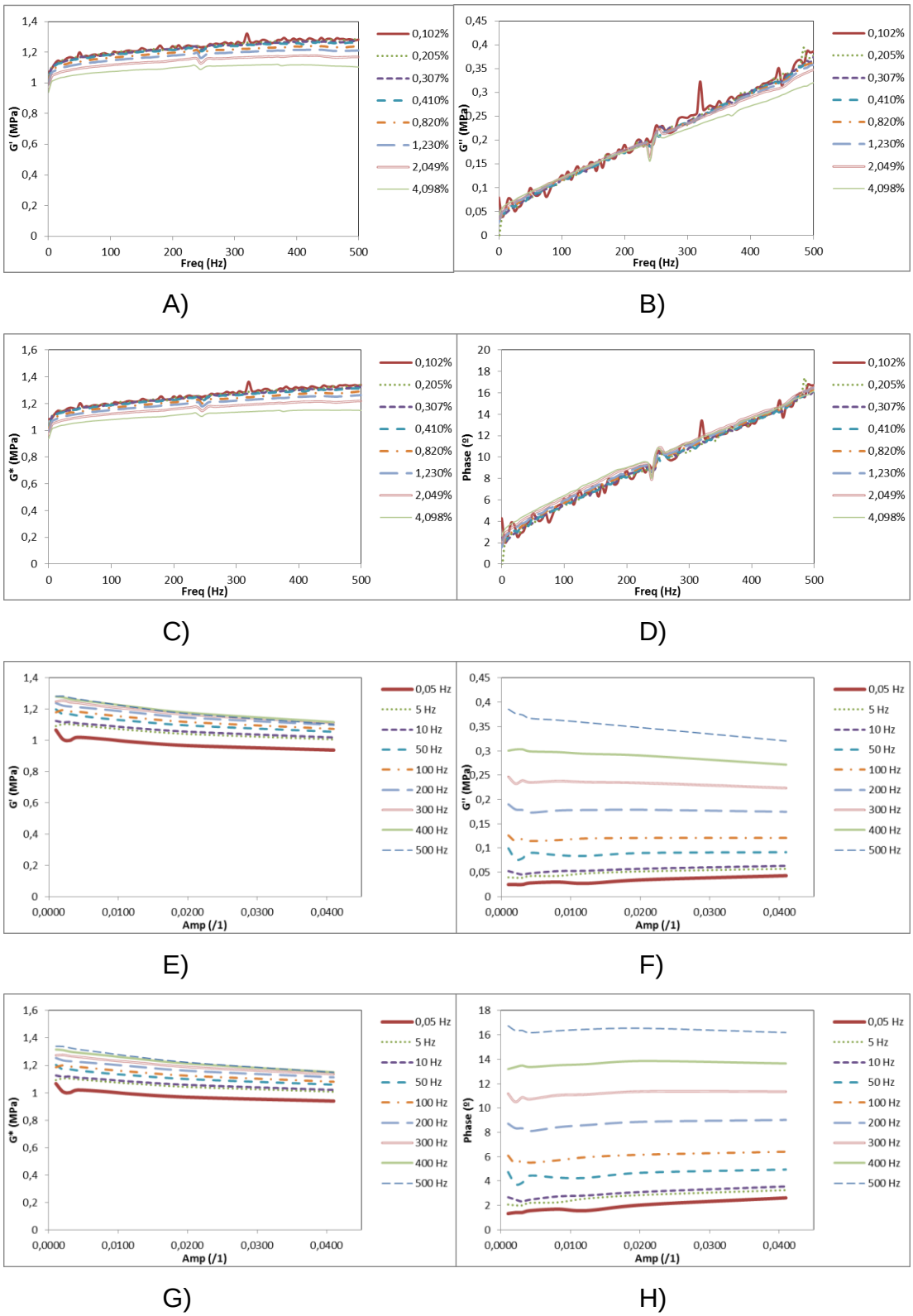

Figure 4.27: Dynamic results of NR2: First, the dynamic properties G', G'', G and δ versus frequency (Hz) are represented, A), B) ,C) and D) respectively. Next, the dynamic properties G', G'', G* and δ versus shear strain (/1) are represented, E), F), G) and H) respectively.*

4.2.5 Conclusions: Rubber behaviour under several amplitude and frequency loads

*Storage modulus G' and dynamic stiffness G**.—

At small deformations, carbon-black agglomerates are not broken and, in addition, they can occlude the rubber producing the mentioned augmentation effect mentioned in section 1.3.3. Hence, the ability to move into the matrix is reduced. As the testing frequency increases, the elastomer stiffness increases. This stiffening of the material with the frequency increase is due to the fact that the cycle time is smaller at higher frequencies. Hence, the non-broken filler agglomerates, and in lower proportion the molecular structure, have less time to return to the relaxed state. This stiffening effect, produced by the frequency increasing, is more pronounced when the amount of filler of the elastomer is higher.

At intermediate deformations, the carbon-black agglomerates are broken into smaller agglomerates. Hence, the elastic modulus or the elastomer stiffness decreases because there are more mobile units into the rubber matrix. Consequently, the material stiffening due to the frequency increasing is smaller. Finally, at high deformations, the carbon-black agglomerates broken down until becoming the aggregates themselves are mobile units. Therefore, the behaviour at high deformations will be similar to the unfilled rubbers.

As the amount of filler of the elastomer decreases, the agglomerates content is lower; consequently the stiffening of the rubber diminishes. Accordingly, the change in the mobility, because of their rupture due to the amplitude, diminishes and, the mobility, because of the frequency change, is not affected. Hence, the frequency and the amplitude dependence diminish as the filler content decreases.

To sum up, the dynamic stiffness slope when plotted over frequency, the slope is higher at low amplitudes than at high ones, which tends to be horizontal when the amplitude is higher. This effect is more evident as the amount of filler of the elastomer increases. Hence, the storage modulus G' and the dynamic stiffness G* curves versus frequency at different amplitudes are not parallel

and the slope goes from smaller to higher, this latter being low at high amplitudes and high at low amplitudes.

Loss modulus G" and phase angle δ.—

Amplitude dependence: When increasing the amplitude, the structure of the agglomerates, that are present at intermediate amplitudes, break down in smaller agglomerates. Those internal frictions increase with the consequent increase in the loss modulus. From the critical amplitude, the increase in the loss modulus changes the trend and decreases with the amplitude. During the cyclic strain, while the stable filler network at low amplitudes can reduce the hysteresis of the filled rubber, the breakdown and reformation of the filler network cause an additional energy dissipation resulting in the higher hysteresis at intermediate amplitudes. Finally, at high amplitudes, as the filler agglomerates are broken down in aggregates, the rubber compound becomes more stable and the reformation of the filler network does not occur. Hence, at high amplitudes, the loss modulus is reduced again.

Frequency dependence: As the frequency is increased, it produces a greater loss of energy because the filler and molecular structure change their configuration in a shorter period of time. Therefore, when the frequency is increased, the number of internal friction increases producing a greater heat release. In unfilled elastomers the internal frictions are lower. Consequently, when increasing the frequency, the loss modulus *G"* does not vary as much as in filled elastomers.

In general, the results are in accordance with those existing in literature. Additionally, a dataset is obtained, which covers a wider frequency or strain ranges, characterising highly filled, filled and unfilled elastomers than usual. This accurate database, which is generated with a current servo-hydraulic machine, can be used to develop or validate new or existing constitutive models. These results could be considered as a reference dataset generated with modern servo-hydraulic test systems; they could be used for further studies in the development and validation of new and existing constitutive models on the prediction of the dynamic properties of rubbers.

4.3 Simulating experimental tests by means of FEA.

In this work, the mentioned EPVE model proposed by Olsson and Austrell is improved in two ways. First, a novel fitting procedure of three EP elements for static cyclic loading tests at four strain levels is proposed; then these elastoplastic elements are fused in a multilinear (ML) curve. The use of a multilinear kinematic hardening constitutive model (MKIN model in ANSYS) reduces the various meshes required for each elastoplastic element to one mesh. After, the second mesh is divided into equivalently strained elements groups (see Figure 4.29) and then, each element group is characterised by the corresponding viscoelastic (VE) material.

The VE materials are characterised by their corresponding Prony constants. The equivalent VE part of the model characterises the rate-dependent stiffness and damping at a number of strain levels. The method presented in this thesis report reduces to two the number of required superposed meshes. One mesh will be characterised by the multilinear constitutive model and the elements of the second mesh are characterised by the equivalent viscoelastic materials characterised with Prony series explained in section 4.3.1.2. This reduction in the number of required meshes reduces the calculation time.

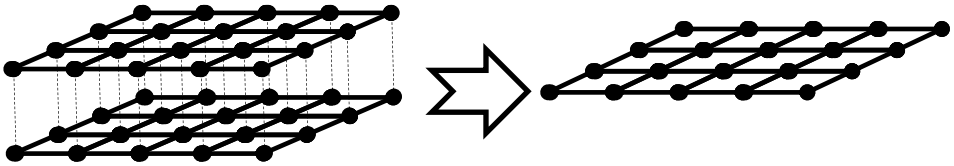

Figure 4.28: Overlay model. The object to simulate is meshed and the mesh is copied at the same location. The first mesh characterised by the multilinear kinematic hardening constitutive model (ML or MKIN) and the second mesh characterised by a number of VE materials, each one characterised by its corresponding Prony series as it is shown in Figure 4.29-B.

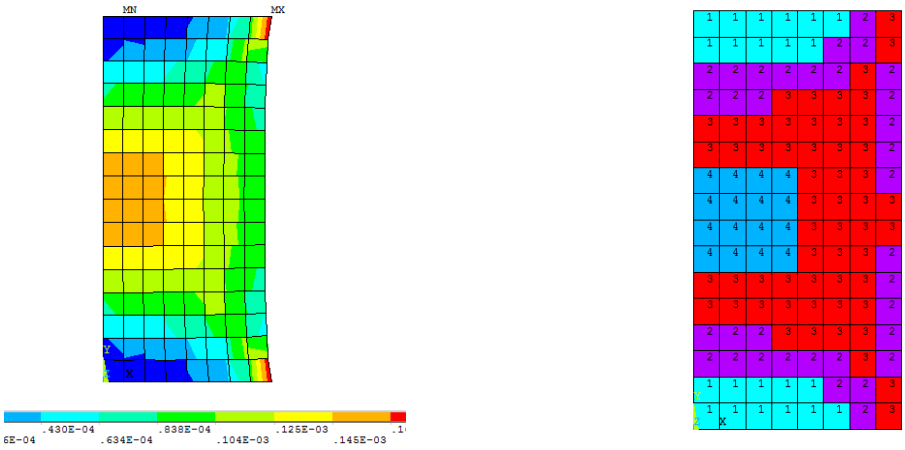

A) B)

Figure 4.29: A) Represents the strain energy density of the deformed geometry. B) Represents the mesh of the model divided in four materials characterised by the equivalent Prony series.

For the fitting step, some considerations are taken into account. The elastomer is considered incompressible and isotropic material, and the fitting procedure is done by the one-dimensional model.

The type of characterisation specimen used is the simple shear sample (see section 4.1.1: Dual simple-shear testing specimens Option B. The main advantage of the used test specimen is that test set up is the same for both static and dynamic test, referring to the clamping devices and the testing machine. On the other hand, dynamic properties of elastomers are characterised in simple shear in order to reduce the influence of elastic nonlinearities. Simple shear strain state characteristics are studied in section 4.1.1, and exposed that the initial shear modulus G_0 as the shear modulus for small strains may be characterised by the use of such type of characterisation specimen. For convenience, the initial modulus G_0 is renamed as relaxed modulus G_∞.

Several fitting procedures are studied for similar material models *Berg* [98,105], *Austrell* [99,141], *Olsson* [68,109], *Gil-Negrete* [113] or *Ahmadi* [111]. Each method has its advantages and disadvantages; hence, after the exposition of existing suggestions, a clear and simple method will be exposed.

The elastoplastic (static mechanical properties) and viscoelastic (dynamic mechanical properties) can be modelled independently *Austrell* [99], *Olsson and Austrell* [68], *Kaliske and Rothert* [148] and *Miehe and Keck* [45].

4.3.1 MLVE model with equivalent viscoelastic approach and its implementation in Ansys

The constitutive model proposed in this work is divided into two parts in order to fit the model parameters to the experimental data. The first part modelled as a single spring and a number of elastoplastic elements (see Figure 4.30 into dashed lines named as ‘EP model’ in this thesis report) characterises the amplitude dependence. Firstly the EP part of the model is fitted and then the characterisation constants are transferred into the ML model (Multilinear model).

The second part modelled as various Maxwell elements (see Figure 4.30 into dash-dot lines known as ‘VE model’ in this document) characterises by the use of Prony series the rate-dependence of elastomers. As it is shown in the experimental section, the rate-dependence of elastomers depends on the applied strain amplitude. Consequently, the viscoelastic material (VE model) has to change as the deformation of the elastomer changes. Therefore, the elements similarly strained of a finite element mesh have to be characterized with the same VE material.

In brief, the proposed MLVE with equivalent viscoelastic approach consists of the reduction of various EP models in a unique ML model. The rate dependence is characterised with several VE materials which depend on the strain level of the element once it is loaded.

The algorithms created to fit the multilinear-viscoelastic (MLVE) model to the experimental data were created with the Matlab software.

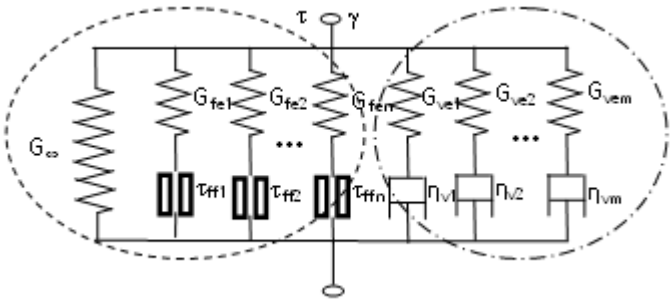

Figure 4.30: Dashed line: Representation of the expanded elastoplastic model (EP model). Dash-dot line: Representation of the expanded viscoelastic model (VE model).

4.3.1.1 Quasi-static and amplitude dependence material fitting

The part of the model which characterises the Payne effect or amplitude dependence is the generalised Zener friction model. This model is composed of a number of elastoplastic elements coupled in series with a hyperelastic spring. The elastoplastic behaviour of this model is piece-wise kinematic hardening. The rate-independent elastoplastic elements are used to define the static hysteresis. When coupled together with elastic springs, as shown in Figure 4.31 (equivalent to Figure 4.9), it is obtained a rather smooth response as well as a good fit to a larger range of amplitudes. The experimental data needed to characterise this part of the model come from the first measurement performed at each strain level or amplitude. Specifically, the required input data come from the first frequency of 0.05Hz of each frequency sweep.

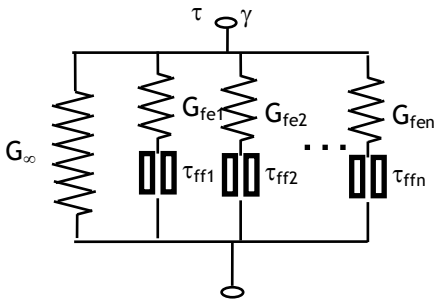

Figure 4.31: Elastoplastic or Generalised Zener friction model.

Hyperelastic spring.— The model used in this study is the Neo-Hookean or also known as *Yeoh's* first order model [25]. The hyperelastic spring element

of the EP model characterises the completely relaxed shear *G* modulus or the commonly known G_∞ of the elastomer. In this work, the elastomer NR1 is characterised up to the maximum peak strain of 4.1%. Hence, when the Zener model is fitted to experimental data, the spring element can be linearized to calculate the initial relaxed shear modulus G_∞ . Then, this G_∞ is used to calculate the Yeoh's constant C_{10}. The Yeoh's first order equation for incompressible materials is written as follows:

$$W_0 = C_{10}(I - 3) \qquad \textit{Eq. 4.60}$$

$$C_{10}=G_\infty/2 \qquad \textit{Eq. 4.61}$$

Bilinear kinematic hardening or Elastoplastic elements.— The elastoplastic elements are used to characterise the quasi-static hysteresis loop and the amplitude dependence. The constitutive model, which fits better the characterised properties, is the kinematic hardening rule. Kinematic hardening assumes that the yield surface remains constant in size when plasticity starts.

In this thesis, a fitting procedure based on a detailed fitting procedure from *Olsson and Austrell* [68] is proposed. Firstly, the dynamic properties are specified for an easier comprehension of the fitting procedure. Storage modulus *E',* loss *E"* modulus, the phase angle δ, dynamic stiffness *E** and the hysteresis *area* are defined for uniaxial strain state in section 1.3.2, and for shear strain state the dynamic properties can be written equivalently as follows:

$$G' = G^* cos\delta \qquad \textit{Eq. 4.62}$$

$$G'' = G^* sin\delta \qquad \textit{Eq. 4.63}$$

$$\delta = \frac{G"}{G'} \qquad \textit{Eq. 4.64}$$

$$G^* = \frac{\tau_0}{\gamma_0} = \sqrt{G'' + G'} \qquad \textit{Eq. 4.65}$$

$$area = \pi G'' \gamma_0^2 \qquad \textit{Eq. 4.66}$$

The dynamic properties used in the fitting process are *G'* and *G"*.

When an elastoplastic element is strained, two situations may occur:

1. $\gamma < \gamma_{ff}$:No sliding occurs in the Coulomb element. Hence, the chain behaves as a linear spring and the damping is zero. Consequently, $\tau = G\gamma$ and the hysteresis $area_f = 0$.
2. $\gamma \geq \gamma_{ff}$: sliding occurs in the Coulomb element then, $\tau = \tau_{ff}$, and the hyteresis $area_f = 4\tau_{ff}(\gamma - \gamma_{ff})$

Then, the total elastoplastic shear stress and hysteretic areas of the Zener model are calculated as follows:

$$\tau_{0,k}^{tot} = \tau_\infty + \sum_{i=1}^{n} \tau_i \qquad \textit{Eq. 4.67}$$

$$\tau_{0,k}^{tot} = G_{f,k}^* \gamma_{0,k} \qquad \textit{Eq. 4.68}$$

$$area_{f,k}^{tot} = \sum_{i=1}^{n} area_{f,i} \qquad \textit{Eq. 4.69}$$

k indicates the frequency sweep number done between 0.05 to 500.05Hz from the lowest to the highest strain level. *i* indicates the number of the elastoplastic element where the total stresses and areas for each *k* strain level are calculated by 'BKIN' (Figure 4.32) and 'df' (Figure 4.33) functions respectively,

```
Function Bkin(Ginf, Gf1, Y1, Gf2, Y2, Gf3, Y3, E)
If E <= Y1 / Gf1 Then
Sigma1 = Gf1 * E
Else
Sigma1 = Y1
End If
If E <= Y2 / Gf2 Then
Sigma2 = Gf2 * E
Else
Sigma2 = Y2
End If
If E <= Y3 / Gf3 Then
Sigma3 = Gf3 * E
Else
Sigma3 = Y3
End If
Bkin = Ginf * E + Sigma1 + Sigma2 + Sigma3
End Function
```

Figure 4.32: BKIN Function programmed in Visual Basic. The output gives the total stress of the generalised friction model, which is composed by an elastic spring and three elastoplastic elements in parallel.

```
Function df(Gf1, Y1, Gf2, Y2, Gf3, Y3, E)
es1 = Y1 / Gf1
If E <= es1 Then
df1 = 0
Else
df1 = 4 * Y1 * (E - es1) 'area
End If
es2 = Y2 / Gf2
If E <= es2 Then
df2 = 0
Else
df2 = 4 * Y2 * (E - es2) 'area
End If
es3 = Y3 / Gf3
If E <= es3 Then
df3 = 0
Else
df3 = 4 * Y3 * (E - es3) 'area
End If
df = df1 + df2 + df3
End Function
```

Figure 4.33: df Function programmed in Visual Basic. The output gives the area of the generalised friction model, which is composed by an elastic spring and three elastoplastic elements in parallel.

The experimentally obtained input values of $G^*_{exp,k}$ and $area^{tot}_{exp,k}$ are obtained from each strain level at the frequency of 0.05Hz, which is considered to be quasi-static (Figure 4.34).

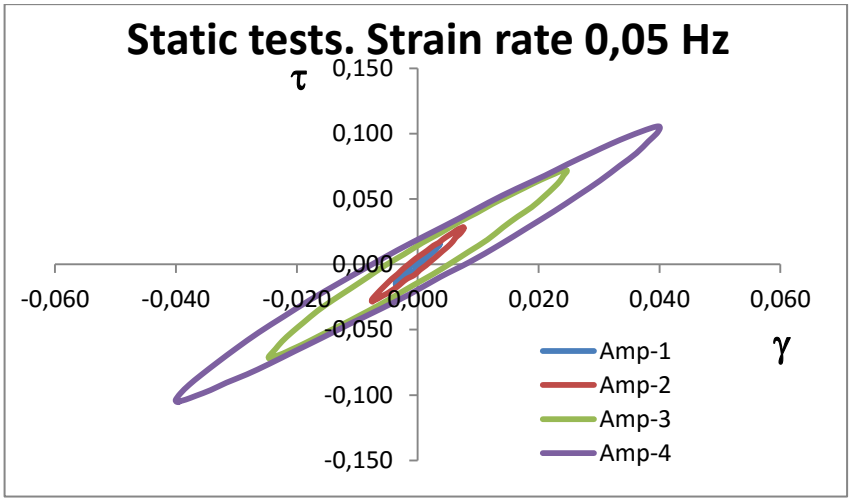

Figure 4.34: Typical cyclic static tests. Four different amplitudes tests are plotted .

The Zener friction model is fitted to the experimental input, which is given by the relation $\tau^{tot}_{0exp,k} = G^*_{exp,k}\gamma_{0,k}$ and the hysteresis $area_{fexp,k}$. The error function used in the optimization approach is the one presented by *Olsson and Austrell* [68].

$$err = \sum_{i=1}^{n}\left(\frac{\tau^{tot}_{0,k} - \tau^{0.05Hz}_{0exp,k}}{\tau^{0.05Hz}_{0exp,k}}\right)^2 + J\sum_{i=1}^{n}\left(\frac{area^{tot}_{f,k} - area^{0.05Hz}_{fexp,k}}{area^{0.05Hz}_{fexp,k}}\right)^2 \qquad \textit{Eq. 4.70}$$

where *k* and *J* are the shear strain amplitude and the scale factor respectively.

Multilinear kinematic hardening.— Once the material constants of the EP model are determined, they are transformed in a multilinear ML curve. *Ahmadi et al* [147] or *Austrell* [99] showed the method to determine multilinear kinematic parameters from the initial loading curve. In this work, for fitting purposes, the way taken was more extensive; each characterisation cycle at each strain level is considered. Once elastoplastic constants are calculated as detailed above, they are transformed in a multilinear curve as it is shown in Figure 4.35-A and B, using for this purpose the next equations: Eq. 4.71 and Eq. 4.72.

$$\gamma_{ff,i} = \frac{\tau_{ff,i}}{G_{f,i}} \qquad \textit{Eq. 4.71}$$

$$\tau_{pj} = u(j)\sum_{j=1}^{j-1}\tau_{p,j} + \gamma_{ff,j}\sum_{i=j}^{n} G_{f,i} \quad u(j)\begin{cases} j=1 & u(j)=0 \\ j\neq 1 & u(j)=1 \end{cases} \qquad \textit{Eq. 4.72}$$

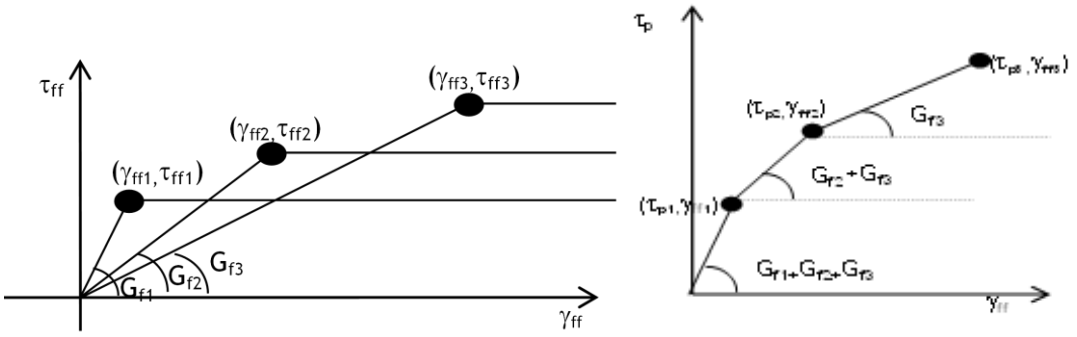

A) B)

Figure 4.35: A) Elastoplastic elements: represents three bilinear plasticity curves. Each constitutive model works as a linear elastic model with stiffness G_{fi} up to the yield strain and then becomes perfectly plastic. B) Multilinear constitutive model

In commercial finite element software as ANSYS, MARC or ABAQUS, elastoplastic data must be introduced in terms of uniaxial tension σ and uniaxial strain ε. For infinitesimal strain theory in an incompressible material, the elastic energy density in simple shear and uniaxial deformation state are the same. Hence, the yield stress in tension σ_p is related to the yield stress in simple shear [147] τ_p,

$$\sigma_{p,i} = \tau_{p,i}\sqrt{3} \qquad \textit{Eq. 4.73}$$

$$\varepsilon_{ff,i} = \gamma_{ff,i}/\sqrt{3} \qquad \textit{Eq. 4.74}$$

4.3.1.2 Frequency or rate dependence characterisation of elastomers

In order to characterise the rate-dependency of the dynamic properties of elastomers, viscoelastic elements are used to define the change in the material behaviour as the testing load becomes non-static. In this work, the frequency of 0.05Hz is considered quasi-static. Hence, the contribution of the VE part of the MLVE model is zero at this frequency.

One of the simplest models to define the viscoelasticity of any material is the Maxwell element. In order to achieve a better fit to a larger range of frequencies, the viscoelasticity is defined by Prony series. The Prony series consists of an expansion of several Maxwell elements coupled in parallel. This VE model is also known as the generalised Maxwell model and it can be represented as shown in Figure 4.36 (equivalent to Figure 4.13).

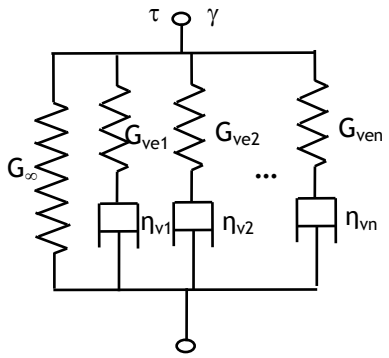

Figure 4.36: Generalised Maxwell model: Prony series

The relaxation time T is defined as the division of the dashpot viscosity constant η_v and the spring elastic modulus G_{ve} (The relaxation time known as τ in section 4.1.2.2 is renamed as T for convenience):

$$T_i = \frac{\eta_{v,i}}{G_{ve,i}} \qquad \textit{Eq. 4.75}$$

The stress of the Prony series is calculated as follows and it shows that the stress decays exponentially with a characteristic time constant (equivalent to Eq. 4.35)[15,99,149]:

$$\tau = \gamma_0 \left(G_\infty + \sum_{i=1}^{N} G_{vei} e^{\frac{-t}{T_i}} \right) \qquad \textit{Eq. 4.76}$$

The previous Eq. 4.76 can be written as follows (equivalent to Eq. 4.36):

$$G_{ve} = G_\infty + \sum_{i=1}^{N} G_{vei} e^{\frac{-t}{T_i}} \qquad \textit{Eq. 4.77}$$

The viscoelastic behaviour of a material is determined from harmonic experiments [139]. In these experiments, the material is exposed to small sinusoidal strain vibrations and the resulting dynamic properties are determined as a function of frequency ω. The mentioned dynamic properties are the storage modulus $G'_{ve}(\omega)$ and loss modulus $G''_{ve}(\omega)$. The Prony series generally defined in time domain (Eq. 4.77) as showed in Annex II-G can be converted to frequency domain with the application of the Fourier transformation (Annex II-H) and, as a result, the next equations are written (equivalently to Eq. 4.43 and Eq. 4.44)[145]:

$$G_0 = G_\infty + \sum_{i=1}^{n} G_{ve,i} \qquad \textit{Eq. 4.78}$$

$$G'_{ve}(\omega) = G_0 - \sum_{i=1}^{n} G_{ve,i} + \sum_{i=1}^{n} \frac{G_{ve,i} T_i^2 \omega^2}{1 + T_i^2 \omega^2} \qquad \textit{Eq. 4.79}$$

$$G''_{ve}(\omega) = \sum_{i=1}^{n} \frac{G_{ve,i} T_i \omega}{1 + T_i^2 \omega^2} \qquad \textit{Eq. 4.80}$$

The amplitude dependence and rate dependence can be considered as two independent types of behaviour, i.e. the frequency response is the same for all strain amplitudes and vice versa. This assumption holds rather well for unfilled materials and it requires some modifications for filled or highly filled materials.

The simplest MLVE model is equivalent to the 5 parameters EPVE presented by *Austrell* [99] shown in Figure 4.37-A. This model can be used to characterise the unfilled rubbers dynamic behaviour and some low filled elastomers when the model is expanded to more EP and VE elements as it can be observed in Figure 4.37-B. As it is shown in Figure 4.38, when shear strain decreases the slope of the curve *G'* is increased. In Figure 4.38, the EV Prony series are characterised by the experimental results performed with the shear strain peak amplitude of γ_2. In consequence, the simulation at this amplitude is correct, but in case of lower amplitude of γ_1, the error increases when the frequency is increased. The use of only one VE characterisation (the same Prony series for every element of the mesh) for any strain level is erroneous because it generates parallel curves displaced by the elastoplastic model. To solve this problem requires the use of equivalent γ_{eq} VE characterisations.

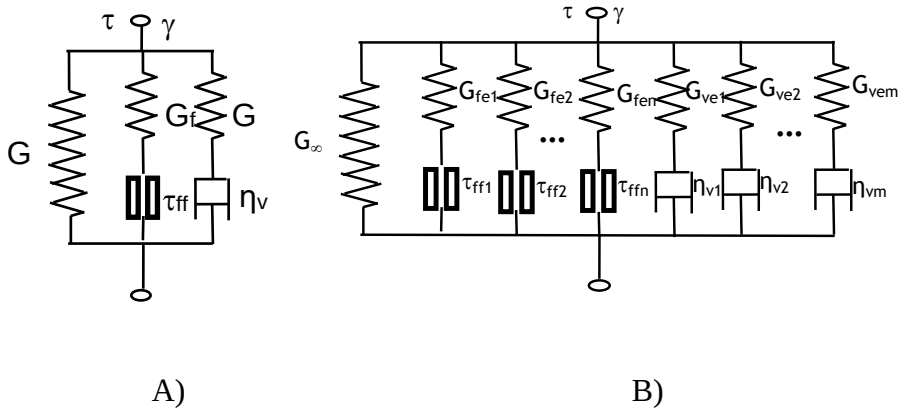

Figure 4.37: A) Representation of the simplest EPVE five parameter constitutive model. B) Representation of the expanded EPVE constitutive model

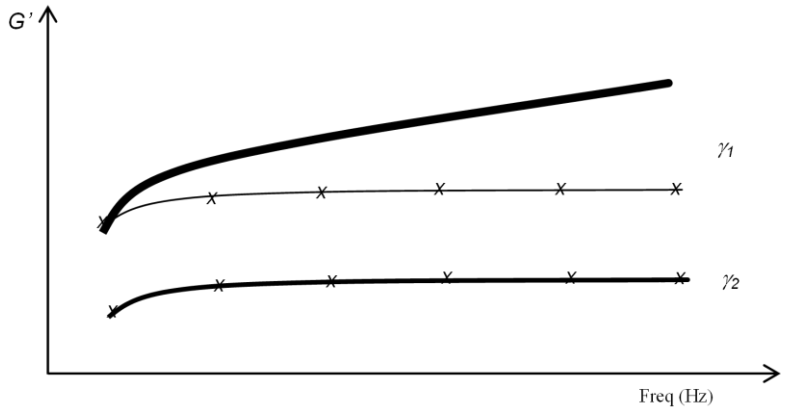

Figure 4.38: EPVE model and MLVE models representation. Solid line represents the experimental tests performed with amplitude γ_1 and γ_2 where $\gamma_1<\gamma_2$. The 'x' marked lines are the EPVE and MLVE models simulations where the Prony series are characterised by γ_2 experimental results.

The G_∞ is a known value which comes from the quasi-static multi-linear fitting step. In this second VE fitting step, Prony series are calculated from different frequency sweeps performed with different strain levels. It is interesting to characterise the widest possible range of strain amplitudes. Hence, in this work, four curves of the eight characterised amplitudes of the material NR1 (see ANNEX IV) will be used to characterise the Prony series. The four input curves are given by the test performed at γ_1=0.0031, γ_2=0.0082, γ_3=0.021 and γ_4=0.042 (/1) in a frequency range from 0.05 to 500.05Hz.

Preparing input data.— The experimental data (the frequency sweep performed at a constant amplitude) is composed of the amplitude dependent static component and the frequency dependent dynamic component. Hence, the amplitude dependent static component is first removed from the experimental data.

$$G^*_{v\exp}(\omega) = G^*_{\exp}(\omega) - G^{*0.05Hz}_{\exp} + G_\infty \qquad \textit{Eq. 4.81}$$

$$area_{v\exp}(\omega) = area_{\exp}(\omega) - area^{0.05Hz}_{\exp} \qquad \textit{Eq. 4.82}$$

The Prony series (see Eq. 4.79 and Eq. 4.80) are fitted to the prepared input data given by Eq. 4.81 and Eq. 4.82. The error function is defined as:

$$err = \sum_{i=1}^{n} \left(\frac{G^*_{ve,k} - G^*_{vexp,k}}{G^*_{vexp,k}} \right)^2 + J \sum_{i=1}^{n} \left(\frac{area_{ve,k} - area_{vexp,k}}{area_{vexp,k}} \right)^2 \qquad Eq.\ 4.83$$

Material properties assignation to the simulation object.— The finite element simulation of the component is divided by two simulations. First, it is required to know what deformation of each element of the mesh is once they are loaded with the testing amplitude. Once the deformation of each element is known, it is characterised by the corresponding Prony series. Hence, the first simulation consists of a simple initial tension as it is shown in Figure 4.29-A. This load is the peak amplitude which will be used in the posterior frequency sweep. In this first step, an initial guess of the rubber shear modulus is used to calculate the maximum equivalent shear strain [141].

Austrell [141] proposed a method to determine an equivalent simple shear strain of a general strain state of a finite element. To this end, a neo-Hooke hyperelastic model having the strain energy potential $W_0 = C_{10}\,(I_1-3)$, with I_1 being the first strain invariant (and the shear modulus $G=2C_{10}$) is defined. The neo-Hookean model is simple and useful in cases of moderate compression and shear dominated load cases. From Eq. 4.6 and Eq. 4.10, for a simple shear load case, the first strain invariant is $I_1=\gamma^2+3$, (γ is the direct shear strain defined as shear displacement divided by the sheared height). For a general load case, an equivalent shear strain γ_{eq} can be calculated from the strain energy amplitude W_0 of each element by putting the elastic strain energy of the simple shear load case equal to the strain energy of the general element load case, giving

$$\gamma_{eq} = \sqrt{W_0 / C_{10}} \qquad Eq.\ 4.84$$

The equivalent shear strain of each element is compared with the characterised Prony series (here four materials characterised by Prony series

tested with γ_1, γ_2, γ_3 and γ_4 shear strain levels), and the material is assigned. Some considerations:

a) $\gamma_{eq} < \gamma_1$: all these elements will be characterised by the material property characterised in the smallest strain testing condition.

b) $\gamma_{eq} > \gamma_4$ All these elements will be characterised by the material property characterised at the highest strain.

c) if the strain range γ_{eq} goes from γ_1 to γ_4, each element will be characterised by one of the levels γ_1, γ_2, γ_3 and γ_4 respectively

The elements of the viscoelastic model that will be assigned to the mesh, belonging to the four different load levels 1 to 4, are shown in Figure 4.29-A and Figure 4.29-B.

4.3.2 Material fitting to MLVE model

This section is directed to verify that the MLVE model with viscoelastic approach presented in the previous section 4.3.1 can simulate all the studied experimental cases correctly. For this purpose, the studied parts are the simple shear specimen and a rubber block is an industrial part.

In the previous section 4.2 we have studied three types of elastomers. As it is shown in the experimental work of the latter section, rubbers behave as linear materials as the filler quantity decreases. Consequently, the amplitude and rate-dependency diminishes as the filler quantity decreases. Therefore, as unfilled rubbers have near linear dynamic behaviour, they have historically been characterised by linear viscoelastic models. The problem begins when the filler content increases. Hence, in this thesis, the objective is the validation of the proposed model for very nonlinear rubbers. The elastomer showing higher nonlinearities of the three presented in the experimental work of the latter section is the rubber NR1, being the most appropriate elastomer to perform the validation of the presented model.

Once the model is fitted as presented in section 4.3.1, the Finite Element Analysis (FEA) simulations of the experimental NR1 are carried out in ANSYS. For a better representation of the obtained results, different sections are presented. First, the simple shear characterisation tests used to fit the material model are inversely simulated to validate both the methodology and the developed programs. Secondly, an industrial part presented as rubber block is simulated and correlated to its experimental tests in several amplitude conditions.

Concerning to material modelling, the ML model constants written in Table 4.2, are common for any strain and frequency condition. Therefore, the first element layer is characterised by a unique material characterised by the ML model.

MULTILINEAR PARAMETERS	
$E_{pini}(MPa)$	14.726
$\varepsilon_{ff,i}$ *(/1)*	$\sigma_{p,i}$ *(MPa)*
0.000186	0.002739
0.00217	0.01476
0.008139	0.028

Table 4.2: ANSYS MKIN model: Multi-linear kinematic hardening model fitting constants. Elastomer NR1.

In addition, the parameter G_∞ calculated in the previous static characterisation step remains constant for any VE Prony series fitted to the mentioned four shear strain amplitude sweeps as shown in Table 4.3.

PRONY SERIES: MATERIAL PARAMETERS FOR EQUIVALENT SHEAR STRAINS γ_{eq}

$G_\infty(MPa)$ common for any model		1.8806
γ_{eq}	$G_{ve,i}$	T_i
0.0031	0.3699	0.00402
	1.0603	0.29351
	3.9994	0.000139
0.0082	0.1767	0.00324
	1.0615	1
	3.5692	0.00012
0.02	0.1739	0.0018
	0.6858	1
	3.5	0.000083
0.041	0.2662	0.0015
	0.5072	0.1002
	5	0.000044

Table 4.3: ANSYS PRONY model. Viscoelastic Prony series parameters. Elastomer NR1

4.3.3 Simple shear: Experimental and FEA correlation.

4.3.3.1 Simple shear: Real model vs. Brick model in FEA

The experimental data for the material characterisation is performed in simple shear strain state. The simple shear specimen used for that purpose is the dual simple-shear specimen presented in section 4.1.1.

Once the material parameters of the MLVE model are fitted to the experimental data by the use of a Matlab application developed on this purpose, the next step consists of the ANSYS simulations of the simple shear specimen and correlation with the experimental data. For that purpose, an APDL program into ANSYS software (called Dynstiff) is developed to carry out the simulations.

When simulating by finite element methods, the computational time of calculation increases as the number of elements of the mesh is increased. The main goal is to reduce the model size (number of elements and nodes) as much as possible. To perform the ideal simple shear state simulation, only one brick element is required, which is the highest possible simplification. Sometimes, the mentioned simplifications of the models of finite elements produce an increase in the error when the predictions are correlated with

experimental tests. To avoid external errors produced by the simplifications, first, the predictions are performed by the finite element brick and the full model of the simple shear specimen used in the experimental data is compared. The work scheme is shown in the next Figure 4.39:

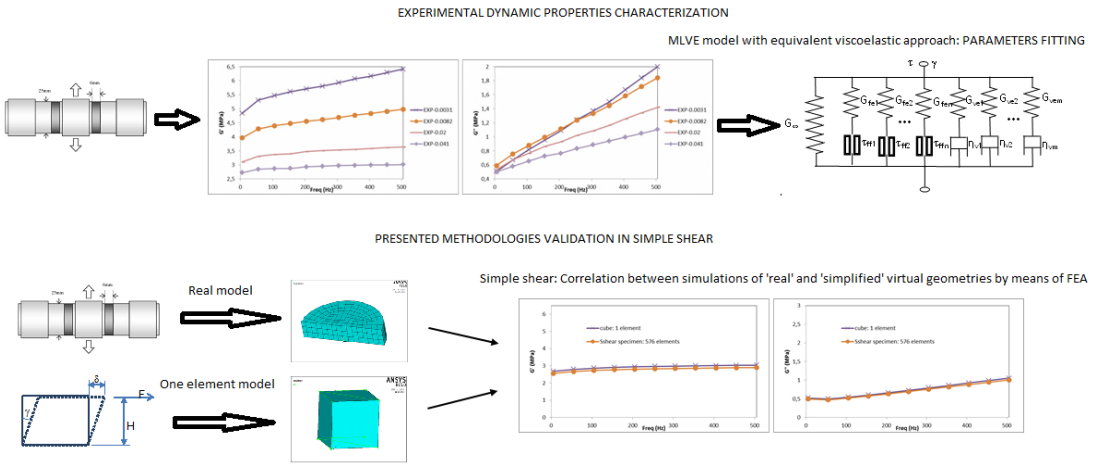

Figure 4.39: Work scheme to validate the simplified cube model. 1st the MLVE model is fitted to the experimental data obtained testing a real simple shear specimen in several testing conditions. 2nd the real and the brick models are characterised with previously fitted MLVE model to carry out simulations and correlate with the experimental data.

As explained in section 4.1.1, finite element calculations of the test specimen show that the shear modulus obtained from this test has to be increased by 6 percent to yield the same values as the ideal simple shear test, indicating that a perfect simple shear load case, is not obtained [141]. Firstly, this affirmation is verified for the studied rubber compound NR1, the applied characterisation and for the novel model presented in this work.

Two finite element models are correlated. One of them is a brick element sided by 1x1x1 millimetres, meshed with a SOLID 185 element (8 node hexahedral type elements). The second, which is a reproduction of the used simple shear specimen (The B option of dual simple-shear specimen presented in section 4.1.1), meshed with the same type of element are presented in Figure 4.40-A and B respectively.

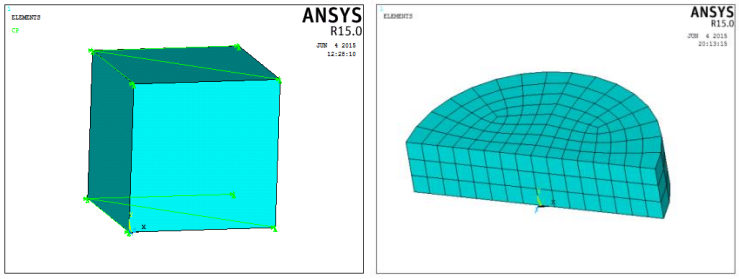

Figure 4.40: Simple shear specimens A) Simplified shear cube meshed with a unique element. B) Reproduction of the used simple shear characterisation specimen composed by 576 brick elements.

For the simple shear specimen due to symmetry, only half of the full geometry was modelled in ANSYS (see Figure 4.40-B). The finite element for this model consisted of 452 nodes and 576 elements.

The loading on both specimens consisted of a constant sinusoidal load with a peak strain amplitude of 4,1% and a frequency sweep between 5 and 505 Hz with a linear step size of 50 Hz.

The first objective is to achieve a good agreement in the correlation between both simulations of the simplified shear cube and the simple shear characterisation specimen in ANSYS.

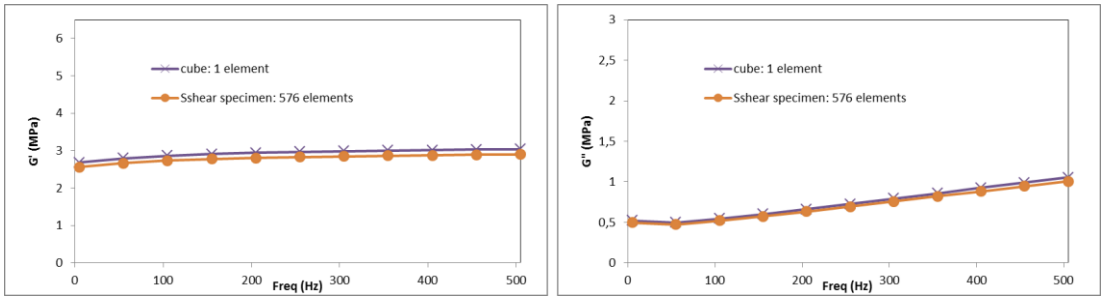

A) B)

Figure 4.41: Simulation correlations of simplified shear cube and simple shear characterisation specimen: Dynamic properties G' and G'' versus frequency (Hz) A) and B) are represented respectively.

Results and discussion.—

For this material, the finite element calculations of the test specimen, the characterisation method and the presented material model show that the storage and loss shear modulus obtained from this test have to be increased by 4.5 instead of 6 percent mentioned in literature to yield the same values as the ideal simple shear test (1 brick element), indicating that a perfect simple shear load case is not obtained.

4.3.3.2 Experimental and simulation correlations in simple shear

As concluded in section 4.3.3.1, the experimental data must be treated and the obtained results increased in 4.5% to have a real simple shear values for this material.

These simulations are performed using the 1 cube or brick element presented in the previous section 4.3.3.1. These experimental and simulation correlations are performed to validate the MLVE model with equivalent VE approach, the proposed characterisation method, the program built in MATLAB to fit the material constants, the overlay technique and the program built in ANSYS with ADPL programming language [150] to perform the dynamic predictions of industrial elastomeric parts.

The studied peak amplitudes in the validation test and simulations are 0.31, 0.82, 2.05 and 4.1 percent respectively and the material is NR1 as presented in Table 4.1. The work scheme is shown in the next figure,

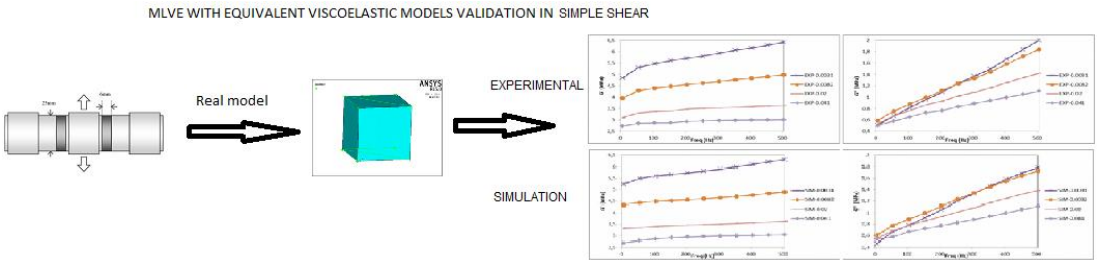

Figure 4.42: Work scheme to validate the MLVE model with equivalent VE approach in simple shear.

In the next Figure 4.43, the experimental results of the simple shear specimen are presented,

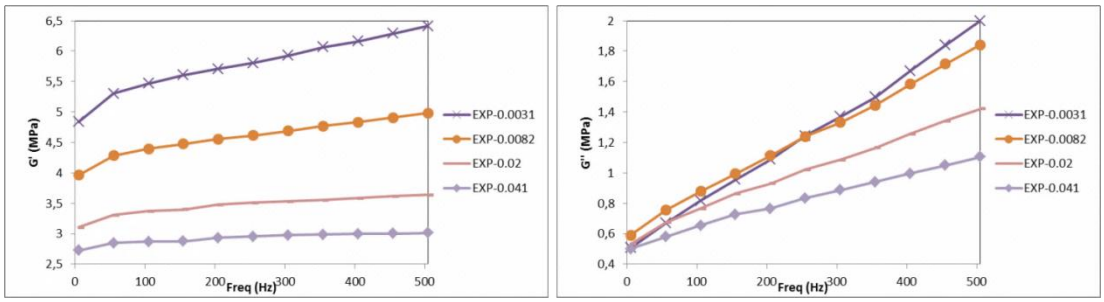

A) B)

Figure 4.43: Experimental dynamic results of the simple shear specimen: Dynamic properties G' and G'' versus frequency (Hz) A) and B) respectively are represented.

In the next Figure 4.44, the simulations of the simple shear strain state (simplified brick element model in section 4.3.3.1) performed in ANSYS are presented:

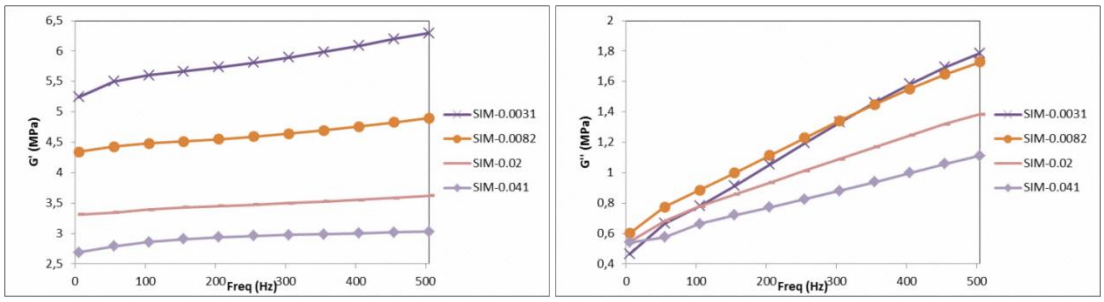

A) B)

Figure 4.44: Simulation with MLVE model with equivalent VE approach of the dynamic results of the simple shear strain state: Dynamic properties G' and G'' versus frequency (Hz) A) and B) respectively are represented.

4.3.3.3 Results and discussion

Figure 4.43 shows four of the eight experimental curves obtained from *Kareaga* [139] (Figure 4.25-A and B).

The MLVE model is fitted to the studied elastomer NR1 using an application programmed in Matlab, which gives the required material constants. The

parameters of the ML model written in Table 4.2 are common for any strain level and frequency. As mentioned before, the viscoelastic model depends on the strain level. The viscoelastic parameters are given in Table 4.3. where, G_∞ is common for all viscoelastic models fitted to the mentioned four shear strain levels.

Experimental results of *G'* and *G"* shown in Figure 4.43 are correlated to the simulations shown in Figure 4.44 performed with the MLVE model with equivalent VE approach programmed in ANSYS. The maximum deviation between experimental and simulations produced with the presented characterisation method do not cross the barrier of 11%. In the next Table 4.4 it is shown the deviation between experimental and simulation results for all of the studied amplitude cases presented in Figure 4.43 and Figure 4.44:

% DEVIATION TABLE (EXPERIMENTAL AND SIMULATION CORRELATION)								
Amp (unitary)	0,0031		0,008		0,0205		0,041	
Frqcy(Hz)	Ksto	Kloss	Ksto	Kloss	Ksto	Kloss	Ksto	Kloss
5	8,38	8,14	9,54	1,75	6,70	1,71	1,25	8,22
55	3,66	0,57	3,39	2,42	1,23	1,26	2,16	0,48
105	2,51	4,59	2,02	0,78	0,76	1,74	0,32	1,33
155	1,07	4,61	0,94	0,31	0,94	0,77	1,12	0,80
205	0,40	3,04	0,16	0,09	0,70	0,55	0,12	1,02
255	0,01	3,97	0,51	0,90	1,07	0,84	0,15	0,85
305	0,60	2,78	1,09	0,72	0,88	0,43	0,00	0,53
355	1,27	2,44	1,48	0,38	0,76	0,29	0,06	0,05
405	1,15	5,23	1,53	2,07	0,84	0,81	0,20	0,22
455	1,45	7,94	1,62	3,94	0,76	1,56	0,51	0,76
505	1,82	10,69	1,69	6,11	0,48	2,48	0,54	0,60

Table 4.4: Deviation table. Experimental and simulation correlation of the studied simple shear cases. Four amplitudes are studied in the frequency range between 5 and 505 Hz.

4.3.4 Rubber block: Experimental and FEA simulations correlation

Once the characterisation methods and programs are validated satisfactorily at specimen level, the second objective consists of performing the MLVE model validation in an industrial part. When the studied industrial part is deformed, the strain range varies between different points of the geometry which does not happen in the characterisation, the specimen being constant in all the geometry. In addition, the strain states of the elements which

compose the mesh are more complex than in the characterisation specimen. The work scheme is shown in the next figure:

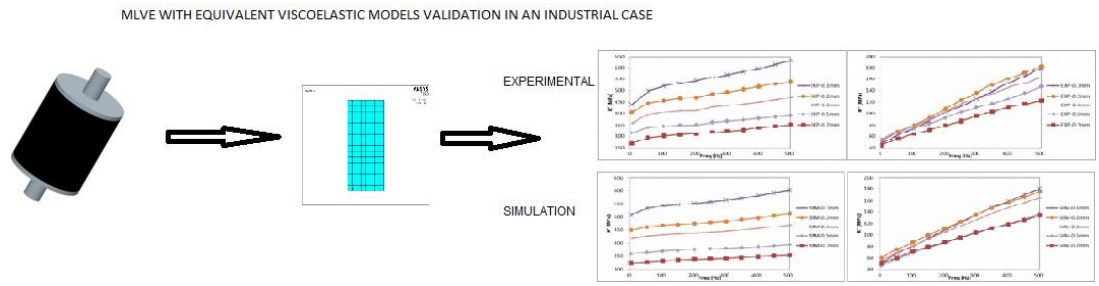

Figure 4.45: Work scheme to validate the MLVE model with equivalent VE approach in an industrial case (rubber block).

4.3.4.1 Geometry definition and testing conditions

The industrial part consists of a 35mm diameter and 35 mm thick rubber cylinder (see Figure 4.46).

Figure 4.46: Industrial part: Rubber block. In black, a 35mm diameter and 35mm thickness rubber cylinder sandwiched between two metal end pieces. One of the two metal end pieces is fixed and the other end piece is displaced in the axial direction.

The degree of cure is directly related to the measured stiffness and damping and it is one of the most important parameters to be taken into account. The thickness differences of the studied simple shear specimen and rubber block with 6mm and 35 mm thicknesses respectively require the use of different cure times in each type of geometry in order to obtain the same degree of cure in both. To this end, the first characterisation method proposed to control the degree of cure between different geometries can be applied (explained in section CHAPTER 2.)

The tests consist of five different amplitude frequency sweeps: from 0.05Hz to 500.05 Hz. The tested peak displacement amplitudes are 0.05, 0.1, 0.15, 0.25 and 0.35 millimetres. The experimental results are presented in Figure 4.48. The MTS test system presented in section 4.2.3 is used to perform the mentioned essays. Hence, the material properties characterisation (carried out by simple shear specimens) and the dynamic measurements of the industrial part (rubber to metal bonded rubber block) are performed in the same servo-hydraulic machine.

The finite element model as the loading conditions of the rubber block that are presented above is meshed with the element type PLANE182 used for 2-D modelling of solid structures. The mentioned element can be used as an axisymmetric element. It is defined by four nodes having two degrees of freedom at each node: translations in the nodal x and y directions. The rubber block geometry is simplified in an axisymmetric cross sectional area in order to reduce the number of the mesh elements (See Figure 4.47):

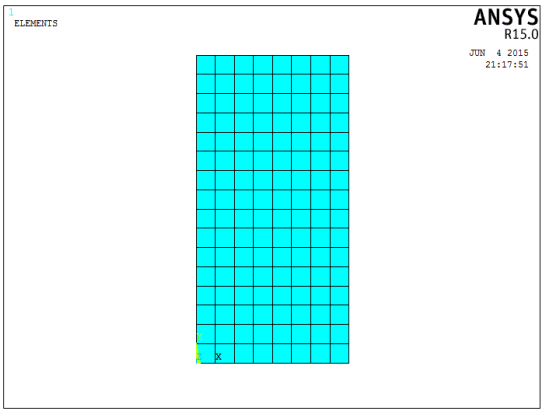

Figure 4.47: The rubber block finite element model is composed by 153 nodes and 256 quad elements.

4.3.4.2 Results and discussion

The geometry and testing conditions are detailed in section 4.3.4.1. In the next Figure 4.48, the experimental results of the industrial part (rubber block) are presented:

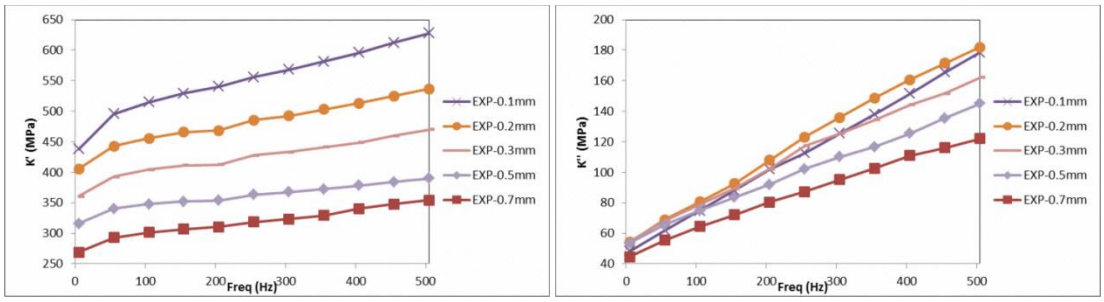

A) B)

Figure 4.48: Experimental dynamic results of the industrial case rubber block: Dynamic properties K' and K" versus frequency (Hz) A) and B) are represented respectively.

In the next Figure 4.49, the simulations of the industrial part performed in ANSYS are presented:

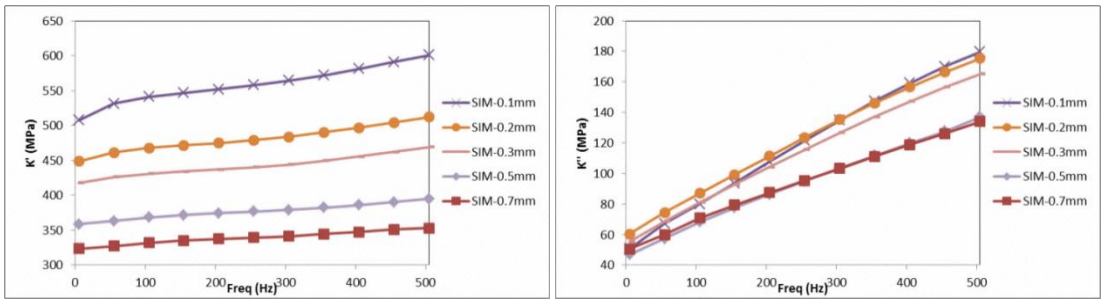

A) B)

Figure 4.49: Simulation with MLVE model with equivalent VE approach of the dynamic results of the industrial case rubber block: Dynamic properties K' and K" versus frequency (Hz) A) and B) are represented respectively.

The validation of the MLVE model with equivalent VE approach model has been performed. Experimental results of *K'* and *K"* shown in Figure 4.48 are correlated to the simulations shown in Figure 4.49 performed with the MLVE model with equivalent viscoelastic model programmed in ANSYS (Dynstiff

application). The range of the studied frequencies is between 5 and 505 Hz. Five peak to peak amplitude levels (0.1, 0.2, 0.3, 0.5 and 0.7mm) are tested experimentally and correlated with the ANSYS simulations. The maximum deviation in the experimental and simulation correlations is around 20%. The mayor deviation is produced in the correlation of the storage stiffness *K'* performed with the peak to peak amplitude of 0.7mm (see Figure 4.48-A and Figure 4.49-A). This deviation could be avoided by the use of more equivalent VE models. This implies that it would be necessary to characterise more equivalent strain levels than the four used in the present work (see Table 4.3). In the next Table 4.5 it is shown the deviation between experimental and simulation results for all of the studied peak to peak amplitude cases presented in Figure 4.48 and Figure 4.49:

% DEVIATION TABLE (EXPERIMENTAL AND SIMULATION CORRELATION)										
Amp p-p (mm)	0,1		0,2		0,3		0,5		0,7	
Frqcy(Hz)	Ksto	Kloss	Ksto	Kloss	Ksto	Kloss	Ksto	Kloss	Ksto	Kloss
5	15,83	5,24	10,62	11,37	15,74	1,47	13,53	12,15	20,37	13,47
55	7,24	8,71	4,18	8,31	8,45	0,70	6,77	12,50	11,69	8,14
105	5,10	6,77	2,69	7,82	6,55	3,09	5,81	8,78	10,19	9,72
155	3,33	6,19	1,23	7,18	5,53	3,66	5,56	7,33	9,27	9,99
205	2,10	5,48	1,32	3,24	5,98	2,12	5,76	6,09	8,73	8,88
255	0,38	7,85	1,42	0,26	2,91	1,42	3,63	7,11	6,55	9,47
305	0,72	7,49	1,76	0,56	2,58	0,96	3,12	6,03	5,60	8,65
355	1,69	6,83	2,61	1,69	1,96	2,03	2,74	4,12	4,66	8,25
405	2,45	5,05	3,16	2,51	1,54	2,09	2,16	4,45	2,14	7,08
455	3,53	2,66	3,99	2,99	0,53	3,17	1,69	5,79	0,84	8,62
505	4,27	0,66	4,62	3,61	0,23	1,93	1,25	5,60	0,37	9,84

Table 4.5: Deviation table. Experimental and simulation correlation of the studied cases. Five peak to peak amplitude cases are studied in the frequency range between 5 and 505 Hz.

CHAPTER 5 CONCLUSIONS

Two characterisation methods are proposed in CHAPTER 3 and CHAPTER 4. The first is related to the strain rate influence on the static stiffness of elastomers and the last is related to a novel characterisation method for the prediction of dynamic properties of filled rubbers by the use of finite element method. Previously, in the CHAPTER 2, a method focused on the determination of the degree of cure of rubber parts is developed. One of the most important parameters to avoid is a different degree of cure between the characterisation specimens used to characterise the static/dynamic behaviour of rubbers and the industrial parts to be predicted. The latter method is applied in CHAPTER 3 and CHAPTER 4 to assure the same degree of cure of various parts manufactured by the use of the same material.

Degree of cure:

When vulcanizing a rubber formulation, it is necessary to take into consideration the cure temperature and the cure time because of their effect on the decomposition of the curing agents. The cure time could also lead to a reversion phenomenon or even to a non-completed cure stage. This reversion phenomenon is exhibited as an increase of the swelling ratio of the rubber formulation and a reduction of the mechanical properties such as the modulus values at Tensile Tests, together with a reduction of the oscillating torque in ODR measurements.

The aim of the study presented in Annex-I to check the applicability of simple swelling tests to evaluate the degree of cure achieved in rubber parts. Other swelling procedures, such as those being based on the *Flory-Rehner* equation, are considered to be too complicated and too time consuming for a practical industrial application. The analysis of swelling data obtained by simple procedures allows a reasonable assessment of the degree of cure in a rapid and uncomplicated way. This could be exemplary demonstrated within a broad test programme covering the examination of laboratory and regular production samples from two formulations, i.e. a conventionally sulphur cured NR and a peroxide cured EPDM. The determined swelling rates are in good conformity with the data from the rheometer traces and the tensile moduli reflecting

realistically the progress of the crosslinking reaction. In addition to that, the swelling data gave valuable insights on how the manufacturing process influences the complete vulcanization of a rubber part. This work dimensions, the way of heat transfer and the curing time are factors which should not be underestimated. When vulcanizing rubber formulations, the fixing of cure temperature and cure time needs a special attention to avoid reversion effects, incomplete decomposition of the curing agents, and irregular vulcanization.

The swelling test can be useful, but it is a simple tool for checking the degree of cure of rubber parts for quality control and even development purposes or in situations where other test methods fail to obtain reasonable results.

When comparing ODR test torque results and the swelling ratios for these samples, the swelling values show a minimum value point which represents the maximum degree of cure point; this point matches with the point of maximum torque in ODR tests. After this point, the NR-sulfur formulation shows a clear reversion phenomenon, which is indicated as a torque decay in the ODR tests and as an increase of the swelling values. EPDM formulation does not exhibit this behaviour at low temperatures (the cure is not completed), but a small torque decrease is displayed when tested at high temperatures.

This is also checked for tensile test specimens, for which swelling tests and measurements of modulus values as test tensile at 100 and 200 % elongation were made. The modulus values achieve a maximum value after which the value goes decreasing in NR formulation for higher cure times (related to the reversion phenomenon); EPDM formulation show similar values (a decay is not shown) for larger cure times. Swelling values give a minimum value, after which the value goes increasing for NR formulation because of the reversion, whereas it can be considered that EPDM formulation keeps the value (it really goes increasing slowly as time goes on). The point of minimum swelling matches in time with the point of maximum modulus values. No matching between the minimum swelling values measured for tensile test samples and ODR samples is seen; it is concluded this difference is related to different processing procedures of each sample, and, as a consequence, the materials suffer different thermal histories. This affects the crosslink densities, and as a result, the swelling values.

It is clearly seen that swelling ratio on a specific solvent can be matched to torque values measured in an ODR test (and each torque value can be associated to a specific degree of cure), or it can be matched to modulus values measured in tensile tests. As a consequence, the degree of cure of rubber parts can be defined using a simple procedure, so that it will be a useful procedure for quality control purposes of rubber parts and even for other more scientific purposes. Measurements done in an industrial area show the usefulness of the present method, illustrating that the external layer of the part achieves a full degree of cure whereas, the core material is not completely cured.

Quasi static characterisation methods: Conditioning research:

The static tests are carried out following some specifications. It is common to find test speeds that can range from 1 mm/min up to 500 mm/min. Therefore, the tests known as static tests can be really quasi-static or non-static depending on the test speed. It is known that mechanical stiffness of rubber compounds are very influenced by its deformation rate.

When a complex geometry is tensioned, the different points of the tested part are strained. The strain range can be very wide, which means that the strain rate of the zones that are more strained is higher than the less strained zones. Then, in the same geometry manufactured with one rubber compound, it can be said that the material behaves differently.

The ESED functions programmed in commercial finite element software have the capability to fit the hyperelastic behaviour of rubber compounds when they are tested statically (when the test speed is near zero). This ‘problem’ may be solved by influencing the experimental test of the characterisation specimen. In this way, several characterisation methods are presented in the literature but no one solved the mentioned problem of the difference of the strain rate in different zones of the tested part.

Correlating the standard two characterisation methods with the proposed method, the best choice to predict the behaviour of an industrial part is the new proposed method. The main advantages of the new method are: it considers

the strain range, the strain rates of each point of the simulated part and the cycles of the mechanical conditioning. Besides, any existing hyperelastic model (ESED Function) could be used to carry out this kind of non-static simulations by means of FEA.

Modelling of dynamic properties of rubbers

The MLVE model with equivalent VE approach has been studied. The experimental vs. simulation agreement demonstrates that the presented method is valid to characterise and simulate the amplitude/frequency dependence on the dynamic properties of highly filled elastomers in a wide range of amplitudes and frequencies.

The MLVE model with equivalent VE approach can be characterised with a number of friction and viscoelastic elements. This model requires only two superposed meshes being independent from the number of friction and viscoelastic elements of the model. This method reduces considerably the calculation time required by the classical elastoplastic-viscoelastic model.

The first correlation performed in simple shear demonstrates the suitability of the MLVE model for each characterised strain level in simple shear. In order to characterise the frequency influence at different amplitudes, the use of equivalent VE fitting is required and each of the mentioned four amplitudes has been characterised and simulated with a very good agreement. In simple shear, the strain is the same in any point of the specimen which helps to fit the experimental data and to achieve a good correlation in posterior simulations. A second correlation has been performed in geometry with a considerable difference between the maximum and minimum strains of the deformed mesh when it is loaded. The good agreement between experimental and simulation correlation demonstrates the validity of the mesh division in equivalent shear strain groups and the assignation of the equivalent VE characterisations.

Finally, it is foreseen that more divisions of the mesh in equivalently deformed element groups and more VE fittings at more strain amplitudes will even reduce the error percentage when experimental and simulation results are correlated.

CHAPTER 6 CONTRIBUTION TO KNOWLEDGE ACADEMIC CHALLENGE AND FUTURE WORK

6.1 Contribution to knowledge

The intention of the present work is to develop a methodology where the main studied area is the testing and simulating of dynamic behaviour of elastomers. Previously, two characterisation methods are developed with the objective to supply valuable information.

The first characterisation method is directed to propose a simple method which consists of various swelling tests of rubber pieces into compatible solvent. The swelling degree of the latter pieces is a value which is used to determine the degree of cure. First, the procedure to create the swelling trace is presented where the samples used in the characterisation are obtained from several ODR Rheometer tests. Later, the degree of cure of any vulcanized part (both material characterisation samples as industrial parts) can be correlated to the swelling trace obtaining their vulcanization degree.

In the second part of the thesis, a procedure related to the conditioning of rubbers in quasi-static tests is developed. This conditioning method takes into account how the stiffness is changed as the strain rate is increased. The presented conditioning method is correlated with two of the most used conditioning methods, obtaining a better agreement in the correlation of experimental and simulation tests than in standard methods.

The intention of the third and most important part of the thesis is the implantation of characterisation and simulation methodologies to simulate the dynamic stiffness and damping of rubber made complex geometries using the finite element code ANSYS. The current procedure allows:

- A simple characterisation of the dynamic properties of rubber.
- The material model to be built by the use of standard material models programmed in commercial finite element software avoiding the need of subroutines implementation.

- The use of a multilinear single curve to characterise the amplitude dependence on the stiffness and damping. This method smoothen the sharp edges produced by a single elastoplastic element in a load cycle.
- The need of several elastoplastic elements to smooth the hysteresis loop that is replaced with a unique multilinear curve.
- The different strain rates present in the finite element mesh to be correctly characterised with various equivalent viscoelastic models characterised as Prony series. The model captures the most marked stiffening at lower amplitudes when frequency is increased.
- First, the use of a multi-linear kinematic hardening elasto-plastic model for the frictional behaviour and second, the viscoelastic approach that requires only two superimposed meshes when using the overlay method. This reduces considerably the calculation time.

To the consecution of the present objective, two mathematical applications were created:

- MLVE Fitting algorithm in Matlab: This program is used to calculate the parameters of the proposed model to fit the model to the experimental data.
- ANSYS APDL program: This application is programmed to reproduce the experimental tests performed with a servo-hydraulic testing machine. This program is used to assign the material properties to each element and calculate the dynamic properties at the frequencies and amplitudes applied.

6.2 Future work

In order to improve the predictions of dynamic stiffness and damping of rubber parts, some new research areas could be considered:

- Discuss the application of the proposed model including temperature and pre-load dependency.
- Check the applicability of the model in bushings where the external metallic ring is pre-strained.
- Investigate how the model could be applied in transient analysis.

- Implement fractional derivatives to characterise the equivalent viscoelastic materials in order to reduce the number of material parameters
- Investigate the design of the simple shear characterisation sample to enable a wider range of testing amplitudes in the same testing machine.

NOMENCLATURE

Abbreviation	Name
σ	Uniaxial stress
ε	Uniaxial strain
F	Force
ESED	Elastic strain energy density
K	Stiffness
δ	Displacement
E	Young Modulus
L_0	Initial length
L	Final length
G	Shear modulus
τ	Shear stress
γ	Shear strain
V_0	Initial volume
V_f	Final volume
ε_v	Volumetric strain
p	Hydrostatic pressure
k	Bulk modulus
d	Compressibility constant
λ	Stretch
EPVE	Elastoplastic-viscoelastic constitutive model
EP	Elastoplastic constitutive model
VE	Viscoelastic constitutive model
MLVE	Multilinear-viscoelastic constitutive model
ML	Multilinear constitutive model
/1	Unitary strain
G_∞	Relaxed shear modulus
W_0	Elastic strain energy density
C_{10}	Hyperelastic parameter
G’	Storage modulus
G”	Loss modulus
G_{ve}	Shear modulus of the viscoelastic component
G^*	Dynamic shear modulus
G^*_{exp}	Experimental dynamic shear modulus
δ	Phase angle
area	Hysteresis area
τ	Shear stress
τ_0	Shear stress amplitude

τ_{ff}	Yield stress in shear
τ_p	Shear stress point in a multilinear curve
γ_0	Shear strain amplitude
γ_{ff}	Yield strain of the elastoplastic element
γ_{eq}	Equivalent shear strain
T	Relaxation time
η_v	Dashpot viscosity constant
t	time
ω	Angular frequency
DSC	Differential Scanning Calorimeter
NR	Natural rubber
EPDM	Ethylene-propylene-diene rubber
ODR	Oscillating Disc Rheometer
MDR	Moving Die Rheometer
SBR	Styrene-butadiene rubber
NBR	Acrylonitrile-butadiene rubber
ti	Scorch or induction time
α	Alpha, degree of cure. Its value goes between 0 (0% cure) and 1 (100% cure).

REFERENCES

[1] Arrillaga A, Kareaga Z, Retolaza E, Zaldua AM. Bestimmung des Vulkanisations grades von Gummi durch Quellung. Gummi Fasern Kunststoffe 2011;64.

[2] Arrillaga A, Kareaga Z, Retolaza E, Zaldua AM. Determining the state of cure of rubber by means of swelling. Rubber Fibres Plast Int 2012;7.

[3] Kareaga Z, Guraya T, Arriaga A, Austrell P-E. Extending the overlay method in order to capture the variation due to amplitude in the frequency dependence of the dynamic stiffness and loss during cyclic loading of elastomers. Const. Models Rubber IX, Prague: 2015.

[4] Gent AN. Engineering with rubber: how to design rubber components. Carl Hanser Verlag GmbH Co KG; 2012.

[5] ISO 1629:2013 Rubbers and latices-Nomenclature. International Organization for Standards; 2013.

[6] Manual for the Rubber Industry. Bayer AG, Rubber Business Group, Research and Development Section, D-51368 Leverkusen 1995.

[7] Ward IM, Sweeney J. An Introduction to the Mechanical Properties of Solid Polymers. John Wiley & Sons; 2004.

[8] Peng SH, Shimbori T, Naderi A. Measurement of Elastomer's Bulk Modulus by Means of a Confined Compression Test. Rubber Chem Technol 1994;67:871–9. doi:10.5254/1.3538718.

[9] Charlton DJ, Yang J, Teh KK. A Review of Methods to Characterize Rubber Elastic Behavior for Use in Finite Element Analysis. Rubber Chem Technol 1994;67:481–503. doi:10.5254/1.3538686.

[10] Gent AN. Rubber Elasticity: Basic Concepts and Behavior. In: Mark JE, Erman B, Eirich FR, editors. Sci. Technol. Rubber Third Ed., Burlington: Academic Press; 2005, p. 1–27.

[11] Oden JT. Finite Elements of Nonlinear Continua. Mineola, N.Y.: Dover Publications; 2006.

[12] Malvern LE. Introduction to the Mechanics of a Continuous Medium. 1st edition. Englewood Cliffs, N.J.: Prentice Hall; 1977.

[13] Beatty MF. Topics in Finite Elasticity: Hyperelasticity of Rubber, Elastomers, and Biological Tissues—With Examples. Appl Mech Rev 1987;40:1699–734. doi:10.1115/1.3149545.

[14] Turner MJ. R. W. Clough, H. C. Martin and L. J Topp'Stiffness Deflection Anal Complex Struct J Aero Space Sci 1956;23:805–823.

[15] ANSYS IC. 11.0 Help Manual. ANSYS Inc 2009.

[16] ANSYS A. programmer′ s guide. ANSYS. Inc March 2002.

[17] Kuhn W. Beziehungen zwischen Molekülgröße, statistischer Molekülgestalt und elastischen Eigenschaften hochpolymerer Stoffe. Kolloid-Z 1936;76:258–71. doi:10.1007/BF01451143.

[18] James HM, Guth E. Theory of the elastic properties of rubber. J Chem Phys 1943;11:455–81. doi:10.1063/1.1723785.

[19] Flory PJ, Rehner J. Statistical mechanics of cross-linked polymer networks I Rubberlike elasticity. J Chem Phys 1943;11:512–20. doi:10.1063/1.1723791.

[20] Treloar LRG. The Physics of Rubber Elasticity. Oxford University Press; 1975.

[21] Ratsimba CHH. Fatigue crack growth of carbon black reinforced elastomers. Ph.D. Dissertation. Queen Mary and Westfield College, 2000.

[22] Rivlin RS. Large Elastic Deformations of Isotropic Materials. I. Fundamental Concepts. In: Barenblatt GI, Joseph DD, editors. Collect. Pap. RS Rivlin, Springer New York; 1997, p. 23–54.

[23] Mooney M. A theory of large elastic deformation. J Appl Phys 1940;11:582–92. doi:10.1063/1.1712836.

[24] Rivlin RS. Large elastic deformations. In: Eirich FR, editor. Rheology, Academic Press; 1956, p. 351–85.

[25] Yeoh OH. Characterization of Elastic Properties of Carbon-Black-Filled Rubber Vulcanizates. Rubber Chem Technol 1990;63:792–805. doi:10.5254/1.3538289.

[26] Tschoegl NW. Constitutive Equations for Elastomers. Rubber Chem Technol 1972;45:60–70. doi:10.5254/1.3544713.

[27] James AG, Green A. Strain energy functions of rubber. II. The characterization of filled vulcanizates. J Appl Polym Sci 1975;19:2319–30. doi:10.1002/app.1975.070190822.

[28] Gregory MJ. The stress/strain behaviour of filled rubbers at moderate strains. Plast Rubber Mater Appl 1979;4:184–8.

[29] Varga OH, Dill EH. Stress-Strain Behavior of Elastic Materials. J Appl Mech 1967;34:254.

[30] Ogden RW. Recent Advances in the Phenomenological Theory of Rubber Elasticity. Rubber Chem Technol 1986;59:361–83. doi:10.5254/1.3538206.

[31] Valanis KC, Landel RF. The Strain-Energy Function of a Hyperelastic Material in Terms of the Extension Ratios. J Appl Phys 1967;38:2997–3002. doi:10.1063/1.1710039.

[32] Rivlin RS, Sawyers KN. The Strain-Energy Function for Elastomers. In: Barenblatt GI, Joseph DD, editors. Collect. Pap. RS Rivlin, Springer New York; 1997, p. 405–17.

[33] Gent AN. A New Constitutive Relation for Rubber. Rubber Chem Technol 1996;69:59–61. doi:10.5254/1.3538357.

[34] Fukahori Y, Seki W. Molecular behaviour of elastomeric materials under large deformation: 1. Re-evaluation of the Mooney-Rivlin plot. Polymer 1992;33:502–8. doi:10.1016/0032-3861(92)90726-D.

[35] Davies CKL, De DK, Thomas AG. Characterization of the Behavior of Rubber for Engineering Design Purposes. 1. Stress-Strain Relations. Rubber Chem Technol 1994;67:716–28. doi:10.5254/1.3538706.

[36] Othman AB, Gregory MJ. A stress strain relationship for filled rubber. J Nat Rubber Res n.d.;44:440–78.

[37] Gregory IH, Muhr AH, Stephens IJ. Engineering applications of rubber in simple extension. Plast. Rubber Compos. Process. Appl., vol. 26, Institute of Materials; 1997, p. 118–22.

[38] Yeoh OH, Fleming PD. A new attempt to reconcile the statistical and phenomenological theories of rubber elasticity. J Polym Sci Part B Polym Phys 1997;35:1919–31. doi:10.1002/(SICI)1099-0488(19970915)35:12<1919::AID-POLB7>3.0.CO;2-K.

[39] Arruda EM, Boyce MC. A three-dimensional constitutive model for the large stretch behavior of rubber elastic materials. J Mech Phys Solids 1993;41:389–412. doi:10.1016/0022-5096(93)90013-6.

[40] Simo JC. On a fully three-dimensional finite-strain viscoelastic damage model: Formulation and computational aspects. Comput Methods Appl Mech Eng 1987;60:153–73. doi:10.1016/0045-7825(87)90107-1.

[41] Govindjee S, Simo J. Transition from micro-mechanics to computationally efficient phenomenology: Carbon black filled rubbers incorporating mullins' effect. J Mech Phys Solids 1992;40:213–33. doi:10.1016/0022-5096(92)90324-U.

[42] Hawkes J, Harris J, Stevenson A, Becker E, Miller T, McMullen M. Fatige life calculations for elastomeric engineering components. Manchester: Proceedings of the international Rubber Conference; 1996.

[43] Ogden RW, Roxburgh DG. A pseudo–elastic model for the Mullins effect in filled rubber. Proc R Soc Lond Ser Math Phys Eng Sci 1999;455:2861–77. doi:10.1098/rspa.1999.0431.

[44] Miehe C. Discontinuous and continuous damage evolution in Ogden-type large-strain elastic materials. Eur J Mech Solids 1995;14:697–720.

[45] Miehe C, Keck J. Superimposed finite elastic–viscoelastic–plastoelastic stress response with damage in filled rubbery polymers. Experiments, modelling and algorithmic implementation. J Mech Phys Solids 2000;48:323–65. doi:10.1016/S0022-5096(99)00017-4.

[46] Hamed GR, Hatfield S. On the Role of Bound Rubber in Carbon-Black Reinforcement. Rubber Chem Technol 1989;62:143–56. doi:10.5254/1.3536231.

[47] Medalia AI. Elastic Modulus of Vulcanizates as Related to Carbon Black Structure. Rubber Chem Technol 1973;46:877–96. doi:10.5254/1.3547416.

[48] Caruthers JM, Cohen RE, Medalia AI. Effect of Carbon Black on Hysteresis of Rubber Vulcanizates: Equivalence of Surface Area and Loading. Rubber Chem Technol 1976;49:1076–94. doi:10.5254/1.3534990.

[49] Medalia AI. Effect of Carbon Black on Dynamic Properties of Rubber Vulcanizates. Rubber Chem Technol 1978;51:437–523. doi:10.5254/1.3535748.

[50] Holt WL. Behavior of Rubber under Repeated Stresses. Rubber Chem Technol 1932;5:79–89. doi:10.5254/1.3539319.

[51] Mullins L. Softening of Rubber by Deformation. Rubber Chem Technol 1969;42:339–62. doi:10.5254/1.3539210.

[52] Bueche F. Molecular Basis for The Mullins Effect. Rubber Chem Technol 1961;34:493–505. doi:10.5254/1.3540224.

[53] Harwood JAC, Mullins L, Payne AR. Stress Softening in Natural Rubber Vulcanizates. Part II. Stress Softening Effects in Pure Gum and Filler Loaded Rubbers. Rubber Chem Technol 1966;39:814–22. doi:10.5254/1.3547145.

[54] Harwood JAC, Payne AR. Stress Softening in Natural Rubber Vulcanizates III. Carbon Black Filled Vulcanizates. Rubber Chem Technol 1966;39:1544–52. doi:10.5254/1.3547069.

[55] Houwink R. Slipping of Molecules during the Deformation of Reinforced Rubber. Rubber Chem Technol 1956;29:888–93. doi:10.5254/1.3542602.

[56] Kraus G, Childers CW, Rollmann KW. Stress Softening in Carbon Black Reinforced Vulcanizates. Strain Rate and Temperature Effects. Rubber Chem Technol 1966;39:1530–43. doi:10.5254/1.3547068.

[57] Harris J, Stevenson A. On the Role of Nonlinearity in the Dynamic Behavior of Rubber Components. Rubber Chem Technol 1986;59:740–64. doi:10.5254/1.3538231.

[58] Rendek M, Lion A. Strain induced transient effects of filler reinforced elastomers with respect to the Payne-Effect: experiments and constitutive modelling. ZAMM-J Appl Math Mech Für Angew Math Mech 2010;90:436–458.

[59] UNE 53510:1985. Elastómeros. Determinación de las propiedades en tracción. AENOR; 1985.

[60] ISO37:2005(E). Rubber, vulcanized or thermoplastic – Determination of tensile stress-strain properties. International Organization for Standards; 2005.

[61] ASTM D412 - 06a(2013) Standard Test Methods for Vulcanized Rubber and Thermoplastic Elastomers—Tension n.d.

[62] UNE 53536:2001. Elastómeros. Determinación de las propiedades esfuerzo/deformación en compresión. AENOR; 2001.

[63] ISO7743. Rubber, vulcanized or thermoplastic – Determination of compression stress-strain properties. International Organization for Standards; 2004.

[64] ASTM D575 - 91(2012) Standard Test Methods for Rubber Properties in Compression n.d.

[65] UNE 53630:2010. Elastómeros. Determinación del módulo de elasticidad en cizalla. Método del cuádruple cizallamiento. AENOR; 2010.

[66] ISO 1827,ISO/TC 45. Rubber, vulcanized or thermoplastic – Determination of modulus in shear or adhesion to rigid plates. Quadruple shear method. International Organization for Standards; 1991.

[67] Nashif AD, Henderson JP. Vibration damping. John Wiley & Sons; 1985.

[68] Olsson A, Austrell P. A fitting procedure for a viscoelastic-elastoplastic material. Const. Models Rubber II, 2001.

[69] Sjöberg MM, Kari L. Non-Linear Behavior of a Rubber Isolator System Using Fractional Derivatives. Veh Syst Dyn 2002;37:217–36. doi:10.1076/vesd.37.3.217.3532.

[70] Dynamic Characterization Process. MTS System Corporation 2000.

[71] Fletcher WP, Gent AN. Nonlinearity in the Dynamic Properties of Vulcanized Rubber Compounds. Rubber Chem Technol 1954;27:209–22. doi:10.5254/1.3543472.

[72] Lion A, Kardelky C, Haupt P. On the Frequency and Amplitude Dependence of the Payne Effect: Theory and Experiments. Rubber Chem Technol 2003;76:533–47. doi:10.5254/1.3547759.

[73] Payne AR. The Dynamic Properties of Carbon Black-Loaded Natural Rubber Vulcanizates. Part I. Rubber Chem Technol 1963;36:432–43. doi:10.5254/1.3539570.

[74] Payne AR. The Dynamic Properties of Carbon Black Loaded Natural Rubber Vulcanizates. Part II. Rubber Chem Technol 1963;36:444–50. doi:10.5254/1.3539571.

[75] Warnaka GE, Miller HT. Strain-Dependent Properties of Polymers I. Rubber Chem Technol 1966;39:1421–7. doi:10.5254/1.3547057.

[76] Payne AR, Whittaker RE. Low Strain Dynamic Properties of Filled Rubbers. Rubber Chem Technol 1971;44:440–78. doi:10.5254/1.3547375.

[77] Warnaka GE. Dynamic Strain Effects in Elastomers. Rubber Chem Technol 1963;36:407–21. doi:10.5254/1.3539568.

[78] Huber G, Vilgis TA, Heinrich G. Universal properties in the dynamical deformation of filled rubbers. J Phys Condens Matter 1996;8:L409. doi:10.1088/0953-8984/8/29/003.

[79] Lindley PB. Engineering design with natural rubber. 4th ed. Brickendonbury: Malaysian Rubber Producers Research Association; 1974.

[80] Wang M-J. Effect of Polymer-Filler and Filler-Filler Interactions on Dynamic Properties of Filled Vulcanizates. Rubber Chem Technol 1998;71:520–89. doi:10.5254/1.3538492.

[81] Wang M-J. The Role of Filler Networking in Dynamic Properties of Filled Rubber. Rubber Chem Technol 1999;72:430–48. doi:10.5254/1.3538812.

[82] Mullins L, Tobin NR. Theoretical Model for the Elastic Behavior of Filler-Reinforced Vulcanized Rubbers. Rubber Chem Technol 1957;30:555–71. doi:10.5254/1.3542705.

[83] Lion A. Phenomenological Modelling of Strain-Induced Structural Changes in Filler-Reinforced Elastomers. KGK-Kautsch Gummi Kunststoffe 2005;58:157–162.

[84] Wang MJ, Patterson WJ, Ouiang GB. Dynamic stress-softening of filled vulcanisates. Pap Present Spring ACS Rubber Div Meet Montr 5-8 May 1996.

[85] Dutta NK, Tripathy DK. Effects of types of fillers on the molecular relaxation characteristics, dynamic mechanical, and physical properties of rubber vulcanizates. J Appl Polym Sci 1992;44:1635–48.

[86] Lion A. Constitutive modeling of the dynamic properties of elastomers. Const. Models Rubber V, 2008, p. 9.

[87] Voet A, Morawski JC. Adaptation of the Rheovibron to the Measurement of Dynamic Properties of Vulcanizates at Elongations up to Sample Rupture. Rubber Chem Technol 1974;47:758–64. doi:10.5254/1.3540462.

[88] Asare S, Thomas AG, Busfield JJC. Cyclic Stress Relaxation (Csr) of Filled Rubber and Rubber Components. Rubber Chem Technol 2009;82:104–12. doi:10.5254/1.3557000.

[89] Höfer P. Strain-induced nonlinearities of filler-reinforced rubber undeer cyclic deformations: Experiments and modelling. Const Models Rubber V 2008:41–6.

[90] Ferry JD. Viscoelastic Properties of Polymers. John Wiley & Sons; 1980.

[91] Williams ML, Landel RF, Ferry JD. The Temperature Dependence of Relaxation Mechanisms in Amorphous Polymers and Other Glass-forming Liquids. J Am Chem Soc 1955;77:3701–7. doi:10.1021/ja01619a008.

[92] Fletcher WP, Gent AN. Dynamic shear properties of some rubber-like materials. Br J Appl Phys 1957;8:194. doi:10.1088/0508-3443/8/5/303.

[93] Miller HT, Warnaka GE. Strain-Dependent Properties of Polymers II. Rubber Chem Technol 1966;39:1428–35. doi:10.5254/1.3547058.

[94] Coveney VA, Johnson DE, Turner DM. A Triboelastic Model for the Cyclic Mechanical Behavior of Filled Vulcanizates. Rubber Chem Technol 1995;68:660–70. doi:10.5254/1.3538765.

[95] Coveney VA, Johnson DE. Modeling of Carbon Black Filled Natural Rubber Vulcanizates by the Standard Triboelastic Solid. Rubber Chem Technol 1999;72:673–83. doi:10.5254/1.3538825.

[96] Coveney VA, Johnson DE. Rate-Dependent Modeling of a Highly Filled Vulcanizate. Rubber Chem Technol 2000;73:565–77. doi:10.5254/1.3547606.

[97] Lion A. Thixotropic behaviour of rubber under dynamic loading histories: Experiments and theory. J Mech Phys Solids 1998;46:895–930. doi:10.1016/S0022-5096(97)00097-5.

[98] Berg M. A model for rubber springs in the dynamic analysis of rail vehicles. Proc Inst Mech Eng Part F J Rail Rapid Transit 1997;211:95–108.

[99] Austrell PE. Modeling of elasticity and damping for filled elastomers. Ph.D. Dissertation. Lund University. Lund Institute of Technology, 1997.

[100] Ulmer JD. Strain Dependence of Dynamic Mechanical Properties of Carbon Black-Filled Rubber Compounds. Rubber Chem Technol 1996;69:15–47. doi:10.5254/1.3538354.

[101] Kraus G. Mechanical losses in carbon-black-filled rubbers. J Appl Polym Sci Appl Polym Symp 1984;39:75–92.

[102] Lion A. Strain-Dependent Dynamic Properties of Filled Rubber: A Non-Linear Viscoelastic Approach Based on Structural Variables. Rubber Chem Technol 1999;72:410–29. doi:10.5254/1.3538811.

[103] Rendek M, Lion A. Modelling and finite element simulation of Filler-Reinforced elastomers under dynamic deformations. KGK Kautsch Gummi Kunststoffe 2009;62:463–470.

[104] Rendek M, Lion A. Amplitude dependence of filler-reinforced rubber: Experiments, constitutive modelling and FEM – Implementation. Int J Solids Struct 2010;47:2918–36. doi:10.1016/j.ijsolstr.2010.06.021.

[105] Berg M. A non-linear rubber spring model for rail vehicle dynamics analysis. Veh Syst Dyn 1998;30:197–212.

[106] García MJ, Kari L, Viñolas J. Axial stiffness of carbon black filled rubber bushings including frequency and amplitude dependence. Kautsch Gummi Kunsts 2007;60:1.

[107] García MJ, Kari L, Vinolas J, Gil-Negrete N. Frequency and amplitude dependence of the axial and radial stiffness of carbon-black filled rubber bushings. Polym Test 2007;26:629–38. doi:10.1016/j.polymertesting.2007.03.011.

[108] Austrell P-E, Olsson AK, Jonsson M. A method to analyse the non-linear dynamic behaviour of carbon-black-filled rubber components using standard FE-codes. Const Models Rubber II 2001:231–236.

[109] Olsson AK, P. Austrell, Sandberg G. Approximate viscoelastic FE-procedures in frequency and time domain to account for the Fletcher-Gent effect. Const. Models Rubber IV, 2005, p. 313.

[110] Olsson AK, Austrell PE. Finite element analysis of a rubber bushing considering rate and amplitude dependent effects. Const Models Rubber III 2003:133–140.

[111] Ahmadi H, Darymple T, Kingston J, Muhr AH. Dynamic properties of filled rubber – Part III use of nonlinear kinematic hardening plasticity material models. Pap Present Autumn ACS Rubber Div Meet 12 Oct 2010.

[112] Gil-Negrete N, Vinolas J, Kari L. Dynamic stiffness prediction of filled rubber mounts: Comparison between a fractional derivative viscoelastic-elastoplastic model and a simplified procedure. Const. Models Rubber IV, Balkema; 2005, p. 479.

[113] Gil-Negrete N. On the modelling and dynamic stiffness prediction of rubber isolators. Univ Navar Spain 2004.

[114] Ahmadi HR, Muhr AH. Dynamic properties of filled rubber – Part II: physical basis of contributions to the model. Rubber Chem Technol 2011;84:24–40. doi:10.5254/1.3518519.

[115] Fung Y. Foundations of solid mechanics. Prentice-Hall; 1965.

[116] Bagley RL, Torvik . J. Fractional calculus - A different approach to the analysis of viscoelastically damped structures. AIAA J 1983;21:741–8. doi:10.2514/3.8142.

[117] Oldham KB. The fractional calculus. Elsevier; 1974.

[118] Enelund M, Lesieutre GA. Time domain modeling of damping using anelastic displacement fields and fractional calculus. Int J Solids Struct 1999;36:4447–72. doi:10.1016/S0020-7683(98)00194-2.

[119] Enelund M, Olsson P. Damping described by fading memory—analysis and application to fractional derivative models. Int J Solids Struct 1999;36:939–70. doi:10.1016/S0020-7683(97)00339-9.

[120] Enelund M, Mähler L, Runesson K, Josefson BL. Formulation and integration of the standard linear viscoelastic solid with fractional order rate laws. Int J Solids Struct 1999;36:2417–42. doi:10.1016/S0020-7683(98)00111-5.

[121] Eldred LB, Baker WP, Palazotto AN. Numerical application of fractional derivative model constitutive relations for viscoelastic materials. Comput Struct 1996;60:875–82. doi:10.1016/0045-7949(95)00447-5.

[122] Bellander M. High pressure Vulcanization: Crosslinking of Diene Rubbers without Vulcanization Agents. Dep Polym Technol R Inst Technol 1998.

[123] Arrillaga A, Zaldua AM, Atxurra RM, Farid AS. Techniques used for determining cure kinetics of rubber compounds. Eur Polym J 2007;43:4783–99. doi:10.1016/j.eurpolymj.2007.08.024.

[124] Rivlin RS. Large Elastic Deformations of Isotropic Materials. IV. Further Developments of the General Theory. Philos Trans R Soc Lond Ser Math Phys Sci 1948;241:379–97. doi:10.1098/rsta.1948.0024.

[125] Brazier DW, Nickel GH. Thermoanalytical Methods in Vulcanizate Analysis I. Differential Scanning Calorimetry and the Heat of Vulcanization. Rubber Chem Technol 1975;48:26–40. doi:10.5254/1.3545037.

[126] Saville B, Watson AA. Structural Characterization of Sulfur-Vulcanized Rubber Networks. Rubber Chem Technol 1967;40:100–48. doi:10.5254/1.3539039.

[127] Warley RL, Vecchio RJD. Comparisons of Methods of State-of-Cure Determination. Rubber World 1987;196:30–38.

[128] Flory PJ, Rehner J. Statistical mechanics of cross-linked polymer networks II Swelling. J Chem Phys 1943;11:521–6. doi:10.1063/1.1723792.

[129] Gent AN, Hartwell JA. Effect of Carbon Black on Crosslinking. Rubber Chem Technol 2003;76:517–32. doi:10.5254/1.3547758.

[130] Hergenrother WL, Hilton AS. Use of χ As a Function of Volume Fraction of Rubber to Determine Crosslink Density by Swelling. Rubber Chem Technol 2003;76:832–45. doi:10.5254/1.3547775.

[131] Hayes RA. A New Look at Measurements of Network Density. Rubber Chem Technol 1986;59:138–41. doi:10.5254/1.3538181.

[132] Crowther BG, Lewis PM, Metherell C. Natural Rubber Science and Technology, Ed. n.d.

[133] Chow CL, Cundiff CH. On the Characterization of Mechanical Properties of Rubber Vulcanizates. Tire Sci Technol 1987;15:73–96. doi:10.2346/1.2148786.

[134] Kawabata S, Yamashita Y, Ooyama H, Yoshida S. Mechanism of Carbon-Black Reinforcement of Rubber Vulcanizate. Rubber Chem Technol 1995;68:311–29. doi:10.5254/1.3538745.

[135] Gent AN, Kim HJ. Tear Strength of Stretched Rubber. Rubber Chem Technol 1978;51:35–44. doi:10.5254/1.3535725.

[136] Yang LM, Shim VPW, Tan VBC, Lim CT, Yuan JM. Experimental Characterisation and Modelling of Rubber for ABAQUS, 2001, p. 609–24.

[137] Przybylo PA, Arruda EM. Experimental Investigations and Numerical Modeling of Incompressible Elastomers during Non-Homogeneous Deformations. Rubber Chem Technol 1998;71:730–49. doi:10.5254/1.3538501.

[138] Moreau C, Thuillier S, Rio G, Grolleau V. The Mechanical Behavior of a Slightly Compressible Rubber-Like Material: Correlation of Simulations and Experiments. Rubber Chem Technol 1999;72:269–82. doi:10.5254/1.3538800.

[139] Kareaga Z, Guraya T, Arriaga A. A Review of Amplitude and Frequency Dependency of Elastomers. Submitt Publ n.d.

[140] ASTM D945 - 06(2012) Standard Test Methods for Rubber Properties in Compression or Shear (Mechanical Oscillograph) n.d.

[141] Austrell P-E, Olsson AK. Considering amplitude dependence during cyclic loading of elastomers using an equivalent viscoelastic approach. Polym Test 2012;31:909–15. doi:10.1016/j.polymertesting.2012.05.005.

[142] Park SW. Analytical modeling of viscoelastic dampers for structural and vibration control. Int J Solids Struct 2001;38:8065–8092.

[143] Tschoegl NW. The phenomenological theory of linear viscoelastic behavior: an introduction. Berl Springer-Verl 1989:143–5.

[144] Findley WN, Davis FA. Creep and Relaxation of Nonlinear Viscoelastic Materials. Courier Dover Publications; 1976.

[145] Bergström J. Calculation of Prony series parameters from dynamic frequency data. Polym FEM 2005.

[146] Olsson AK. Finite element procedures in modelling the dynamic properties of rubber. Ph.D. Dissertation. Lund University. Lund Institute of Technology, 2007.

[147] Ahmadi HR, Kingston JGR, Muhr AH. Dynamic Properties of Filled Rubber – Part I: Simple Model, Experimental Data and Simulated Results. Rubber Chem Technol 2008;81:1–18. doi:10.5254/1.3548196.

[148] Kaliske M, Rothert H. Constitutive approach to rate-independent properties of filled elastomers. Int J Solids Struct 1998;35:2057–71. doi:10.1016/S0020-7683(97)00182-0.

[149] Bódai G, Goda T. A new, tensile test-based parameter identification method for large-strain generalized Maxwell-model. Acta Polytech Hung 2011;8:89–108.

[150] ANSYS Programmer’s guide. ANSYS Inc 2002.

ANNEX I

A) Bestimmung des Vulkanisations grades von Gummi durch Quellung

B) Determining the state of cure of rubber by means of swelling

Bestimmung des Vulkanisationsgrades von Gummi durch Quellung

A. Arrillaga, Z. Kareaga, E. Retolaza, A. M. Zaldua*

Die Gummiindustrie benötigt ein zweckmäßiges Verfahren zur Bestimmung des Vulkanisationsgrades von Formteilen. Die Prüfung des Quellverhaltens und der Restexothermie (mittels DSC) kann man in diesem Kontext als nützliche Verfahren ansehen. DSC-Messungen erwiesen sich jedoch wegen der niedrigen Exothermie der untersuchten Mischungen als nicht sinnvoll. Aus diesem Grund wurde die Veränderung des Vulkanisationsgrades eines schwefelvernetzten Naturkautschuks und eines peroxidvernetzten EPDMs über Quellungsmessungen in Cyclohexan bestimmt. Als Fazit resultierte, dass die Quellergebnisse sowohl mit den Daten rheologischer Tests, als auch mit den Modulwerten aus Zugversuchen in Einklang stehen. Die Methode wurde zusätzlich bei einem industriell hergestellten Gummiteil angewendet, um Unterschiede des Vulkanisationsgrades als Funktion der Dicke des Teils herauszufinden.

The rubber industry requires a practical technique to determine the degree of cure achieved in moulded parts. In this context tests regarding the swelling characteristics and residual exothermicity (by means of DSC) can be considered as helpful techniques. DSC measurements, however, were not useful due to the low exothermicity of the formulations having been investigated. The cure variation of a NR crosslinked with sulphur and an EPDM crosslinked with peroxide was examined using swelling measurements in cyclohexane. It could be observed that swelling results agreed with data from rheological tests as well as modulus values from tensile testing. The method was also applied to an industrial rubber part to evaluate differences in the degree of cure across the part thickness.

1. Einleitung

Gummiteile werden in Verfahren wie Formpressen, Spritzpressen, Extrusion, Kalandrieren usw. hergestellt. In allen Fällen wird die Gummimischung zunächst in die Form des herzustellenden Artikels gebracht und anschließend vulkanisiert, um die endgültigen Eigenschaften zu erhalten. Vulkanisation oder Vernetzung bezeichnet den Vorgang, bei dem Bindungen (so genannte Vernetzungsstellen) zwischen den Kautschukmolekülen gebildet werden, so dass ein ursprünglich viskoses und klebriges Material in ein elastisches umgewandelt wird. Dabei entsteht ein dreidimensionales Polymernetzwerk **(Abb. 1)** [1]. Ein Material mit Gummieigenschaften muss drei Voraussetzungen erfüllen:

- langkettige Moleküle mit frei rotierenden Bindungen besitzen
- schwache Wechselwirkungen zwischen den Molekülketten aufweisen
- wenige, feste Verknüpfungen der Ketten untereinander bilden, um ein dreidimensionales Netz zu bilden

Der Einbau von Querverknüpfungen verhindert die vollständig freie Beweglichkeit der Ketten, der Gummi wird elastisch. Neben chemischen Bindungen tragen Verflechtungen zur Elastizität des Polymernetzwerks bei. Sie können permanenter oder temporärer Natur sein. Die Vorstellung von solchen Verflechtungen wurde über viele Jahrzehnte diskutiert und in Frage gestellt. Heute jedoch wird mehr oder weniger akzeptiert, dass solche Verflechtungen zu den elastischen Eigenschaften von Gummimaterialien beitragen. In Gegenwart von Füllstoff kommt es zusätzlich zu Polymer-Füllstoff-Wechselwirkungen. Diese tragen ebenfalls zum dreidimensionalen elastischen Netzwerk bei. Den drei genannten Mechanismen zu Netzwerkinteraktionen stehen lose Kettenenden und elastisch unwirksame Schlaufen gegenüber. Erstere erhöhen durch ihre unbegrenzte Beweglichkeit (keine Vernetzungsstellen, die die Kettenenden binden) das freie Volumen des Materials. Kettenschlaufen können sich während der Vulkanisation bilden. Sie erniedrigen die Anzahl von elastisch effektiven Ketten im Material.

Der Begriff „Vernetzungsdichte" verdient eine ausführlichere Erläuterung. Sie kann entweder als die Anzahl von Vernetzungsstellen oder als die Zahl elastisch effektiver Ketten pro Volumeneinheit ausgedrückt werden. Diese beiden Größen sind einander proportional und ihre genaue Beziehung hängt von der Funktionalität der Vernetzungsstellen ab, d. h. der Anzahl von Ketten, die von der Vernetzungsstelle ausgehen. Im Folgenden wird die Vernetzungsdichte als Zahl der Vernetzungsstellen pro Volumeneinheit definiert. Darüber hinaus ist die Vernetzungsdichte umgekehrt proportional zum durchschnittlichen Mo-

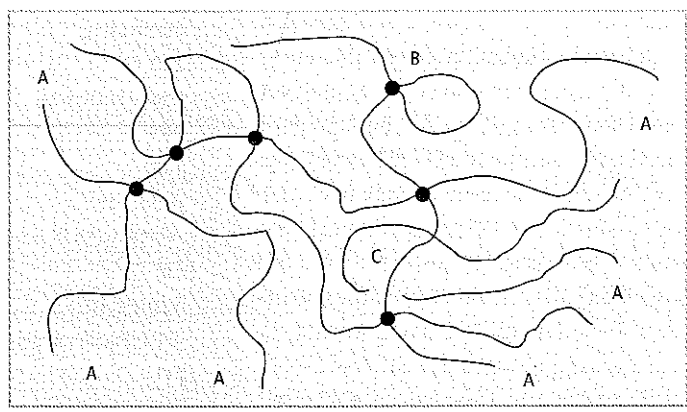

Abb. 1:
Schematische Darstellung eines Gummineztzwerks [1]
A: lose Kettenenden,
B: elastisch inaktive Schlaufe,
C: Kettenverflechtung
• chemische Bindung

* Dr. Alexander Arrillaga,
aarrillaga@leartik.com
Zorion Kareaga,
Egoitz Retolaza,
Dr. Ane M. Zaldua

Leartiker, Materials Dept.,
Lea-Artibai Ikastetxea S. Coop.,
Vizcaya, Spanien

lekulargewicht der Ketten zwischen den Vernetzungsstellen. Auch das ist ein Weg, Netzwerke zu charakterisieren. Für ein typisches Gummimaterial liegt der Wert für die Vernetzungsdichte in der Größenordnung von 10^{-3} bis 10^{-5} mol/cm³. Das entspricht 15 – 1 500 Monomereinheiten zwischen den Vernetzungsstellen. Die Vernetzungsdichte ist für Polymernetzwerke von fundamentaler Bedeutung, weil sie viele physikalische Eigenschaften des Materials bestimmt. **Abbildung 2** [2] zeigt, wie einige Eigenschaften eines Gummimaterials generell von der Vernetzungsdichte abhängen.

Der Vulkanisationsprozess erfordert eine bestimmte Zeit, die grundsätzlich von der Mischungsrezeptur und der Vulkanisationstemperatur abhängt, in einigen Fällen auch vom Druck. Bei Press- oder Spritzgießverfahren überträgt die geheizte Form Wärme auf das Material. Seine Temperatur steigt und die Vernetzungsreaktion beginnt. Abhängig von der Vulkanisationszeit wird eine gewisse Vernetzungsdichte erreicht, die, wie in **Abbildung 2** detailliert gezeigt, die spezifischen Werte für die physikalischen Eigenschaften zur Folge hat.

Mit der vorliegenden Untersuchung sollte eine einfache und schnelle Methode zur Messung des jeweils erreichten Vulkanisationsgrades des Materials entwickelt werden. Der Begriff „Vulkanisationsgrad" bezeichnet den Anteil vom möglichen Maximalwert einer physikalischen Eigenschaft, der schon in Abhängigkeit von Vulkanisationszeit oder -temperatur erzielt worden ist. Der Vulkanisationsgrad (manchmal auch Vernetzungsgrad) steht in Wechselbeziehung zur Vernetzungsdichte.

Um die Kinetik von Vernetzung oder Vulkanisation zu untersuchen, sind verschiedene Verfahren verfügbar. In einer früheren Arbeit [3] wurde deren Anwendung und Nutzen schon diskutiert. Ihr Ziel bestand darin, die Kinetik über empirische/phänomenologische Näherungen zu definieren, um darauf aufbauend den Vernetzungsverlauf zu simulieren. Dies schloss Messmethoden wie ODR (oscillating disc rheometer), MDR (moving die rheometer) und DSC (differential/dynamic scanning calorimetry) ein. Das Ziel der vorliegenden Arbeit war jedoch, ein Verfahren zu erarbeiten, mit dem sich der Vulkanisationsgrad teilweise vulkanisierter Proben ermitteln lässt.

Nach der Literatur kann die Vernetzungsdichte auf verschiedene Weisen bestimmt werden:

- Zug-Dehnungs-Messungen unter Einsatz der Mooney-Rivlin-Gleichung [4 – 5]
- Ermittlung des elastischen Moduls bei einer bestimmten Temperatur im Plateaubereich der Gummielastizität [6]
- Quellungsmessungen unter Verwendung der Flory-Rehner-Gleichung [7]
- Bestimmung der verbleibenden exothermen Vernetzung [8 – 10]

Die aktuelle Studie befasst sich mit der Verwendung von Quellungsmessungen, um den in unterschiedlichen Teilen (Teilbezirken) erreichten Vulkanisationsgrad herauszufinden. Weitere Resultate aus rheologischen Tests (ODR) und Zugversuchen dienten zur Untersuchung ihrer Korrelierbarkeit mit den Quellwerten. Obwohl die mit DSC messbare Restwärme der Vulkanisationsreaktion als nützliche Methode zur Feststellung des Vernetzungsgrades angesehen werden kann, wurde in der vorliegenden Arbeit auf sie verzichtet. Zum einen weisen Gummimischungen nur einen sehr niedrigen exothermen Peak auf. Dies führt zu einer mangelhaften, schlecht auswertbaren Auflösung. Zum anderen sind die einsetzbaren Probemengen sehr gering und nicht immer repräsentativ. Als ergänzender Hinweis mag dienen, dass der Vulkanisationsgrad bei dieser Analysemethode als das Verhältnis zwischen der Restwärme einer teilweise vulkanisierten Probe und der Wärme einer nicht vulkanisierten Probe bestimmt wird [10].

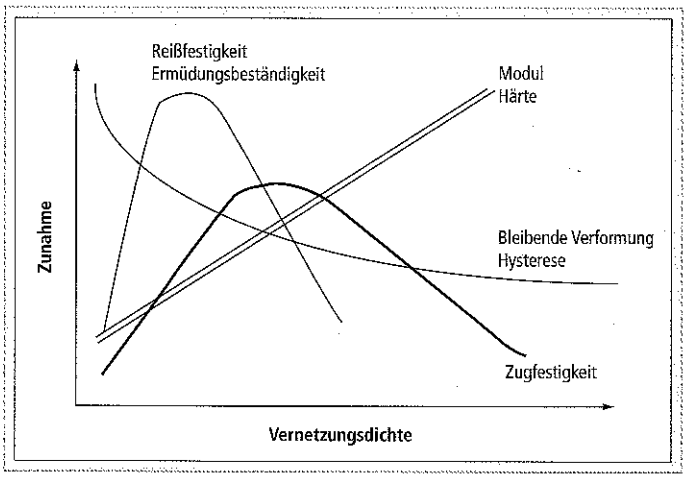

Abb. 2: Abhängigkeit der Gummieigenschaften von der Vernetzungsdichte

Tab. 1: Mischungsrezepte

CK-NR 1	phr
BR	30
NR	70
Verzögerer	1
Stearinsäure	1,5
ZnO	4
Ozonschutzwachs	4
PAN	1
TMQ	0,5
Ruß N-539	91
Aromatisches Öl	12
CBS	1,5
Schwefel 80 %	1,8
4,4' Dithiodimorpholin	1,1
PVI	0,2

CK-EPDM 1	phr
EPDM, 50 % Propylen, 5 % Dien	70
EPDM, 70 % Propylen, 5 % Dien	30
MgO	6
TMQ	1
Polyethylenglykol	2
Stearinsäure	1
Ruß N-539	58,3
Paraffinöl	29
Gleitwachs	4
Perkadox 14/40	5,5
Coagenz	3,5

Abschließend durchlief die Quellmethodik einen Test an einem realen, aus den hier eingesetzten Gummimischungen angefertigten Industrieartikel. Damit sollte überprüft werden, inwieweit sich mögliche Unterschiede des Vulkanisationsgrades in Abhängigkeit von der Dicke des Teils herausfinden lassen.

2. Experimenteller Teil

2.1 Materialien

Für die Versuche wurden zwei Gummisorten, eine schwefelvernetzte NR- und eine peroxidvernetzte EPDM-Mischung, eigens für diesen Verwendungszweck entwickelt und bei Firma Cikautxo S. Coop. in einem 150 l Innenmischer hergestellt. **Tabelle 1** zeigt die vollständigen Rezepte.

2.2 Rheologische Prüfungen

Sie erfolgten gemäß Norm ASTM D2084. Die Probe kommt in eine beheizte Prüfkammer mit Temperaturkontrolle, in der sich eine doppelt kegelförmige Scheibe, der Rotor, befindet. Er schwingt mit einer Frequenz von 1,57 Hz und einer Amplitude von ± 3°. Das auf diese Schwingscheibe wirkende Drehmoment wird über die Prüfzeit aufgezeichnet. Das Schwingscheibenrheometer (ODR/oscillating disc rheometer) misst nicht nur den Scorch oder die Induktionszeit, sondern auch die Vulkanisationsgeschwindigkeit und den jeweiligen Stand der Vulkanisation, d. h. es wird die komplette Vulkanisationskurve aufgezeichnet. Der Drehmomentwert kann mit dem Vernetzungsgrad korreliert werden. Es lassen sich drei Kurventypen unterscheiden **(Abb. 3).** Der Vulkanisationsverlauf selbst besteht aus ebenfalls drei Abschnitten:

- Induktionsperiode oder Scorch-Zeit (t_i): Die Zeit vom Messbeginn bis zum Einsetzen des Vernetzungsprozesses (wenn die Kurve wieder ansteigt) wird als „Scorch-Zeit" oder auch als Induktionsperiode bezeichnet. Sie stellt das Zeitintervall dar, in dem bei Vulkanisationstemperatur keine Vernetzung festzustellen ist.
- Vulkanisations- oder Vernetzungsverlauf: Nach der Induktionsperiode setzt die Vernetzung ein. Die Geschwindigkeit hängt von Temperatur und der Zusammensetzung der Mischung ab.
- Vollständiger Vulkanisationsumsatz: Im Idealfall erreicht die Vulkanisationskurve nach vollständigem Umsetzen des Vernetzungssystems ein Plateau, d. h. die Vernetzungsreaktion hat ihren Gleichgewichtszustand eingenommen (Kurve B in **Abb. 3).** In manchen Fällen stellt sich ein solches Gleichgewicht nicht ein und das Drehmoment nimmt kontinuierlich zu (Kurve A in **Abb. 3).** Dies nennt man „marching modulus" und tritt häufig bei peroxidvernetzten Formulierungen auf. Wählt man für solche Materialien zu lange Vulkanisationszeiten (= Übervulkanisation), treten Verhärtung, höherer Modul, kleinere Reißdehnung auf. Bei anderen Gummirezepten durchläuft die Rheometerkurve ein Maximum (= maximales Drehmoment) und fällt dann wieder ab (Kurve C in **Abb. 3).** Dies ist typisch für NR-Mischungen, die mit einem konventionellen Schwefelsystem vulkanisiert werden. Lange Vulkanisationszeiten (= Übervulkanisation) führen zum Abbau des Netzwerks (= Reversion) [11].

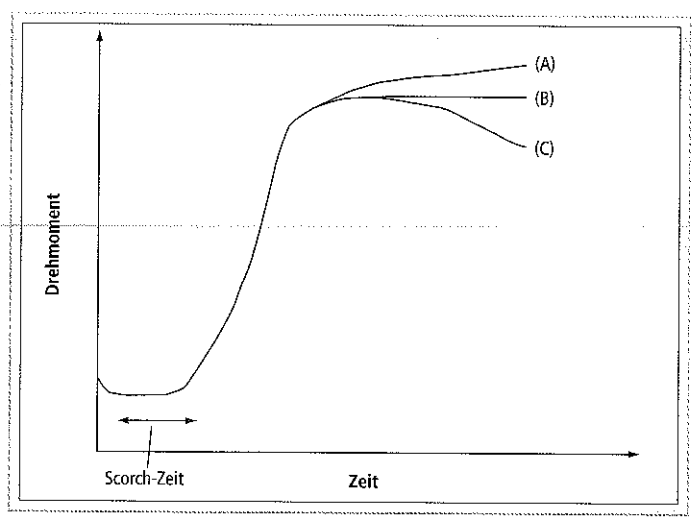

Abb. 3:
Typische Vulkanisationscharakteristiken
A: kontinuierlicher Anstieg,
B: Plateau,
C: Reversion

Die beiden Testmischungen wurden jeweils bei zwei Temperaturen geprüft, CK-NR 1 bei 165 °C und 150 °C, CK-EPDM 1 bei 180 °C und 160 °C. Die Messzeiten waren lang genug ausgelegt, um die Rheokurve möglichst vollständig aufzuzeichnen. Die Tests fanden in jedem Fall mit mindestens fünf Messungen je Mischung statt. Daraus ergaben sich die Durchschnittswerte für die spätere Auswertung. Bezeichnet man das Drehmoment als M und den Vulkanisationsgrad als α, ordnet ihm beim niedrigsten Drehmoment den Wert „0" und beim maximalen Drehmoment den Wert „1" zu, dann lässt sich nach **Gleichung 1** leicht der zeitliche Verlauf des Vulkanisationsgrades berechnen:

$$\alpha_{(t)} = \frac{M_{(t)} - M_{(min)}}{M_{(max)} - M_{(min)}} \qquad 1$$

Nach Registrierung der Vulkanisationskurven wurden zusätzliche Messungen bei gleichen Temperaturen aber mit dazwischenliegenden Prüfzeiten vorgenommen:

- CK-NR 1 bei 165 °C mit 100, 120, 150, 180, 220, 300, 600 und 1 000 s
- CK-NR 1 bei 150 °C mit 260, 290, 320, 350, 390, 430, 470 und 720 s
- CK-EPDM 1 bei 180 °C mit 60, 90, 110, 140, 200, 300 und 500 s
- CK-EPDM 1 bei 160 °C mit 100, 210, 320, 440, 550, 660 und 900 s

Diese Zeiten sind Zwischenpunkte auf der Vernetzungskurve und liegen im Bereich von Reversion/Plateau. Direkt nach Erreichen der festgelegten Prüfzeit kamen die Proben aus der Prüfkammer in Eiswasser, um die Vernetzungsreaktion zu stoppen.

2.3 Zugprüfungen

Die Prüfkörper für die Zugversuche, jeweils sechs pro Kombination, wurden auf einer IM-Presse REP V37 gespritzt: CK-NR 1 bei 165 °C Formtemperatur und Vulkanisationszeiten von 60, 90, 120, 160, 200, 260, 290, 320, 350, 390, 430, 470 und 720 s, CK-EPDM 1 bei 180 °C Formtemperatur und Zeiten von 30, 60, 80, 100, 210, 320, 440, 550, 660 und 900 s.

Nach Ablauf der Vulkanisationszeit mussten die Proben so schnell wie möglich der Form entnommen und in Eiswasser getaucht werden, um eine weitere Vulkanisation zu verhindern. Danach folgten die Zugprüfungen nach ASTM D412-97 und die Bestimmung der Spannungswerte bei 100 und 200 % Dehnung an jeweils drei Prüfkörpern pro Presszeit.

2.4 Quellprüfungen

Die Ermittlung der Gleichgewichtsvolumenquellung ist eine der besten Methoden zur Charakterisierung der Vernetzungsstruktur. Nachweislich sind der Quellwert ebenso wie die Gleichgewichtsquellung eines Vulkanisates in einem Lösemittel eine Funktion des Vulkanisationsgrades. Als Index dafür kann man entweder das durchschnittliche Molekulargewicht der Polymerkettensegmente zwischen den Vernetzungsstellen oder seinen Kehrwert, die Zahl der effektiven Vernetzungsstellen pro Volumeneinheit Gummi benutzen. Vernetzungsgrade werden gewöhnlich unter Anwendung der Flory-Rehner-Gleichung [7] bestimmt:

$$\overline{M_c} = \frac{\rho V_0 (V_r^{1/3} - V_r/2)}{-\mathrm{Ln}(1-V_r) - V_r - \mu V_r^2} \qquad 2$$

Darin sind ρ die Dichte des Materials (Gummimischung), V_0 das Molvolumen des Lösemittels, μ der Wert des Wechselwirkungsparameters Gummi-Lösemittel und V_r die Volumenfraktion des Polymers im gequollenen Vulkanisat. Sie ist eine Funktion der gequollenen Gummimasse, der getrockneten Gummimasse, der Dichte der Mischung und der Dichte des Lösemittels, das zum Quellen der Probe verwendet wurde.

Abb. 4: Getesteter Industrieartikel – VW-Teil Nr. 7H0-253-144

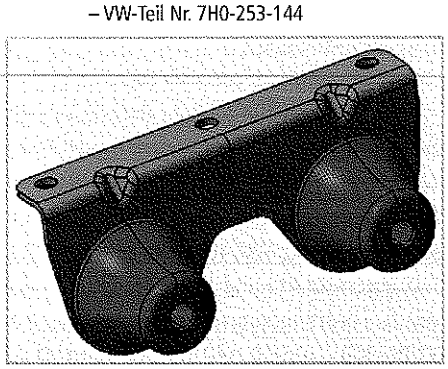

Warley und Del Vecchio [10] benutzten eine ähnliche Gleichung für die Berechnung der Vernetzungsdichte in mol/cm³:

$$-\nu = \frac{\mathrm{Ln}(1-V_r) + V_r + \mu V_r^2}{V_0 (V_r^{1/3} - V_r/2)} \qquad 3$$

Darin ist ν die Vernetzungsdichte in mol/cm³, die wiedergegeben werden kann als:

$$-\nu = \frac{\rho}{\overline{M_c}} \qquad 4$$

Dieser Ausdruck gilt für ungefüllte Mischungen. Die Berechnung wird wesentlich komplizierter bei rußgefüllten Mischungen [7, 12 – 13]. Der Parameter für die Polymer-Lösemittel-Wechselwirkung muss ebenfalls ermittelt werden. Hierzu kann das von Hayes [14] beschriebene Verfahren mit den zwei Lösemitteln dienen. Wegen der Komplexität dieser Methodik wurde hier aber der Quellgrad verwendet. Er ergibt sich nach der Formel

$$\%\ \text{Quellung} = [(m_1 - m_0)/m_0] \cdot 100 \qquad 5$$

mit m_0 = Probengewicht vor der Quellung und m_1 = Probengewicht nach der Quellung. Die beschriebene Messmethodik erfordert ein gängiges sowie geeignetes Lösemittel, d. h. es muss eine ausreichend große Quellung (im Bereich 90 – 100 %) hervorrufen und darf nicht zu schnell verdampfen. Von den geprüften Lösemitteln erfüllte nur Cyclohexan diese Anforderungen. Prüflinge mit den unterschiedlichen Vulkanisationszeiten waren aus den rheologischen Tests und den Zugprüfungen verfügbar. Testbedingun-

Abb. 5: Vulkanisationskurven Mischung CK-NR 1 (ODR)

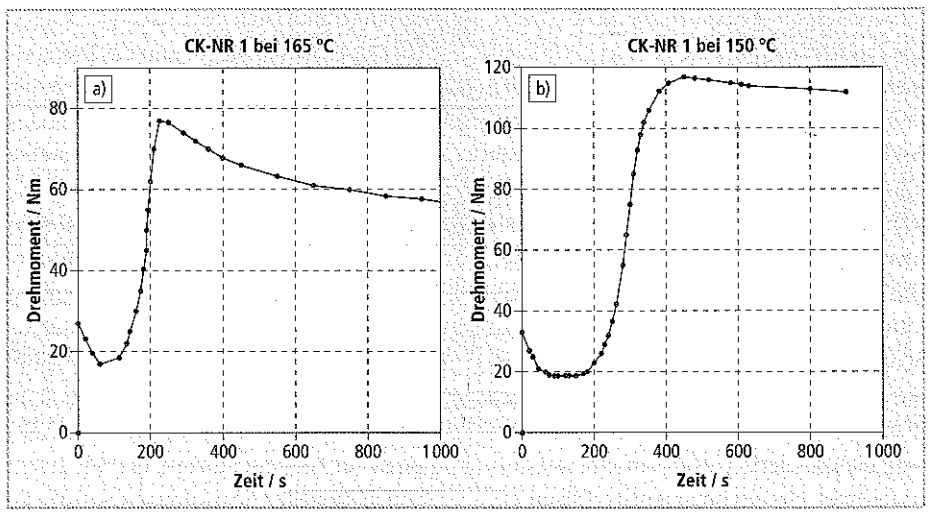

Abb. 6: Vulkanisationskurven Mischung CK-EPDM 1 (ODR)

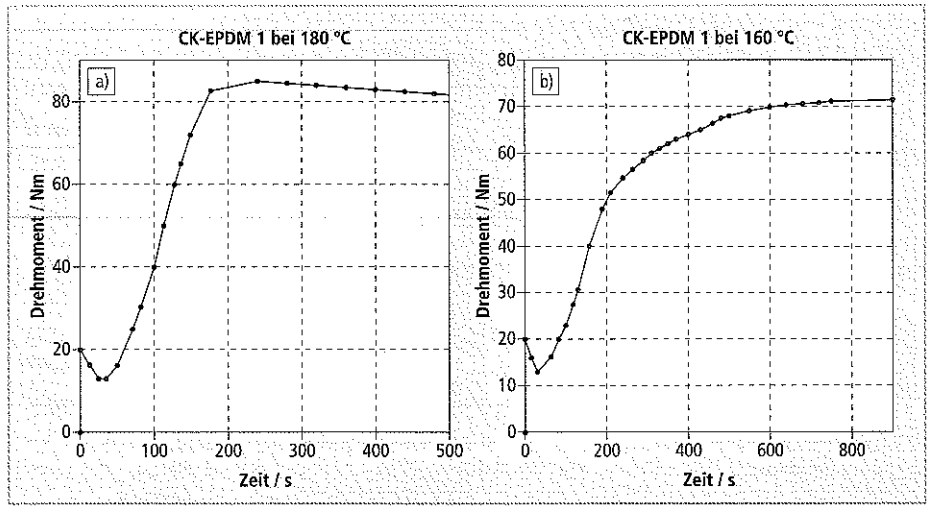

gen: Probengewicht 0,4 – 0,5 g, jede Probe für 24 h in einer verschlossenen Flasche mit 6 ml Lösemittel bedeckt bei Raumtemperatur gelagert. Vor dem Auswiegen von m_1 wurden die Probekörper an der Oberfläche mit einem Papiertuch getrocknet. Es ist zu beachten, dass der auf diese Weise gemessene Quellgrad ein Durchschnittswert ist. Der Vulkanisationsgrad muss bezogen auf den Querschnitt der Probe nicht unbedingt konstant sein.

2.5 Quellprüfungen industriell gefertigter Teile

Hier wurde die Schwankung des Vulkanisationsgrades über den Querschnitt eines industriellen Artikels (Referenz-Nr. VW 7H0-253-144) untersucht. Es handelte sich um ein Gummi-Metallteil **(Abb. 4).** Die maximale Wandstärke des Gummis betrug ca. 15 mm. Die Fertigung des Teils fand sowohl mit der NR-, als auch der EPDM-Mischung statt. Die Prüflinge (je 3) stammten aus zwei Zonen. Probe 1 wurde aus der äußeren Gummischicht (Kontaktfläche mit der Form) herausgeschnitten, Probe 2 aus dem Zentrum. Die Testbedingungen entsprachen denen aus Abschnitt 2.4 mit einem Lösemittel-Gummi-Verhältnis von 15:1.

3. Diskussion der Ergebnisse

3.1 Vulkanisationskurven

Abb. 5 und **Abb. 6** stellen die ODR-Kurven für die zwei untersuchten Gummimischungen dar. CK-NR 1 lässt klar eine Reversion (typisch für mit Schwefel vulkanisierte Mischungen) bei beiden Messtemperaturen, 150 und 160 °C, erkennen. Sie zeigt sich als ein Abfall des Drehmomentes nach dem Erreichen des Maximalwertes. CK-EPDM 1 ist ein mit Peroxid vulkanisierter EPDM. Die höhere Prüftemperatur führt zu einem größeren Wert für das Drehmomentmaximum. Bei der niedrigeren Temperatur von 160 °C ist die Zersetzungsgeschwindigkeit des Peroxids noch gering. Es resultiert eine langsame Vernetzungsreaktion und die Kurve strebt erst nach etwa 900 s ihrem Plateau zu. Da sich bei der Messung mit 180 °C ein höheres Drehmomentmaximum einstellt, kann bei 160 °C noch nicht der maximale Vernetzungsgrad erzielt worden sein.

Wertet man die Rheokurven nach **Gleichung 1** aus, d. h. berechnet man den Vulkanisationsgrad α aus den Drehmomentwerten, so ergibt sich jeweils der Zeitverlauf für den Vulkanisationsfortschritt **(Abb. 7** und **Abb. 8).** Der Vulkanisationsgrad ist bis zu dem Punkt, an dem das Drehmoment ansteigt, gleich „0" gesetzt. Diese Zeit wird als Induktions- oder Scorch-Zeit bezeichnet.

Abb. 7: Vulkanisationsgrad Mischung CK-NR 1 (ODR)

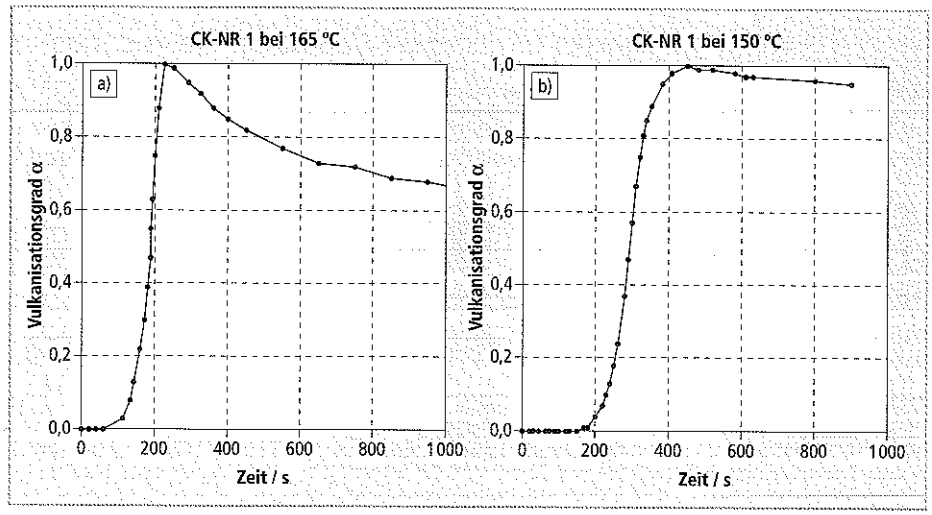

Abb. 8: Vulkanisationsgrad Mischung CK-EPDM 1 (ODR)

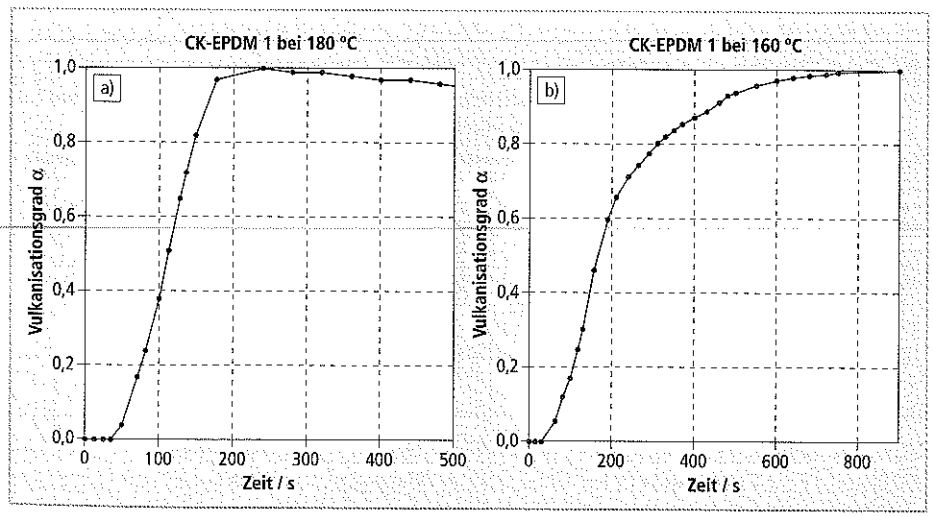

3.2 Quellung der ODR-Vulkanisate

Wie schon in Abschnitt 2.2 dargelegt, wurden im Rheometer Prüflinge mit Vulkanisationszeiten im Bereich des Plateaus/der Reversion hergestellt und ihr Quellverhalten analysiert. In den **Abbildungen 9** und **10** sind diese Quellwerte als Funktion der Vulkanisationszeit eingetragen.

Die NR-Mischung besitzt bei niedriger Temperatur ihr größtes Drehmoment **(Abb. 5).** Demnach sollte an diesem Punkt die Zahl der Vernetzungsstellen pro Volumeneinheit ebenfalls am höchsten liegen. Dieses Verhalten ist auch aus den Quellergebnissen abzulesen. Bei der Prüftemperatur von 165 °C wird der kleinste Quellwert, der mit der maximalen Vernetzungsdichte korreliert, bei 107 % erreicht, mit 150 °C reduziert er sich auf 95 %. Ein höherer Wert des Drehmomentes ist also mit geringerer Quellung gleichzusetzen. Ist der optimale Vernetzungspunkt überschritten (= kleinster Quellgrad), geht der Naturkautschuk in Reversion, die Quellung nimmt zu **(Abb. 9).**

Die peroxidvernetzte EPDM-Mischung läuft erst mit der höheren Vulkanisationstemperatur von 180 °C in ihr maximales

Drehmoment **(Abb. 6).** Bei 160 °C zersetzt sich das Peroxid nicht restlos und es kommt nicht zu einer vollständigen Vulkanisation. Betrachtet man die Quellgrade, so liegt für die Versuchstemperatur von 180 °C die kleinste Quellung bei etwa 166 %. Für 160 °C ist die minimale Quellung mit 172 % höher. Dies kann ebenfalls als Indiz dafür gewertet werden, dass die Reaktion bei 160 °C nicht vollkommen abläuft. Wieder bedeutet ein höherer Drehmomentwert eine geringere Quellung. In der 180 °C-Kurve tritt im Zeitverlauf ein leichter Abfall des Drehmomentes ein, was sich auch in einem wachsenden Quellgrad widerspiegelt **(Abb. 10).**

Für beide Mischungen, NR und EPDM, stimmt die Zeit, zu der das maximale Drehmoment beobachtet wird, mit der Zeit, bei der sich der niedrigste Quellwert ergibt, überein. Damit bestätigt sich die Äquivalenz von maximalem Drehmoment und minimaler Quellung.

Nach diesen Ergebnissen ist es notwendig, bei der Vulkanisation einer Gummimischung sowohl die Vulkanisationstemperatur wegen ihres Einflusses auf die Zersetzung der Vernetzungsmittel, als auch die Vulkanisationszeit richtig anzupassen. Wird eine zu lange Zeit gewählt, können abhängig von der Rezeptur Reversionserscheinungen auftreten.

Zwischen den gemessenen Drehmomenten (jedes Drehmoment ist spezifisch einem Vulkanisationsgrad assoziiert) und der Größe der Quellung kann ein Abgleich hergestellt werden. Nachdem diese Beziehung für die jeweils untersuchte Gummimischung einmal definiert ist, hat man die Möglichkeit an der Hand, den Vernetzungsgrad des Gummiteils nach dem diskutierten Quellverfahren zu bestimmen. Auf diese Weise ist es nicht mehr notwendig, die viel komplexeren Untersuchungen, die in der Literatur beschrieben sind und auf der Flory-Rehner-Gleichung beruhen, durchzuführen [11].

3.3 Zugversuche und Quellung der Zugversuchprüflinge

Entsprechend Abschnitt 2.3 wurden jeweils drei Prüfhanteln für die Zugtests und drei für Quelltests hergestellt. Die Resultate der Zugtests finden sich in den **Abbildungen 11** und **12,** die der Quellung in den **Abbildungen 13** und **14.**

Die Mischung CK-NR 1 weist anfänglich einen Anstieg des Moduls bis zu einem Maximum auf. Danach beginnen die Werte abzufallen. Diese Abnahme beruht auf der Reversion der NR-Mischung bei längeren Vulkanisationszeiten. CK-EPDM 1 verhält sich ähnlich, doch tritt keine Reversion auf und der Maximalwert bleibt erhalten.

Abbildungen 13 und **14** zeigen jeweils eine minimale Quellrate über die Zeit. NR erreicht bei 165 °C ca. 93 %, EPDM bei 180 °C etwa 172 %. Die Daten entsprechen nahezu den Minimumwerten, die für 150 °C (NR) und 160 °C (EPDM) bei den ODR-Vulkanisaten gefunden wurden, also dem Zustand bei niedrigerer Temperatur. Man kann demnach keine direkte Kongruenz zwischen den Quellwerten der ODR-Proben und denen der Prüfhanteln ableiten. Die Ursache dürfte in der (durch die Herstellverfahren bedingte) unterschiedlichen thermischen Vorgeschichte der Proben zu suchen sein. Im Ergebnis sind die nach beiden Methoden erreichten Vulkanisationsgrade, d. h. ihre via Quellverfahren gemessenen Werte, nicht äquivalent. Analog den ODR-Proben stimmen jedoch die Vulkanisationszeiten der minimalen Quellung und des maximalen Moduls (bei 100 und 200 % Dehnung) überein.

3.4 Quellung Industrieartikel

Die Prüfungen erfolgten gemäß Abschnitt 2.5. Die zugehörigen Quellwerte sind in **Tabelle 2** angegeben. Bei beiden Mischungen zeigt sich, dass die äußere Schicht weniger quillt als das Material im Kern. Dies hängt mit den Unterschieden im Vulkanisations-

Abb. 9: Quellung Mischung CK-NR 1 (ODR)

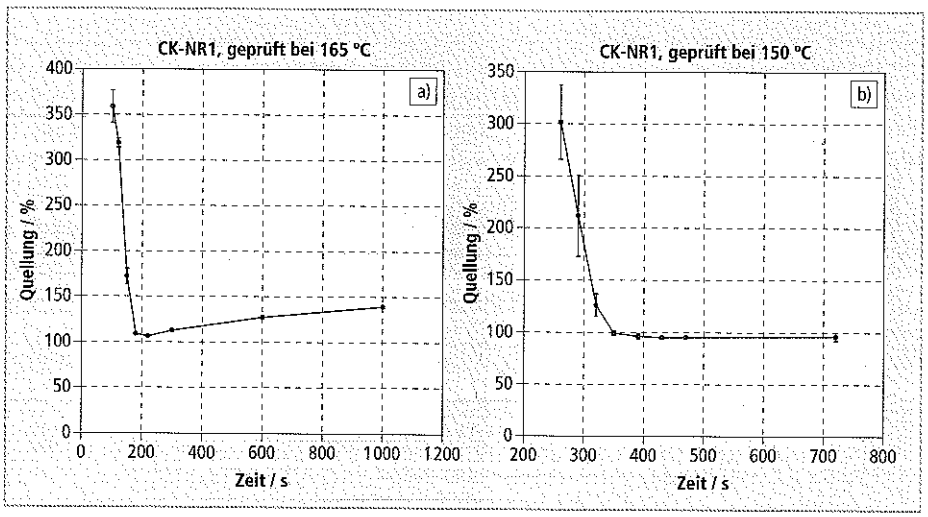

Abb. 10: Quellung Mischung CK-EPDM 1 (ODR)

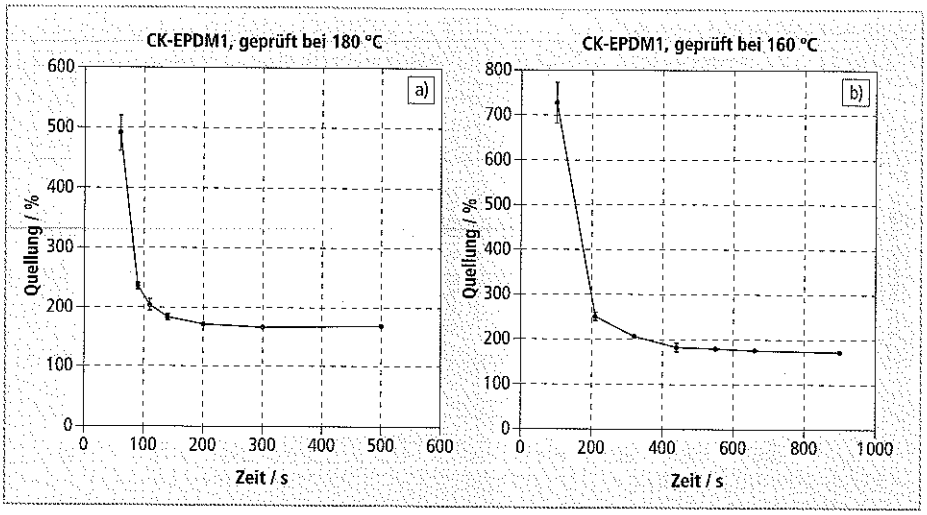

grad zusammen. Nach den in **Abbildung 10** dargestellten Ergebnissen für die ODR-Vulkanisate, die unter ähnlichen Bedingungen gequollen wurden, erreichte die NR-Mischung bei vollständiger Vulkanisation eine Minimalquellung von ca. 95 %. Dieser Wert stimmt mit dem an der Außenschicht des Industrieartikels gemessenen überein. Daraus ist zu schließen, dass das NR-Teil außen ausvulkanisiert ist. Die innere Schicht kommt auf einen Wert von ca. 102 % und ist demnach nicht völlig vulkanisiert. Es erhärtet sich die Erkenntnis aus den Quellversuchen mit den Rheoprüflingen: Das Quellverhalten eines Gummimaterials ist ein Maß für seinen Vulkanisationsgrad. Die Quellgrade für den ausvulkanisierten Zustand lagen

Tab. 2: Quellgrad Industrieartikel – VW-Teil Nr. 7H0-253-144

Material	Probe 1 / %	Probe 2 / %	Probe 3 / %	Durchschnitt / %
CK-NR 1 außen	96,56	95,06	96,76	96,13
CK-NR 1 innen	101,99	101,27	102,24	101,84
CK-EPDM 1 außen	169,04	169,14	170,57	169,59
CK-EPDM 1 innen	175,56	175,95	176,56	176,02

Abb. 11: Modulwerte Mischung CK-NR 1

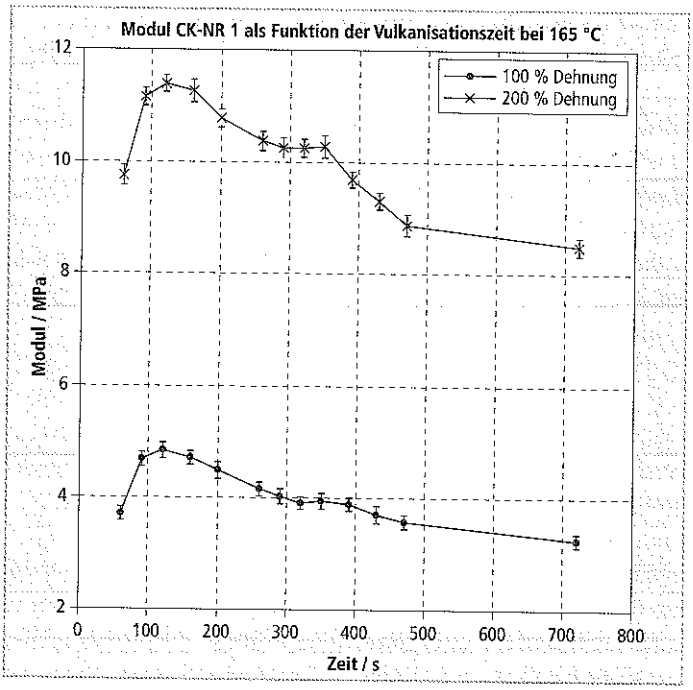

Abb. 12: Modulwerte Mischung CK-EPDM 1

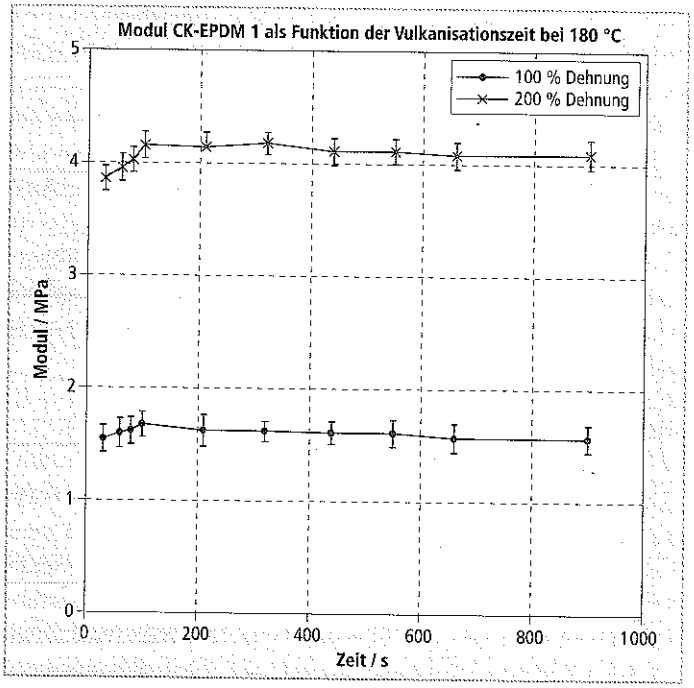

Abb. 13: Quellung Mischung CK-NR 1 (Prüfhantel)

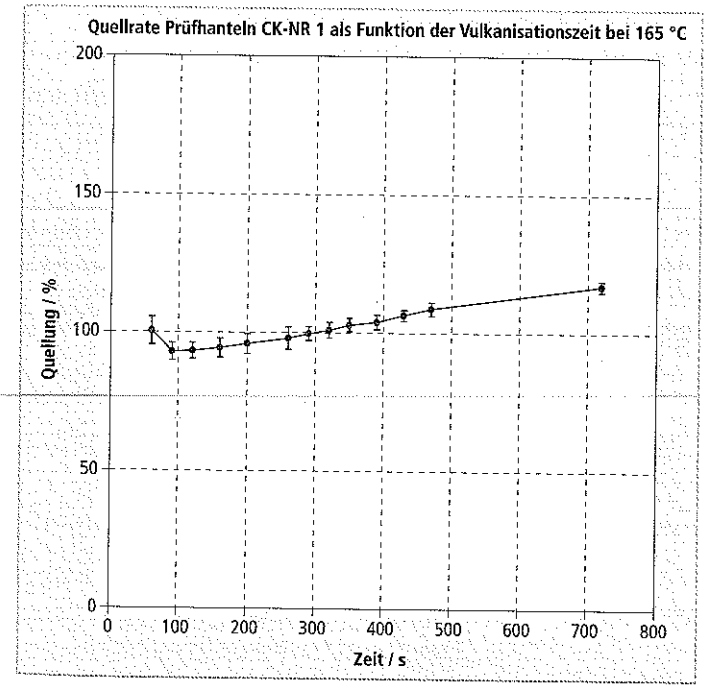

Abb. 14: Quellung Mischung CK-EPDM 1 (Prüfhantel)

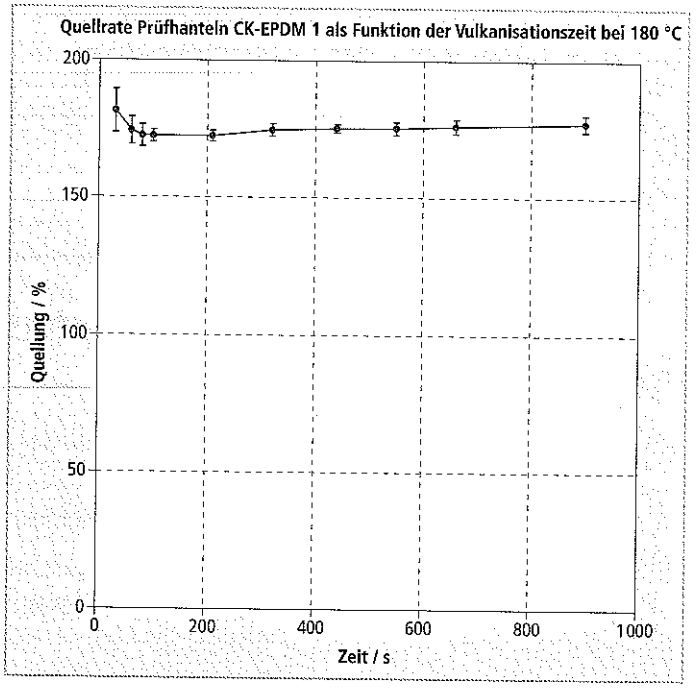

bei der EPDM-Mischung entsprechend Abschnitt 2.5 je nach Temperatur im Bereich von 166 – 172 %. Im Außenbezirk des Teils wird ein entsprechender Wert eingehalten. Die Innenschicht weist jedoch eine erhöhte Quellrate auf. Der Gummikern ist somit nicht vollkommen vulkanisiert.

4. Fazit und Schlussfolgerungen

Das Ziel der vorliegenden Studie bestand darin nachzuprüfen, inwieweit sich einfache Quellungsprüfungen in der Praxis zur Kontrolle der Ausvulkanisation eines Gummiteils eignen. Die auf der Flory-Rehner-Gleichung [7] basierenden Verfahren sind für den praktischen Einsatz in der Industrie zu komplex und zu langwierig. Beschränkt man sich auf die Auswertung von Daten aus der Gewichtsquellung, so gelangt man rasch und unkompliziert zu vernünftigen Aussagen über den Vulkanisationsgrad. Dies konnte in einem breit angelegten Prüfprogramm beispielhaft an zwei unterschiedlichen Mischungen, nämlich konventionell mit Schwefel vulkanisiertem Naturkautschuk und mit Peroxid vernetztem EPDM, mit entsprechenden Proben aus dem Labor und repräsentativen Mustern aus regulärer IM-Fertigung gezeigt werden. Die ermittelten Quellraten stehen in gutem Einklang mit den Messungen der Vulkanisationskurven und den Modulwerten bei Dehnung und spiegeln somit den zeitlichen Verlauf der Vernetzungsreaktion realistisch wider. In diesem Zusammenhang war anhand der Quellwerte ebenfalls festzustellen, wie sich das Herstellverfahren auf die Ausvulkanisation eines Gummiartikels auswirkt. Die Faktoren Artikeldimensionen, Art des Wärmeeintrags und Vulkanisationszeit spielen eine nicht zu unterschätzende Rolle. Man muss also bei der Herstellung von Gummiartikeln der Festlegung von Vulkanisationstemperatur und -zeit ausreichend Aufmerksamkeit widmen, um Reversionserscheinungen, unzureichende Vernetzungsreaktion und ungleichmäßige Ausvulkanisation sicher zu vermeiden.

Die Quellungsprüfung kann als nützliches Werkzeug zur Überprüfung des Vulkanisationsgrades, sei es in der Entwicklung, sei es in der Qualitätskontrolle, auch in Situationen herangezogen werden, in denen andere Messverfahren versagen.

5. Dank

Dank gilt der Cikautxo S. Coop. für die Auswahl und Herstellung der Gummimischungen sowie der Lea Artibai Ikastetxea S. Coop. Azaro Fundazioa, Feder und baskischen Provinzregierung für die finanzielle Unterstützung bei der Durchführung dieses Projekts.

6. Literatur

[1] Bellander, M., High pressure Vulcanization: Crosslinking of Diene Rubbers without Vulcanization Agents, Dissertation 1998, Department of Polymer Technology, Royal Institute of Technology, Stockholm

[2] Kramer, H., Rubber World Juli (1994), IRC'93 und 144. ACS Rubber Division Meeting (1993)

[3] Arrilaga, A., Zaldua, A. M., Achurra, R. M., Farid, A. S., Eur. Polym. J. 43/11 (2007), 4783 (2007)

[4] Mooney, M., J. Appl. Phys. 11 (1940), 582

[5] Rivlin, R. S., Phi. Trans. Roy. Soc. A241 (1948), 319

[6] Saville, B., Watson, A. A., Rubber Chem. Technol. 40 (1967), 100

[7] Flory, P. J., Rehner, J., J. Chem. Phys. 11 (1943), 521

[8] Brazier, D. W., Nickel, G. H., Rubber Chem. Technol. 48 (1975), 26

[9] Brazier, D. W., Thermochim. Acta 18 (1977), 147

[10] Warley, R. L., Del Vecchio, R. J., 131. ACS Rubber Division Meeting (1987), 29

[11] Crowther, B. G., Lewis, P. M., Methrell, C., Natural Rubber Science and Technology, 6 (1988), Roberts, A. D., Ed., Oxford University Press, New York

[12] Gent, A. N., Hartwell, J. A., Lee, G., Rubber Chem. Technol. 76 (2003), 517

[13] Hergenrother, W. L., Hilton, A. S., Rubber Chem. Technol. 76 (2003), 832

[14] Hayes, R. A., Rubber Chem. Technol. 59 (1986), 138

Determining the state of cure of rubber by means of swelling

A. Arrillaga, Z. Kareaga, E. Retolaza, A. M. Zaldua*

The rubber industry requires a practical technique to determine the degree of cure achieved in moulded parts. In this context tests regarding the swelling characteristics and residual exothermicity (by means of DSC) can be considered as helpful techniques. DSC measurements, however, were not useful due to the low exothermicity of the formulations having been investigated. The cure variation of a NR crosslinked with sulphur and an EPDM crosslinked with peroxide was examined using swelling measurements in cyclohexane. It could be observed that swelling results agreed with data from rheological tests as well as modulus values from tensile testing. The method was also applied to an industrial rubber part to evaluate differences in the degree of cure across the part thickness.

1. Introduction

Rubber parts are manufactured using processes such as compression moulding, injection moulding, extrusion, calendering, and so on. In all cases, first the rubber takes the shape of the part to be manufactured, and later on it vulcanises to achieve the final properties. Vulcanisation is known as the process during which a number of bonds (so called crosslinks) between the rubber molecules are formed, so that a viscous and tacky material is converted into an elastic material. As a consequence, a polymer network is created, resulting in a three-dimensional structure **(fig. 1)** [1]. Three requirements have to be fulfilled for a material to show rubber-like properties:

- the presence of long chain-like molecules with freely rotating links
- weak secondary forces between the molecules
- an interlocking of the molecules at a few places along their length to form a three-dimensional network

Due to the introduction of crosslinks, the chains are prevented from sliding from each other and the rubber becomes elastic. Besides chemical crosslinks, chain entanglements contribute to the elasticity of the polymer network. They can be either of permanent or temporary nature. The concept of entanglements has been discussed, and even questioned, during many decades. Today, however, it is more or less accepted that entanglements contribute to the elastic forces in rubber materials. When filler is incorporated, polymer-filler interactions appear and will also contribute to the three-dimensional network. Opposing these three mechanisms of networking are loose chain ends and elastically ineffective loops. The former increase the free volume of the material by their non-restricted mobility (no crosslinks that tighten the chain end). Chain loops may be formed during vulcanisation and will lower the number of elastically effective chains in the material.

The term "crosslink density" deserves a more elaborate explanation. It can be expressed as the number of crosslink points or the number of elastically effective chains per unit volume. These two quantities are proportional to each other, and their exact relationship depends on the functionality of the crosslink points, i. e. the number of chains that start from the crosslink. Henceforth crosslink density will be defined as the number of crosslink points per unit volume. Furthermore, crosslink density is inversely related to the average molecular weight of the chains between the crosslinks, which is also a way to express the network properties. The value of crosslink density may be in the order of $10^{-3} - 10^{-5}$ mol/cm^3 for a typical rubber material, corresponding to 15 – 1,500 monomer units between the crosslinks. Crosslink density is fundamental for polymeric networks as it determines many physical properties of the resulting material. **Figure 2** [2] shows how some properties of a rubber material generally depend on the crosslink density.

This vulcanisation process requires a time, which basically depends on the formulation recipe and the cure temperature, and in some cases pressure. For instance, when using a compression or injection moulding process, the heated mould transfers heat to the material, its temperature increases, and cure reaction starts. Depending on the cure time, a certain crosslink density will be achieved, and as detailed in **figure 2**, this leads to specific values of the physical properties.

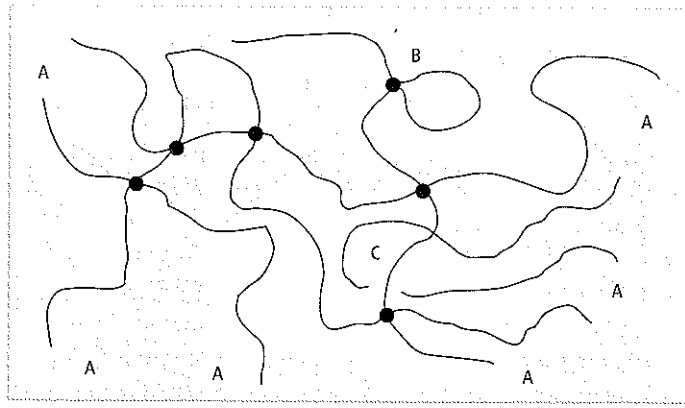

Fig. 1:
Model of a rubber network [1]
A: loose chain ends,
B: elastically inactive loop,
C: chain entanglement
• chemical crosslink

* Dr. Alexander Arrillaga
aarrillaga@leartik.com
Zorion Kareaga,
Egoitz Retolaza,
Dr. Ane M. Zaldua

Leartiker, Materials Dept.,
Lea-Artibai Ikastetxea S. Coop.,
Vizcaya, Spain

In the present study, the authors wanted to develop a very simple and quick method to evaluate (measure) the degree of cure achieved by the material. The term "state of cure of a vulcanisate" means the degree to which some property of the vulcanisate has approached the maximum attainable value as a result of change in time or temperature of cure. It is rather directly related to the degree of crosslinking.

Several techniques are available to study the kinetics of curing or vulcanisation. A previous publication [3] discusses their application and usefulness with the aim of defining the kinetics by empirical/phenomenological approaches for realising curing simulations. This includes techniques such as ODR, MDR and DSC. Nevertheless, the aim of the present work was not to have a procedure to obtain the complete cure curve, but to have a procedure to determine the degree of cure achieved in partially cured samples.

According to literature, crosslink density can be measured in different ways:

- stress-strain measurements using the Mooney-Rivlin equation [4, 5]
- determination of the elastic modulus at a certain temperature in the rubbery plateau range [6]
- by swelling measurements using the Flory-Rehner equation [7]
- by determination of the residual exothermicity [8 – 10]

The current work is concerned with the use of swelling measurements to evaluate the degree of cure achieved in several parts. ODR measurements and tensile tests are also done to correlate the results obtained to the swelling value. Although the use of residual exothermicity measured by DSC was considered as an useful procedure to evaluate the degree of cure, this procedure was not utilized for the present study because of its poor resolution, related to the low exothermal peak of rubber formulations and the very small samples that need to be used. The degree of cure is determined as the ratio between the residual heat given by a partially cured sample and the heat given by a non-cured sample [10].

The swelling based procedure was finally used to evaluate differences in curing degree values across the thickness, for a real industrial part manufactured with the rubber formulations studied in the present work.

2. Experimental

2.1 Materials

The present study was based on the use of two rubber formulations, one based on a NR cured with sulphur and the other one on an EPDM cured by peroxides. They are proprietary developments and were manufactured at Cikautxo S. Coop. Company. **Table 1** summarises the complete recipe for both formulations, which were prepared in a 150 l internal mixer.

2.2 Rheological tests

All tests were conducted according to the ASTM D2084. The sample was put into a temperature controlled die cavity fitted with a bi-conical disk (rotor) oscillating in a sinusoidal way at a frequency of 1.57 Hz and an amplitude of ± 3°. The torque counteracting the disk oscillation is monitored over the test time. ODR measures not only the scorch or induction period, but also the cure rate and the state of cure. Thus the complete cure curve can be recorded and the torque level is correlating to the degree of crosslinking. There occur three different cure characteristics being illustrated in **figure 3**. The vulcanisation proceeds in three steps:

- Induction period or scorch time (t_i): The time from the start of the measurement to the onset of the crosslinking process (i. e. when the curve begins to slope upwards) is called scorch time, also defined as induction period. It represents the time interval at curing temperature during which no crosslinking can be defined.
- Curing or crosslinking stage: Following the induction period, crosslinking occurs at a rate which is dependent on temperature and the nature of the composition.
- Reversion or overcure stage: When the crosslinking has proceeded to a full cure, subsequent heating produces an overcure which may be evidenced by continued stiffening or by reversion. The upper curve (A) shows a marching behav-

Fig. 2: Dependence of some properties of a rubber material on crosslink density

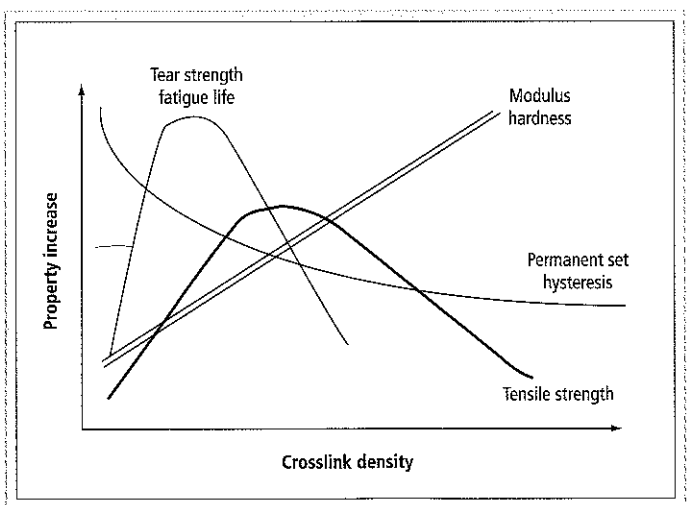

Fig. 3: Typical rheometer traces;
A) marching characteristic, B) plateau level, C) reversion

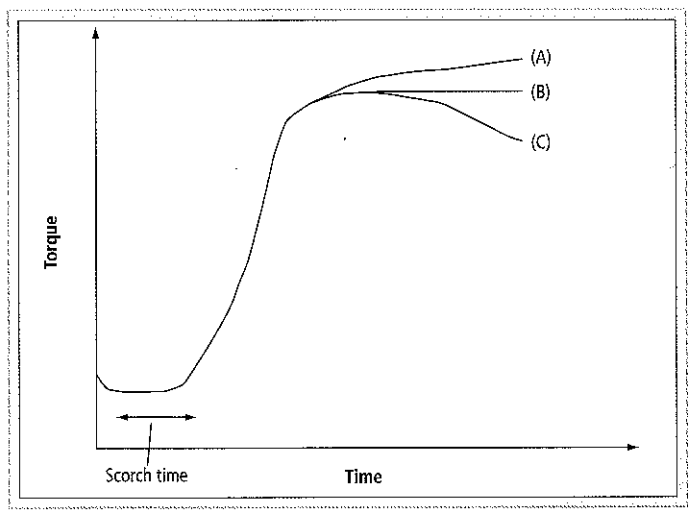

iour that can be observed for chloroprene rubber and SBR-based compounds. B) is the ideal behaviour where the cure level reaches a plateau (equilibrium), typically for NBR. C) shows reversion, a phenomenon that appears for example, when NR is vulcanised with a conventional sulphur system as described by Crowther, Lewis and Methrell [11].

The CK-NR 1 formulation was tested at two temperatures, 165 °C and 150 °C. CK-EPDM 1 was tested also at two temperatures, 180 °C and 160 °C. Sufficiently long cure times were set to see the complete curve. Tests were done with at least five samples for each case, and an average was calculated for later evaluation. If the minimum torque (M) is set to "degree of cure α"= 0 and the maximum torque to "degree of cure α"= 1 then the cure curve α vs. t (t = time) can be calculated for each temperature according to the following equation:

Tab. 1: Compound recipes

CK-NR 1	phr
BR	30
NR	70
Inhibitor	1
Stearic acid	1.5
ZnO	4
Antiozonant	4
PAN	1
TMQ	0.5
Carbon black N539	91
Aromatic oil	12
CBS	1.5
Sulphur 80 %	1.8
4,4' Dithiodimorpholine	1.1
PVI	0.2
CK-EPDM 1	**phr**
EPDM, 50 % propylene, 5 % diene	70
EPDM, 70 % propylene, 5 % diene	30
MgO	6
TMQ	1
Polyethylene glycol	2
Stearic acid	1
Carbon black N539	58.3
Paraffinic oil	29
Slipping wax	4
Perkadox 14/40	5.5
Co-agent	3.5

$$\alpha_{(t)} = \frac{M_{(t)} - M_{(min)}}{M_{(max)} - M_{(min)}} \quad 1$$

Once the complete cure curves were obtained further measurements were made at the same temperatures, but using intermediate test times, as described below:

- CK-NR 1 tested at 165 °C: 100, 120, 150, 180, 220, 300, 600, and 1,000 s
- CK-NR 1 tested at 150 °C: 260, 290, 320, 350, 390, 430, 470, and 720 s
- CK-EPDM 1 tested at 180 °C: 60, 90, 110, 140, 200, 300, and 500 s
- CK-EPDM 1 tested at 160 °C: 100, 210, 320, 440, 550, 660, and 900 s

These times are intermediate values within the cure range and the reversion/plateau range. After reaching the test time the samples were removed as quickly as possible from the ODR and were immersed into iced water to stop curing.

2.3 Tensile tests

The tensile test specimens were pressed on a REP V37 injection machine. CK-NR 1 was injected at a 165 °C mould temperature with curing times of 60, 90, 120 160, 200, 260, 290, 320, 350, 390, 430, 470, and 720 s. CK-EPDM 1 was injected at 180 °C mould temperature with curing times of 30, 60, 80, 100, 210, 320, 440, 550, 660, and 900 s.

After moulding samples were removed as quickly as possible from the mould and immersed into iced water to stop further curing. Five samples were manufactured at each cure time and then tensile tests were done according to ASTM D412-97 for getting the information on modulus at 100 and 200 % elongation.

2.4 Swelling tests

The determination of equilibrium swelling volumes is one of the best methods for characterising crosslinked structures. The rate of swell as well as the equilibrium swell of a vulcanisate in a solvent has been shown to be a function of the state of cure. Either the molecular weight between crosslinks or its reciprocal, the number of effective network chains per unit volume of rubber, may be used as an indication of the cure state. Curing degrees are usually determined by applying the Flory-Rehner formula [7], which is as:

$$\overline{M}_c = \frac{\rho V_0 (V_r^{1/3} - V_r/2)}{-\mathrm{Ln}(1-V_r) - V_r - \mu V_r^2} \quad 2$$

where ρ is the density of the material (rubber formulation), V_0 is the molar volume of the solvent, μ is the value of the rubber-solvent interaction parameter, and V_r is the polymer volume fraction in the swollen vulcanisate, which is a function of the swollen rubber mass, dried rubber mass, density of the formulation, and the density of the solvent used for swelling.

Warley and Del Vecchio [10] proposed a similar expression to calculate the crosslink density in mol/cm³:

$$-\nu = \frac{\mathrm{Ln}(1-V_r) + V_r + \mu V_r^2}{V_0 (V_r^{1/3} - V_r/2)} \quad 3$$

where ν is the crosslink density, in mol/cm³, which can be rewritten as:

$$-\nu = \frac{\rho}{\overline{M}_c} \quad 4$$

This is true for non-filled formulations. The calculation becomes much more complex when testing carbon black loaded formulations [7, 12, 13]. The polymer-solvent interaction parameter must be also determined using the two solvent procedure described by Hayes [14]. Due to the complexity of this procedure the option of using just only the value of the swelling degree was chosen. The swelling degree is defined simply as:

$$\%\ \mathrm{Swelling} = [(m_1 - m_0)/m_0] \cdot 100 \quad 5$$

where m_0 = sample weight before swelling and m_1 = sample weight after swelling.

To apply this technique it is necessary to use appropriate solvents. It should give a sufficient swelling rate in the range of 90 – 100 % and a low evaporation rate. From the solvents tested cyclohexane was the only one fulfilling these requirements. Samples cured at different times were available from the ODR tests and the tensile tests specimens. Samples (0.4 – 0.5 g) were immersed into a bottle containing 6 ml

of solvent and maintained into the solvent for 24 h. Before measuring m_1 the sample was dried briefly with tissue. It is necessary to remind that the swelling degree measured in this way is an average value because in reality there is a distribution of the curing degree across the thickness of the sample.

2.5 Swelling tests of industrial parts

For evaluating the test method with regard to applicability the degree of cure variation across the thickness of an industrial part (Reference: Volkswagen 7H0-253-144) was checked. Parts were manufactured with both formulations. **Figure 4** displays the part studied. It is a rubber-metal part, where rubber has a maximum thickness of about 15 mm. Two types of samples were analysed. Sample 1 was cut from the external layer of the rubber (that one in contact with the mould) and sample 2 was taken from the centre of the rubber part. Test conditions were conforming with section 2.4 with a solvent-rubber ratio of 15 : 1.

3. Results and discussion

3.1 Rheometer traces

Figures 5 and **6** show the ODR test results obtained for both rubber formulations. CK-NR 1 exhibits a clear reversion phenomenon (being typical for sulphur cured formulations), both when testing at 150 and 165 °C. This is represented as a torque decrease after achieving the maximum value. CK-EPDM 1 is an EPDM crosslinked with peroxide. When testing at low temperature, 160 °C, the decomposition rate of the peroxide is low. This slows down the cure kinetics and it seems that the trace arrives at the plateau after 900 s. Nevertheless the maximum torque achieved at 180 °C was slightly higher. This means that at 160 °C the maximum curing degree was not attained. Using the information of the aforementioned curves and **equation 1** the curing degree curves detailed in **figures 7** and **8** can be calculated from the torque values. The degree of

Fig. 4: Industrial part tested – VW Reference 7H0-253-144

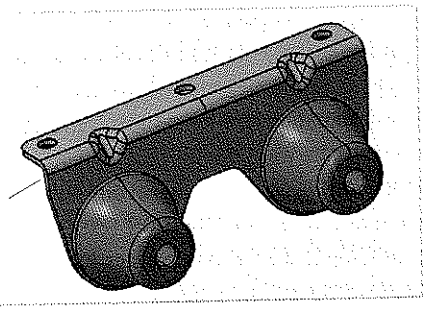

Fig. 5: Rheometer traces of CK-NR 1 (ODR)

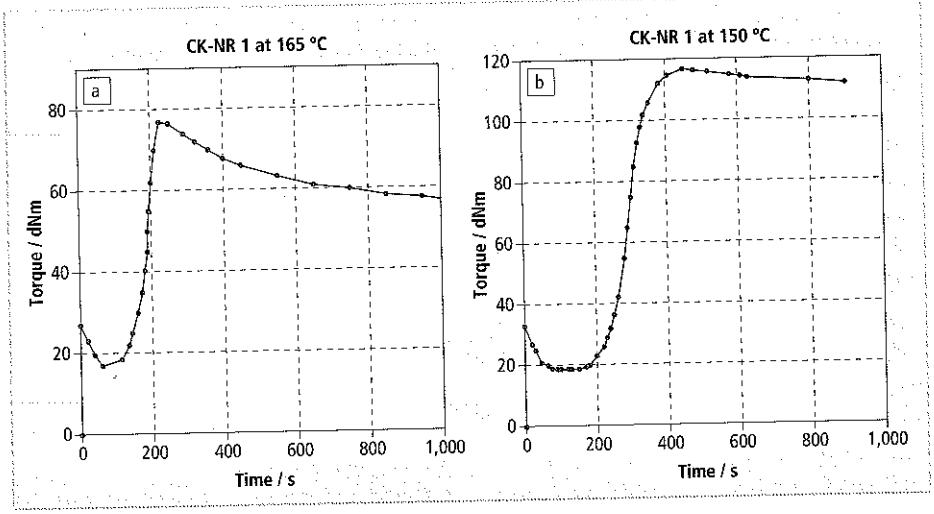

Fig. 6: Rheometer traces of CK-EPDM 1 (ODR)

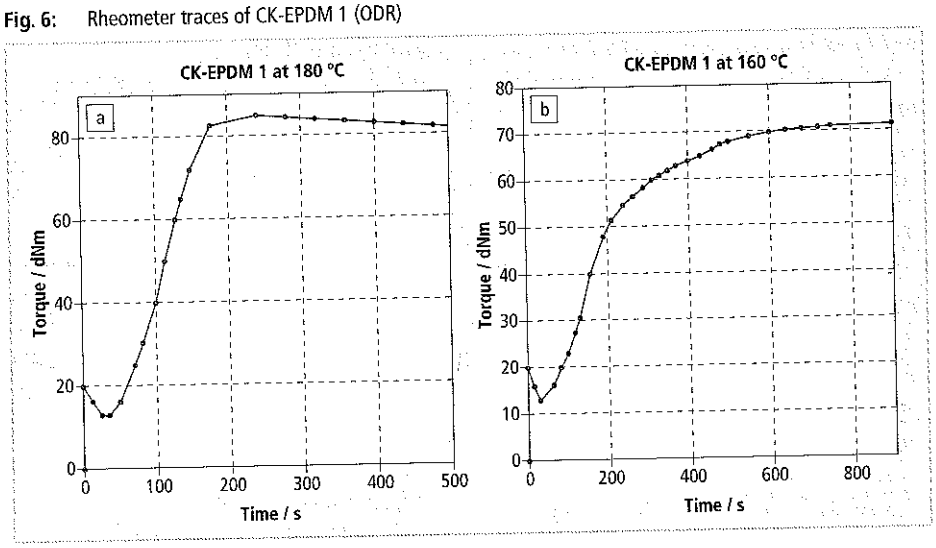

Fig. 7: State of cure of CK-NR 1 (ODR)

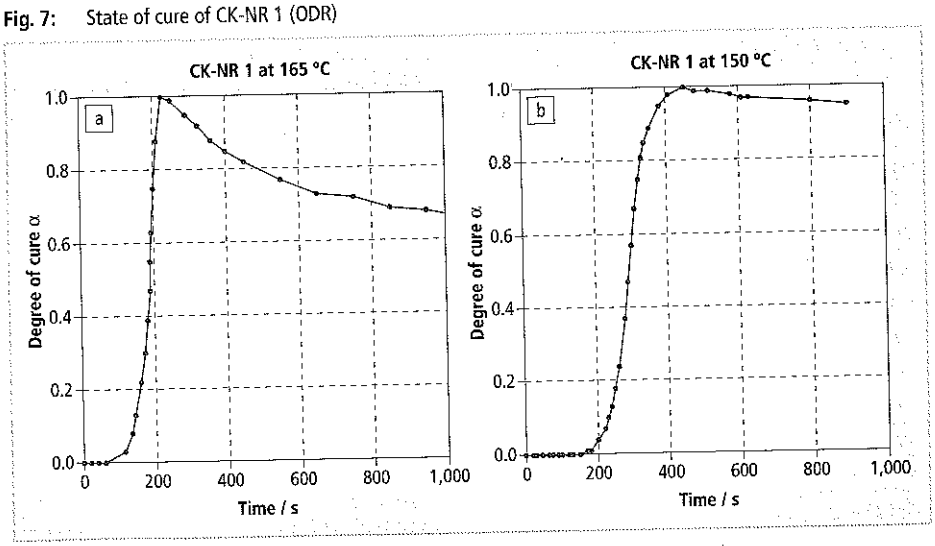

cure was set at zero up to the point where the torque starts to increase after achieving the minimum value. This period is defined as the induction or scorch time.

3.2 Swelling of ODR samples

As already discussed in section 2.2 additional tests were performed with keeping the compound in the ODR chamber for the specified times and the resulting samples being checked for swelling. **Figures 9** and **10** represent the swelling values obtained vs. curing time.

Fig. 8: State of cure of CK-EPDM 1 (ODR)

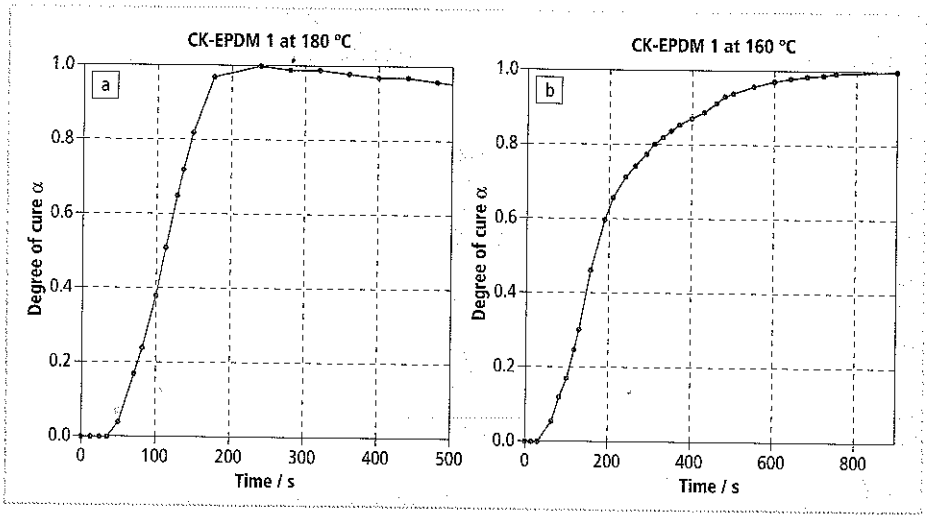

Fig. 9: Swelling of CK-NR 1 (ODR)

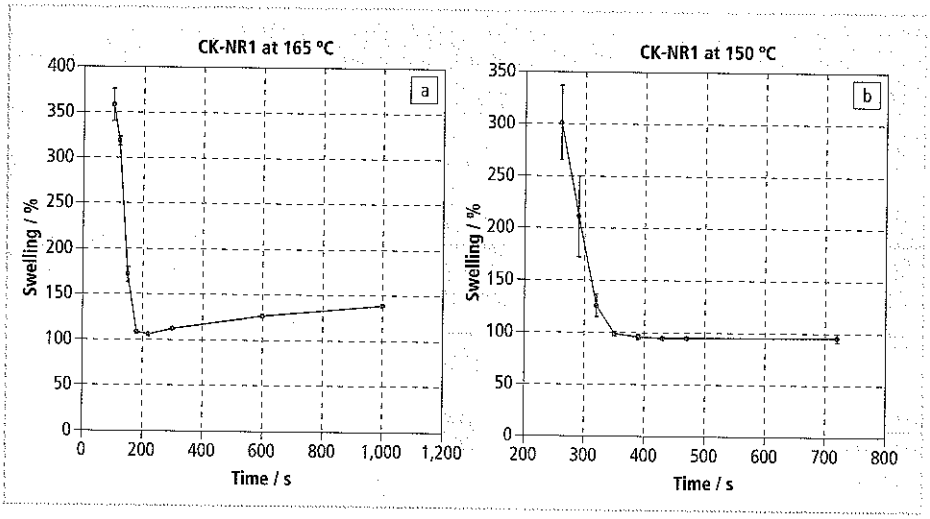

Fig. 10: Swelling of CK-EPDM 1 (ODR)

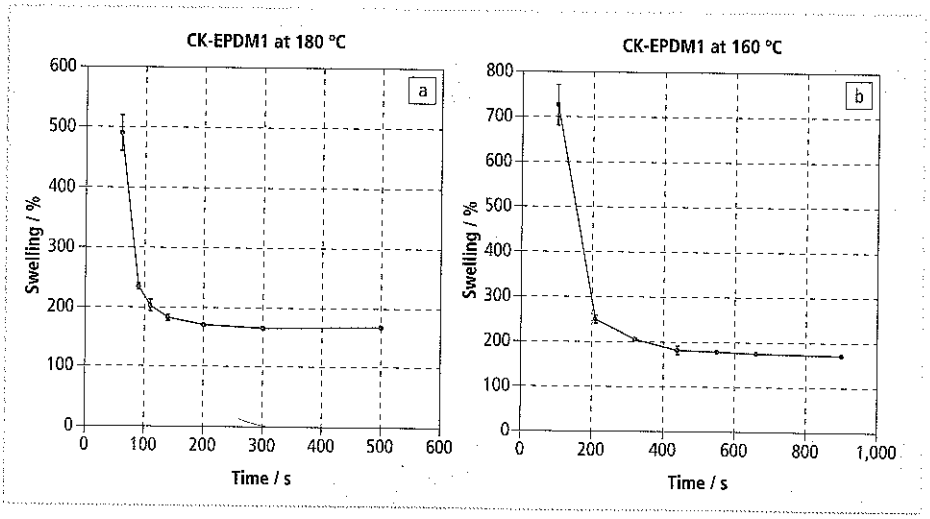

The NR formulation gives a higher torque at the maximum cure point when the test is done at lower temperature **(fig. 5).** The number of crosslinks per unit volume becomes higher. This behaviour is verified by the swelling results **(fig. 9)** where the minimum value of swelling (that is related to the maximum crosslink density) is at 107 % for the material having been cured at 165 °C and goes down to 95 % at a curing temperature of 150 °C. A higher torque value means a lower swelling ratio. Once the optimum cure point is achieved (that is the minimum swelling point) the NR exhibits its reversion character, which results in an increase of the swelling ratio as detailed in **figure 9.**

The EPDM formulation was cured with peroxides. In this case, as illustrated in **figure 6,** the material gives a higher maximum torque when the test is done at higher temperature (180 °C instead of 160 °C). When a temperature of 160 °C is applied, the peroxide does not decompose completely, so that the curing remains incomplete. When the information of the swelling tests is evaluated **(fig. 10),** a minimum swelling ratio of about 166 % is achieved at a temperature of 180 °C whereas the minimum value at 160 °C is 172 %. This means that the cure reaction is not completed at 160 °C. Again, a higher torque value correlates to a lower swelling ratio. A small torque decay as time goes on is exhibited at 180 °C, which is also represented as an increased swelling ratio.

For both NR and EPDM there is a match in time for the time values at which the material reaches the maximum torque value in ODR tests and the time value for which the minimum value of swelling ratio is achieved; which means that there exists an equivalence of maximum torque and minimum swelling ratio.

According to these results, when vulcanising a rubber formulation it is necessary to take the cure temperature into account because it affects the decomposition of the

curing agents and also the cure time. In addition to that it could lead to reversion phenomena depending on the composition of the formulation.

A match can be found between the torque values measured in the ODR test (and each torque value can be associated to a specific degree of cure) and the swelling ratios. In this way, once this relationship has been defined for the rubber formulation to be studied it is possible to determine the curing degree of a rubber part using the swelling method discussed above. So, it is not necessary to apply the methods described in the literature (being much more complex) and that are based on the Flory-Rehner relationship [11].

3.3 Tensile testing and swelling of tensile test samples

Tensile test specimens were manufactured in accordance with section 2.3, three samples each for tensile testing and swelling. The results are collected in **figures 11** and **12** (tensile tests) and in **figures 13** and **14** (swelling tests).

Fig. 11: Modulus values of CK-NR 1

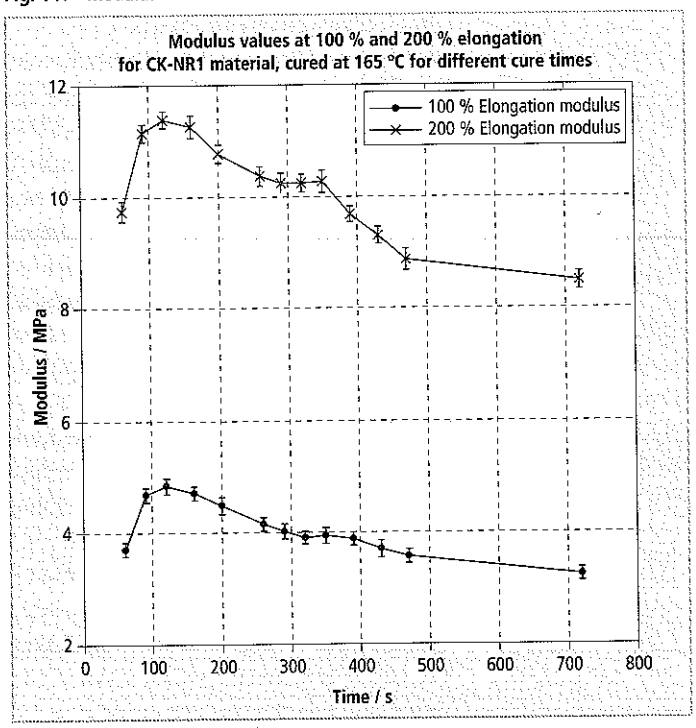

Fig. 12: Modulus values of CK-EPDM 1

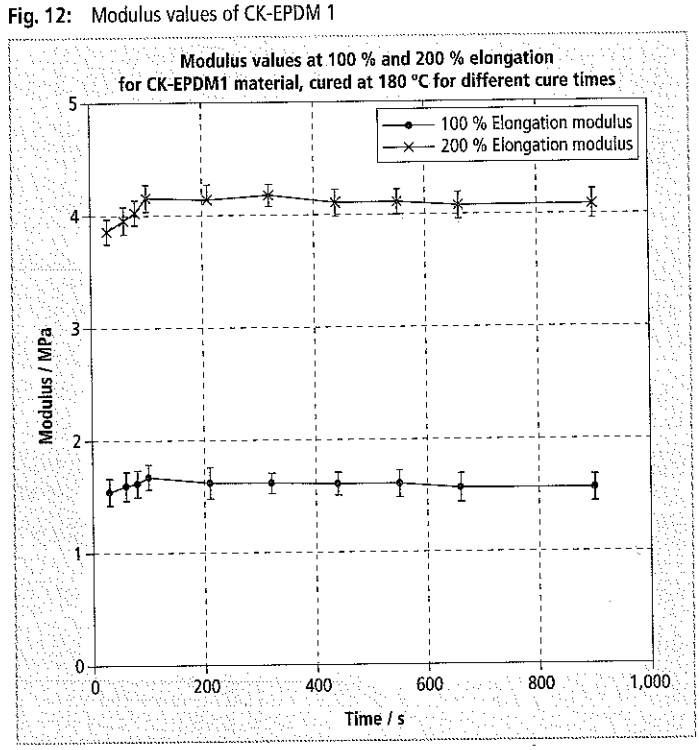

Fig. 13: Swelling of CK-NR 1 (dumbbell)

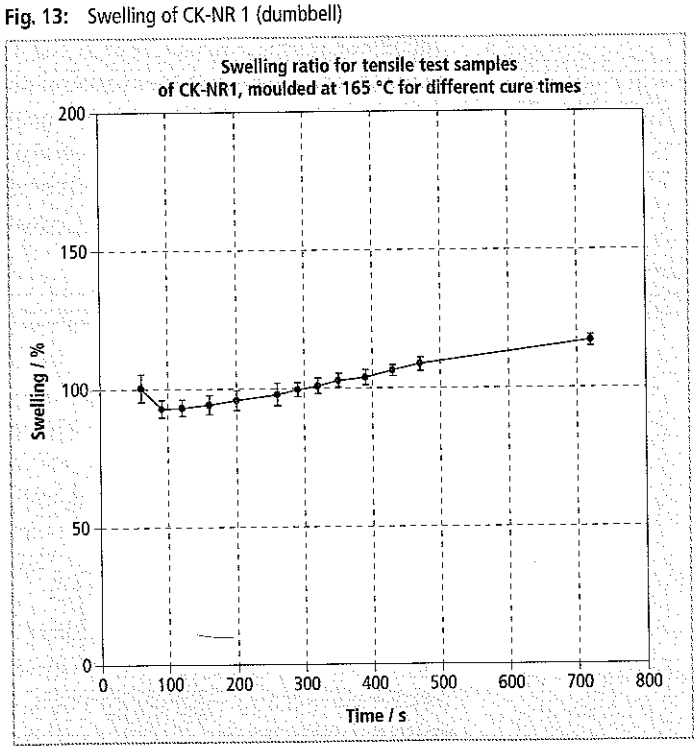

Fig. 14: Swelling of CK-EPDM 1 (dumbbell)

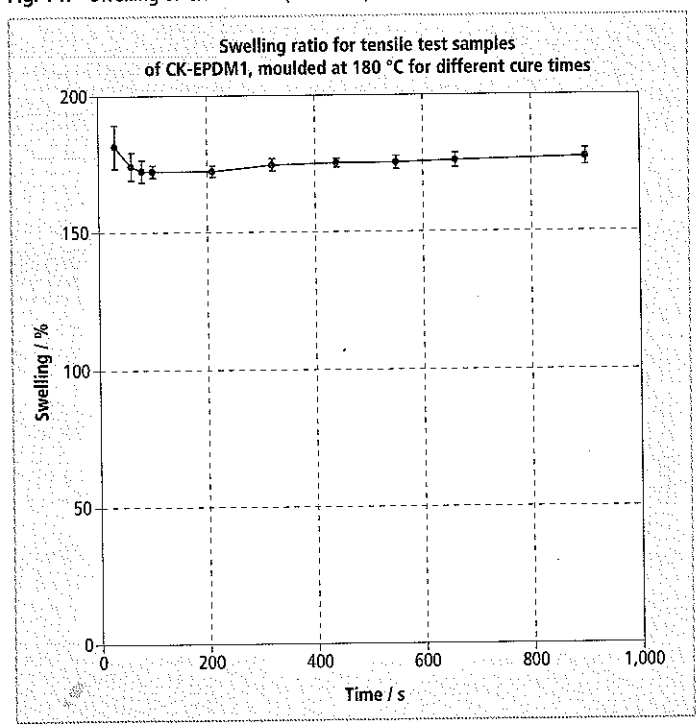

Regarding CK-NR 1 there occurs an initial increase of the moduli up to a maximum followed by an on-going decrease. That decrease is associated with the reversion character exhibited by the formulation. CK-EPDM 1 shows a similar increase at the beginning, but no reversion behaviour. The maximum value is maintained.

Figures 13 and **14** display a minimum swelling ratio point. Values of about 93 and 172 % are attained for NR (165 °C) and EPDM (180 °C) samples respectively. The values are close to the minimum swelling values seen for the ODR samples tested at 150 °C (NR) and 160 °C (EPDM), i. e. tested at lower temperatures than the mould temperature for manufacturing the tensile samples. This means a direct relationship of swelling values from ODR and tensile test samples cannot be deduced, because the manufacturing process and as a consequence the thermal history of those samples are completely different. Concerning the curing degrees measured by swelling both methods (ODR and tensile) do not lead to equivalent results. Analogous to the ODR samples, however, the tensile specimens have a match in time for the point of minimum swelling ratio and the point of maximum modulus value (both at 100 and 200 % elongation).

3.4 Swelling of industrial parts

Preparation and testing of the samples followed section 2.5. The results are presented in **table 2.** Both materials show that the external layer leads to lower swelling ratio values than the core material, which is related to differences in the degree of cure. According to the results presented in **figures 9** and **10** where samples from the ODR tests were swollen under similar conditions, the NR formulation arrives at a minimum level of about 95 % for a completely cured sample. This value matches with the value measured for the external layer of the industrial part; so it can be concluded that the external layer of the NR part is completely cured. The internal layer reaches about 102 %, which corresponds to an incomplete cure. Considering the swelling values obtained for the ODR samples it can be deduced, that the swelling behaviour gives a good indication of the curing degree. Referring to the EPDM formulation ODR test samples attain a minimum swelling ratio of about 170 % for a complete curing stage. Results from the industrial part show that the external layer achieves these values, whereas the internal layer gives higher swelling ratios, which corresponds to an incomplete cure again.

Material	Sample 1 / %	Sample 2 / %	Sample 1 / %	Average / %
CK-NR 1 outside	96.56	95.06	96.76	96.13
CK-NR 1 inside	101.99	101.27	102.24	101.84
CK-EPDM 1 outside	169.04	169.14	170.57	169.59
CK-EPDM 1 inside	175.56	175.95	176.56	176.02

Tab. 2:
Swelling industrial part – VW Reference 7H0-253-144

4. Conclusions

The aim of the present study was to check the applicability of simple swelling tests for evaluating the curing degree achieved in rubber parts. Other swelling procedures such as those being based on the Flory-Rehner equation [7] are considered to be too complicated and too time consuming for a practical industrial application. The analysis of swelling data obtained by simple procedures allows a reasonable assessment of the curing degree in a rapid and uncomplicated way. This could be exemplary demonstrated within a broad test programme covering the examination of laboratory and regular production samples from two formulations, i. e. a conventionally sulphur cured NR and a peroxide cured EPDM. The swelling rates determined are in good conformity with the data from the rheometer traces and the tensile moduli reflecting realistically the progress of the crosslinking reaction. In addition to that the swelling data gave valuable insights how the manufacturing process influences the complete vulcanisation of a rubber part. The article dimensions, the way of heat transfer, and curing time are factors which should not be underestimated. When vulcanising rubber formulations the fixing of cure temperature and cure time needs special attention to avoid reversion effects, incomplete decomposition of the curing agents, and irregular vulcanisation.

The swelling test can be a useful, but simple tool for checking the degree of cure of rubber parts for quality control and even development purposes or in situations where other test methods fail to obtain reasonable results.

5. Acknowledgements

The authors wish to thank Cikautxo S. Coop. for defining and manufacturing the rubber formulations. Additional thanks go to Lea Artibai Ikastetxea S. Coop., Azaro Fundazioa, Feder, and Basque Country Government for funding this study.

6. References

[1] Bellander, M., High pressure Vulcanisation: Crosslinking of Diene Rubbers without Vulcanisation Agents, PhD thesis 1998, Department of Polymer Technology, Royal Institute of Technology, Stockholm, Sweden
[2] Kramer, H., Rubber World July (1994), IRC'93 and 144th ACS Rubber Division Meeting (1993)
[3] Arrilaga, A., Zaldua, A. M., Achurra, R. M., Farid, A. S., Eur. Polym. J. 43/11 (2007), 4783
[4] Mooney, M., J. Appl. Phys. 11 (1940), 582
[5] Rivlin, R. S., Phi. Trans. Roy. Soc. A241 (1948), 319
[6] Saville, B., Watson, A. A., Rubber Chem. Technol. 40 (1967), 100
[7] Flory, P. J., Rehner, J., J. Chem. Phys. 11 (1943), 521
[8] Brazier, D. W., Nickel, G. H., Rubber Chem. Technol. 48 (1975), 26
[9] Brazier, D. W., Thermochim. Acta 18 (1977), 147
[10] Warley, R. L., Del Vecchio, R. J., 131st ACS Rubber Division Meeting (1987), 29
[11] Crowther, B. G., Lewis, P. M., Methrell, C., Natural Rubber Science and Technology, 6 (1988), Roberts, A. D., Ed., Oxford University Press, New York, USA
[12] Gent, A. N., Hartwell, J. A., Lee, G., Rubber Chem. Technol. 76 (2003), 517
[13] Hergenrother, W. L., Hilton, A. S., Rubber Chem. Technol. 76 (2003), 832
[14] Hayes, R. A., Rubber Chem. Technol. 59 (1986), 138

ANNEX II

Mathematical relations

ANNEX II-A: ON THE TENSILE AND SHEAR MODULUS RELATION

Figure 0.1 represents the pure shear state. When the inside cube is rotated 45º, it is only loaded by the maximum possible shear. The unique deformations in this geometry are angular deformations.

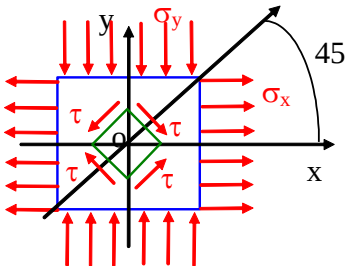

Figure 0.1: Pure shear

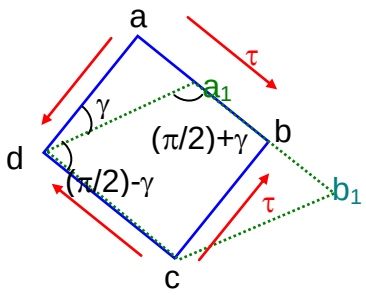

Figure 0.2: Pure shear representation

The diagonal d-b (Figure 0.2) is extended and the diagonal *a-c* is shortened. $\sigma_x = \tau$; $\sigma_y = -\tau$; $\sigma_z = 0$. Applying the generalized Hooke's law:

$$\varepsilon_x = \frac{1}{E}\left[\sigma_x - \nu\left(\sigma_y + \sigma_z\right)\right] = \frac{\tau}{E}\left(1+\nu\right) \qquad \textit{Eq. 0.1}$$

$$\varepsilon_y = \frac{1}{E}\left[\sigma_y - \nu\left(\sigma_z + \sigma_x\right)\right] = -\frac{\tau}{E}\left(1+\nu\right) \qquad \textit{Eq. 0.2}$$

$$\varepsilon_z = \frac{1}{E}\left[\sigma_z - \nu\left(\sigma_x + \sigma_y\right)\right] = 0 \qquad \textit{Eq. 0.3}$$

$$\varepsilon_v = \frac{\Delta V}{V_0} = \varepsilon_x + \varepsilon_y + \varepsilon_z = 0 \qquad \textit{Eq. 0.4}$$

The variation of the unitary volume is zero in pure shear. So the diagonals variation is calculated as follows (Figure 0.3):

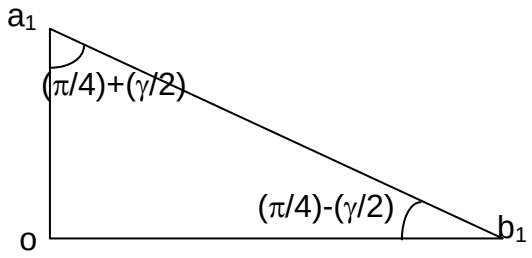

Figure 0.3: Pure shear: diagonals variation

$$\overline{ob_1} = \overline{ob}(1+\varepsilon_x) = \overline{ob}\left[1+\frac{\tau}{E}(1+\nu)\right] \qquad \textit{Eq. 0.5}$$

$$\overline{oa_1} = \overline{oa}(1+\varepsilon_y) = \overline{oa}\left[1-\frac{\tau}{E}(1+\nu)\right] \qquad \textit{Eq. 0.6}$$

$$\mathrm{tg}\,\hat{oa_1}b_1 = \mathrm{tg}\left(\frac{\pi}{4}+\frac{\gamma}{2}\right) = \frac{\overline{ob_1}}{\overline{oa_1}} = \frac{\overline{ob}\left[1+\frac{\tau}{E}(1+\nu)\right]}{\overline{oa}\left[1-\frac{\tau}{E}(1+\nu)\right]} = \frac{1+\frac{\tau}{E}(1+\nu)}{1-\frac{\tau}{E}(1+\nu)} \qquad \textit{Eq. 0.7}$$

$$tg\left(\frac{\pi}{4}+\frac{\gamma}{2}\right) = \frac{tg\frac{\pi}{4}+tg\frac{\gamma}{2}}{1-tg\frac{\pi}{4}tg\frac{\gamma}{2}} \approx \frac{1+\frac{\gamma}{2}}{1-\frac{\gamma}{2}} \qquad \textit{Eq. 0.8}$$

From the last two Eq. 0.7 and Eq. 0.8,

$$\frac{1+\frac{\gamma}{2}}{1-\frac{\gamma}{2}} = \frac{1+\frac{\tau}{E}(1+\nu)}{1-\frac{\tau}{E}(1+\nu)} \Rightarrow \frac{\gamma}{2} = \frac{\tau}{E}(1+\nu) = \varepsilon \qquad \textit{Eq. 0.9}$$

$$2\varepsilon = \gamma = \frac{2(1+\nu)}{E}\tau = \frac{\tau}{G} \Rightarrow \boxed{G = \frac{E}{2(1+\nu)}} \qquad \textit{Eq. 0.10}$$

$$G = \frac{\tau}{\gamma} \Rightarrow \boxed{\tau = G\gamma} \qquad \textit{Eq. 0.11}$$

It is assumed that $V_0=1$,

$$V_f = (1+\varepsilon_x)(1+\varepsilon_y)(1+\varepsilon_z) \qquad \textit{Eq. 0.12}$$

Rejecting a higher order this expression yields to:

$$V_f = 1+\varepsilon_x+\varepsilon_y+\varepsilon_z \qquad \textit{Eq. 0.13}$$

$$\varepsilon_v = \frac{\Delta V}{V_0} = \frac{V_f - V_0}{V_0} = \frac{(1+\varepsilon_x+\varepsilon_y+\varepsilon_z)-1}{1} = \varepsilon_x+\varepsilon_y+\varepsilon_z \qquad \textit{Eq. 0.14}$$

where V_0 and V_f are the initial and the final volume values respectively and εv is known as the volumetric strain or cubic dilatation.

Substituted by the generalized Hooke's law,

$$\varepsilon_v = \frac{\sigma_x+\sigma_y+\sigma_z}{E}(1-2\nu) \qquad \textit{Eq. 0.15}$$

The deformation of any point which is modelled as a cube and loaded with hydrostatic pressure p is solved with the following equation:

$$\sigma_x = \sigma_y = \sigma_z = -p \qquad \varepsilon_x = \varepsilon_y = \varepsilon_z = -\frac{p}{E}(1-2\nu) \qquad \textit{Eq. 0.16}$$

Y.C. Fung [1]: The Bulk modulus k may be expressed as follows

$$k = -p/\varepsilon_v \qquad \textit{Eq. 0.17}$$

From Eq. 0.15, Eq. 0.16 and Eq. 0.17,

$$k = \frac{E}{3(1-2\nu)}$$ *Eq. 0.18*

ANNEX II-C: ENERGY DISSIPATED PER CYCLE AND THE MAXIMUM STORED ELASTIC ENERGY (Wc).

When a sample is subjected to oscillatory deformations, the strain varies sinusoidally with time as:

$$\varepsilon = \varepsilon_0 sin\omega t \qquad \textit{Eq. 0.19}$$

And the stress can be defined as,

$$\sigma = \varepsilon_0 \, \mathrm{E}' \sin \omega t + \varepsilon_0 \, \mathrm{E}'' \cos \omega t \qquad \textit{Eq. 0.20}$$

The dissipative energy per cycle is calculated as:

$$U_c = \int \sigma d\varepsilon = \int_0^{2\pi/\omega} \sigma \frac{d\varepsilon}{dt} dt \qquad \textit{Eq. 0.21}$$

From Eq. 0.19 the following equation can be defined as:

$$\frac{d\varepsilon}{dt} = \varepsilon_0 \omega \cos \omega t \qquad \textit{Eq. 0.22}$$

Using expressions Eq. 0.20 and Eq. 0.22, Eq. 0.21 can be rewritten as:

$$U_c = \int_0^{2\pi/\omega} \left(\varepsilon_0 \varpi \cos \omega t\right)\left(\varepsilon_0 E' sen\omega t + \varepsilon_0 E'' \cos \omega t\right) dt \qquad \textit{Eq. 0.23}$$

$$U_c = \int_0^{2\pi/\omega} {\varepsilon_0}^2 \varpi \left(E' sen\omega t \cos \omega t + E'' \cos^2 \omega t\right) dt \qquad \textit{Eq. 0.24}$$

This integral is solved taking into account the next trigonometric relations;

$$\begin{cases} \operatorname{sen}\omega t\cos\omega t = \dfrac{1}{2}\operatorname{sen}2\omega t \\ \cos^2\omega t = \dfrac{1}{2}(1+\cos 2\omega t) \end{cases}$$

$$U_c = \varpi\varepsilon_0^{\,2}\int_0^{2\pi/\omega}\left(E'\frac{1}{2}sen2\omega t + E''\frac{1}{2}(1+\cos 2\omega t)\right)dt \qquad \textit{Eq. 0.25}$$

$$U_c = \frac{\varpi\varepsilon_0^{\,2}}{2}\int_0^{2\pi/\omega}\left(E'sen2\omega t + E''+E''\cos 2\omega t\right)dt \qquad \textit{Eq. 0.26}$$

$$U_c = \frac{\varpi\varepsilon_0^{\,2}}{2}\left[-\frac{E'}{2\omega}\cos 2\omega t + E''t + \frac{E''}{2\omega}sen2\omega t\right]_0^{2\pi/\omega} \qquad \textit{Eq. 0.27}$$

$$U_c = \frac{\varpi\varepsilon_0^{\,2}}{2}E''\frac{2\pi}{\omega} \qquad \textit{Eq. 0.28}$$

$$U_c = \pi E''\varepsilon_0^{\,2} \qquad \textit{Eq. 0.29}$$

If the integral U_c is evaluated for a quarter of a cycle, instead of the entire cycle, the first term gives the maximum stored elastic energy (W_c).

$$E'\varpi\varepsilon_0^{\,2}\int_0^{\pi/2\omega} sen\omega t\cos\omega t dt \qquad \textit{Eq. 0.30}$$

$$W_c = E'\varpi\varepsilon_0^{\,2}\int_0^{\pi/2\omega}\frac{1}{2}sen2\omega t dt = E'\varpi\varepsilon_0^{\,2}\left[-\frac{1}{4\omega}\cos 2\omega t\right]_0^{\pi/2\omega} \qquad \textit{Eq. 0.31}$$

$$W_c = E'\varpi\varepsilon_0^{\,2}\left[\frac{1}{4\omega}+\frac{1}{4\omega}\right] = E'\varpi\varepsilon_0^{\,2}\frac{1}{2\omega} \qquad \textit{Eq. 0.32}$$

$$W_c = \frac{1}{2} E' \varepsilon_0^{\,2} \qquad \textit{Eq. 0.33}$$

ANNEX II-D: APPROXIMATED RELATION BETWEEN SIMPLE SHEAR AND PURE SHEAR

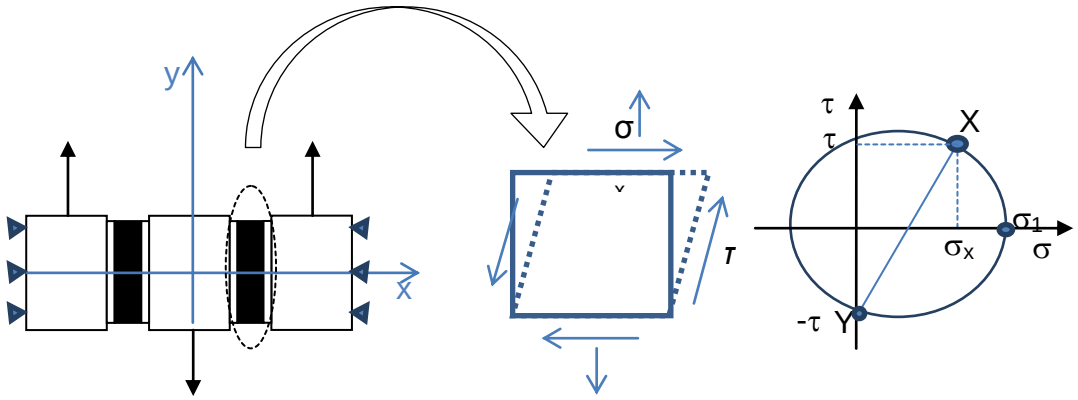

Figure 0.4: Simple shear specimen, strain state representation & Mohr's circle representation.

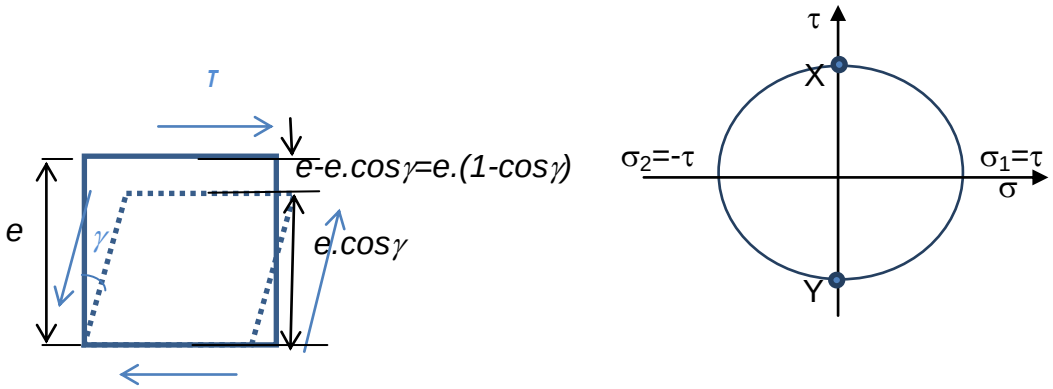

Figure 0.5: Pure shear, strain state representation & Mohr's circle representation

$$\varepsilon_x = \frac{e(1-cos\gamma)}{e} \qquad \textit{Eq. 0.34}$$

The Generalized Hooke's law is valid only for isotropic materials; the strain for '*x*' direction is calculated as follows,

$$\varepsilon_x = \frac{1}{E}\left[\sigma_x - \nu(\sigma_y + \sigma_z)\right] \qquad \textit{Eq. 0.35}$$

In pure shear strain state σ_y and σ_z are zero, hence,

$$\varepsilon_x = \frac{\sigma_x}{E} = \frac{e(1 - cos\gamma)}{e} \qquad \textit{Eq. 0.36}$$

$$\sigma_x = E(1 - cos\gamma) \qquad \textit{Eq. 0.37}$$

$$\sigma_1 = \frac{\sigma_x}{2} + \sqrt{\left(\frac{\sigma_x}{2}\right)^2 + \tau^2} \qquad \textit{Eq. 0.38}$$

When the angular deformation γ takes small values it is known that $tan\gamma \approx sin\gamma \;\&\; cos\gamma \approx 1$, hence, $\varepsilon_x = 0$, $\sigma_x = 0$ and $\sigma_1 = \tau$ which implies that both strain states (pure shear and simple shear states) are equivalent states.

ANNEX II-E: CORRELATION BETWEEN SIMPLE SHEAR AND PURE SHEAR

The strain invariants I_1 and I_2 in pure shear Eq. 0.39 as in simple shear Eq. 0.40 are equal;

$$I_1 = tr(B) = I_2 = tr(B^{-1}) = 1 + \lambda^2 + \frac{1}{\lambda^2} \qquad \textit{Eq. 0.39}$$

$$I_1 = tr(B) = I_2 = tr(B^{-1}) = 3 + \tan^2 \gamma \qquad \textit{Eq. 0.40}$$

As explained in the thesis document when the elastomer is considered as incompressible the third strain invariant $I_3 = 1$. In addition, in both pure shear and simple shear strain states the first and second invariants are equal as demonstrated in Eq. 0.39 and Eq. 0.40. Hence, a relation between the shear angle γ in simple shear and the stretch $\lambda = \lambda_1$ in pure shear can be obtained by comparing the first strain invariant expressions;

$$1 + \lambda^2 + \frac{1}{\lambda^2} = 3 + \tan^2 \gamma \qquad \textit{Eq. 0.41}$$

and solve for the shear angle giving,

$$\gamma = atan\left(\sqrt{\lambda^2 + \tfrac{1}{\lambda^2} - 2}\right) \text{ then } \gamma = atan\left(\lambda - \tfrac{1}{\lambda}\right) \qquad \textit{Eq. 0.42}$$

From this equation, we find the shear angle that produces the same strain invariants in simple shear as in pure shear, given a specific stretch λ in pure shear.

Work is the result of a force on a point that moves through a distance. For a constant force that is not directed along the line it is defined as the product of force vector and the displacement in the direction of movement,

$$W = F.cos\gamma.ds \qquad Eq.\ 0.43$$

where γ is the angle between force and displacement direction vectors.

In pure shear the only work done is the work done by σ_1 (λ_2=1 in pure shear is constant and the third direction is 90º displaced with the force application direction, then, Cos90º=0),

$$dW = \sigma_1 d\lambda \qquad Eq.\ 0.44$$

In the same way, in simple shear the only work done is that done by the shear stress τ,

$$dW = \tau d\gamma \qquad Eq.\ 0.45$$

These two expressions Eq. 0.44 and Eq. 0.45 must be identical,

$$\tau = \sigma_1 \frac{d\lambda}{d\gamma} \qquad Eq.\ 0.46$$

Hence, from measurements of stress σ_1 in the principal direction λ_1 done in pure shear permits the calculation of the equivalent simple shear stress τ.

As mentioned above, the pure shear stress σ_1 /strain ε data can be transformed in simple shear stress τ/strain γ data. After, two ways are presented. First, the simplified relation for small strain level and after, the complete relation for every strain level are presented.

Pure shear and simple shear relation for small strains.—

For small strains, the principal axes are inclined at 45º to the direction of sliding. *Love* [2] explained that the amount of the shear may be related either to angle γ or to the principal extension ratios λ as follows (from Eq. 0.42),

$$\gamma = tan\gamma = \lambda - \frac{1}{\lambda} \qquad \textit{Eq. 0.47}$$

Hence, the derivative of the previous expression Eq. 0.47 can be written as follows,

$$\frac{d\gamma}{d\lambda} = 1 + \frac{1}{\lambda^2} = \frac{1+\lambda^2}{\lambda^2} \qquad \textit{Eq. 0.48}$$

Hence,

$$\frac{d\lambda}{d\gamma} = \frac{\lambda^2}{1+\lambda^2} \qquad \textit{Eq. 0.49}$$

Rewriting Eq. 0.47, the pure shear stretch λ can be defined as follows *Gil-Negrete* [3],

$$\lambda\gamma = \lambda^2 - 1 \rightarrow \lambda^2 - \gamma\lambda - 1 = 0 \text{ then} \qquad \lambda = \frac{\gamma + \sqrt{\gamma^2+4}}{2} \qquad \textit{Eq. 0.50}$$

The elongation or stretch λ is defined as,

$$\lambda = \frac{L}{L_0} = \frac{L_0 + \Delta L}{L_0} = \frac{L_0}{L_0} + \frac{\Delta L}{L_0} = 1 + \varepsilon \qquad \textit{Eq. 0.51}$$

From Eq. 0.50 and Eq. 0.51 pure shear strain ε_1 and simple shear strain γ can be related as follows,

$$\varepsilon_1 = \frac{\gamma + \sqrt{\gamma^2+4}}{2} - 1 \qquad \textit{Eq. 0.52}$$

Rewriting Eq. 0.46 we have,

$$\sigma_1 = \tau \frac{d\gamma}{d\lambda} \qquad \textit{Eq. 0.53}$$

From Eq. 0.53 and Eq. 0.48, the pure shear stress σ_1 and simple shear stress can be related for a known pure shear stretch λ.

$$\sigma_1 = \tau \frac{1+\lambda^2}{\lambda^2} \quad \text{or} \quad \tau = \sigma_1 \frac{\lambda^2}{1+\lambda^2} \qquad \textit{Eq. 0.54}$$

Pure shear and simple shear relation for every strain level.—

The derivative of Eq. 0.42 which relates simple shear angle γ and pure shear stretch λ gives,

$$\frac{d\lambda}{d\gamma} = \frac{\lambda^4 - \lambda^2 + 1}{1 + \lambda^2} \qquad \textit{Eq. 0.55}$$

When $\lambda_1 \simeq 1$, Eq. 0.49 and Eq. 0.55 gives a similar result.

From Eq. 0.46 and Eq. 0.55 , the pure shear stress σ_1 and simple shear stress can be related for a known pure shear stretch λ as follows,

$$\sigma_1 = \tau \frac{1+\lambda^2}{\lambda^4-\lambda^2+1} \text{or} \quad \tau = \sigma_1 \frac{\lambda^4-\lambda^2+1}{1+\lambda^2} \qquad \textit{Eq. 0.56}$$

From Eq. 0.42 the pure shear stretch λ can be related with simple shear strain γ as follows,

$$\lambda = \frac{tan\gamma + \sqrt{tan^2\gamma + 4}}{2} \qquad \textit{Eq. 0.57}$$

Finally, from Eq. 0.51 and Eq. 0.57 the pure shear strain ε can be related with simple shear strain γ as follows,

$$\varepsilon = \frac{tan\gamma + \sqrt{tan^2\gamma + 4}}{2} - 1$$ *Eq. 0.58*

Pot element or Dashpot.—

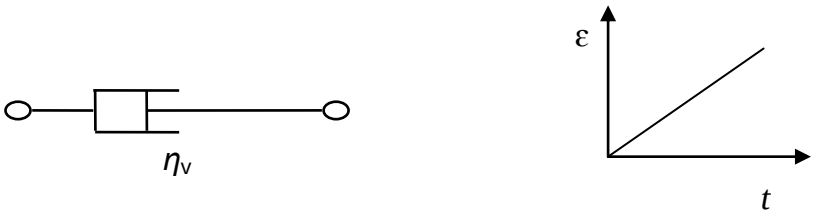

A) B)

Figure 0.6: A) Dashpot element. B) Deformation vs. time representation when a constant stress is applied

This element is a frictionless piston which represents the viscous behavior (Figure 0.6-A). If a stress σ is applied between times t_0 and t_1, the deformation ε will vary linearly with time of application of stress (Figure 0.6-B).

$$\frac{d_\varepsilon}{d_t} = \frac{\sigma}{\eta_v} \qquad \textit{Eq. 0.59}$$

if σ is constant (Creep case):

$$\varepsilon = \frac{\sigma}{\eta_v} t \qquad \textit{Eq. 0.60}$$

where η_v is the viscosity constant.

When the applied stress σ stops acting, deformation ε remains (irreversible) because the work provided by the external force is not stored by the material and it is dissipated as heat (internal friction). Deformation is faster for smaller values of viscosity.

Elastic solid. Spring model.—

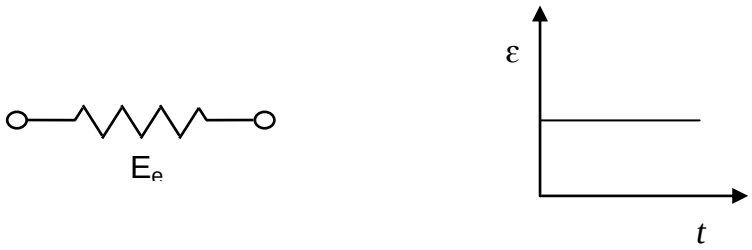

A) B)

Figure 0.7: A) Elastic Spring. B) Deformation vs. time representation when a constant stress is applied

The elastic solid follows Hooke's law $\sigma=E_e\varepsilon$ (Figure 0.7-A). When a load is applied, the instantaneous strain originated is due to changes in the length and angles of atomic bonds (Figure 0.7-B). The solid stores all the energy supplied by the external forces. When the load is removed, the stored energy is able to restore the original shape instantly (reversible deformation)

Maxwell model.—

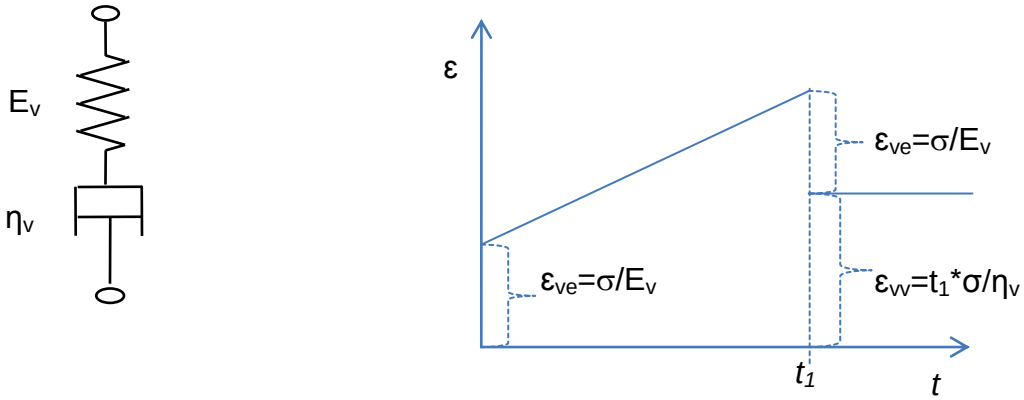

A) B)

Figure 0.8: A) Maxwell models representation. B) Creep case (σ is constant) Maxwell models loading and unloading representation. The model is unloaded at time t_1.

Most polymers exhibit elastic and viscous behavior together (only glassy polymers are perfectly elastic solids and thermoplastics; high temperature

shows a viscous behavior only), which can be assimilated to the juxtaposition of the models described above.

Maxwell's element or model is formed by connecting in series a dashpot and a spring (Figure 0.8-A). By applying the spring force *F*, it instantly lengthens the magnitude ε and the dashpot moves to the speed σ/η while applying the load (between t_o and t_1). By stopping the application of the load, the elastic component is recovered instantaneously while the viscous component of the deformation remains indefinitely (Figure 0.8-B).

The total deformation is therefore distributed between the two elements, which are subjected to the total stress. Thus,

$$\sigma_v = \sigma_{ve} = \sigma_{vv} \qquad \textit{Eq. 0.61}$$

$$\varepsilon_v = \varepsilon_{ve} + \varepsilon_{vv} \qquad \textit{Eq. 0.62}$$

Where subscripts *ve, vv* and *v* indicate the stresses σ and strains ε in the elastic spring, dashpot and the totals of the Maxwell element.

The spring is the elastic component of the model and behaves according to Hooke's law:

$$\varepsilon_{ve} = \left(\frac{1}{E_{ve}}\right)\sigma_v \qquad \textit{Eq. 0.63}$$

and the dashpot is the viscous component of the model and behaves according to Newton's law:

$$\frac{d\varepsilon_{vv}}{d_t} = \left(\frac{1}{\eta_v}\right)\sigma_v \qquad \textit{Eq. 0.64}$$

The total strain variation over time is obtained by differentiating the Eq. 0.62:

$$\frac{d\varepsilon_v}{d_t} = \frac{d\varepsilon_{ve}}{d_t} + \frac{d\varepsilon_{vv}}{d_t} \qquad \textit{Eq. 0.65}$$

Substituting in Eq. 0.65 the Eq. 0.64 and Eq. 0.63 derivative with respect to time yields:

$$\frac{d\varepsilon_v}{d_t} = \left(\frac{1}{E_{ve}}\right)\frac{d\sigma_v}{d_t} + \left(\frac{1}{\eta_v}\right)\sigma_v \qquad \textit{Eq. 0.66}$$

which is the equation that governs the behavior of the Maxwell model.

A simple viscous or standard viscoelastic solid model: Zener model.—

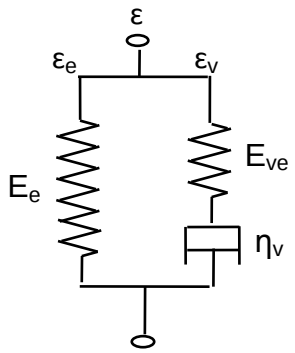

Figure 0.9: Three elements model. It is known as the Zener or standard linear solid (SLS) model.

A response closer to a real polymer is obtained by adding a second spring of modulus E_e in parallel with Maxwell unit (Figure 0.9). This model is known as Zener model [4].

$$\varepsilon = \varepsilon_e = \varepsilon_v \qquad \textit{Eq. 0.67}$$

$$\sigma = \sigma_e + \sigma_v \qquad \textit{Eq. 0.68}$$

where:

$$\varepsilon = \frac{\sigma_e}{E_e} \qquad \textit{Eq. 0.69}$$

Using these relationships, their time derivatives and the above stress-strain relationships for the spring and the dashpot elements, the system can be modelled as follows:

$$(E_e + E_{ve})\frac{d\varepsilon}{dt} + \frac{E_e E_{ve}}{\eta}\varepsilon = \frac{d\sigma}{dt} + \frac{E_{ve}}{\eta_v}\sigma \qquad \textit{Eq. 0.70}$$

Generalization of the Maxwell model.—

This model is based on the Zener model. One or more Maxwell chains are added to that model to improve the fitting of experimental data (Figure 0.10).

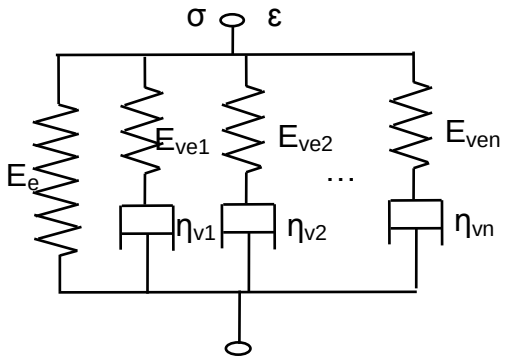

Figure 0.10: Generalization of the Maxwell model.

Considering a relaxation test, the total stress in this model will be obtained with the addition of the elastic stress to the solitary spring of stiffness E_e which is known as E_∞, plus the sum of stresses in each Maxwell element.

These viscoelastic models can be written so that they can characterize the mechanical behavior as a function of both time and frequency. When these models are written according to time, they can be used for characterizing the creep and stress relaxation tests. This thesis will examine the last mentioned tests because this latter is the most related to the objectives of the thesis.

Maxwell models stress relaxation behavior.—

In this mode of time-dependent stress, $\boldsymbol{\varepsilon}$ is constant, then Eq. 0.66 is converted into:

$$\left(\frac{1}{E_{ve}}\right)\frac{d\sigma_v}{d_t}+\left(\frac{\sigma_v}{\eta_v}\right)=0 \qquad \textit{Eq. 0.71}$$

Where,

$$\frac{d\sigma_v}{\sigma_v}=-\left(\frac{E_{ve}}{\eta_v}\right)dt \qquad \textit{Eq. 0.72}$$

The solution of the previous differential equation between the initial time of application of stress σ until it takes a time t gives:

$$\sigma=\sigma_{v0}e^{\frac{-E_{ve}t}{\eta_v}}=\sigma_{v0}e^{\frac{-t}{\tau}}=\varepsilon_{v0}E_{ve}e^{\frac{-t}{\tau}} \qquad \textit{Eq. 0.73}$$

And,

$$E(t)=E_{ve}e^{\frac{-t}{\tau}} \qquad \textit{Eq. 0.74}$$

The initial stress is defined entirely by the elastic spring, and the initial condition for the differential equation is the load acting on the body is disappearing gradually and disappears completely after an infinite time (Figure 0.11). This equation shows that the stress decays exponentially with a characteristic time constant:

$$\tau=\frac{\eta_v}{E_{ve}} \qquad \textit{Eq. 0.75}$$

where τ is called the “relaxation time”.

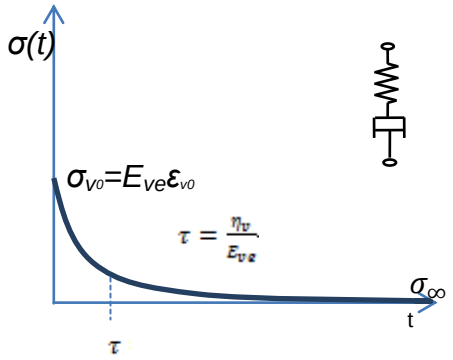

Figure 0.11: Stress relaxation phenomenon: Maxwell model.

This model is too simple to explain the actual behavior of polymers since it has two major limitations: the strain rate is constant while applying the constant load and also the relaxed stress $\sigma_\infty=0$ at constant strain conditions.

The complex modulus $E^*(\omega)$ can be determined by solving Eq. 0.66 for a steady-state sinusoidal strain history,

$$\varepsilon^* = \varepsilon_0 e^{i\omega t} \qquad \textit{Eq. 0.76}$$

Inserting a trial solution,

$$\sigma = Ce^{i\omega t} \qquad \textit{Eq. 0.77}$$

into Eq. 0.66 yields in the stationary solution,

$$C = E_{ve}\frac{i\omega}{i\omega + E_{ve}/\eta}\varepsilon_0 = E_{ve}\frac{i\omega\tau}{i\omega\tau + 1}\varepsilon_0 \qquad \textit{Eq. 0.78}$$

Finally the complex modulus can be written as follows,

$$E^*(\omega) = E_{ve}\frac{i\omega\tau}{1 + i\omega\tau} \qquad \textit{Eq. 0.79}$$

Zener models stress relaxation behavior.—

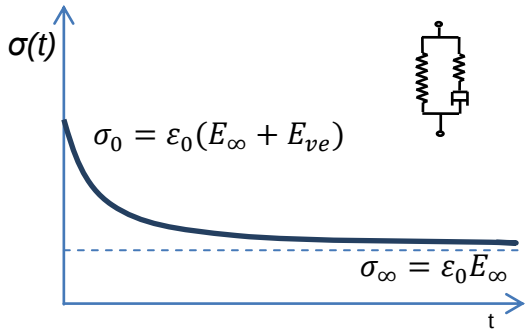

Figure 0.12: Stress relaxation phenomenon: Zener model.

The total stress is given by,

$$\sigma = \sigma_\infty + \sigma_{Maxwell} \qquad \textit{Eq. 0.80}$$

Once the material is relaxed, the stress is not zero (Figure 0.12), but it reaches a value depending on the additional spring (compared to the Maxwell model).

In this case, integrating the Eq. 0.70 from the initial time of application of stress σ until it takes a time t gives:

$$\sigma(t) = \varepsilon_0 \left(E_\infty + E_{ve} e^{\frac{-t}{\tau}} \right) \qquad \textit{Eq. 0.81}$$

Then, Young's relation modulus can be written as follows:

$$E(t) = E_\infty + E_{ve} e^{\frac{-t}{\tau}} \qquad \textit{Eq. 0.82}$$

The stress is given by inserting the Maxwell stress Eq. 0.79 into Eq. 0.80 according to,

$$\sigma^*(\omega) = E_\infty \varepsilon^* + E_{ve} \frac{i\omega\tau}{1 + i\omega\tau} \varepsilon^* \qquad \textit{Eq. 0.83}$$

Hence, the Zener models complex modulus yields in,

$$E^*(\omega) = E_\infty + E_{ve}\frac{i\omega\tau}{1+i\omega\tau} \qquad \textit{Eq. 0.84}$$

Generalization of the Zener model or generalized Maxwell model.—

The generalized Maxwell model (Figure 0.10), widely used to characterize the modulus functions of linear viscoelastic media, consists of a spring and *N* Maxwell units connected in parallel *Tschoegl* [5].

$$\sigma_0 = \sigma_\infty + \sum_{i=1}^{N}\sigma_{ve,i} \qquad \textit{Eq. 0.85}$$

$$\sigma = \varepsilon_0\left(E_\infty + \sum_{i=1}^{N}E_{ve,i}e^{\frac{-t}{\tau_i}}\right) \qquad \textit{Eq. 0.86}$$

$$Eve(t) = E_\infty + \sum_{i=1}^{N}E_{ve,i}e^{-\frac{t}{\tau_i}} \qquad \textit{Eq. 0.87}$$

where τ_i is the relaxation time for each Prony component E_{vei}.

In this model, when the time is zero (*t=0),* the instantaneous modulus E_o is,

$$E_0 = E_\infty + \sum_{i=1}^{N}E_{vei} \qquad \textit{Eq. 0.88}$$

where the long term or the relaxed modulus ($t=\infty$) is E_∞. E_{vei} and τ are the relaxation modulus and relaxation time respectively; the relaxation time of the i^{th} Maxwell element defined by $\tau_i = \eta_i/E_{vei}$ where η_i is the viscosity of the dashpot unit. The typical term under the summation symbol in the previous equation, represents the relaxation modulus of the i^{th} Maxwell unit. The series expression in the equation is often referred to as a Prony series.

Findley et all [6] studied some common models including the generalized Voigt model and generalized Maxwell model.

This model can be used to simulate sinusoidal dynamic tests. If the mentioned test is simulated with the latter model, the dynamic modulus does not change with the loading strain amplitude (Figure 0.13):

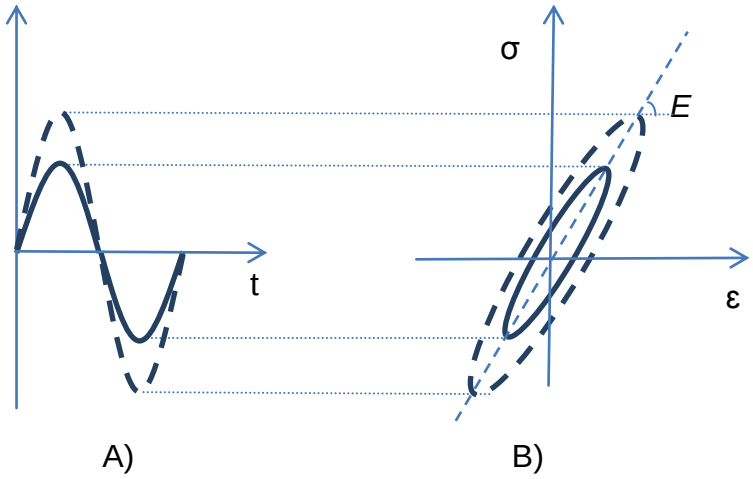

Figure 0.13: Sinusoidal Dynamic test: Linear viscoelasticity. The dynamic modulus does not change with the load strain amplitude. A) Two sinusoidal loads with different strain amplitude are presented. B) The dynamic modulus is the same in both load strain cases presented in Figure A.

The complex modulus for the generalized Zener model can be derived in a similar manner that made before in Eq. 0.84,

$$E^*(\omega) = E_\infty + \sum_{j=1}^{n} E_{vej} \frac{i\omega\tau_j}{1 + i\omega\tau_j} \qquad \textit{Eq. 0.89}$$

ANNEX II-G: GENERALIZED MAXWELL MODEL: PRONY SERIES IN TIME DOMAIN

The Prony series can be used to characterize the variation of relaxation modulus of elastomers subjected to a constant deformation [7],

$$Eve(t) = E_{\infty} + \sum_{i=1}^{N} E_{vi} e^{-\frac{t}{\tau_i}} \qquad \textit{Eq. 0.90}$$

where τ_i is the relaxation time for each Prony component E_i. E_o is the instantaneous modulus (t=0) whereas E_∞ is the long-term modulus (t=∞).

If we call E_{ve} (t) the relaxation modulus of shear stresses. The limits take the following values,

$$E_{\infty} = \lim_{t \to \infty} E_{ve}(t)$$

$$E_0 = E_{ve}(0)$$

A dimensionless relaxation modulus is defined as follows,

$$\alpha_i = \frac{E_{vi}}{E_0} \qquad \textit{Eq. 0.91}$$

The sum of α_i should be less than or equal to 1. If the sum of α_i is equal to 1, that means that E_{ve}(t=∞)=0.

Hence, Prony series can be rewritten as follows,

$$Eve(t) = E_0 \left[\alpha_{\infty} + \sum_{i=1}^{N} \alpha_i e^{-\frac{t}{\tau_i}} \right] \qquad \textit{Eq. 0.92}$$

and if it is rewritten based on the dimensionless relaxation modulus,

$$\alpha_\infty = 1 - \sum_{i=1}^{N} \alpha_i \qquad \textit{Eq. 0.93}$$

$$Eve(t) = E_0 \left(1 - \sum_{i=1}^{N} \alpha_i\right) + E_0 \sum_{i=1}^{N} \alpha_i e^{-\frac{t}{\tau_i}} \qquad \textit{Eq. 0.94}$$

$$\alpha_{ve}(t) = 1 - \sum_{i=1}^{N} \alpha_i + \sum_{i=1}^{N} \alpha_i e^{-\frac{t}{\tau_i}} \qquad \textit{Eq. 0.95}$$

$$\alpha_{ve}(t) = 1 - \sum_{i=1}^{N} \alpha_i \left[1 - e^{-\frac{t}{\tau_i}}\right] \qquad \textit{Eq. 0.96}$$

ANNEX II-H: GENERALIZED MAXWELL MODEL: PRONY SERIES IN FREQUENCY DOMAIN:

Prony series generally defined in time domain can be converted to frequency domain with the application of the Fourier transform.

The application of Fourier transformation to Eq. 0.96 gives,

$$\mathfrak{F}(\alpha_{ve}(t)) = \int_{-\infty}^{\infty} \alpha_{ve}(t)\, e^{-i\omega t} dt \qquad \textit{Eq. 0.97}$$

$\alpha_{ve}(t)$ is defined only between (0,∞), hence,

$$\mathfrak{F}\big(\alpha_{ve}(t)\big) = \int_{-\infty}^{\infty} \left\{1 - \sum_{i=1}^{N} \alpha_i \left[1 - e^{-\frac{t}{\tau_i}}\right]\right\} e^{-i\omega t} dt$$

$$= -\frac{e^{-i\omega t}}{i\omega}\Bigg]_{-\infty}^{\infty} + \sum_{i=1}^{N} \frac{e^{-i\omega t}}{i\omega}\alpha_i\Bigg]_{0}^{\infty} - \sum_{i=1}^{N} \frac{e^{-t\left(\frac{1}{\tau_i}+i\omega\right)}}{\frac{1}{\tau_i}+i\omega}\alpha_i\Bigg]_{0}^{\infty} =$$

$$-\sum_{i=1}^{N} \frac{\alpha_i}{i\omega} + \sum_{i=1}^{N} \frac{\alpha_i}{\frac{1}{\tau_i}+i\omega} = -\sum_{i=1}^{N} \frac{\alpha_i}{i\omega} + \sum_{i=1}^{N} \frac{\alpha_i\tau_i}{1+i\omega\tau_i}$$

That is, α_{ve} in the frequency domain is,

$$\alpha_{ve}(\omega) = -\sum_{i=1}^{N} \frac{\alpha_i}{i\omega} + \sum_{i=1}^{N} \frac{\alpha_i\tau_i}{1+i\omega\tau_i} \qquad \textit{Eq. 0.98}$$

Taking the last expression and equation 9.9 of *Austrell* [8], we have the same expression given by *Jörgen Bergström* [9]:

From *Austrell* [8],

$$E^* = E_0\big(1 + i\omega\alpha_{ve}(\omega)\big) \qquad \textit{Eq. 0.99}$$

Hence,

$$E^* = E_0\left(1 - \sum_{i=1}^{N}\alpha_i + \sum_{i=1}^{N}\frac{\alpha_i i\omega\tau_i}{1 + i\omega\tau_i}\right) \qquad \textit{Eq. 0.100}$$

As $\alpha_i = \frac{E_i}{E_0}$, then,

$$E^*(\omega) = E_0 - \sum_{i=1}^{N}E_i + \sum_{i=1}^{N}\frac{E_i i\omega\tau_i}{1 + i\omega\tau_i} \qquad \textit{Eq. 0.101}$$

Real and imaginary parts are obtained by multiplying by the conjugate of the,

$$E^*(\omega) = E_0 - \sum_{i=1}^{N}E_i + \sum_{i=1}^{N}\frac{E_i i\omega\tau_i(1 - i\omega\tau_i)}{(1 + i\omega\tau_i)(1 - i\omega\tau_i)} \qquad \textit{Eq. 0.102}$$

Rewritting the previous equation,

$$E'(\omega) = E_0 - \sum_{i=1}^{N}E_i + \sum_{i=1}^{N}\frac{E_i\tau_i^2\omega^2}{1 + \tau_i^2\omega^2} \qquad \textit{Eq. 0.103}$$

$$E''(\omega) = \sum_{i=1}^{N}\frac{E_i\tau_i\omega}{1 + \tau_i^2\omega^2} \qquad \textit{Eq. 0.104}$$

ANNEX II-I: RELATION BETWEEN TENSILE AND PURE SHEAR YIELD STRESSES

The next development relating the shear yield stress and the tensile yield stress has been extracted from [10].

Clasical plasticity: Hypothesis

The so-called classic plasticity involves the application of four hypotheses, which are described below,

1st Hypothesis: **Fluency function:**

It is supposed that there exists a function that determines the fluency and that the initial yield or fluency depends only on the state of stress. Hence, it does not take into account how it has achieved this status. The yield function $f(\sigma_{ij})$ defines the elastic limit in the tensional space and determines the yield criterion. $f(\sigma_{ij})$ depends on the principal stresses and their directions.

2nd Hypothesis: The material is Isotropic:

It is assumed that satisfies the condition isotropy. In this case, there would be no preferred direction and $f(\sigma_{ij})$ could be expressed in main directions. Furthermore, function *f* is not changed if the axes are exchanged (in the representation of the principal stresses, instead of the principal stresses, we can use strain invariants, which are logically independent also of the order of the principal stresses.

3rd Hypothesis: The yield stress and the hydrostatic stress are not directly related:

It is considered that the hydrostatic stress does not influence the plastic flow condition. Plastic deformation occurs when there are only tangential or shear stresses. Therefore, in a state of uniform tri-axial tension or compression (hydrostatic stress state) no plastic deformation is generated, regardless of the presented stress magnitude, since it does not appear shear stresses in any plane.

4th Hypothesis: Traction behavior is identical to that in compression:

It is supposed that the tension and compression behaviour are identical. Hence, if all the stresses change sign, the *f* function continues invariable: $f(\sigma_{ij})$=$f(-\sigma_{ij})$.

Mises Fluency criterion: Criterion J_2

There are several fluency criterions which fulfil the above mentioned four hypotheses. The Mises criterion is widely applied in ductile materials.

Mises criterion postulates that the yield begins when the modulus of the second invariant of deviatoric stress tensor reaches a critical value K_M^2, it depends on the material (but not on the stress state). Consequently means that fluency is

$$J_2 = K_M^2 \qquad \textit{Eq. 0.105}$$

and in terms of main directions:

$$J_2 = \frac{1}{6}[(\sigma_1 - \sigma_2)^2 + (\sigma_2 - \sigma_3)^2 + (\sigma_1 - \sigma_3)^2] \qquad \textit{Eq. 0.106}$$

In a state of pure shear, i.e. in plane 1-2, the fluency implies that $\sigma_{12} = k$, where *k* is the fluency for shear stress. Hence,

$$J_2 = \sigma_{12}^2 = k^2 \qquad \textit{Eq. 0.107}$$

and the Mises constant yields in,

$$K_M = k \qquad \textit{Eq. 0.108}$$

K_M also can be found from tensile test, i.e. in direction 1, where

$$\sigma_{11} = Y \qquad \textit{Eq. 0.109}$$

in fluency,

$$J_2 = \frac{\sigma_{11}^2 + \sigma_{11}^2}{6} = \frac{Y^2}{3} \qquad \textit{Eq. 0.110}$$

Where Y is the tensile yield stress, hence,

$$K_M = \frac{Y}{\sqrt{3}} \qquad \textit{Eq. 0.111}$$

For this value, in the pure shear test fluency for a shear stress would be:

$$k = K_M = \frac{Y}{\sqrt{3}} \qquad \textit{Eq. 0.112}$$

REFERENCES

[1] Fung Y. Foundations of solid mechanics. Prentice-Hall; 1965.

[2] Love AEH. The mathematical theory of elasticity. 1927.

[3] Gil-Negrete N. On the modelling and dynamic stiffness prediction of rubber isolators. Univ Navar Spain 2004.

[4] Zener C. Elasticity and anelasticity of metals. University of Chicago press; 1948.

[5] Tschoegl NW. The phenomenological theory of linear viscoelastic behavior: an introduction. Berl Springer-Verl 1989:143–5.

[6] Findley WN, Davis FA. Creep and Relaxation of Nonlinear Viscoelastic Materials. Courier Dover Publications; 1976.

[7] ANSYS IC. 11.0 Help Manual. ANSYS Inc 2009.

[8] Austrell PE. Modeling of elasticity and damping for filled elastomers. Ph.D. Dissertation. Lund University. Lund Institute of Technology, 1997.

[9] Bergström J. Calculation of Prony series parameters from dynamic frequency data. Polym FEM 2005.

[10] Alcaraz G. Comportamiento No Lineal de los Materiales. Escuela Técnica Superior de Ingenieria de Bilbao. Sección de Publicaciones; 2011.

ANNEX III

Extending the overlay method in order to capture the variation due to amplitude in the frequency dependence of the dynamic stiffness and loss during cyclic loading of elastomers

Extending the overlay method in order to capture the variation due to amplitude in the frequency dependence of the dynamic stiffness and loss during cyclic loading of elastomers

Z. Kareaga, T. Guraya
EMERG. EUITI. UPV/EHU. Pª Rafael Moreno Pitxitxi 3, Bilbo 48013, Bizkaia, Spain. Tel.: Int. 34 94 6169171

A. Arriaga
Materials Department, Lea-Artibai Ikastetxea S.Coop., Xemein etorbidea 12, Markina-Xemein, 48270, Bizkaia, Spain

P-E. Austrell
Structural Mechanics Lund University, P.O. Box 118, SE 221 00 Lund, Sweden

ABSTRACT: The current work focus on the overlay method proposed by Austrell concerning frequency dependence of the dynamic modulus and loss angle that is known to increase more with frequency for small amplitudes than for large amplitudes. The original version of the overlay method yields no difference in frequency dependence with respect to different load amplitudes. However, if the elements in the viscoelastic layer of the finite element model are given different stiffness and loss properties depending on the loading amplitude level, frequency dependence is shown to be more accurate compared to experiments. The commercial finite element program Ansys is used to model an industrial metal rubber part using two layers of elements. One layer is a hyper viscoelastic layer and the other layer uses an elasto-plastic model with a multi-linear kinematic hardening rule. The model, being intended for stationary cyclic loading, shows good agreement with measurements on the harmonically loaded industrial rubber part.

1 INTRODUCTION

The dynamic stiffness and loss angle of elastomers increases with higher filler content. Fillers can also introduce a non-linear dynamic behavior shown as an amplitude dependence of the dynamic stiffness and loss angle. Although it is a bit inappropriate the linear viscoelastic stiffness and loss measures are used also for the non-linear dynamics of filled rubbers.

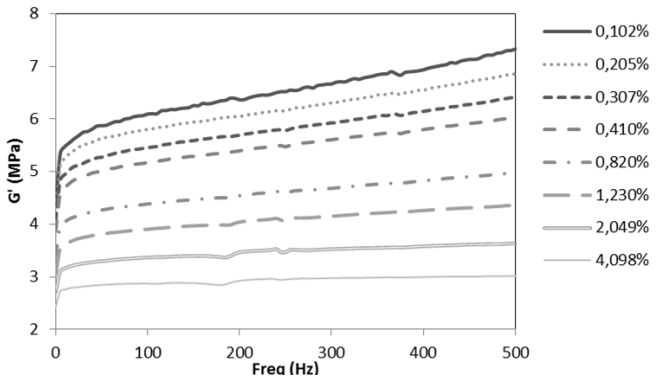

Figure 1. Filled elastomers: The upturn of the storage modulus with increasing frequency is greater at smaller amplitudes (to the right).

In this work storage G' and loss modulus G" are used to characterize the cyclic dynamic behavior of a particular rubber used to validate the proposed modeling method.

While unfilled rubbers can be properly modeled by purely viscoelastic models, filled rubbers, on the other hand, show amplitude dependence of stiffness and loss as shown in Figures 1 and 2 giving the storage and loss modulus respectively for a highly filled natural rubber. The amplitude dependence is pronounced in both plots.

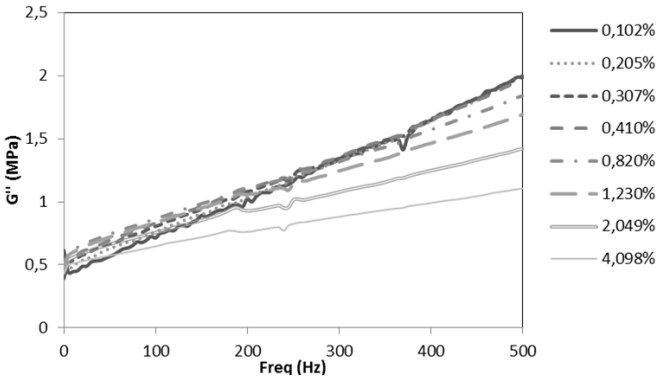

Figure 2. Filled elastomers: The upturn of the loss modulus with increasing frequency is significant.

The behavior shown in the figures can be captured by using the overlay method proposed by Austrell et al. (2001). However, the frequency dependence shows a steeper slope for the smaller

amplitudes than for the larger amplitudes in both Figure 1 and 2. This cannot be modeled by the original version of the overlay method. In a wide frequency range, as shown here, it is important to be able to model this behavior.

Österlöf et al. (2014) modeled this phenomena in a one-dimensional model coupling a generalized Maxwell model in series with an elasto-plastic model by Dafalias & Popov (1977). They thus added strain instead of stress from the two branches.

Here it is shown in a finite element context, using the overlay method, how different dynamic stiffness and loss values in the elements of the viscoelastic mesh (in the overlay) can capture this phenomena.

2 THE OVERLAY METHOD AND THE PROPOSED EXTENSION

The overlay method consists of three fundamental steps, illustrated in Figure 3.

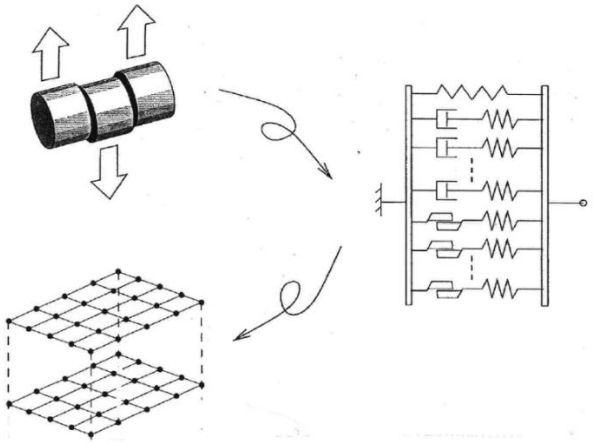

Figure 3. The basic steps in the overlay method: 1) material test, 2) one-dim. model fit, and 3) viscoelastic and elasto-plastic mesh overlay

The first is a cyclic material test. Here a dynamic harmonic displacement shear test is used to characterize the dynamic properties of the rubber material. On the basis of the expected working condition of the component, the test is carried out for a range of different frequencies and amplitudes. For simple shear, the elastic part of the rubber behavior is more or less linear, making it easier to observe the rate and amplitude dependence in this mode of deformation.

The second step is the parameter identification using a one-dimensional viscoelastic elasto-plastic model. This model contains a number of material parameters that are fitted to the experimental data using a minimization procedure, focusing on a good fit of dynamic modulus and damping.

The third step is to establish the finite element model. By using a straightforward engineering approach, it is possible to create a finite element model containing both frequency and amplitude dependence. This is done by means of an overlay of viscoelastic and elasto-plastic finite element models. The meshes are simply assembled on top of each other to the same nodes. This approach makes it possible to use commercially available finite element codes, using only the constitutive models that have already been implemented.

These three steps describe shortly the original version of the method presented on the second EC-CMR conference in 2001 by Austrell & Olsson. A fitting procedure for the material parameters was also presented at the same conference (Olsson & Austrell 2001).

In this work, as mentioned, an extension of the method is proposed in order to capture the different slopes of the frequency dependence shown in Figures 1 and 2. As can be seen from the figures, smaller amplitudes give a steeper frequency dependence for both the storage and the loss modulus, compared to larger amplitudes. This effect is more significant the wider the frequency range is that one wants to cover. The modeling method proposed here is to let the values of dynamic stiffness and loss be dependent on the load amplitude level of the element. This means that different viscoelastic models are used in the elements of the viscoelastic mesh. The way this is done is similar to the equivalent viscoelastic approach (Olsson & Austrell 2005). In that work the frictional behavior was approximated by using only one viscoelastic mesh with different viscoelastic models in different elements.

The big difference compared to the present work is that here the viscoelastic mesh is assembled on top of an elasto-plastic mesh according to the overlay method. Moreover, the existence of a multi-linear kinematic hardening elasto-plastic large displacement model in Ansys makes it possible to use only one elasto-plastic mesh.

It should be pointed out that the method proposed here is strictly speaking only suitable for stationary cyclic loading cases although the loading need not be harmonic. This is due to the need of predicting load levels in the elements. Thus, vibration problems, rolling contact problems etc. are suitable for the method proposed here.

3 MATERIAL MODEL AND PARAMETERS

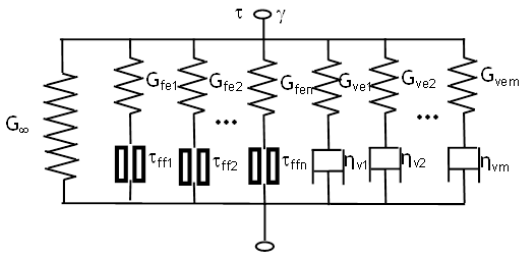

Figure 4. The material parameters are obtained from this uniaxial model by fitting it to the simple shear experimental data.

The parameters of the viscoelastic and the elasto-plastic mesh are given by a fit of the uniaxial model, shown in Figure 4, to the harmonic simple shear experiments. The spring-dashpot elements with parameters shown in the figure are material input to the viscoelastic mesh. The spring-friction block elements with parameters corresponds to the multi-linear kinematic hardening model, being material parameters of the elasto-plastic mesh.

The fitting of the material parameters shown in Figure 4 is done by using algorithms implemented in Matlab. In this work three viscoelastic elements and three elasto-plastic elements were used in the uniaxial model. The viscoelastic material parameters was characterized at four amplitude levels in order to capture the different slopes of the frequency dependence.

4 LABORATORY TESTING

A natural rubber compound was used to manufacture a double shear specimen shown in Figure 5 (left) and a cylindrical metal rubber part shown in Figure 5 (right).

Figure 5. The double shear material test object (left) and the metal rubber cylinder used for model verification (right).

The compound is a highly filled natural rubber based on the formulation given in Table 1.

Table 1. Formulation of the filled natural rubber

Rubber compound	*Phr
SMR CV 60 (NR)	100
ZnO	5.0
SFR N-774 (carbon black)	80
TMQ	1.0
IPPD	1.5
Zinc Stearate	3.0
MBS	1.5
TBTD	0.9
Sulfur	0.8

*Phr= parts per hundred rubber.

The double shear specimen, consists of two rubber discs, 25mm diameter and 6 mm thick, vulcanized to metal cylinders. The second object is a metal rubber cylinder, diameter of 35mm and a height of 35 mm, used for verification of the proposed model.

The degree of cure is directly related to the measured stiffness and damping and it is one of the most important parameters to take into account in manufacturing test objects. The thickness differences of the studied material test specimen and the validation component require the use of different curing times in order to obtain the same degree of cure in both. To this end, a previously developed swelling method, was used presented by Arrillaga & Kareaga (2012).

The testing of the double shear specimen consist of different frequency sweeps for constant amplitudes from 0.05Hz up to 500.05 Hz. Four amplitudes were used to characterize the elastomer: γ_1=0.0031, γ_2=0.0082, γ_3=0.020 and γ_4=0.041 in terms of direct shear strain γ, being the ratio of the displacement and the thickness of the rubber disc. These levels where chosen to match the load levels in the cylindrical metal rubber part used for verification. This matching will be discussed in Section 5.

Fig 1 and 2 show the measured storage and loss modulus for the amplitudes given above together with four extra amplitudes.

The testing of the rubber cylinder was done in another mode of deformation being alternating tension/compression, using five different amplitudes in frequency sweeps covering the same frequency interval i.e. 0.05 to 500.05 Hz. The tested peak displacement amplitudes were (determined according to the discussion in Section 5) 0.05, 0.1, 0.15, 0.25 and 0.35 millimeters. In Section 6 the results of these measurements will be compared to the finite element model output for the cylindrical component.

5 MATERIAL FITTING PROCEDURE

The method presented in this work reduces, as mentioned, the number of required superimposed meshes to two due to the existence of the multi-linear kinematic hardening elasto-plastic model.

The components of the first, rate independent, mesh are characterized by the elasto-plastic constitutive model. The components of the second superimposed rate dependent mesh are characterized by a conventional viscoelastic model with the relaxation modulus defined by a Prony series approach. However, one viscoelastic model for each selected amplitude need to be determined (i.e. four in this case). The load level in the component can be determined through a purely elastic simulation with a simple hyperelastic approximate model. The values of the shear strain levels to be used in the material testing can be determined from the span of strain energy in different elements of the component giving equivalent shear strain values γ_{eq} to be used in the laboratory testing of the material. The procedure of obtaining the equivalent shear strain is described by Austrell & Olsson (2005).

5.1 *Obtaining the elasto-plastic parameters*

In this work three frictional components, with associated material parameters, are chosen in order to take care of the elasto-plastic branch of the material behavior. Here the fitting of this rate independent part of the model is done by quasi static cyclic loading tests at four strain levels. The experimental data needed to characterize this part of the model come from the first measurement performed at each strain level (i.e. amplitude). Specifically, the required experimental data come from the first frequency, i.e. 0.05Hz, used for each frequency sweep.

A procedure based on a two-step fitting procedure similar to the one used by Ahmadi et al (2005) is used to obtain material parameters according to Figure 4. These elasto-plastic parameters are then converted into the format of the multi-linear kinematic hardening model as follows:

$$\gamma_{ff,i} = \frac{\tau_{ff,i}}{G_{f,i}} \tag{1}$$

$$\tau_{pj} = u(j)\sum_{j=1}^{j-1}\tau_{p,j} + \gamma_{ff,j}\sum_{i=j}^{n}G_{f,i} \tag{2}$$

where, $u(j)\begin{cases} j=1 & u(j)=0 \\ j\neq 1 & u(j)=1 \end{cases}$

where $\gamma_{ff,i}$ is the i^{th} friction element yield shear strain, $\tau_{ff,i}$ is the i^{th} friction element yield shear stress, and $\tau_{p,j}$ is the shear stress point in a multi-linear loading curve of quasi static behavior.

In the commercial finite element software Ansys being used, elasto-plastic data must be introduced in terms of uniaxial tension σ and uniaxial strain ε. By using infinitesimal strain theory and an incompressible material, the yield stress in tension σ_p is related to the yield stress in simple shear τ_p according to

$$\sigma_{p,i} = \tau_{p,i}\sqrt{3} \tag{3}$$

$$\varepsilon_{ff,i} = \frac{\gamma_{ff,i}}{\sqrt{3}} \tag{4}$$

The material model is fitted to the NR elastomer using an application programmed in Matlab, which gives the required material constants. The elasto-plastic model parameters are given in Table 2.

Table 2. Elasto-plastic parameters.

$E_p^{ini}=\sigma_{p,1}/\varepsilon_{ff,1}$ *[MPa]*		14.726
i	$\varepsilon_{ff,i}$	$\sigma_{p,i}$ *[MPa]*
1	0.000186	0.002739
2	0.002170	0.01476
3	0.008139	0.028

5.2 *Obtaining the viscoelastic parameters*

The viscoelastic part of the model characterizes the rate-dependent stiffness and damping at a number of strain levels (four here). In order to determine these levels (amplitudes) a preliminary elastic finite element simulation of the component is required. For this problem, using an axi-symmetric model, a simple initial tension as shown in Figure 6a, is applied. The model used in this first step, is based on a neo-Hooke material with only one hyperelastic constant C_{10}, being half the shear modulus of the material. It can for example approximately be determined from the hardness of the material.

The strain energy density in each element is used to calculate the equivalent shear strain γ_{eq} to be used in the material testing

$$\gamma_{eq} = \sqrt{W_0 / C_{10}} \tag{5}$$

The equivalent shear strain of each element is divided into (here) four level γ_1, γ_2, γ_3 and γ_4 of simple shear strain amplitudes chosen according to:

a) $\gamma_{eq} < \gamma_1$: all these elements will be characterized by the material property characterized in the smallest strain testing condition.

b) $\gamma_{eq} > \gamma_4$ All these elements will be characterized by the material property characterized at the highest strain.

c) if the strain range γ_{eq} goes from γ_1 to γ_4, each element will be characterized by one of the levels γ_1, γ_2, γ_3 and γ_4 respectively.

The elements of the viscoelastic model that will be assigned to the mesh, belonging to the four different load levels 1 to 4, are shown in Figure 6b.

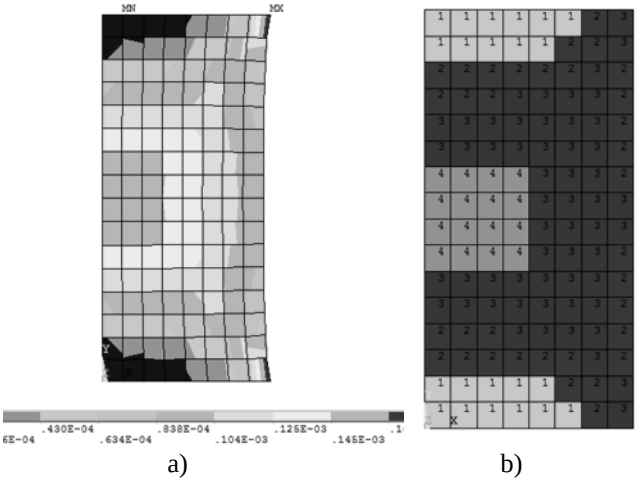

a) b)

Figure 6. a) The strain energy density of the elastic (neo-Hooke) preliminary model in tension. b) The viscoelastic mesh division into four categories depending on the load level in a) yielding their equivalent shear strain γ_{eq}.

The experimental data from the frequency sweeps performed at the different constant amplitudes show a behavior originating from both frictional and viscous material properties. Hence, the viscoelastic part of the complete response have to be extracted from

the experimental data to calculate the Prony series parameters at the four amplitudes. Hence, the previously characterized elasto-plastic part of the stress has to be removed from the experimental data. For each constant shear strain amplitude the viscous dynamic modulus and loss is obtained as

$$G^*_{v\exp}(\omega) = G^*_{\exp}(\omega) - G^{*0.05Hz}_{\exp} + G_\infty \quad (6)$$

$$A_{v\exp}(\omega) = A_{\exp}(\omega) - A^{0.05Hz}_{\exp} \quad (7)$$

$G^*_{v\ exp}(\omega)$ is the experimental dynamic shear modulus for the viscoelastic part of the material model at the particular amplitude used. $G^*_{exp}(\omega)$ is the experimental dynamic shear modulus. $G^{*0.05Hz}_{exp}$ is the experimental dynamic shear modulus at 0.05Hz, and G_∞ is the relaxed shear modulus. A is the hysteretic area and ω is angular frequency.

From the extracted experimental data according to (6) and (7), the Prony series parameters can be calculated (Bergström 2005)

$$G_0 = G_\infty + \sum_{i=1}^{n} G_{ve,i} \quad (8)$$

$$G'_{ve}(\omega) = G_0 - \sum_{i=1}^{n} G_{ve,i} + \sum_{i=1}^{n} \frac{G_{ve,i} T_i^2 \omega^2}{1 + T_i^2 \omega^2} \quad (9)$$

$$G''_{ve}(\omega) = \sum_{i=1}^{n} \frac{G_{ve,i} T_i\ \omega}{1 + T_i^2 \omega^2} \quad (10)$$

G_0 is the initial shear modulus; G'_{ve} and G''_{ve} are the storage and the loss shear modulus, T is the relaxation time.

The viscoelastic parameters are given in Table 3. G_∞ is common for all viscoelastic models fitted to the mentioned four shear strain sweeps with different amplitudes.

Table 3. Viscoelastic Prony series parameters for simple shear strains γ_i at four amplitude levels (i).

G_∞ *[MPa]* common for all viscoel. models		1.8806
γ_i	$G_{ve,i}$*[MPa]*	T_i *[s]*
0.0031	0.3699	0.00402
	1.0603	0.29351
	3.9994	0.000139
0.0082	0.1767	0.00324
	1.0615	1.0
	3.5692	0.00012
0.02	0.1739	0.00180
	0.6858	1.0
	3.5	0.000083
0.041	0.2662	0.0015
	0.5072	0.1002
	5.0	0.000044

Comparing the fitted material model (according to Figure 4) with parameters in Table 2 and 3 show that the experimental results of *G'* and *G"* given in Figures 1 and 2 yields errors not exceeding 10%. The correlation is not presented because the agreement is very good and all curves are almost superimposed.

6 MODEL VALIDATION

In order to validate also the finite element model the testing of the cylindrical component discussed in Section 2, was simulated using Ansys. Figures 7 and 8 show the experimental tests and simulation results respectively, for the dynamic storage stiffness. Figures 9 and 10 show the experimental tests and simulation results respectively, for the dynamic loss stiffness.

There is a slight discrepancy between the model and the experiments concerning the storage stiffness with the slopes of the model being slightly lower than the experiments. However, experiments and simulation are otherwise in good agreement.

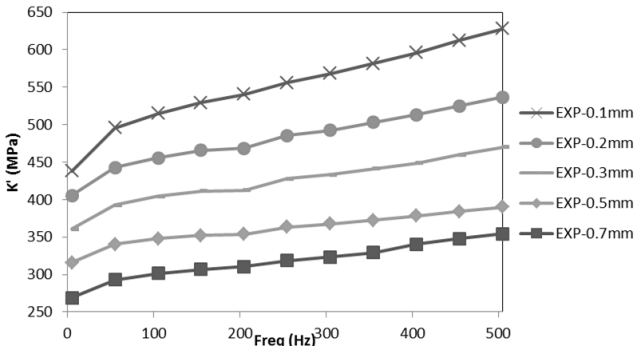

Figure 7. Experimental dynamic storage stiffness versus frequency at different amplitudes.

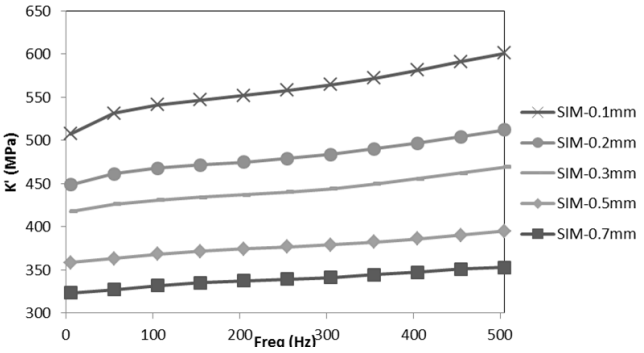

Figure 8. Simulation of the dynamic storage stiffness versus frequency at different amplitudes.

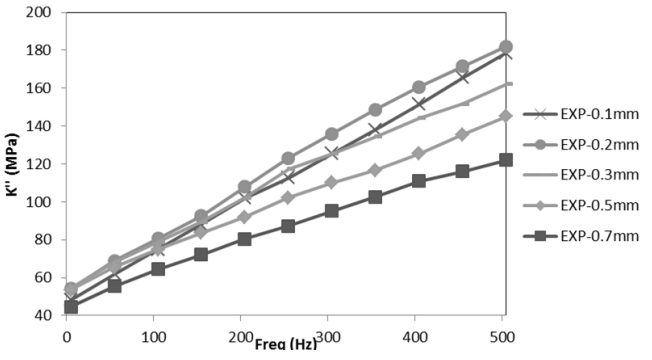

Figure 9. Experimental dynamic loss stiffness versus frequency at different amplitudes.

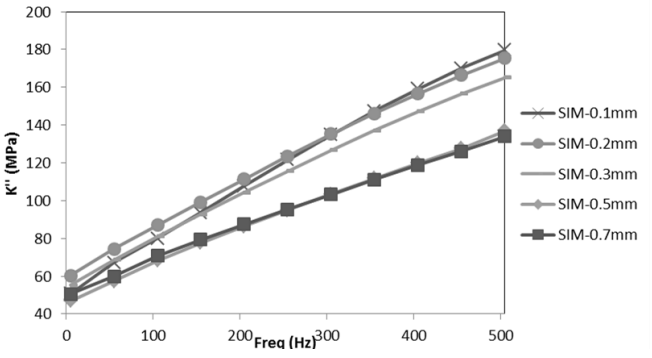

Figure 10. Simulation of the dynamic loss stiffness versus frequency at different amplitudes.

7 CONCLUSIONS

A modified overlay approach was developed and compared to experiments in harmonic loading in a wide frequency interval at different amplitudes The purpose is to handle the difference in frequency dependence of the dynamic stiffness and loss for different amplitudes during stationary cyclic loading.

The method was validated using a cylindrical natural rubber component of the same material as the material test samples. The model was shown to be in good agreement with experiments.

Moreover, the use of a multi-linear kinematic hardening elasto-plastic model for the frictional behavior requires only two superimposed meshes. This reduces considerably the calculation time.

REFERENCES

Ahmadi H.R., Kingston J.G.R., Muhr A.H., Gracia L.A. & Gomes B. 2005. *Interpretation of the high low strain modulus of filled rubbers as an inelastic effect.* Third European Conference on Constitutive Models for Rubber. England.

Arrillaga A., Kareaga Z., Retolaza E., Zaldua A.M., 2012. *Determining the state of cure of rubber by means of swelling.* Rubber Fibres Plastics International. 7,1.

Austrell P-E, Olsson A.K. & Jonsson M. 2001. *A method to analyse the non-linear dynamic behaviour of carbon-black-filled rubber components using standard FE-codes.* Second European Conference on Constitutive Models for Rubber. Germany.

Austrell P-E & Olsson A.K. 2012. *Considering amplitude dependence during cyclic loading of elastomers using an equivalent viscoelastic approach.* Polymer testing. 31, 7, 909-915.

Bergström J. 2005. *Calculation of Prony series parameters from dynamic frequency data*. Polymer FEM.

Dafalias Y. & Popov E. 1977. *Cyclic loading for materials with a vanishing elastic region.* Nucl. Eng. Des.41.

Olsson A.K. & Austrell, P-E. 2001. *A Fitting Procedure for Viscoelastic-Elastoplastic Material Models.* Second European Conference on Constitutive Models for Rubber. Germany.

Österlöf R., Wentzel H., Kari L., Diercks N. & Wollscheid D. 2014. *Constitutive modelling of the amplitude and frequency dependency of filled elastomers utilizing a modified Boundary Surface Model.* Int. J. of Solids and Structures 51

ANNEX IV

A Review of Amplitude and Frequency Dependency of Elastomers.

A REVIEW ON THE AMPLITUDE AND FREQUENCY DEPENDENCY ON ELASTOMERS IN DYNAMIC TESTING

Contributing authors:

Z. KAREAGA*, T. GURAYA

EMERG. EUITI. UPV/EHU. Pª Rafael Moreno Pitxitxi 3, Bilbo 48013, Bizkaia, Spain Tel.: Int. 34 94 616 9002 Fax.: Int. 34 94 616 9171

A. ARRIAGA

Materials Department, Lea-Artibai Ikastetxea S.Coop., Xemein etorbidea 12, Markina-Xemein 48270 , Bizkaia, Spain Tel.: Int. 34 94 616 9002 Fax.: Int. 34 94 616 9171

* Corresponding author. Email: zkareaga@leartiker.com

ABSTRACT

The current paper is focused on the experimental characterization of elastomers and the dynamic properties in simple shear mode are investigated. For this purpose, three carbon black-filled rubber compounds are loaded with 8 harmonic peak strain levels between 0.01 and 4.1 % shear strains, in a frequency range between 0.05 and 500Hz. The stationary stress response is evaluated in terms of the storage and the loss modulus and equivalently, in terms of the dynamic modulus and the loss angle. The formulae of the essayed elastomers, NR1 and NR2, are identical with a unique exception, the carbon black-filler quantity. The formulae of the third compound which is named as elastomer CKR, is completely different and the carbon black-filler quantity is intermediate between the others. The theories and conclusions of the literature review are contrasted and the stiffening of the rubber with frequency sweeps is studied. The first objective which consists of developing a dynamic properties database with a highly-filled, filled and unfilled elastomer covering a wider frequency/strain ranges than existing literature has been fulfilled. Concerning results, as filler content diminishes the influence of the amplitude and frequency on dynamic properties is reduced and tends to be linear. In filled and more markedly in highly filled elastomers the storage modulus G' increases with the frequency being this increment higher at smaller amplitudes. The loss modulus G'' increases as frequency increase and the amplitude influence is depreciable at small amplitudes where above critical amplitude the filler network starts breaking down with the consequent diminution in the reformation property and increasing internal frictions. This complete database, which has been generated with a current servo-hydraulic machine, could use to develop or validate new or existing constitutive models.

The experimental results are in accordance with the literature review. The range of frequency wider than it is in the literature at eight strain levels of three reproducible highly filled, filled and unfilled elastomers gives valuable information.

INTRODUCTION

The motivation for carrying out this work is to develop a material test database of the dynamic properties of three natural rubbers covering a wide range of frequencies usually given in the automotive industry. In literature the characterization is generally done at a unique frequency as in the work of Wang[1,2], at a constant frequency of 10Hz, or the frequency ranges hardly pass the barrier of 100 Hz as shown in existing studies from as Olsson *et al*[3], up to 50Hz or Lion *et al* [4] up to 70Hz. In literature there are not many characterized materials, some of the results are partially published or the formulation of the characterized elastomers is not specified. Hence, on the one hand, the test may not be reproduced and on the other hand, it is not possible the testing of other strain states or more complicated geometries by other researchers to advance in the knowledge of the dynamic properties of elastomers. Additionally, this work provides material characterizations performed in current testing devices, which enable more accurate measurements than those reported in most of the previous researches. In early seventies, Payne and Whittaker[5] explained that little work had been carried out on the effect of frequency on dynamic properties. This was presumably due to the difficulty of obtaining sufficient frequency and strain ranges together in one apparatus. The current testing devices permit a characterization of wider frequency and amplitude ranges. Furthermore, in this paper the dynamic results are presented in several dynamic terms versus amplitude and frequency, although both types of graphs give the same results. However, they are shown in two forms to facilitate the understanding of the results.

From one side, the dynamic characterization of the mentioned three elastomers are used to review the influence of the testing strain amplitude and frequency in elastomers with different amounts of carbon black filler and on the other side, the goal was to generate a database for future works for verification of existing constitutive models or developing new models. To this end, and to cover the widest range of all variables, the dynamic characterizations are performed as follows:

(1) Three elastomers are characterized: NR1, CKR and NR2, highly-filled, filled and un-filled elastomers respectively.

(2) The simple shear specimens used to characterize the dynamic properties are used by recognized researchers [6], the shape of the specimen is shown in FIG. 1.

(3) The tested frequency range is defined between 0.05 and 500Hz

(4) The tested shear strain range (peak amplitude) is defined between 0.1 and 4.1%.

Elastomers NR1 and NR2 have almost the same formulation where the only difference consist of the amount of carbon black of its composition. Elastomer NR2 is formulated with the minimum amount of carbon black

possible to avoid problems in injection processing. Finally, elastomer CKR is an industrial rubber compound which has a different formulation with an intermediate amount of carbon black in comparison with the elastomers NR1 and NR2.

Most researches have been directed to studying the Payne effect. These studies are composed by several amplitude sweeps changing the testing cycle frequency after each amplitude sweep. Then, these curves were have been used to demonstrate the amplitude and frequency dependence on the dynamic properties of elastomers [4,7]. In this way, firstly, a short literature review of the Payne effect is presented in this study to continue with the experimental work where the dynamic properties versus frequency and amplitude of the three characterized elastomers are presented. Initially the dynamic properties versus frequency, related to the Payne effect, are exposed and after, these properties are presented versus amplitude to check if the literature review is in accordance with these characterized materials.

STRAIN AMPLITUDE DEPENDENCE ON THE DYNAMIC MODULUS: PAYNE EFFECT

Strain amplitude dependence has been deeply studied in the last years. Two phenomena are the responsible for the stiffness dependence in the amplitude: On the one hand the well-known Mullins effect [8–13] which is related with the stress-softening produced when an elastomer is cyclically deformed as shown in FIG. 2 and on the other hand the Payne effect which is reviewed in this paper. The term "Mullins softening" is sometimes used interchangeably with the Payne effect, but the former is a different phenomenon that occurs at larger strains. To investigate the Payne effect without influence of the Mullins-effect, in our study all specimens were preconditioned with sufficient large strain amplitude so that the Mullins-effect was eliminated.

One of the earlier studies of this phenomenon was made by Fletcher and Gent [14] (afterwards called Payne effect [4,5,15–18]) that made extensive studies of the mentioned effect. When a constant strain load at constant frequency is applied cyclically, the modulus decreases with increasing strain amplitude, for a wide range of filler types and concentrations.

The investigations made by Payne [15] concluded that the elastomer modulus declines, increasing strain amplitude as a result of the breaking of the filler structure. As the molecular structure is composed of aggregates held together by van der Waals bonds, the modulus is almost recoverable due to the permanent breaking and recombination of the mentioned weak bonds in the filler network. As Huber *et al* [19] described the rate of these breaking and recombination processes generally differs but under stationary conditions they are equal and

depend on the dynamic deformation amplitude. In FIG. 3-A and FIG. 3-B where the dynamic mechanical properties are plotted as the storage *E'* and loss modulus *E''* respectively, it is observed that *E''* takes a maximum value in the strain range corresponding to the maximum rate of change of the storage modulus with amplitude. At small amplitudes of oscillation, little structure is broken down, the storage modulus *E',* which is large due to filler structure, is not modified and hence *E''* is small, even though the reformation of structure is probably easier at these small separations of the black particles. At large amplitudes, the structure is so extensively broken down, that reformation of structure is very much slower than the cycle time and *E''* is again low. A maximum in *E''* and phase angle is expected somewhere in the middle strain region where considerable structure breakdown occurs, but where reformation is also most easy and rapid. Consequently, the decrease in dynamic modulus *E** and increase in loss factor *tanδ* are not maintained in all range of amplitudes. At large amplitudes the change in dynamic modulus *E** is softer than in intermediate ones as shown in FIG. 3-C. The loss factor (FIG. 3-D) shows a peak in the region where *E** decreases more markedly as shown for example by Lindley [20], Payne and Whittaker [5] and Rendek and Lion [7]. Theoretically, there is a critical amplitude where bellow it the storage *E'* and loss modulus *E"* do not change due to amplitude variation.

Effect of fillers.— Carbon black fillers are added to rubber in order to increase both the dynamic modulus *E** and the phase angle δ (and hence damping) of rubber. Consequently, these dynamic properties become amplitude-dependent. The magnitude of the mentioned dynamic properties depends on the type and the amount of filler. In FIG. 4 it is shown the variation of the dynamic properties of Vulcanizates A to E over the normal operating range of shear strain. The rubbers are all of approximately the same hardness (about 55 IRHD). This was accomplished by using three different types of carbon-black and by balancing the reinforcing effect by addition of high-viscosity aromatic oil. The modulus increase was greater at small amplitudes, particularly for vulcanizates with higher proportions of filler [21]. The level of damping and the variation of the damping through the strain range increased with increasing the filler content. The filler agglomerate which is broken down on cycling above a certain strain range may reform, leading to a reduction in modulus and peak in damping. This material behavior, even in shear, is clearly nonlinear [21]. Fletcher and Gent [14], Lindley [20] and more recently Rendek and Lion [7] carried out some experimental tests to study the amount of filler influence on the mentioned dynamic properties which shown again a stronger dependence on filled elastomers than on unfilled ones.

Meng-Jiao Wang [1,2] carried out experimental investigations to show the impact of the filler network, both its strength and architecture on the dynamic modulus and hysteresis during the dynamic straining. It was found

that the filler network can substantially increase the effective volume of the filler due to rubber trapped in the agglomerates, leading to high elastic modulus (FIG. 5-B). During the cyclic straining, while the stable filler network can reduce the hysteresis of the filled rubber, the breakdown and reformation of the filler network would cause an additional energy dissipation resulting in the higher hysteresis. The experiments were done at double strain amplitudes ranging from 0.2% to 120% with a constant frequency of 10Hz under constant temperatures of 0 and 70ºC and filler phr of 0 and 70.

Payne effect and the augmentation of the elastic modulus.— The augmentation of elastic modulus at low amplitudes has been explained by Payne [5,15] or Mullins and Tobin [22] as being due to a network structure modification of carbon black particles (known as aggregates in Medalias [23] studies). From the viewpoint of Payne, the particles or aggregates are associated in agglomerate groups which when deformed are broken into smaller agglomerates of different dimensions. The particles or aggregates are fused carbon entities and are associated by the van der Waals or other secondary attractive forces into agglomerates (known as well as aggregates network).

At small deformations, the elastic modulus is higher because the carbon-black agglomerates which are the "hardest" regions are not broken. These agglomerates or "hard regions" must immobilize some rubber in addition to that occluded within the aggregates (see FIG. 5-A), and thus cause an augmentation of the effective volume fraction beyond that due to the aggregates themselves. In addition, as the effective volume fraction of the filler increases, the agglomerates ability to move into the matrix is diminished, hence, elastic modulus increases. Both effects become more important as the amplitude is diminished or as the frequency is increased.

As the deformation is increased, the agglomerates are broken into smaller agglomerates. Hence, the elastic modulus decreases because there are more mobile units or "soft" regions into the rubber matrix. At high deformations, the carbon-black agglomerates break down until the aggregates themselves are mobile units. The augmentation effect is of minor practical importance in well-dispersed formulation batches.

The agglomerates present at intermediate amplitudes may be identified with the "hard" regions. The breaking of the structure is often described as a frictional behavior, which is an energy dissipation mechanism. Hence, the loss factor of the elastomer increases, Medalia [24].

EXPERIMENTAL

MATERIALS

The present research is based on the use of three rubber formulations. Two formulations, NR1 and NR2 are own designed formulations and manufactured at Elastorsa company (Rioja, Spain) and the third formulation is an industrial formulation manufactured at Cikautxo S.Coop. company (Basque Country, Spain). Table I. summarizes the complete recipe for each formulation, which were prepared in an internal mixer.

CHARACTERIZATION DEVICE

Dynamic tests have been carried out in Cikautxo S.Coop. The MTS servohydraulic test systems are precisely configured to characterize dynamic properties of several materials and components. Specifically the MTS Model 831.50 (10 kN) 1000 Hz shown in FIG. 6. Elastomer Testing System with FlexTest 60 Control System. The MTS Model 831.50 is a high frequency elastomer test system incorporating all the elements necessary to provide static and dynamic characterization data for elastomeric components and materials. The standard configuration features a frequency range of 0.01 to 1000 Hz with ±50N to ±10 kN force range and ±0.005 to ±20 mm dynamic displacement range.

Acceleration compensation is built into the force measurement system and is used on both the strain gauge load cell and piezoelectric load washer. Accuracy at high frequency is ensured by utilizing acceleration based displacement measurement with the accelerometer located at the specimen interface to the piston rod.

TESTING CONDITIONS

To assure the repeatability of the tests some considerations are taken:

(1) The laboratory atmosphere was adjusted to 23ºC and 50% relative humidity.

(2) 5 simple shear specimens were tested per condition and the mean curve of these curves is presented.

(3) One frequency sweep per amplitude, where the starting frequency is 0.05Hz with 5Hz linear step increments up to 500.05Hz.

(4) The studied 8 shear strains are 0.1, 0.2, 0.31, 0.41, 0.82, 1.23, 2.05 and 4.1 %.

Each specimen is preconditioned at each of the eight different amplitudes, cycling 10 times, and then the frequency sweep starts.

Each specimen is tested in the defined frequency sweep at mentioned eight shear strains from the smaller to the higher. Once the eight frequency sweeps are finished, the test are repeated again to assure that no relaxation factor have influence in the initial results.

At the end of each test, there are captured eight frequency sweeps, one frequency sweep per amplitude

DYNAMIC CHARACTERIZATION AND MEASUREMENTS

The simple shear specimen type used to perform the characterizations was shown in FIG. 1. This type of simple shear specimen is composed by two rubber cylinders. Hence, it must take into account and divide the measured forces *F* by 2. Rubber cylinders of the shear specimen are sheared as it is shown in FIG. 7. where thickness *H* as the area *A* are constants every time. Applied force *F* produces a displacement *d* of the upper area *A* as shown in FIG. 7 and consequently a shear strain γ.

$$\tan\gamma = d/H \tag{1}$$

For small deformations the previous Equation 1 can be simplified as follows,

$$\tan\gamma = d/H \approx \gamma \tag{2}$$

The shear stress τ and the simple shear modulus *G* are defined as,

$$\tau = F/A \tag{3}$$

$$G = \tau/\gamma \tag{4}$$

When a simple shear specimen is subjected to oscillatory deformations, the strain varies sinusoidally with time as it can be seen in FIG. 8. The shear strain and the shear strain can be written as,

$$\gamma = \gamma_0 sin\omega t \tag{5}$$

$$\tau = \tau_0 \sin(\omega t + \delta) \tag{6}$$

where γ_0 is the shear strain amplitude, ω the angular frequency (2π times the frequency in Hertz), and *t* the time. The sinusoidal oscillation of the shear stress τ and the shear strain γ with the angular frequency ω and a phase lag δ is illustrated in FIG. 8.

The software from the testing machine (MTS Elastomer Configuration Program ®) used to calculate the dynamic properties, considers an elliptical hysteresis area U_c (FIG. 9). The results of the dynamic characterizations will be shown in terms of storage *G'*, loss *G''*, dynamic *G** modulus and phase angle δ. Hence, the storage *G'*, loss *G"* and dynamic *G** modulus and the damping *tan* δ are defined as[25],

$$G' = \frac{\tau_0}{\gamma_0} cos\delta \quad (7)$$

$$G'' = \frac{\tau_0}{\gamma_0} sin\delta \quad (8)$$

$$G^* = \sqrt{G' + G''} \quad (9)$$

$$tan\delta = G''/G' \quad (10)$$

If no damping is present in the system, the modulus *G** is real *G'* but it becomes complex when damping exists as in the case of elastomers.

RESULTS AND DISCUSSION

The dynamic results of three elastomers are presented. These elastomers are highly filled, filled and unfilled, NR1, CKR and NR2 respectively. The characterization results of each elastomer are divided in two groups. On the one hand, four graphs will be presented defining the dynamic properties versus frequency (Hz) and these properties are simple shear storage *G'*, loss *G"*, dynamic *G** modulus and phase angle δ. On the other hand, the same dynamic properties versus shear strain amplitude γ_0 are presented.

The most widely studied parameters in literature, are the storage *G'* and loss *G"* modulus and they are the dynamic properties which give the most valuable information. The dynamic stiffness *G** and phase angle δ can be derived from them. Hence, the conclusions will be focused mostly in these two modulus *G'* and *G"* and the other two dynamic properties *G** and phase angle δ will be presented as additional information. Moreover, the dynamic stiffness *G** has the same tendencies as the storage modulus *G'*.

FREQUENCY VERSUS DYNAMIC PROPERTIES

As it can be seen from FIG. 10-12-A-C, as frequency is increased, storage *G'* and dynamic modulus *G** increase too. This stiffening effect due to frequency increasing is more pronounced as the amplitude tends to zero. However, at high amplitudes the frequency change almost does not affect the magnitude of *G'* and *G**.

Loss modulus *G"* and phase angle δ as shown from FIG. 10-12-B-D increase as frequency is increased. At the studied highest amplitudes, the increase of the loss modulus *G"* due to frequency increasing becomes less significant.

AMPLITUDE VERSUS DYNAMIC PROPERTIES

The magnitudes of storage *G'* and dynamic *G** modulus from FIG. 10-12-E-G decrease as amplitude is increased. As it is shown in FIG. 13 this reduction in the stiffness is more pronounced as higher is the testing frequency.

The maximum of the loss modulus *G"* shown in FIG. 10-12-F is given at the amplitude where the storage modulus *G'* shown in FIG. 10-12-E drops more rapidly. The phase angle δ (FIG. 10-12-H) increase as the frequency is increased. The magnitude of loss modulus *G"* arises as frequency is increased but this effect becomes less significant as the amplitude increase.

THE EFFECT OF THE AMOUNT OF FILLER ON DYNAMIC PROPERTIES

In general the dynamic stiffness of all testing conditions is greater in elastomers with a higher content of filler. On the one hand, storage modulus *G'* as dynamic stiffness *G** arise as the amount of filler is increased due to its reinforcing effect. The stiffening of the storage *G'* and dynamic modulus *G** plotted against frequency slope at low amplitudes has more noticeable influence as a filler content of the elastomer increase. On the other hand, the offset between *G'* & *G** versus frequency curves at the tested amplitudes is more noticeable in elastomers with a greater amount of filler. Finally, as the filler content tends to zero, the amplitude and frequency dependence tends to be negligible and the material behavior tends to be linear.

The loss modulus magnitude increases with increasing the filler content, FIG. 10-11-B. The slope of *G''* versus frequency decrease as the amplitude increase in highly filled and filled rubbers, FIG. 10-11-B.

CONCLUSIONS

STORAGE MODULUS G' AND DYNAMIC STIFFNESS G*

At small deformations carbon-black agglomerates are not broken and in addition they can occlude rubber producing the mentioned augmentation effect mentioned above. Hence, the ability to move into the matrix is reduced. As the testing frequency increases the elastomer stiffness increases. This stiffening of the material with the frequency increase is due to the fact that the cycle time is smaller at higher frequencies. Hence, the non-broken filler agglomerates and in lower proportion the molecular structure, has less time to return to the relaxed state. This stiffening effect produced by the frequency increasing is more pronounced as higher is the amount of filler of the elastomer.

At intermediate deformations, the carbon-black agglomerates are broken into smaller agglomerates. Hence, the elastic modulus or the elastomer stiffness decreases because there are more mobile units into the rubber matrix. Consequently, the material stiffening due to frequency increasing is smaller. Finally, at high deformations, the carbon-black agglomerates broken down until the aggregates themselves are mobile units. Hence, the behavior at high deformations will be similar to the unfilled rubbers.

As the amount of filler of the elastomer decreases, the agglomerates content is lower, consequently the stiffening of the rubber diminishes. Accordingly, the change in the mobility because of their rupture due to the amplitude diminishes and the mobility because frequency change is not affected. Hence, the frequency and amplitude dependence diminishes as the filler content decreases.

In summary, the dynamic stiffness slope when plotted against frequency slope is higher at low amplitudes than higher amplitudes, which tends to be horizontal as higher is the amplitude. This effect is more evident as the amount of filler of the elastomer increase. Hence, the storage modulus G' and the dynamic stiffness G* curves versus frequency at different amplitudes are not parallel and the slope goes from smaller to higher being the slope low at high amplitudes and high at low amplitudes.

LOSS MODULUS G'' AND PHASE ANGLE δ

Amplitude dependence.— With increasing amplitude, the structure of the agglomerates present at intermediate amplitudes break down in smaller agglomerates. Those internal frictions are increasing with the

consequent increase in the loss modulus. From the critical amplitude the increase in the loss modulus changes the trend and decreases with the amplitude. During the cyclic strain, while the stable filler network at low amplitudes can reduce the hysteresis of the filled rubber, the breakdown and reformation of the filler network would cause an additional energy dissipation resulting in the higher hysteresis at intermediate amplitudes. Finally, at high amplitudes as the filler agglomerates are breakdown in aggregates, the rubber compound becomes more stable and the reformation of the filler network could not happen. Hence, at high amplitudes the loss modulus is reduced again.

Frequency dependence.— As frequency is increased it produces a greater loss of energy because the filler and molecular structure are changing their configuration in a shorter period of time. Therefore, when frequency is increased the number of internal friction increases producing a greater heat release. In unfilled elastomers the internal frictions are lower. Consequently, increasing the frequency the loss modulus *G"* does not vary as much as in filled elastomers.

In general, the results are in accordance with those existing in literature. Additionally a dataset is obtained, which covers a wider frequency/strain ranges than usual and characterizing highly filled, filled and unfilled elastomers. This accurate database, which is generated with a current servo-hydraulic machine, can be used to develop or validate new or existing constitutive models. The presented results, could be considered as a reference dataset generated with modern servo-hydraulic test systems, which could be used for further studies in the development and validation of new and existing constitutive models on the prediction of the dynamic properties for rubbers.

ACKNOWLEDGEMENTS

The definition and manufacturing of rubber formulations, as the characterization tests are a result of a collaborative work with Cikautxo S.Coop.

EMERG. EUITI. UPV/EHU, Leartiker, Lea Artibai Ikastetxea S.Coop., AZARO Fundazioa, FEDER and Basque Country Government, for research funding for the development of this study.

REFERENCES

[1] M.-J. Wang, Rubber Chem. Technol. **71**, 520 (1998).
[2] M.-J. Wang, Rubber Chem. Technol. **72**, 430 (1999).
[3] Olsson, A. K.; Austrell, P. E. *Const. Models for Rubber III* **2003**, 133–140.
[4] A. Lion, C. Kardelky, and P. Haupt, Rubber Chem. Technol. **76**, 533 (2003).
[5] A.R. Payne and R.E. Whittaker, Rubber Chem. Technol. **44**, 440 (1971).
[6] H.R. Ahmadi and A.H. Muhr, Rubber Chem. Technol. **84**, 24 (2011).
[7] M. Rendek and A. Lion, ZAMM-J. Appl. Math. Mech. Für Angew. Math. Mech. **90**, 436 (2010).
[8] W.L. Holt, Rubber Chem. Technol. **5**, 79 (1932).
[9] L. Mullins, Rubber Chem. Technol. **42**, 339 (1969).
[10] F. Bueche, Rubber Chem. Technol. **34**, 493 (1961).
[11] J.A.C. Harwood, L. Mullins, and A.R. Payne, Rubber Chem. Technol. **39**, 814 (1966).
[12] R. Houwink, Rubber Chem. Technol. **29**, 888 (1956).
[13] G. Kraus, C.W. Childers, and K.W. Rollmann, Rubber Chem. Technol. **39**, 1530 (1966).
[14] W.P. Fletcher and A.N. Gent, Rubber Chem. Technol. **27**, 209 (1954).
[15] A.R. Payne, Rubber Chem. Technol. **36**, 432 (1963).
[16] A.R. Payne, Rubber Chem. Technol. **36**, 444 (1963).
[17] G.E. Warnaka and H.T. Miller, Rubber Chem. Technol. **39**, 1421 (1966).
[18] G.E. Warnaka, Rubber Chem. Technol. **36**, 407 (1963).
[19] G. Huber, T.A. Vilgis, and G. Heinrich, J. Phys. Condens. Matter **8**, L409 (1996).
[20] P.B. Lindley, *Engineering Design with Natural Rubber.*, 4th ed. (Malaysian Rubber Producers Research Association, Brickendonbury, 1974).
[21] J. Harris and A. Stevenson, Rubber Chem. Technol. **59**, 740 (1986).
[22] L. Mullins and N.R. Tobin, Rubber Chem. Technol. **30**, 555 (1957).
[23] A.I. Medalia, Rubber Chem. Technol. **46**, 877 (1973).
[24] A.I. Medalia, Rubber Chem. Technol. **51**, 437 (1978).
[25]MTS Systems Corporation (2000).

FIGURES

FIG. 1.— Simple Shear specimen for measuring dynamic properties. In black: two rubber cylinders. In grey: metallic rubber supports.

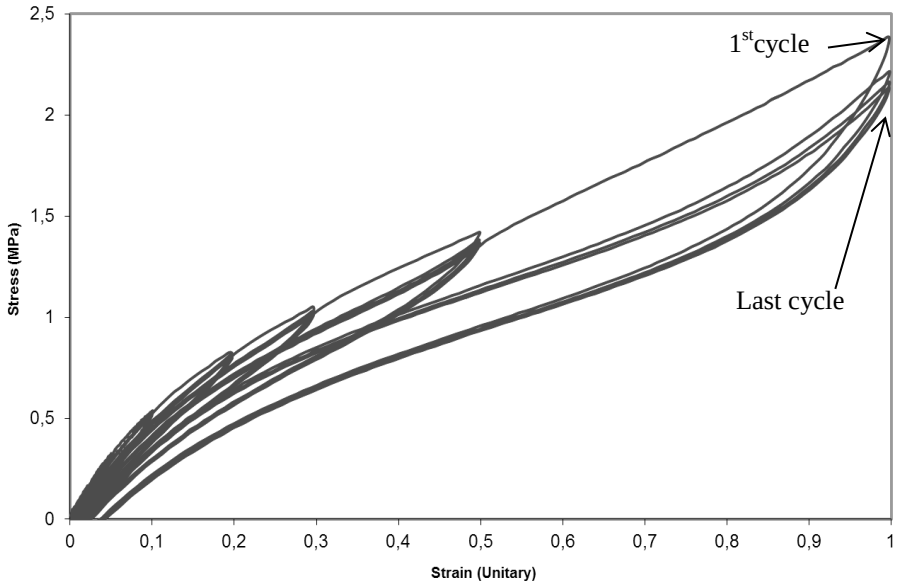

FIG. 2.— Mullins effect: The greatest softening occurs during the first cycle, with subsequent cycles a stabilization is observed.

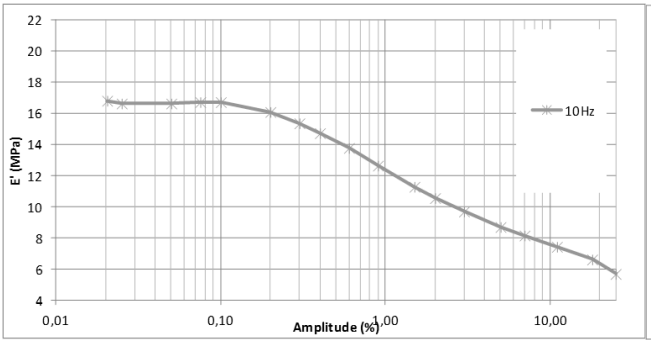

A)

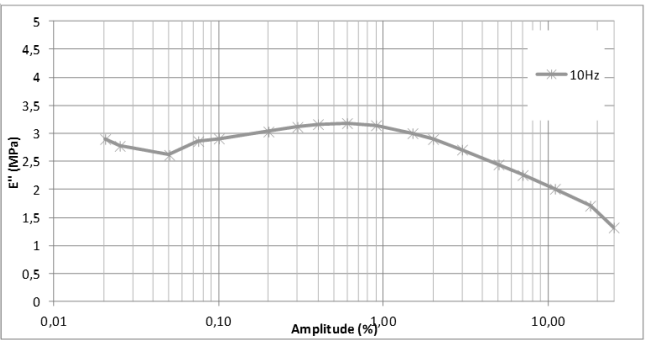

B)

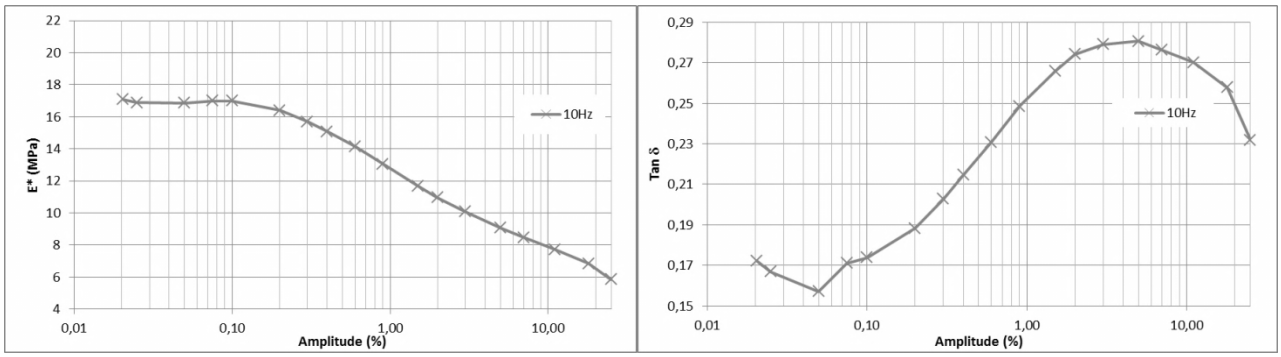

C) D)

FIG. 3.— Amplitude sweep test. Testing frequencie: 10 Hz. Figures A, B, C and D are the storage, loss and complex modulus respectively and D is the tan δ (Figure reproduced from Rendek and Lion [7])

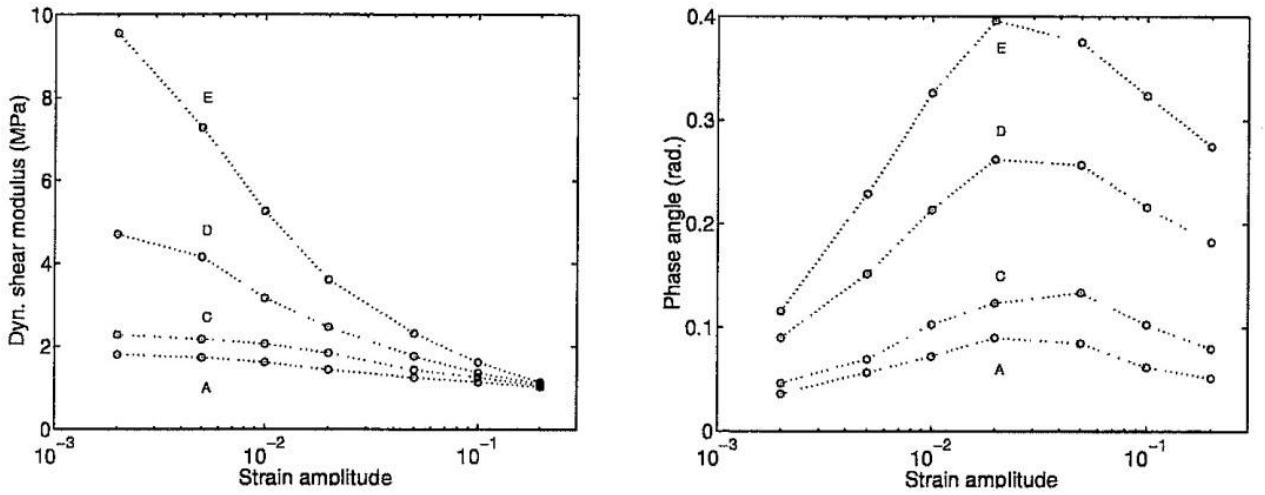

FIG. 4.— Amplitude dependence of dynamic shear modulus and phase angle for some filled natural rubbers of various filler contents (Reproduced from Harris and Stevenson [21]). From A to E, different compounds are represented, the amount of carbon-black being higher in E than in A). From C to E have the same type of filler.

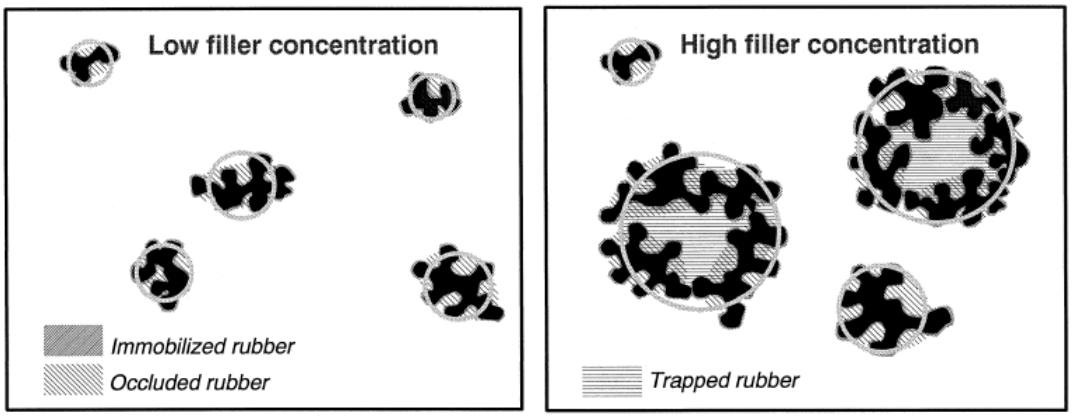

A) B)

FIG. 5.— A) Low filler concentration: Immobilized and occluded rubber representation around filler agglomerates. B) High filler concentration: Trapped rubber representation into filler agglomerates (Figure taken from Wang [2]).

FIG. 6.—MTS Model 831.50 (10 kN) 1000 Hz. Elastomer Testing System.

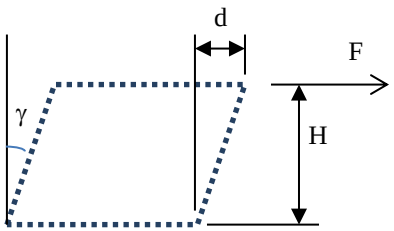

FIG. 7.— Simple shear specimen: representation of the deformed rubber region.

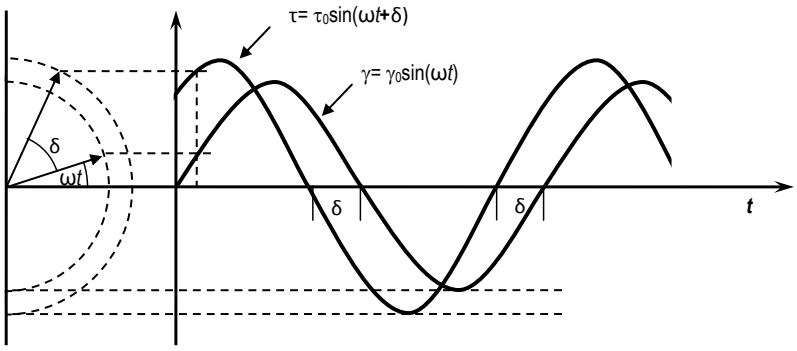

FIG. 8.— Phase shift between stress and strain in dynamic testing of rubber.

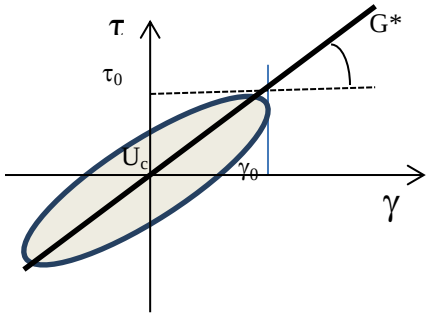

FIG. 9.— Dynamic measurement hysteresis loop.

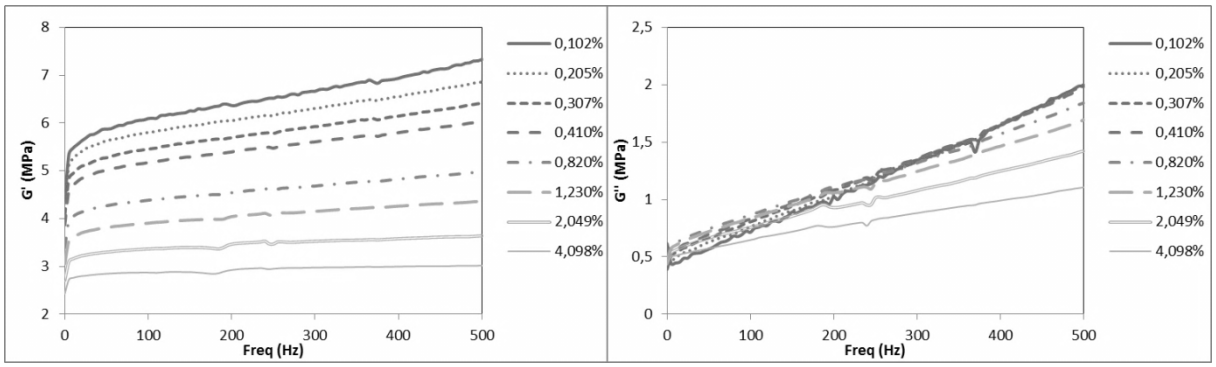

A) B)

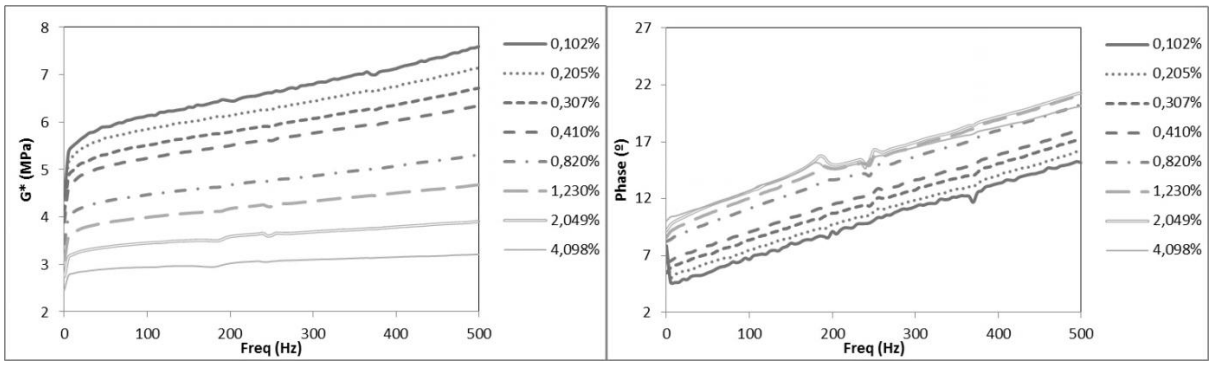

C) D)

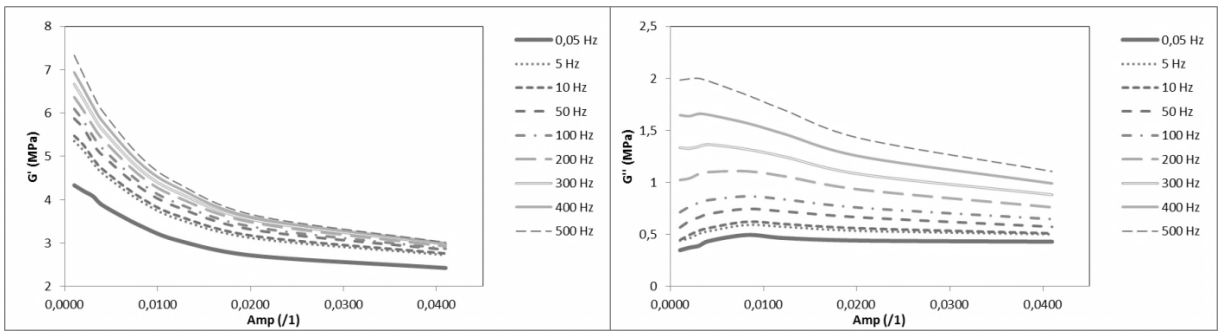

E) F)

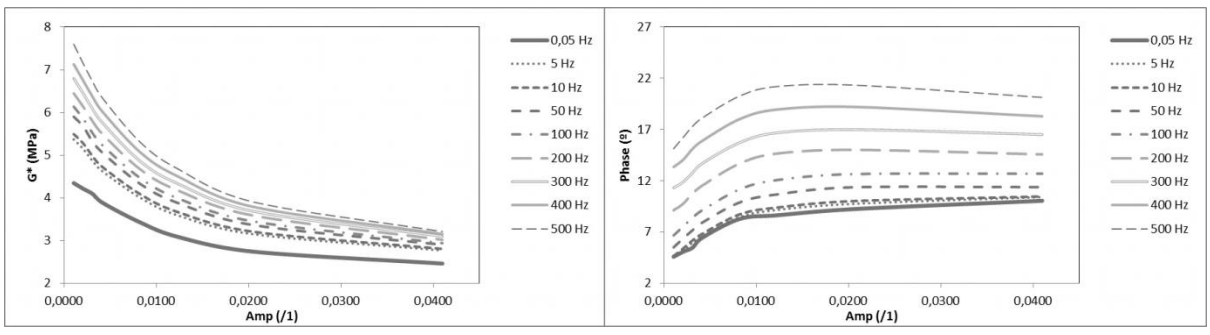

G) H)

FIG. 10.— Dynamic results of NR1: First, the dynamic properties G', G", G* and δ versus frequency (Hz) are represented, A), B) ,C) and D) respectively. Next, the dynamic properties G', G", G* and δ versus shear strain (/1) are represented, E), F), G) and H) respectively.

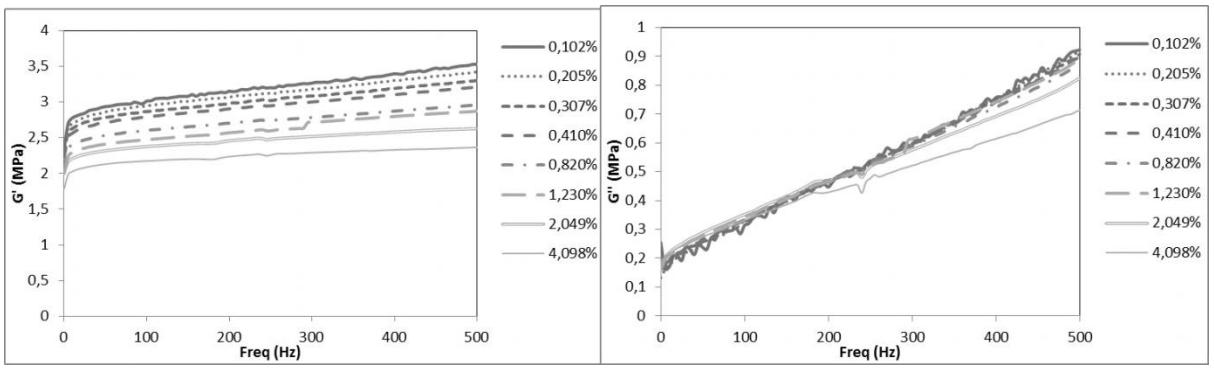

A)

B)

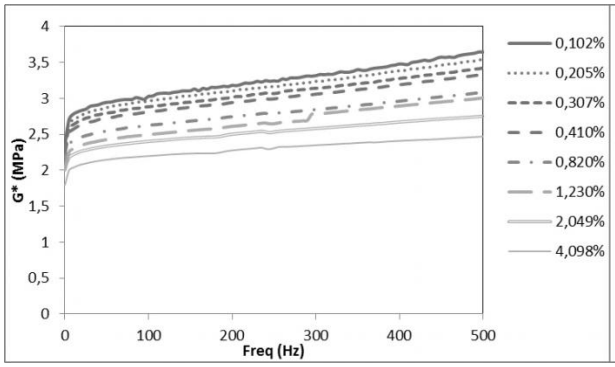

C)

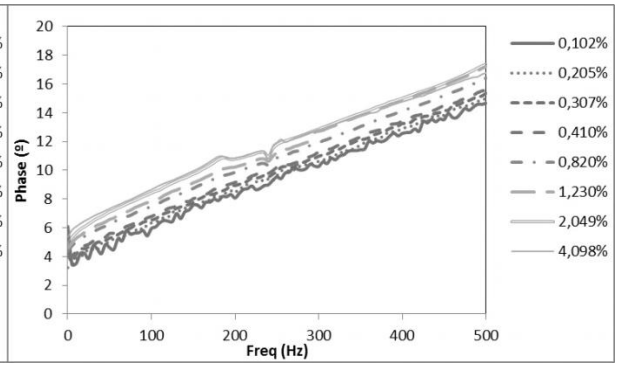

D)

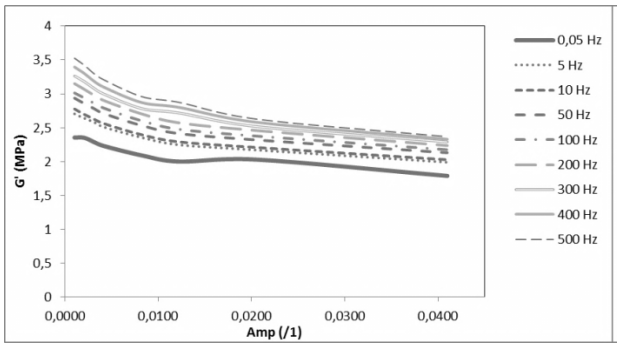

E)

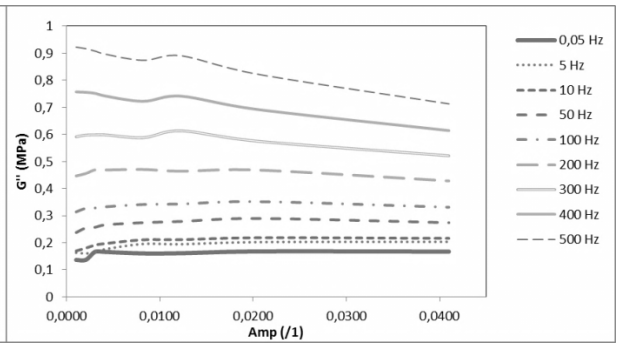

F)

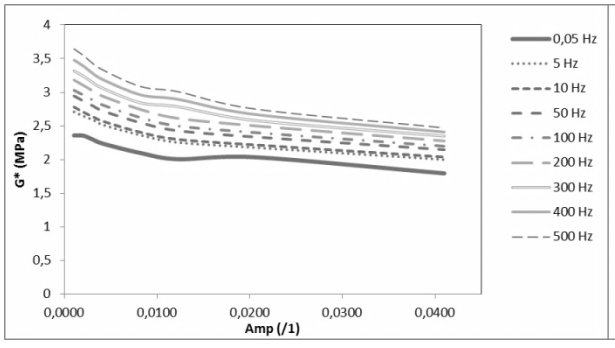

G)

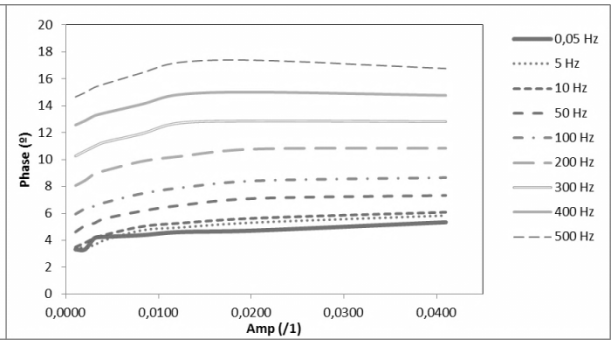

H)

FIG. 11.— Dynamic results of CKR: First, the dynamic properties G', G", G* and δ versus frequency (Hz) are represented, A), B) ,C) and D) respectively. Next, the dynamic properties G', G", G* and δ versus shear strain (/1) are represented, E), F), G) and H) respectively.

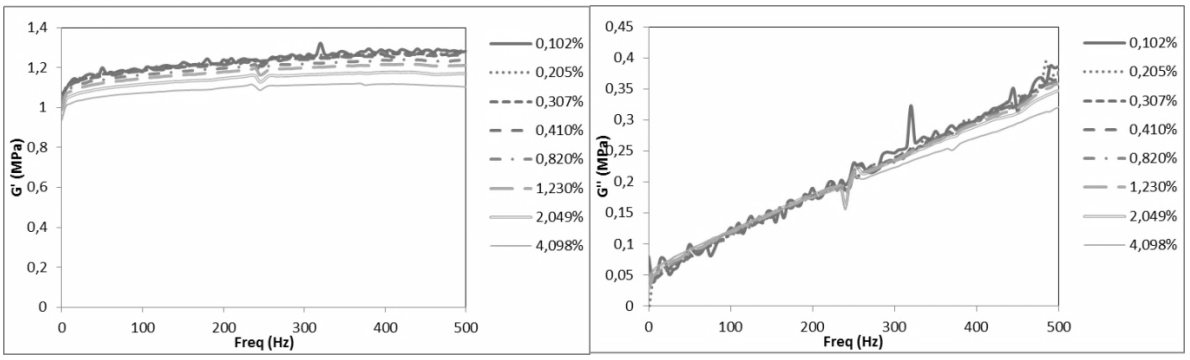

A)

B)

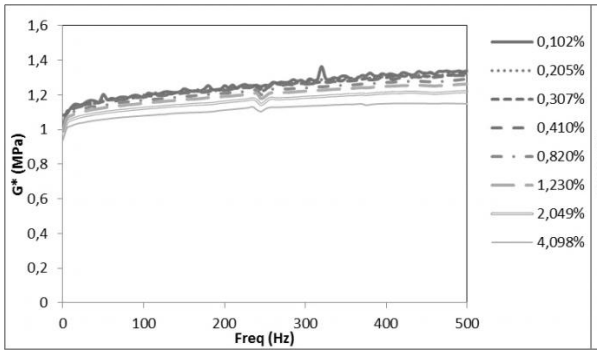

C)

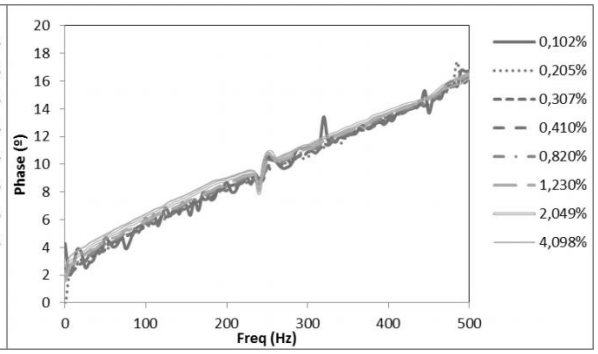

D)

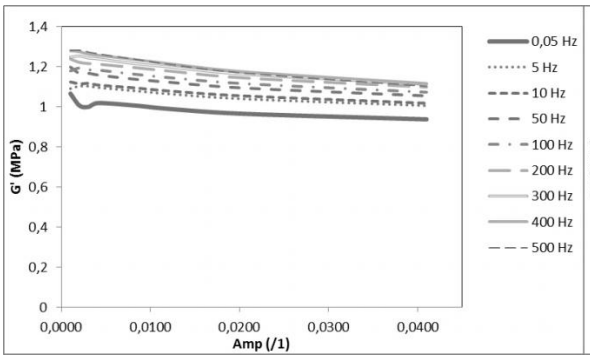

E)

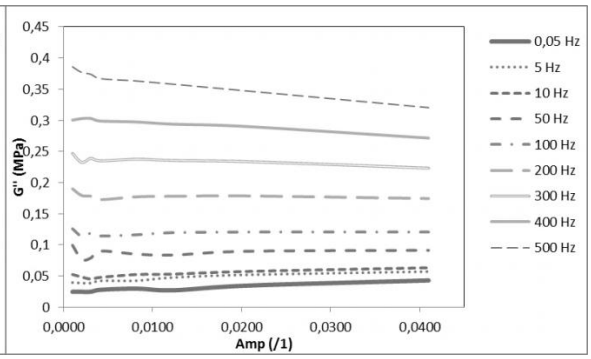

F)

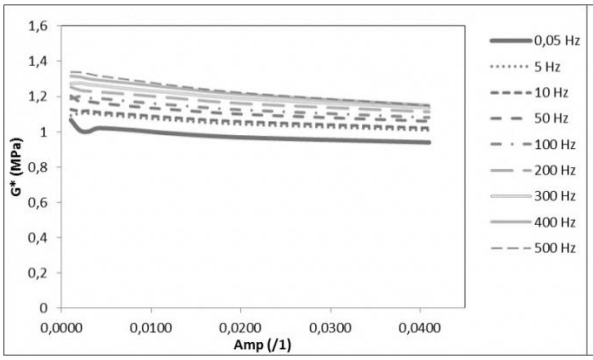

G)

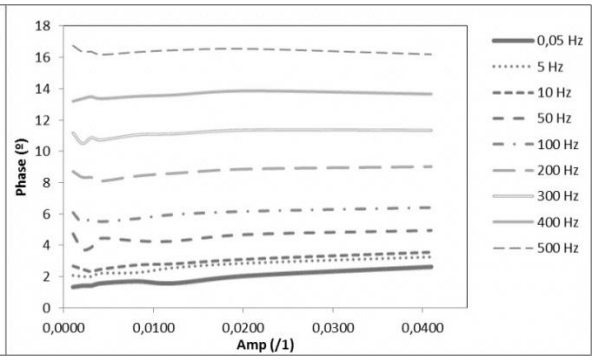

H)

FIG. 12.— Dynamic results of NR2: First, the dynamic properties G', G", G* and δ versus frequency (Hz) are represented, A), B) ,C) and D) respectively. Next, the dynamic properties G', G", G* and δ versus shear strain (/1) are represented, E), F), G) and H) respectively.

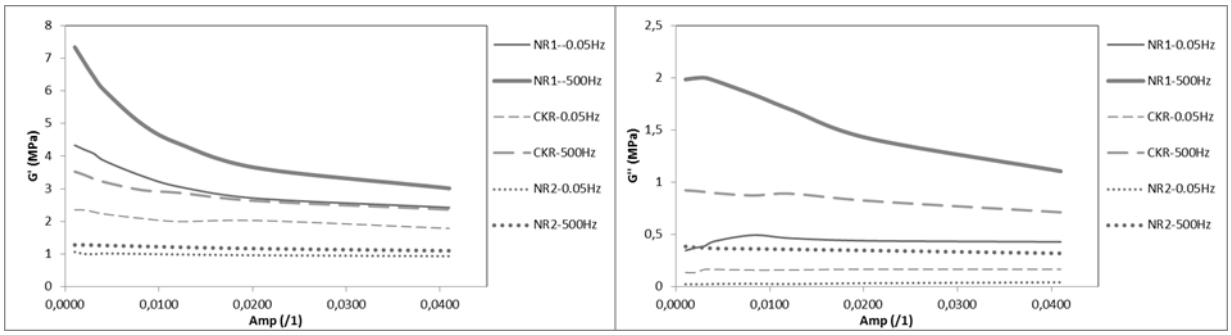

A) B)

FIG. 13.— A) Storage *G'* and B) Loss *G''* modulus versus amplitude representations: Comparison between the three characterized elastomers NR1, CKR & NR2 at the lowest & highest frequencies

TABLES

TABLE I
FORMULATION RECIPES

NR1	*phr*
SMR CV 60	100
ZnO	5
SFR N-774	80
TMQ	1
IPPD	1.5
Zinc Stearate	3
MBS	1.5
TBTD	0.9
Sulfur	0.8

NR2	*phr*
SMR CV 60	100
ZnO	5
SFR N-774	30
TMQ	1
IPPD	1.5
Zinc Stearate	3
MBS	1.5
TBTD	0.9
Sulfur	0.8

CKR	*phr*
BR	30
NR	70
ZnO	4
Stearic acid	1
Peptizing agent	1
Antiozonant Microwax	3.5
Aminic antioxidant	1.5
Aminic antiozonant	3
Aromatic oil	5
N539	50
Sulfur	1.4
CZ	1